University of Alberta

Fundamentals of Rapid Dewatering of Composite Tailings

by

Dennis James Boratynec ©

A thesis submitted to the Faculty of Graduate Studies and Research in partial fulfillment of the Master of Science

in

Geoenvironmental Engineering

Department of Civil and Environmental Engineering

Edmonton, Alberta

Spring, 2003

National Library of Canada
Acquisitions and Bibliographic Services
395 Wellington Street
Ottawa ON K1A 0N4
Canada

Bibliothèque nationale du Canada
Acquisitions et services bibliographiques
395, rue Wellington
Ottawa ON K1A 0N4
Canada

Your file Votre référence

Our file Notre référence

The author has granted a non-exclusive licence allowing the National Library of Canada to reproduce, loan, distribute or sell copies of this thesis in microform, paper or electronic formats.

L'auteur a accordé une licence non exclusive permettant à la Bibliothèque nationale du Canada de reproduire, prêter, distribuer ou vendre des copies de cette thèse sous la forme de microfiche/film, de reproduction sur papier ou sur format électronique.

The author retains ownership of the copyright in this thesis. Neither the thesis nor substantial extracts from it may be printed or otherwise reproduced without the author's permission.

L'auteur conserve la propriété du droit d'auteur qui protège cette thèse. Ni la thèse ni des extraits substantiels de celle-ci ne doivent être imprimés ou autrement reproduits sans son autorisation.

0-612-82250-8

Canada

University of Alberta

Library Release Form

Name of Author: *Dennis James Boratynec*

Title of Thesis: *Fundamentals of Rapid Dewatering of Composite Tailings*

Degree: *Master of Science*

Year this Degree Granted: *2003*

Permission is hereby granted to the University of Alberta Library to reproduce single copies of this thesis and to lend or sell such copies for private, scholarly or scientific research purposes only.

The author reserves all other publication and other rights in association with the copyright in the thesis, and except as herein before provided, neither the thesis nor any substantial portion thereof may be printed or otherwise reproduced in any material form whatever without the author's prior written permission.

D Boratynec

Dennis Boratynec
9 Village Road
Sherwood Park, AB T8A 0Z4

January 22, 2003

Date submitted to FGSR

University of Alberta

Faculty of Graduate Studies and Research

The undersigned certify that they have read, and recommend to the Faculty of Graduate Studies and Research for acceptance, a thesis entitled FUNDAMENTALS OF RAPID DEWATERING OF COMPOSITE TAILINGS submitted by Dennis James Boratynec in partial fulfillment of the requirements for the degree of Master of Science in Geoenvironmental Engineering.

Dr. R.J. Chalaturnyk
Co-Supervisor

Dr. J. D. Scott
Co-Supervisor

Dr. D. Sego

Dr. Selma Guigard

Dr. Zhenghe Xu

Date: January 17, 2003

ABSTRACT

Previous research conducted at the University of Alberta has revealed that addition of phosphogypsum (PG) to a mixture of tailings cyclone underflow and mature fine tailings produces a nonsegregating tailings stream known as composite tailings (CT). The objective of the laboratory testing program was to increase the understanding of the chemical and physical processes which influence the dewatering characteristics of CT. A complete set of equations for defining the compositional characteristics of CT were developed. The results of the testing program showed that CT placed in 5 cm high deposits experiences an immediate downward movement and undergoes hindered sedimentation followed by self-weight consolidation. Increasing the PG dosage up to 3200 g/m^3 results in an increase in the mass of release water and the presence of an optimum dosage was not observed. CT has a compression index consistent the upper limit of with pure kaolinite and hydraulic conductivity which spans two orders of magnitude.

DEDICATION

The author would like to thank, Dr. J.D. Scott for his guidance, expertise, patience, and encouragement during this research project. Also to Dr. R.J. Chalaturnyk for his support, energy, enthusiasm, and teachings both academic and otherwise. Thank you for answering all the long distance phone calls, emails and finally making this happen.

Thanks to Steve Gamble and Gilbert Wong for assisting in the laboratory and being there when things were not going so well and for finishing some much needed laboratory testing.

Thanks to Gord McKenna of Syncrude for providing the tailings samples used in this work.

Special thanks to my parents, Marshall and Mary, for their love, encouragement and instilling in me the value of an education. Also to my brother and sister, Bryan and Susan, for the early morning wake up calls, carpooling and understanding why I needed to stay "one more hour".

Most importantly, I'd like to thank my wife, Zina, for her encouragement and sacrifice during the last five years. Finally.....no more '"thesis weekends".

TABLE OF CONTENTS

1.0 BACKGROUND 1

1.1 Statement of Problem 1
1.2 Objective of Research 3
1.3 Scope of Thesis 3
1.4 Organization of Thesis 4

2.0 LITERATURE REVIEW 6

2.1 OVERVIEW OF OIL SANDS MINING OPERATION 6

2.1.1 Oil Sand Deposits 6
2.1.2 Tailings Disposal 7
2.1.3 Tailings Management 8
2.1.4 Nonsegregating Tailings 9
2.1.5 Composite Tailings 11

2.2 DISSOLUTION OF GYPSUM 12

2.2.1 Sinks for Gypsum 13

2.3 CLAY-WATER ELECTROLYTE SYSTEM 14

2.3.1 Clay Mineralogy 15
2.3.2 Electric Double Layer Theory 16
2.3.2.1 Influences on Diffuse Double Layer Thickness 19

2.4 CATION EXCHANGE CAPACITY (CEC) 20

2.4.1 CEC Reactions 21
2.4.2 Ion Exchange Equilibrium 22
2.4.3 Cation Exchange Rate 23
2.4.4 Interaction of Adjacent Double Layers 23
2.4.4.1 Short and Long Range Repulsive Forces 24
2.4.4.2 Long Range Attractive Forces 25
2.4.4.3 Net Particle Interaction 25
2.4.5 Factors Determining Floc and Aggregate Size 26
2.4.5.1 Soil Fabric 27
2.4.5.1.1 Soil Fabric as it Relates to Compressibility 27
2.4.5.1.2 Soil Fabric as it Relates to Hydraulic Conductivity 28
2.4.6 Effect of Cation Exchange on Void Ratio – Effective Stress Relationship 29
2.4.6.1 Effect of Cation Exchange on Hydraulic Conductivity 31
2.4.6.2 Effect of Cation Exchange on Structure 32

2.5 BEHAVIOR OF A CLAY-WATER SYSTEM 33

2.5.1 Settling Behavior Type 33
2.5.2 Hindered Settling Theory 34
2.5.2.1 Stages of Hindered Settling 35
2.5.2.1.1 Flocculation or Induction Stage 35
2.5.2.1.2 Settling Stage 37
2.5.2.1.3 Solids Content of Hindered Settling Zone 38
2.5.3 Consolidation Settling Theory 38
2.5.3.1 General Discussion on Soil Compressibility 39
2.5.3.1.1 Inclusion of Interparticle Forces to Effective Stress 40
2.5.3.1.2 Factors Affecting the Interparticle Pressure 41
2.5.3.1.3 Quantifying the Interparticle Pressure 42
2.5.3.1.4 Application of the Osmotic Pressure Theory 43
2.5.3.1.5 Physico-Chemical Effects 44

2.5.3.2 Measurement of Hydraulic Conductivity 45

3.0 MULTIPHASE MASS-VOLUME RELATIONSHIPS 61

3.1 INTRODUCTION TO THE MULTIPHASES OF OIL SANDS TAILINGS 61

3.2 FIVE PHASE OIL SANDS TAILINGS DIAGRAM 65

3.3 DEFINITION OF MASS-VOLUME RELATIONSHIPS 66

3.3.1 Bitumen Content 66
3.3.2 Degree of Saturation 66
3.3.3 Density 66
3.3.4 Fines Content 67
3.3.5 Fines-Water Ratio 68
3.3.6 Gas Content 68
3.3.7 Porosity 68
3.3.8 Sand Content 68
3.3.9 Sand Fines Ratio 68
3.3.10 Solids Concentration 69
3.3.11 Solids Content 69
3.3.12 Specific Gravity 69
3.3.13 Unit Weight 70
3.3.14 Void Ratio 71
3.3.15 Fines Void Ratio 71
3.3.16 Fines-Bitumen Void Ratio 71
3.3.17 Sand Void Ratio 71
3.3.18 Volume Concentration 71
3.3.19 Water Content 72

3.4 COMPARISON BETWEEN GEOTECHNICAL AND "MINING" DEFINITIONS 73

3.4.1 Bitumen Content 75
3.4.2 Fines Content 75
3.4.3 Solids Content 76
3.4.4 Water Content 76

3.5 CONVERSION RELATIONSHIPS FOR MASS-VOLUME RELATIONSHIPS 77

4.0 EXPERIMENTAL PROGRAM AND PROCEDURES 82

4.1 FIELD PRODUCTION OF CT 82

4.1.1 Makeup of Field Produced CT 82

4.2 COLLECTION AND STORAGE OF LABORATORY TAILINGS SAMPLES 84

4.2.1 Mature Fine Tails (MFT) Sampling and Storage 85
4.2.2 Recycled Pond Water Sampling and Storage 85
4.2.3 Whole Tailings Sampling and Storage 86

4.3 GEOTECHNICAL TEST RESULTS ON LABORATORY TAILINGS SAMPLES 86

4.3.1 Index Properties of Laboratory Samples 87
4.3.1.1 Summary of Index Properties of Laboratory Samples 88
4.3.2 Gradation of Laboratory MFT 88

4.4 LABORATORY PRODUCTION OF CT 88

4.4.1 Production of Laboratory Manufactured Cyclone Underflow 88
4.4.2 Gradation Laboratory Manufactured Cyclone Underflow 89

4.4.3 MIX DESIGN FOR STANDARD LABORATORY CT 90
4.4.4 GRADATION OF STANDARD LABORATORY CT 90

4.5 WATER RELEASE INDEX TEST (WRIT) 91

4.5.1 DESIGN CONSIDERATION FOR WATER RELEASE INDEX TEST (WRIT) 92
4.5.2 TEST PROCEDURE FOR STANDARD WATER RELEASE INDEX TEST (WRIT) 93

4.6 LABORATORY TEST PROCEDURES 94

4.6.1 EFFECT OF EXPERIMENTAL PROCEDURE 95
4.6.1.1 Effect of Diameter-to-Height Ratio (DHR) *96*
4.6.2 EFFECT OF PHOSPHOGYPSUM DOSAGE 97
4.6.2.1. Water Release Index Tests (WRIT's) *97*
4.6.2.2 Capturing Behavior of CT / Water Interface During WRIT *97*
4.6.2.3 Step Loaded Slurry Consolidometers *98*
4.6.2.4 Scanning Electronic Microscopy (SEM) Images *99*
4.6.2.4.1 Cryogenic SEM 100
4.6.2.4.2 Variable Pressure SEM 101

4.7 SUMMARY 103

5.0 RESULTS ON EFFECT OF EXPERIMENTAL PROCEDURE AND EFFECT OF INCREASING PHOSPHOGYPSUM DOSAGE 115

5.1 INTRODUCTION 115

5.1 DIAMETER TO HEIGHT RATIO (DHR) 115
5.1.1 Effect on Grams of Release Water per cm^2 ..... *116*
5.1.2 Effect on Normalized Grams of Release Water *117*

5.2 EFFECT OF PHOSPHOGYPSUM DOSAGE 117

5.2.1 INDEX TEST RESULTS 117
5.2.1.1 Partial Discussion of WRIT *119*
5.2.1.2 Summary of Index Test Results *121*
5.2.2 BEHAVIOR OF CT / WATER INTERFACE DURING WRIT 122
5.2.3 SLURRY CONSOLIDOMETER TEST RESULTS 123
5.2.3.1 Compressibility Relationship at 900 g/m^3 of PG *123*
5.2.3.2 Compressibility Relationship at 3200 g/m^3 of PG *124*
5.2.3.3 Comparison of Compressibility Relationships at 900 and 3200 g/m^3 of PG *124*
5.2.3.4 Hydraulic Conductivity Relationship at 900 g/m^3 of PG *125*
5.2.3.5 Hydraulic Conductivity Relationship at 3200 g/m^3 of PG *127*
5.2.3.6 Comparison of Hydraulic Conductivity Relationship at 900 and 3200 g/m^3 of PG *127*
5.2.4 SCANNING ELECTRON MICROSCOPY (SEM) 128
5.2.4.1 Introduction *128*
5.2.4.2 Cryogenic SEM Images with 900 g/m^3 of PG *129*
5.2.4.2.1 Cryogenic SEM Images with 1400 g/m^3 of PG. 130
5.2.4.2.2 Cryogenic SEM Images with 2000 g/m^3 of PG. 131
5.2.4.2.3 Cryogenic SEM Images with 2600 g/m^3 of PG. 131
5.2.4.2.4 Cryogenic SEM Images with 3200 g/m^3 of PG. 132
5.2.4.2.5 Variable Pressure SEM Images with 600 g/m^3 of PG. 133
5.2.4.2.6 Variable Pressure SEM Images with 900 g/m^3 of PG. 134
5.2.4.3 Variable Pressure SEM Images with 3200 g/m^3 of PG *134*

6.1 DIAMETER-TO-HEIGHT RATIO (DHR) 177

6.2 FINES AND PHOSPHOGYPSUM INTERACTION 180

6.2.1 Behavior of Interface during WRIT *182*
6.2.1.1 Prevention of Segregation 182

6.2.1.2 Flocculation or Induction Period 183
6.2.1.3 Yield Diameter and Yield Height 185
6.2.1.4 Uniqueness of Soil Forming Void Ratio 186
6.2.2 Effect of PG on Compressibility Characteristics *187*
6.2.2.1 Overall Compressibility of CT 187
6.2.2.2 Effect of Increased PG Dosage on Compressibility of CT 188
6.2.2.3 CT Compressibility Results of Others 190
6.2.3 Effect of PG on Hydraulic Conductivity *191*
6.2.3.1 Quantitative Measurement of Hydraulic Conductivity 191
6.2.3.2 Qualitative Measurement of Hydraulic Conductivity 192
6.2.3.2.1. Effect of Minor Fluctuations in PGFR on Hydraulic Conductivity 193

7.0 CONCLUSIONS AND RECOMMENDATIONS **197**

7.1 RECOMMENDATIONS FOR FURTHER RESEARCH **199**

REFERENCES **201**

APPENDIX A **209**

APPENDIX B **219**

APPENDIX C **222**

APPENDIX D **245**

LIST OF FIGURES

Figure 2.1	Athabasca oil sand deposit	47
Figure 2.2	Cross–section of Athabasca deposit	48
Figure 2.3	Water-wet arrangement of oil sands	49
Figure 2.4	Grain size distribution	50
Figure 2.5	Slurry properties diagram	51
Figure 2.6	Distribution of absorbed cations according to the diffuse double layer theory	52
Figure 2.7	Influence of metastable fabric on void ratio under an effective consolidation pressure	53
Figure 2.8	Theoretical water-retention curves of Na-clays as a function of NaCl concentration	54
Figure 2.9	Experimental water-retention curves for mixed ion Na-Ca-Montmorillonite systems	55
Figure 2.10	Compression curves of Na-montmorillonite and Ca-montmorillonite, fraction < 2 um	56
Figure 2.11	General characteristics of sedimentation of clay-water mixture	57
Figure 2.12	Three generalized types of settling plots	58
Figure 2.13	Interparticle forces in an active clay-water system	59
Figure 2.14	Measured vs. estimated net physico-chemical stress	60
Figure 3.1	Five-Phase Tailings Diagram	65
Figure 4.1	Grain size distribution of laboratory MFT compared to MFT used by Syncrude in 1995 Field Trial	109
Figure 4.2	Grain size distribution of laboratory TFT	110
Figure 4.3	Grain size distribution of laboratory Sand	111
Figure 4.4	Grain size distribution of cyclone underflow (1995) and laboratory simulated cyclone underflow	112
Figure 4.5	Grain size distribution of CT	113
Figure 4.6	Slurry consolidometer	114
Figure 5.1	Effect of Diameter-to-Height Ratio (DHR) on grams of release water per cm^2	145
Figure 5.2	Effect of Diameter-to-Height Ratio (DHR) on normalized grams of release water	146
Figure 5.3	Effect of increasing PG dosage on WRIT results	147
Figure 5.4	Effect of increasing PGFR on WRIT results	148
Figure 5.5	Effect of low PGFR's on WRIT results	149
Figure 5.6	Effect of high PGFR's on WRIT results	150
Figure 5.7	Behavior of interface during WRIT at 900 and 3200 g/m^3	151
Figure 5.8	Compressibility relationship for CT at 900 g/m^3	152
Figure 5.9	Compressibility relationship for CT at 3200 g/m^3	153
Figure 5.10	Comparison of compressibility relationship for CT at 900 and 3200 g/m^3 of PG	154

Figure 5.11 Fines void ratio-hydraulic conductivity relationship for CT with 900 g/m^3 of PG 155
Figure 5.12 Fines void ratio-hydraulic conductivity relationship for CT with 3200 g/m^3 of PG 156
Figure 5.13 Comparison of fines void ratio-hydraulic conductivity relationship for CT at 900 and 3200 g/m^3 157
Figure 5.14 Mass of release water vs. PGFR for all SEM images 158
Figure 5.15 Cryogenic SEM for CT at 61.9 % Solids, 21.2 % Fines with 900 g/m^3 of PG (Magnification X 15) 159
Figure 5.16 Cryogenic SEM for CT at 61.9 % Solids, 21.2 % Fines with 900 g/m^3 of PG (Magnification X 100) 160
Figure 5.17 Cryogenic SEM for CT at 61.9 % Solids, 21.2 % Fines with 900 g/m^3 of PG (Magnification X 200) 161
Figure 5.18 Cryogenic SEM for CT at 61.8 % Solids, 21.0 % Fines with 1400 g/m^3 of PG (Magnification X 100) 162
Figure 5.19 Cryogenic SEM for CT at 61.8 % Solids, 21.0 % Fines with 1400 g/m^3 of PG (Magnification X 500) 163
Figure 5.20 Cryogenic SEM for CT at 61.9 % Solids, 19.8 % Fines with 2000 g/m^3 of PG (Magnification X 15) 164
Figure 5.21 Cryogenic SEM for CT at 61.9 % Solids, 19.8 % Fines with 2000 g/m^3 of PG (Magnification X 200) 165
Figure 5.22 Cryogenic SEM for CT at 61.8 % Solids, 22.2 % Fines with 2600 g/m^3 of PG (Magnification X 15) 166
Figure 5.23 Cryogenic SEM for CT at 61.8% Solids, 22.2 % Fines with 2600 g/m^3 of PG (Magnification X 100) 167
Figure 5.24 Cryogenic SEM for CT at 61.6 % Solids, 20.0 % Fines with 3200 g/m^3 of PG (Magnification X 15) 168
Figure 5.25 Cryogenic SEM for CT at 61.6 % Solids, 20.0 % Fines with 3200 g/m^3 of PG (Magnification X 100) 169
Figure 5.26 Cryogenic SEM for CT at 61.6 % Solids, 20.0 % Fines with 3200 g/m^3 of PG (Magnification X 200) 170
Figure 5.27 Variable Pressure SEM for CT at 62.1 % Solids, 20.1 % Fines with 600 g/m^3 of PG (Magnification X 266) 171
Figure 5.28 Variable Pressure SEM for CT at 62.1 % Solids, 20.1 % Fines with 600 g/m^3 of PG (Magnification X 690) 172
Figure 5.29 Variable Pressure SEM for CT at 61.8 % Solids, 20.9 % Fines with 900 g/m^3 of PG (Magnification X 286) 173
Figure 5.30 Variable Pressure SEM for CT at 61.8 % Solids, 20.9 % Fines with 900 g/m^3 of PG (Magnification X 690) 174
Figure 5.31 Variable Pressure SEM for CT at 62.8 % Solids, 20.5 % Fines with 3200 g/m^3 of PG (Magnification X 227) 175
Figure 5.32 Variable Pressure SEM for CT at 62.8 % Solids, 20.5 % Fines with 3200 g/m^3 of PG (Magnification X 690) 176

LIST OF TABLES

Table 3.1	Mass-Volume Conversion Relationships	78
Table 4.1	Components Required to Produce 1 m^3 of Field CT at 62 % Solids and 20 % Fines	105
Table 4.2	Breakdown of Age Designations for CT Phases	106
Table 4.3	Average Geotechnical Parameters of Laboratory Tailings Samples	107
Table 4.4	Standard Laboratory CT Mix Design (2.0 L)	108
Table 5.1	Effect of Diameter-to-Height Ratio (DHR) at 900 g/m^3	136
Table 5.2	Effect of Diameter-to-Height Ratio (DHR) at 2000 g/m^3	137
Table 5.4	Re-evaluating WRIT Results for PG dosages from 600 to 3200 g/m^3	138
Table 5.5	Summary of Compressibility Test Results at 900 g/m^3	139
Table 5.6	Summary of Compressibility Test Results at 3200 g/m^3	140
Table 5.7	Summary of Hydraulic Conductivity Test Results at 900 g/m^3	141
Table 5.7	Summary of Hydraulic Conductivity Test Results at 900 g/m^3	142
Table 5.8	Summary of Hydraulic Conductivity Test Results at 3200 g/m^3	143
Table 5.9	Summary of SEM Samples	144

1.0 Background

The Athabasca Oil Sands of Northern Alberta have been commercial mined by Syncrude Canada Limited (SCL) and Suncor Inc. since 1978 and 1967, respectively. After extracting the bitumen, a slurry waste consisting of residual bitumen, water, coarse and fined grained material is hydraulically transported and stored within surface tailings ponds. Without chemical treatment prior to deposition, the tailings stream naturally segregates as the coarse particles rapidly fall out of suspension while the finer fraction accumulates towards the center of the tailings pond. Currently, there are approximately 400 million m^3 of mature fine tails (MFT) at a solids content of 30 % (233 % geotechnical water content) in storage and future predictions estimate that 1 billion m^3 will require storage by 2025 if current discharge methods continue (Scott, 2002). The major geoenvironmental issues associated with the untreated tailings slurry are its segregating behavior, bulking factor and the long-term environmental impacts of permanent storage.

Research conducted at the University of Alberta has revealed that addition of lime or a form of gypsum to a mixture of tailings cyclone underflow (CU) and MFT produces a nonsegregating tailings stream known as composite tailings or consolidated tailings (CT). The addition of calcium ions is thought to sufficiently reinforce the strength of the clay structure as to prevent segregation, thereby retaining the coarse fraction to provide an internal surcharge. Field production of CT results in the deposition of relatively thin layers, which subsequently undergo rapid water release during the first 8 to 12 hours after deposition. The clear decant water which flows to the surface of the deposit is collected for re-use in the extraction plant.

1.1 Statement of Problem

In the past, finite strain consolidation models have been used to predict the rate of water release and pore pressure dissipation of various CT field deposits. These models require laboratory data to define the relationship between the hydraulic conductivity and void ratio and the relationship between void ratio and effective stress. Using finite strain consolidation theory the rate and magnitude of the strain can be assessed.

For any modeling work, the accuracy of the prediction is dependent on the physical processes incorporated in the model, quality of the laboratory data and its ability to mimic field conditions and overcome any scale effects. Current modeling efforts of CT depositional processes have identified anomalies which exist between the laboratory based predictions and the field response of CT. Visual observations of recent field deposits suggest that water release rates observed in field deposits are noticeably higher than observed in laboratory tests.

From an accuracy point of view, issues can be raised by the quality and appeal of both field and laboratory derived relationships. From an economic and precision standpoint field results are more costly and due to their size generally suffer from reduced quality control. A laboratory environment provides a controlled setting in which relevant and irrelevant factors can be assessed quickly and economically.

However, a basic understanding of the experimental and physiochemical factors influencing the early stages of water release does not exist. Advancement of this understanding will permit further optimization of CT behavior such that the water release rates can be maximized; thereby reducing the area requiring final reclamation, amount of water brought on site and the time required for the CT deposit to be trafficable. The characterization of factors affecting water release rate must proceed in conjunction with the development of reclamation options

such that a suitable long-term waste management disposal program can be implemented.

1.2 Objective of Research

One of the objectives of the research was to provide mathematical definitions and conversion equations to help understand the multi-phase mass-volume relationships, which are often utilized when discussing oil sand tailings. The objective of the laboratory program was to increase the understanding of the chemical and physical processes which influence the dewatering characteristics of CT using laboratory testing. The importance of the physical and chemical factors were assessed by observing changes in; (1) settling behavior, (2) compressibility and hydraulic conductivity characteristics, and (3) fines structure as observed in SEM images. A discussion which links the experimentally measured behavioral changes and information gathered from the literature is presented to interpret the role of physical and chemical processes in the dewatering of CT.

1.3 Scope of Thesis

Initial experimental results to determine optimum experimental equipment and procedures are first presented. This portion involved performing a series of index test using glass and acrylic standpipes to quantify the effects of diameter to height ratio (DHR), and phosphogypsum dosage on the rate of water release of CT. In each water release index test (WRIT) 5 cm of CT was placed in an acrylic standpipe with a diameter ranging from approximately 5 to 20 cm. At the end of the 24-hour index test the mass of water released was determined using gravimetric analysis. Additionally, using time-lapse photography the movement of the interface as a function of time was captured to characterize the settling behavior of the CT during the WRIT.

Large strain oedometers were used to quantify the effect of PG dosage on the compressibility and hydraulic conductivity of two CT samples. Each sample was subjected to eleven loading steps from approximately 0.2 kPa to 700 kPa in order to determine the variation in void ratio as a function of effective stress. Between loading steps, upward flow then downward flow hydraulic gradients were applied and the variation in hydraulic conductivity as a function of void ratio was also determined.

To complement the results of the WRIT's and the slurry oedometer experiments and to provide further insight into the role of phosphogypsum (PG) as it relates to the fines structure and to the rate of water release, a series of images were captured using Scanning Electron Microscopy (SEM). To help reduce controversy surrounding artifacts of freezing in cryogenics SEMs as a result of preparation techniques, both a cryogenic and variable pressure SEMs were used. These images were used to qualitatively assess changes in the fines fabric of CT as a function of PG dosage and complement the quantitative test results.

1.4 Organization of Thesis

Chapter 2 contains the literature review of the current oil sands mining operation, interaction of calcium and clay particles, and sedimentation and consolidation theory. The initial part of this chapter is intended to provide a general description of both the Syncrude and Suncor operations in Fort McMurray and to quantify the volume of materials currently in storage rather than a comparison of each. The literature review continues with factors controlling flocculation behavior, cation exchange reactions, soil fabric and their impact on soil compressibility and hydraulic conductivity. The literature review contains a discussion of the stages of sedimentation and consolidation behavior, to better understand the physical processes that CT undergoes after deposition.

Chapter 3 contains definitions and conversion factors that were needed for dealing with a five phase material such as CT. Oil sands tailings is an unequaled geotechnical material, in that four different phases; mineral grains (fine and coarse), water, bitumen and gas can be present. The need for standardizing the oil sand tailings definitions and conversion relationships has arisen as different engineering disciplines; geotechnical, mining and chemical in addition to geologic disciplines often work together on different aspects of tailings treatment and disposal within the oil sands industry. It is hoped that this chapter will form the basis for standardizing usage of oil sands tailings parameters and act as an analytical tool to increase the understanding of material behavior.

Chapter 4 summarizes the procedure used to obtain and store tailings samples and the measured geotechnical characteristics of mature fine tails (MFT) and whole tailings. Furthermore, the techniques used in the production of laboratory CT are described along with the design of the standard water release index test (WRIT). The chapter concludes with a detailed summary of the laboratory equipment and test procedures used within.

Chapters 5 contains the results of the laboratory testing program while Chapter 6 contains the discussions of the test results as they related to the role of physical and chemical processes in the dewatering of CT. Conclusions and recommendations for future research are contained in Chapter 7.

2.0 Literature Review

2.1 Overview of Oil Sands Mining Operation

2.1.1 Oil Sand Deposits

Alberta has three oil sands deposits, which together contain 269 billion m^3 of crude bitumen, but only the Athabasca deposit is economically minable using surface mining techniques. As shown in Figure 2.1, the Athabasca oil sands deposit is located 450 km northeast of Edmonton, near Fort McMurray. The surface minable section of this deposit has proven synthetic crude oil (SCO) reserves of 4.8 billion m^3 (Energy Resources Conservation Board, 1991). Currently, Syncrude Canada Ltd. and Suncor Oil Sands Group are the only two companies mining the deposit. Collectively they produce 72 000 m^3/day of Synthetic Crude Oil or approximately 20 % of Canada's domestic production (Energy Resources Conservation Board, 1991).

Figure 2.2 shows a typical cross section of the Athabasca deposit. The Clearwater formation, a highly smectitic overconsolidated clay, overlies the oil sands and must be stripped prior to exposing the oil sands for mining. The underlying Lower Cretaceous oil bearing sand is largely made up of uniform quartz sand and is approximately 44 m thick. Scattered throughout the oil sands are thin seams to thick beds of silty clay-shale, which contribute heavily to the fines content of the resulting tailings stream. The surface minable portion of the deposit contains an average of 5 % water, 11 % bitumen, 12 % fines and 72 % sand. However, significant deviations are apparent across the deposit, the most critical being the bitumen and fines content.

Insitu, the Athabasca oil sands are water-wet as shown in Figure 2.3. That is, the bitumen is not in direct contact with the mineral grains, but rather it is separated by a thin film of water known as connate water. In the coarse clean

sand, bitumen will occupy 90 % of the void spaces - while the other 10 % will be filled with water. Due to this arrangement of the bitumen and mineral grains, the extraction process of choice has been a modified version of the Clark Hot Water Extraction (CHWE) process.

Upon delivery of the oil sands ore to the CHWE extraction plant, it undergoes bitumen extraction in the following three stages: conditioning, primary extraction and final extraction. In the conditioning stage the ore is mechanically mixed with hot water (80 °C), steam and NaOH to promote bitumen separation. The result of the conditioning stage is a slurry with a solids content of 70 - 85 %, a pH of 8.0 - 8.5 (Camp, 1976) and clay minerals in a dispersed state. Geotechnically speaking, a slurry is defined as a soil-water mixture which displays fluid like characteristics and is pumpable. At the end of the conditioning stage, rocks and solid clay 'balls' are removed and the slurry enters the separation vessels. In the primary separation stage additional hot water is added to further enhance separation and bitumen froth is removed from the top while the coarser fraction settles to the bottom. The remainder of the slurry, known as middlings, is made up of water, unrecovered bitumen and dispersed clay. It is further processed using air flotation to separate the bitumen from the fines. Upon completion of the extraction process, the two mineral streams are recombined and additional water is added to increase the pumping efficiency of the whole tailings stream. For each m^3 of ore that is processed an additional 1.3 m^3 is produced (Camp, 1976).

2.1.2 Tailings Disposal

Since both companies operate under the 'zero discharge' policy, no fine tails or process affected water can be discharged or allowed to migrate to an off site location. Prior to 1995 both companies hydraulically transported and discharged the whole tailings into above grade ponds, which provided containment.

Syncrude's whole tailings stream has an average solids content ranging from 35 to 65 % with a fines content between 8 and 25 % with approximately 1 % residual bitumen (based on dry weight). Figure 2.4, shows the gradation of the whole tailings stream as it enters the containment facilities, along with the clay-shale seams and oil bearing sand layer. The sand fraction consists of a uniform sand containing 1 - 2 % fines, while the clay shale contains particles which are exclusively smaller than 45 μm. As mentioned, following extraction these two mineral streams with significantly different grain size distributions are combined. As a result the whole tailings stream grain size distribution is gap-graded.

Due to its gap-graded characteristics, the untreated whole tailings stream naturally segregates upon disposal. The sand falls out of suspension near the point of discharge while 50 % of the finer fraction with most of the water, also known as thin fine tails, flows towards the center of the pond. The thin fine tails enter the tailings ponds at solids content of approximately 8 % and rapidly releases water for the first two years until it reaches a solids content of approximately 30 % and becomes known as mature fine tails (MFT). During the two year period, the thin fine tails undergo hindered sedimentation followed by consolidation. Beyond two years the dewatering rate of MFT approaches zero as a result of thixotropic strength gain and reduced hydraulic conductivity such that full consolidation of MFT would not occur for hundreds of years. As a result of the water retention characteristics, the ponds contain an enormous volume of water, which must be removed in order to reduce the waste volume. This extremely slow rate of consolidation of MFT is the true concern of the mining companies.

2.1.3 Tailings Management

Dewatering is a necessary but not a straightforward process which must be dealt with in order that Syncrude and Suncor can reclaim each mine site in a manner

which is both environmentally and operationally in agreement with their lease. Presently, between the two companies, there are approximately 400 million m^3 of mature fine tails stored, with predictions that it will reach 1 billion m^3 by the year 2025, if production continues following the same processing technique (Lui et al, 1996). Permanent storage within these ponds is not a final solution to the waste management problem, as the two companies must leave the site in a similar environmental state as when mining commenced.

The two major problems that face the oil sands industry are operational and environmental. First and foremost is the environmental concerns imposed by the toxicity of the porewater. Thus any dewatering or volume reduction technique must find a way to reuse the tailings decant water and upgrade its water quality parameters or it has simply separated the waste in two separate locations. The second problem that the oil sand industry faces is that the ponds, which cover over 30 km^2, are partially situated on top of ore deposits, which could be mined in the future. Permanent storage of the segregating whole tailings is not a final solution as it represents additional costs and long-term environmental risks associated with containment breach.

Currently, their is no single reclamation option that can handle the volumes of fine tails in a manner which is technically, environmentally, and economically acceptable. Instead a combination of the so called "wet" and "dry" landscapes will be employed. The dry landscape involves removal of water from within the fine tails to create a trafficable landform while a wet landscape involves creating wetlands. Whichever method is selected, the final goal is to produce a stable, productive, and self sustaining ecosystem.

2.1.4 Nonsegregating Tailings

As mentioned earlier when describing the deposition of whole tailings, sand rapidly falls out of suspension while the thin fine tailings flow towards the center

of the pond. Determining whether or not a tailings stream will segregate depends on its solids content, gradation of the solid material and the depositional energy. Any material possessing a well sorted grain size distribution and hydraulic deposition is subject to internal instability or suffossion. As defined by Chapuis (1992), suffossion is the migration of fine particles of soil within its own pore water, leaving behind large openings between the remaining larger particles. It is possible to predict whether suffossion occurs, based on the grain size characteristics of the material. Despite these theories, according to Chapuis the mathematical formulations must be used with caution since little information regarding the effect of void ratio, the severity of disturbing forces due to vibration or seepage and initial segregation of the soil. Additionally, these theories do not account for the method or the environment by which deposition occurs. Research by Scott, 2002 has shown that the segregation boundary of CT can be altered by changing the grain size distribution of the tailings.

Figure 2.5 shows the segregation boundary for untreated tailings streams as developed by Scott and Cymerman (1984). Scott et al., (1993) defines nonsegregrating oil sands tailings as mixtures in which at least 90 % of the fines are retained. Figure 2.5 shows that the segregation boundary is distinct and requires only a small change in solids content to change the deposition characteristics of a tailings stream from heterogeneous to homogeneous. Untreated tailings streams which plot above the boundary, will naturally segregate while those plotting below are able to trap and hold the fines within the void spaces of the coarse grained material. From Figure 2.5 it is apparent that the segregation boundary is located at a constant fines-water ratio of approximately 0.28. Also shown in Figure 2.5 are the average tailing streams produced by Syncrude and Suncor. It is apparent that without modification, segregation of the whole tailings will occur naturally.

There are several methods available to change the deposition characteristics of the tailings stream such that it becomes nonsegregating. As seen in Figure 2.5, changing the physical properties of the slurry, by increasing the solids or fines content can produce a mixture, which has a reduced tendency to segregate. Other methods include altering the chemical properties of the pore water (chemical concentration, pH) thereby changing the dewatering characteristics.

2.1.5 Composite Tailings

Research conducted at the University of Alberta has revealed that addition of lime (CaO) or phosphogypsum ($CaSO_4 \cdot 2H_2O$) to a mixture of tailings cyclone underflow and MFT produces a nonsegregating tailings stream known as composite tailings or consolidated tailings (CT). The addition of calcium ions is known to alter the clay structure such that segregation is prevented and the coarse fraction is supported within. The retention of sand within the fines matrix provides an increase in the self-weight of CT and causes the void ratio to decrease from approximately 2 to 1 after only a few days of self-weight consolidation. The clear decant water which flows to the surface of the deposit is collected for re-use in the extraction plant.

In the field, Syncrude takes whole tailings, which come straight from the extraction plant, and pass it through a hydrocylcone to increase its solids content. The whole tailing enters the cyclone at 55 % solids and 15 % fines and cycloning produces an underflow containing 75 % solids and 10.1 % fines. The remaining fines and water are passed out the top of the cyclone and are pumped to South West Sand Storage to undergo hindered settling and consolidation. Syncrude slurries gypsum with gland water (release water from Mildred Lake Settling Basin) to produce a gypsum slurry at approximately 10 % solids. This gypsum slurry is added to the MFT, which is then combined with cyclone

underflow. Gypsum dosages in the field are based on grams of gypsum per m^3 of CT.

To date Syncrude continues to deposit much of their naturally segregating whole tailings stream as it did in the past, without any modifications. However, due to limited space in their ponds, they now deposit the whole tailings in the South West Sand Storage. After the whole tailings segregates the thin fine tails are pumped to MLSB. Syncrude is currently producing their version of nonsegregated tailings known as composite tailings (CT). Since 1996 Suncor has been in full commercial production of a nonsegregating stream known as consolidated tailings (CT).

Please note, further references to CT throughout the remainder of this thesis refers to a nonsegregating tailings stream unless noted otherwise.

2.2 Dissolution Of Gypsum

Addition of gypsum ($CaS0_4$) to pure water will cause the gypsum to dissociate according to the following:

$$CaSO_{4\,(s)} \quad \leftrightarrow \quad Ca^{2+}{}_{(aq)} + SO_4^{2-}{}_{(aq)}$$

Initially, the rate of dissolution of the salt is rapid and slowly tapers off until the concentration of the two ions becomes a maximum. When more gypsum is present in solution than can go into solution the relationship shown above is not static, but is highly dynamic. That is, gypsum is continuously dissolving while at an identical rate, calcium and sulfate ions are colliding to form solid gypsum. The amount of gypsum that will dissolves into pure water is given by its solubility product, K_{sp}, which equals $6.1*10^{-5}$ at 25 °C (Zumdahl, 1989). The rate of gypsum dissolution is a function of its surface area and temperature of the

aqueous medium. All other parameters being equal, elevated temperatures increase the dissolution rate, and vice versa.

2.2.1 Sinks for Gypsum

To understand the role that gypsum plays in the production of CT, it is necessary to identify and understand what sinks exist for gypsum. Calcium ions, which go into solution, can be removed as a result of precipitation with other dissolved inorganics and/or association with the clay surfaces through cation exchange reactions.

The dominant anion in CT tailings water, prior to treatment is bicarbonate (HCO_3^-) and as a result, the tailings water is highly buffered against pH changes. The addition of Ca^{2+} to tailings water causes the precipitation of calcium carbonate. Removal of carbonate from the system causes a shift in the carbonate system such that bicarbonate ion concentration is reduced and favors the production of hydrogen and carbonate. The bicarbonate concentration and pH of the water are directly related. A decrease in the bicarbonate concentration produces a resulting decrease in the pH of the water as hydrogen ions are released. These results were confirmed when the addition of Agricultural Grade Gypsum (AGG) caused the pH of the tailings water to decreased from 8.2 to 7.9 during the 1995 NST Field Demonstration (Shaw, 1996) and also during the laboratory testing performed within.

The second major sink for calcium is its adsorption through cation exchange reactions. Prior to treatment, the surface of the kaolinite minerals is sodium rich as sodium is the preferential ion of choice. After treatment with gypsum, calcium becomes the preferential ion and sodium concentrations in the CT release water are greater than pre-gypsum treatment. Test results by Mikula (1996) showed that approximately 0.05 % calcium (by weight) will be uptaken by a given weight of pure kaolinite in tap water. The net effect of PG dosage which exceeds 0.05

% (by mass) is to reduce the bicarbonate concentration and therefore the pH. The existence of these processes were confirmed during the 1995 field demonstration when only 40 % of the calcium which was added during AGG amendment (dosage 1400 g/m^3) was present in the CT release water. Since calcium ions are conserved, the remaining 60 % of the calcium was "lost" during precipitation with carbonate and exchange with sodium as a result of cation ion exchange.

2.3 Clay-Water Electrolyte System

During commercial and laboratory production of CT, phosphogypsum (PG), agricultural grade gypsum (AGG) or Suncor flue gas desulphurization gypsum is added to a mixture of cyclone underflow and MFT to produce a nonsegregating tailings product. Regardless of the grade of gypsum, it is surmised that the active component which is responsible for changing the tailings stream from segregating to nonsegregating, is the calcium ions (Ca^{2+}). Cations such as calcium are known to alter the surface properties of the clay particles as a result of adsorption and to react with carbonate to form calcite. The interaction of calcium ions with the clay particles either causes a change in the grain size distribution as a result of flocculation (Scott et al., 1993) or produces a stronger floc structure which supports the sand internally and prevents segregation (FTFC, 1995 Vol. III). Beyond preempting segregation, the role of gypsum as it relates to the geotechnical characteristics of CT is not well understood.

The following sections review concepts associated with kaolinite mineralogy, double layer theory, cation exchange, particle approach and flocculation. The following sections discuss issues associated with single individual clay minerals, followed by a discussion on interaction of adjacent clay minerals, which occurs in most clay systems. The purpose of the following sections are to understand what impact gypsum has on the flocculation behavior of clay, the interparticle

forces, the structure and ultimately the dewatering behavior of CT. This review is intended to provide a background so that quantitative changes in settling behavior and hydraulic conductivity along with qualitative changes in fines structure as observed using the SEM can be analyzed to explain changes in the observed behavior of CT.

2.3.1 Clay Mineralogy

Clays are known to be lyophobic or hydrophobic colloids despite the fact that water is adsorbed on the particle surface. According to Mitchell (1993) hydrophobic colloids are liquid separations of small solid particles that are:

- two-phase systems with large interfacial surface area;
- have a behavior dominated by surface forces (rather than gravity); and
- can flocculate in the presence of small amounts of salt.

The clay minerals contained within CT are dominated by kaolinite (80 %) (FTFC, 1995, Vol. I). Other clay minerals include illite (15 %) and montmorillonite and chlorite (Roberts, Yong and Erskine, 1980). Structurally, kaolinites are 1:1 type phyllosilicates while illite and montmorillonite are members of the 2:1 clay family.

A single unit sheet of kaolinite is composed of one aluminum octahedral layer and one silica tetrahedral layer joined together by shared oxygen's, and is approximately $0.7 * 10^{-9}$ m thick (Terzaghi et al., 1996). A kaolinite crystal consists of approximately 70 to 100 single units sheets, which are held together by hydrogen bonds between the hydroxyl of the octahedral sheet and oxygens of the tetrahedral sheet. Since the hydrogen bond is very strong no interlayer swelling occurs. The specific surface area of kaolinite ranges from approximately 10 to 20 m^2/gm. The three possible sources which causes the kaolinite mineral to possess a negative surface charge are; (1) isomorphic substitution of Al^{3+} for Si^{4+} in the silica sheet or a divalent ion for Al^{3+} in the octahedral sheet, (2)

broken bonds near the edges, (3) replacement of hydrogen ions on the exposed hydroxyl by exchangeable cations. Whether or not measurable isomorphous substitution exists within the structure of the kaolinites is uncertain (Mitchell, 1993).

Kaolinite is said to be amphoteric as the sign of the charge on the edge depends on the pH of the environment in which the particle resides. At low pH's, positive charges exist on the edges of the particles, while at high pH's, the edges become negatively charged. Hence, the magnitude of the negative charge deficiency of kaolinite is greater in basic environments than acidic environments. The clays which are sensitive to changes in pH, the pH which cause the surface charge to be electrically neural is termed the isoelectric point of zero point charge (ZPC).

A single unit sheet of illite is composed of one octahedral layer sandwiched between two silica tetrahedral layers, and is approximately $1.0 * 10^{-9}$ m thick. Successive unit sheets of illite are held together by van der Waals forces and potassium ions. The bonding provided by the potassium ions is relatively strong. Isomorphic substitution of aluminum for silicon in the silica sheet causes illite to a have a negative charge. Unlike the kaolinite minerals, the total charge is independent of pH. The surface area of illite ranges from approximately 65 to 100 m^2/gm.

2.3.2 Electric Double Layer Theory

As a result of processes mentioned above, clays possess a residual net negative charge and as a result cations in solution are electrostatically attracted to the face of the clay minerals. The typical approach is to regard the clay particle as colloids having a constant surface charge with a variable surface potential. That is, the magnitude of the residual negative charge is constant, however the magnitude of the electric potential is highest near the surface of the clay and continues to diminish as the distance from the clay particle increases. The

condition of constant surface charge is generally the case providing the pH and both the electrolyte make-up and concentration are held constant. Similarly, the assumption of constant surface charge excludes the effects of complexation reactions with surface functional groups, which are known to alter to total charge. As a result of this negative charge and the aforementioned distribution of electric potential, exchangeable cations are not uniformly distributed throughout the solution phase. Instead, the concentration of cations grades continuously from a high concentration near the clay surface and asymptotically approaches the bulk solution concentration as distance increases from the clay particle. Electrical neutrality dictates that the sum of exchangeable cation charge equals the magnitude of the residual negative charge of the clay particle. The residual negative charge on the clay surface and the swarm of positive counter ions adjacent to the clay surface are together called the electric double layer (Tan, 1991).

Several double layer theories exist to quantify the distribution of charge as a function of distance from the clay particle or its "thickness". The more well known theories include, but are not limited to the Helmhotz, Guoy-Chapman and Stern. The major difference between the Helmholtz and Guoy-Chapman theories is that in Helmholtz theory all charges are balanced by cations which are immediately adjacent to the clay surface. Thus, in the Helmholtz model the potential decreases linearly while the in Gouy-Chapman the decrease of potential is exponential. The remaining Stern theory, considers the actual size of the ions (rather than point charges) and denotes the presence of closely packed layers of counter ions immediately adjacent to the clay surface, known as the Stern Layer while the remainder of the charge is satisfied by ions which make-up of the diffuse double layer. Within the Stern Layer, the potential decreases linearly while beyond it, the potential decreases exponentially. The presence of the

Stern Layer helps to explain selectivity based on cation size, during cation exchange reactions.

Implicit within the Guoy-Chapman theory are the following three assumptions; (1) exchangeable cations exist as point charges, (2) colloidal surfaces are planar and essentially infinite in extent, and (3) surface charge is distributed uniformly over the entire colloid surface. These assumptions inaccurately describe actual systems, yet the Guoy-Chapman theory works surprisingly well for soil colloids as the inherent errors tend to cancel out (Bohn, 1985). Although the Guoy-Chapman theory has been shown to accurately describe the actual distribution of ions only in smectite clays with low monovalent concentrations (Sposito, 1989), it provides a good visual tool and is sufficient for the usage required within. The distribution of ions adjacent to the clay surface is shown schematically in Figure 2.6, according to the Gouy-Chapman theory.

As shown, the distribution of cations is greatest near the clay surface and decreases with increasing distance from the clay surface. Additionally, as a result of the increased number of cations adjacent to the clay surface, there is a deficiency of negatively charged ions (anions) within this region as they are electrostatically repelled.

Although not shown in Figure 2.6, in addition to the distribution of cations adjacent to the its surface, highly polar water molecules have the ability to form strong bonds with the surface of soil particles (Terzaghi et al., 1996). This adsorbed water is a result of the short-range adsorption forces holding one to four molecular layers adjacent to the soil particle. Thus, in general a soil particle is covered by a layer of adsorbed water, which in turn is surrounded by a diffuse double layer, and finally enveloped by free water (or water which is not influenced by the force field of the particle).

2.3.2.1 Influences on Diffuse Double Layer Thickness

The thickness of the diffuse double layer can be calculated using equation 2.1 :

$$\frac{1}{K} = \left(\frac{\varepsilon_o DkT}{2\eta_o e^2 v^2} \right)^{1/2} \qquad 2.1$$

Where:

1/ K = thickness of diffuse double layer

D = dielectric constant of the pore fluid

n_0 = electrolyte concentration

T = Temperature

v = cation valence

k = Boltzmann Constant ($1.38 * 10^{-23}$ J°K^{-1})

e = electric charge ($1.602 * 10^{-19}$ coulombs)

This relationship shows that the thickness varies inversely with the valence and the square root of the electrolyte concentration and directly with the square root of the dielectric constant and temperature, other factors remaining constant (Terzaghi et al., 1996).

For a constant surface charge density, the amount of cations required to satisfy the negative charge is constant. Increasing the electrolyte concentration increases the amount of cations present resulting in a reduction of the concentration gradient between the adsorbed phase and solution phase. This reduces the tendency for cations to diffuse away from the adsorbed phase and results in a compressed double layer.

Using equation 2.1, the distances from the surface to the center of the clay layer (1/K), for a "typical" soil colloid in equilibrium with monovalent and divalent cations with a 0.1 M solution concentration, are approximately 10 to 5

Angstroms, respectively. Similarly, decreasing the solution concentration to 0.001 M causes the thickness in a monovalent and divalent system to be approximately 100 and 50 Angstroms, respectively.

2.4 Cation Exchange Capacity (CEC)

Since clay minerals carry residual negative charge, cations in solution are electrostatically attracted to the surface of the clay. The cation exchange capacity (CEC) of soils is defined as the capacity of soils to adsorb and exchange cations (Tan, 1991). CEC represents the amount of readily exchangeable cations that can be replaced easily by leaching with a solution containing other dissolved cations of higher replacing power than the adsorbed cations (Mitchell, 1993). Readily exchangeable cations are generally held on the edges and surfaces of the clay particles and are easily accessed by the outer solution. In contrast, cations, which are held in interlayer spaces of the 2:1 clays, are generally not readily exchangeable. CEC varies with the nature of the exchangeable ion, salt concentration and pH (Bohn, 1985). However, as mentioned previously, clays are assumed to have a constant surface charge unless significant changes in pH or concentration occur.

CEC is related to surface area and surface charge density of the clay, and can be mathematically expressed by equation 2.2.

$$CEC = S * \sigma \qquad 2.2$$

Where: S = specific charge

σ = surface charge density

The CEC of kaolinite is known to range from 3 to 15 meq/100 grams, while montmorillonite ranges from 80 to 150 meq/100 grams. CEC capacity of kaolinite is made up of the CEC_p which the portion associated with the

permanent charge deficiency (isomorphous substitution) and CEC_v which is the variable charge component (pH dependent).

2.4.1 CEC Reactions

Cation ion exchange is a reversible mass action type of reaction, which occurs on a charge equivalent basis (equivalents). Cation ion exchange occurs when cations from the solution phase are adsorbed and replace all or part of the adsorbed ions to balance the charge deficiency of the clay particle. Not all cations within the solution phase are equally attracted; selectivity is based on valence, relative abundance of the different ion types, and ion size (Mitchell, 1993). Of these factors, valency is generally most important. All other conditions being equal, trivalent ions are held tighter than divalent which are held tighter than monovalent ions. Additionally, smaller cations tend to replace larger cations as they can approach the colloidal surface more closely and thus coulombic attraction is greater.

A typical listing, in increasing order, of those cations which are preferred (from a replacement point of view) is known as a lyotrophic series. A typical lyotrophic series is shown below.

$$Na^+ < Li^+ < K^+ < Rb^+ < Cs^+ < Mg^{2+} < Ca^{2+} < Ba^{2+} < Cu^{2+} < Al^{3+} < Fe^{3+} < Th^{4+}$$

A different lyotrophic series exist for different types of clays and selectivity of ions within a heterogeneous solution phase is temperature dependent (Mitchell, 1993). As a result of a clay particle's selectivity for cations, the ratio of monovalent, divalent and trivalent cations will be different in the adsorbed phase than the solution phase. As demonstrated by the lyotrophic series, the ratio of divalent to monovalent cations will be much higher in the adsorbed phase than the solution phase as divalent cations are preferred.

2.4.2 Ion Exchange Equilibrium

Predicting the equilibrium concentrations of ions in the solution phase and adsorbed phase is possible. Several theories including the Vanselow, Davis, Erickson, Gapon and Donnan exist to quantify cation exchange relationships. The primary difference between these theories is their differing treatment of the activities of the exchangeable cations. The Gapon equation has been shown to work reasonably well and is also simpler than most. For these reasons, it is the only theory presented within.

The Gapon equation, Equation 2.3, relates the composition of the solution phase to the composition of the adsorbed phase for a solution containing both monovalent and divalent cations.

$$\frac{[Na-X]}{[Ca-X]+[Mg-X]} = K_G \frac{[Na^+]}{\sqrt{[Ca^{2+}+Mg^{2+}]}} \qquad 2.3$$

In the above equation, the terms of the left hand side of the equation which are denoted with "- X", refer to ions that have been adsorbed by the clay and are expressed in terms of me/100g. The right hand side of the equation 2.3, represents soluble-cations concentration (not activities) expressed in terms of mmoles/L. Each side of the equation presents a ratio of the amount of monovalent to divalent ions. K_G is the Gapon exchange coefficient, which relates the solution phase to the adsorbed. Alternately, equation 2.3 can be written in the following form,

$$ESR = K_G \times SAR \qquad 2.4$$

Where SAR = sodium adsorption ratio (water quality parameter)
ESR = exchangeable sodium ratio
K_G = Gapon exchange coefficient

For practical applications, K_G equals 0.015 for Western Canadian clay with SAR < 30 (Dudas, 1996). K_G is constant over a limited range of cation ratios and has its own value for each pair of cations. As shown in equations 2.3 and 2.4, the ratio of monovalent to divalent cations is lower in the adsorbed phase than in the solution phase, as clay minerals are selective. However, when considering changes in the equilibrium position of equation 2.3, it is the ratio of the right hand side which is important not their individual concentrations.

2.4.3 Cation Exchange Rate

Cation exchange rates vary according to clay type, solution concentration and temperature. The actual exchange reaction itself is virtually instantaneous, however in natural field conditions a rate limiting process may be induced by tortuous paths, or thick water films, or the physical location of the exchange site. In the laboratory setting, shaking and stirring help to minimize time related effects. Exchange reactions in the kaolin minerals are almost instantaneous, while in illites a few hours may be needed as a small portion of the exchange sites may be situated between unit layers (Mitchell, 1993). Cation ion exchange rates are unlike real chemical reactions rates, they decrease as temperature increases (Tan, 1991). Adsorption occurs less rapidly at elevated temperatures because increased kinetic energy of the molecules at elevated temperatures interferes with concentrating constituents at the clay surface (Tan, 1991).

Other factors including complimentary cation effect, valency dilution effect, anion effect are known to alter CEC but have not been discussed within.

2.4.4 Interaction of Adjacent Double Layers

The presence of single, clay particles acting independently is not representative of the actual conditions in most clay systems. The likelihood that adjacent particles and their associated double layers will interact depends on the moisture

content of the soil and thickness of the double layer. As a result of Brownian motion particles collide frequently and their diffuse double layers will interact. However, the net result of interaction is dependent on the balance of repulsive and attractive forces that are present. The following sections summarize the short and long-range repulsive and attractive forces that are present. Ultimately, the net result of these repulsive and attractive forces determine whether a suspension will be colloidally stable or unstable.

2.4.4.1 Short and Long Range Repulsive Forces

Two types of short-range forces of repulsion are generated when particles are brought sufficiently close to one another. One, the Born electrostatic repulsion, becomes effective as soon as extruding lattice points come into contact; it resists the interpenetration of the crystal lattices (van Olphen, 1963) and results from the overlap between electron clouds. The second short range repulsive forces are a result of the layers of molecular water, which are adsorbed to the particle surface. In order for particles to get closer than the thickness of the absorbed water layers, work is required to desorb the water. The work required for desorption manifests itself as a short-range repulsion (solvation repulsion) and may as much as 400 MPa to remove one monolayer of water (van Olphen, 1963).

Long-range electrostatic repulsive forces are a result of the interaction of the diffuse double layers. The range and effectiveness of the long range repulsive forces depend on the thickness of the diffuse double layer, as the magnitude of this repulsive forces decreases exponentially with increasing distance from the particle. As discussed in Section 2.2.2, the thickness of the double layer depends on cation valency, electrolyte concentration and dielectric properties of the pore fluid.

2.4.4.2 Long Range Attractive Forces

In a clay system, when particle edges and surfaces have opposite charge, an electrostatic attraction will be present, between the negative diffuse layer adjacent to the face and positive charged particle edges. The magnitude of this force is dependent on charge deficiency and the distance separating the charges.

The other long-range attractive forces are van der Waals forces. These interparticle attractive forces are electromagnetic in nature and only effective at very close distances and decay rapidly as the distance between two atoms increases. These attractive forces are additive and proportional to the sum of all attractive forces between every atom of one particle and every atom of the other particle. This summation of charge leads to larger attractive force that decays less rapidly with distance. The phenomenon of flocculation demonstrates the existence of interparticle attractive forces (van Olphen, 1963). van der Waals forces are practically independent of electrolyte concentration and are therefore considered equally effective in all environments.

Other sources of interparticle attractive forces including capillary stresses and cementation, are not discussed.

2.4.4.3 Net Particle Interaction

The net interaction of the repulsive and attractive forces determines whether a suspension will be colloidally stable (dispersed) or colloidally unstable (flocculated). If the net result of attractive and repulsive forces between clay particles is attractive, the particles will tend to become attached to one another - flocculated. If the net force is negative they tend to remain apart - dispersed. A thick diffuse double layer prevents adjacent clay particles from approaching close enough for van der Waals attractive forces from dominating and causing a net

agglomeration between adjacent particles. The amount of additional energy require to overcome double layer repulsion is proportional to the thickness of the diffuse double layer. At high electrolyte concentrations repulsive forces are at a minimum and flocculation occurs very fast, while at low electrolyte concentrations long-range repulsive forces tend to retard the process.

The combined effects of surface force attractions and small particle size, create a wide variety of interparticle attractive and repulsive forces. The net result of these forces influences the flocculation behavior and development of soil fabric, which in turn impacts the compressibility and hydraulic conductivity of suspensions.

2.4.5 Factors Determining Floc and Aggregate Size

Within a flocculated suspension, the basic units are not primary particles, but are small clusters of particles (plus enclosed water) which are known as flocs. In low shear rate environments, flocs group together into clusters of flocs, known as aggregates. The previous discussion on particle approach was based on the particle approach under controlled conditions or in low shear environments.

The size of the aggregates is not a fundamental property of a flocculated suspension, but is a dynamic property, which depends upon the rate at which aggregates grow by collision and are broken down by shear forces (Michaels and Bolger, 1962). The rate of formation depends on the number of collisions occurring and the surface characteristics of the particles involved. The number of collision increases with concentration and agitation, while the surface characteristics of the particles, depends on the particle type and surrounding chemical environment.

Michaels and Bolger (1962) found that dilute suspensions experienced higher settling rates when they were prepared by blending the suspension, rather than

mixing the suspension by inversion. They also found that strong mixing produced large aggregates and also increased the overall spread in aggregate size. Reich and Robert (1957) found that average floc size increased with increasing concentration and with decreasing speed of agitation. The nature and duration of the shear forces involved in mixing and agitation can have an important effect on sediment structure (Tiller and Khatib, 1984).

2.4.5.1 Soil Fabric

The term fabric refers to the arrangement of the particle, particle groups and pore spaces in a soil (Mitchell, 1993), whereas structure refers to the combined effects of fabric, composition and interparticle forces including soil composition, history, present state and environmental conditions. Two soils can have the same fabric but exhibit different engineering behavior if the forces between the particles and particle groups are not the same.

2.4.5.1.1 Soil Fabric as it Relates to Compressibility

Conditions which favor aggregation or flocculation of individual clay particles tend to produce larger clusters, than deflocculated dispersive environments. Under natural sedimentation a flocculated suspension will form a looser array of particles with a correspondingly higher void ratio than a deflocculated suspension. The phenomena is further explained by van Olphen (1977) who reasons that in a deflocculated suspension when the particles settle individually, once they begin to crowd in the lower portion of the vessel, the particles will tend to slide and roll along each other, since they repel each other. As a result they are able to reach the lowest possible position and become arranged in a close-packed fashion. However, in a flocculated suspension, the haphazardly formed loose flocs will settle and will pile up at the bottom as voluminous sediment. This voluminous sediment will exist as long as the particles are not so

big that the gravity forces can break the links between the particles (Clay Colloid Chemistry, 1977). Mitchell (1993) indicates that once the maximum precompression stress has been reached, a further increment of pressure causes a greater change in fabric of a flocculated soil structure than in a deflocculated soil structure as a flocculated soil is more compressible.

The principle of chemical irreversibility of clay fabric (Bennett and Hurlbut, 1986) generally applies to fine grained soil. It recognizes that the chemical environment is critical during the initial stages of fabric formation of sediment in water. But beyond initial flocculation, the chemistry is less important in influencing fabric changes as mechanical energy rather than chemical energy dominates. According to Leroueil and Vaughan (1990) fabric is as important in determining the engineering behavior as are the effects of initial porosity and stress-history, which are two basic concepts of soil mechanics.

Research by Scott has shown that the origin of the card house structure seen in SEMs of CT is a result of the extraction process and is not an artifact of flash freezing the sample. Furthermore, his research has shown that it is the presence of bicarbonate, which comes from the oil sands connate water and adsorption from the air at elevated pH of the extraction process, is responsible for the card house structure and not sodium hydroxide which is added during extraction.

2.4.5.1.2 Soil Fabric as it Relates to Hydraulic Conductivity.

The three types of soil fabric are microfabric, minifabric and macrofabric. The microfabric consists of the actual cluster and the intercluster void ratio while the assemblage of the these clusters make up the minifabric. Very little flow will occur as a result of microfabric, while flow through the minifabric will be much greater. Macrofabric consist of cracks, fissure, laminations, or root holes through

which the flow rate can be so great that flow contributions for the other two become negligible.

Olsen (1962) proposed the cluster model to describe the variation of the hydraulic conductivity of fine-grained soils as a function of void ratio. According to Olsen (1962) the total void ratio (e_t) is made up of the sum of the intercluster voids and the intercluster void space. The size of the clusters depends on mineralogy and characteristics of the pore fluids. For soils with the same void ratio the sample which is in the most flocculated state will have the highest permeability, while the sample with the most dispersed state will have the minimum permeability. Soils, which have a dispersed structure, will have particles that are more parallel and thus the flow path is more tortuous. However, the major difference is that the flocculated soil will have some large channels available for flow. Since flow through one large channel will be much greater than flow through a number of small channels having the same total channel area as the one large channel, it is readily apparent that the larger a channel for a given void volume, the higher the permeability (Lambe and Whitman, 1969). The fabric component of structure is one of the most important soil characteristics influencing permeability, especially for fine-grained soils (Lambe and Whitman, 1969).

2.4.6 Effect of Cation Exchange on Void Ratio – Effective Stress Relationship

The structure of a soil is composed of a fabric and interparticle force system that reflects all facets of the soil composition, history, present state and environment (Mitchell, 1993). Due to variety of interparticle forces and soil fabric the number of soil structures that can result are limitless. Structure can account for differences between the actual void ratio and effective stress of a soil and the corresponding void ratio for the same soil in the destructured stated. The

difference between the void ratio under a constant level of effective stress for a soil with some structure, and the void ratio for completely destructured soil are shown in Figure 2.7. The upper void ratio boundary corresponds to a fully structured soil, while the lower boundary corresponds to a fully destructured soil. Fine-grained soils, which have flocculated and undergone sedimentation will tend to have some degree of edge-to-edge and edge-to-face associations. As a result of this fabric the soil is said to be metastable as it can carry effective stresses at void ratios higher than would be possible if the fabric was lost or removed. The result is that metastable fabrics cause the consolidation curve not to be unique as soils with structure will plot above the curve for a fully destructured material (Mitchell, 1993).

Figure 2.8 shows results obtained by Swaify et al. (1967) in which the volume of free liquid (related to water content) versus increasing electrolyte concentration for montmorillonite, vermiculite and kaolinite (< 0.2 um) at equilibrium pressures ranging from 0.1 to 10 atm. From Figure 2.8, both the theoretical and experimental test results demonstrate for a given clay type and constant equilibrium pressure, the water content decreases as the concentration of electrolyte is increased. Swaify et al. (1967) notes that the magnitude of effect of increasing electrolyte concentration varies according to equilibrium pressure, cation saturation and clay mineral species. At lower equilibrium pressures, all three clay-water systems are more sensitive to electrolyte changes, whereas at high pressure, the effect of increasing electrolyte concentration was small, or none existent. Also at lower equilibrium pressures, increasing electrolyte strength has a greater effect in montmorillonite than vermiculite, which in turn is greater than kaolinite. Finally, at higher electrolyte concentrations (cation saturation), the difference in the water retention behavior of the three clay types are reduced. This indicates, that as the flocculation status of the clay is approached, the physical behaviors become similar.

Figure 2.9 shows additional test results from Swaify et al. (1967) that demonstrate the experimental relationship between water retention behavior of montmorillonite as a function of ionic composition for various equilibrium pressures and electrolyte concentration. From the figure it is apparent that for a constant equilibrium pressure and electrolyte strength less water is retained (lower water content) as the ionic composition is increased from 0 to 100 % calcium. The experimental relationships shown in Figure 2.9 are near linear and do not show a threshold value or abrupt or sudden change in water retention behavior. These test results emphasize that the water content for a given pressure depends on the proportion of monovalent to divalent cations which are absorbed. Lastly the changes shown in Figure 2.9, indicate that the effects of electrolyte makeup are most critical at low equilibrium pressure and low electrolyte concentration.

Figure 2.10 shows the theoretical and experimental relationship between void ratio and equilibrium pressure for montmorillonite (< 0.2 μm) in equilibrium with 10^{-3} molar solutions of sodium and calcium chloride (from Bolt, 1956). As shown, as the equilibrium pressure increases the void ratio decreases for both the experimental and theoretical curves for both sodium and calcium rich electrolyte solutions. These results confirm the effect of a higher valency cations such as calcium versus that of sodium, is a lower void ratio for any given pressure. Also noted, is that for a given applied pressure the theoretical void ratio is lower than that which was directly measured from the test specimens. See Section 2.5.3.1.3 for calculation of the theoretical relationship between void ratio and effective stress including effects of electrolyte type and strength.

2.4.6.1 Effect of Cation Exchange on Hydraulic Conductivity

According to Chen et al. (1983) the three major mechanisms that result in the decrease of hydraulic conductivity as a result of exchange reactions are; swelling,

dispersion and clay migration. Swelling decreases the size of the large pores in the soil, while dispersion of clay particles is related to particles moving further apart from one another as the repulsive forces are increased and results in particles moving and blocking channels within the soil. Shainberg and Caiserman (1971) suggest that at low ESP < 15 to 20 the main factor in reducing hydraulic conductivity is clay migration and not dispersion and swelling. However, test results by Chen and Banin (1975) on a clayey sand and sand clay show that swelling occurred even at low SAR values because the electrolyte concentration was low. Chen and Banin (1975) further distinguish short range and long-range migration. Short range migration is a result of clay particle rearrangement following aggregate destruction and results in the pore-size reduction, whereas downward movement of clays, which often needs to the formation of an impeded layer, is considered as long range migration.

2.4.6.2 Effect of Cation Exchange on Structure

The effects of exchangeable cations on the hydraulic conductivity with particular emphasis on the deleterious effects of sodium versus calcium are well documented. Within the literature numerous test results on the effect of decreasing SAR and its effect on hydraulic conductivity were found and often accompanied with SEM images. However, due to the somewhat unique natural of oil sands tailings, little information was found on soils with 62 % solids and 20 % fines.

SEM images of sandy clay (55 % clay [55-60 % smectites, 20 to 25 % kaolinite] and 26 % Sand) by Chen and Banin (1975) show that a low SAR treatments, the fines material is either concentrated in large aggregates or adhered to the sand particles, creating large voids which enable a comparatively high hydraulic conductivity. In higher SAR environments, the fine material is much more dispersed and detached from the sand particles, resulting in a continuous

network of dispersed fine particles within the voids between sand grains and a reduced hydraulic conductivity. They concluded that the modification of the pore shape and reduction of the pore size, resulting from local rearrangement as a result of increased repulsion increased the resistance of the soil structure to water flow.

2.5 Behavior of a Clay-Water System

Sedimentation and consolidation of a mineral-water suspension are two fundamentally different processes which both result in a reduction of void ratio with time. Geotechnically speaking, sedimentation and consolidation can be distinguished based on the absence or presence of effective stresses. Sedimentation occurs in clay-water suspensions when the void ratio is sufficiently high that soil-like conditions are absent and the suspension behaves like a fluid and its behavior is governed by sedimentation theory. During sedimentation the void ratio decreases until a soil like structure has been formed and effective stresses begin to manifest themselves. Once effective stresses are present the suspension transitions to a "soil" and its behavior is governed by the theory of consolidation

2.5.1 Settling Behavior Type

According to Imai (1980) four different settling types have been observed for clay-water systems, they include; dispersed free settling, flocculated settling, hindered settling, and consolidation. Dispersed free settling occurs when both the solids concentration and salt concentration of the supernatant water is low, and the soil particles settle as individuals (Stokian settling). Flocculated settling occurs when the solids concentration is low but the salt concentration is high. Under these conditions the soil particles flocculate into flocs, which then settle freely. The third type of settling behavior is zone settling or hindered settling

(Kynch, 1952) which occurs when the solids concentration is greater than in flocculated free settling and flocs settle together forming a sharp slurry-water interface. Finally, consolidated settling is observed under conditions of high solids concentration and independent of salt concentration. For each of the four aforementioned settling types, determination of how a slurry will behave depends on its solids content and salt concentration.

Previous test results (Caughill (1992)and Scott (1993)) on CT have shown that CT exhibits settling behavior consistent with hindered settling and consolidation. For this reason, dispersed free settling and flocculated free settling will not be discussed further in detail.

2.5.2 Hindered Settling Theory

The theory of hindered settling was first introduced by Kynch (1952), in which the downward velocity of a particle depended only the local concentration of the particles in its immediate neighborhood. His theory of hindered sedimentation was based on batch settling of uniformly dispersed particles, which form a sharp interface between the slurry and supernatant fluid. McRoberts and Nixon (1976) advanced Kynch's theory to include the effects of consolidation of fine grained (and subsequent observation of a change from a linear settling rate to some other rate) and relaxed the requirement of uniform particles assuming the suspension does not segregate. Additionally, they redefined the concentration in terms of the weight of particles in a given volume as follows:

$$c = G_s (1-n) \gamma_w \qquad 2.5$$

where: n = porosity

G_s = specific gravity of solids

γ_w = unit weight of water (g/cm^3)

By considering two horizontal layers within a slurry, the accumulation of particles of between the layers is the difference between the flow of particles in through the upper layer and the flow out through the lower layer. From this statement of continuity, the governing equation for hindered sedimentation becomes:

$$\frac{\partial \rho}{\partial t} + V(\rho)\frac{\partial \rho}{\partial x} = 0 \qquad 2.6$$

where: $V(\rho) = -\frac{dS}{dc}$

Since no effective stresses are present during hindered sedimentation, Darcy's Law (v=ki) can be used to determine the hydraulic conductivity based on the behavior of the soil/water interface. Since the pore water pressure is equal to the total stress, the hydraulic gradient is unity. Therefore, the velocity of the slurry interface is equivalent to the hydraulic conductivity of the soil.

2.5.2.1 Stages of Hindered Settling

According to Imai (1980), hindered settling is generally divided into three stages as shown in Figure 2.11; flocculation, settling and consolidation.

2.5.2.1.1 Flocculation or Induction Stage

Imai (1980), Fitch (1966), Guadin et al. (1964), Thomas (1963), Mitchell (1960), Coe and Clevenger (1916) identify a flocculation or induction stage. They describe it as a period of the time when the interface is static, and floc formation takes place. Laboratory results by Imai (1981) on kaolin with a 9.0 % solids concentration, prepared with salt water, reveal that during an eight minute flocculation stage the solids content in the 21.5 cm standpipe was uniform throughout.

Others including Michaels and Bolger (1962), Shannon and Tory (1965) and Scott (1968) report that during the induction stage, the slurry is undergoing the gradual formation of the optimum shape of flow channel between flocs. As settling proceeds, the aggregates tend to coalesce and line up into vertical rows, contraction and sharp bends are smoothed out, and the flow path straightens out. As a result the settling rate increases to a maximum as shown in Figure 2.12, by curve 'b'.

This acceleration of the interface only occurs if the diameter of the standpipe exceeds the "yield diameter" and the height of the standpipe exceeds the "yield height". Michaels and Bolger (1952) provide equations necessary to determine the yield diameter and yield height for a given slurry and standpipe. Failure to meet these two criteria results in the interface subsiding at an ever decreasing rate as shown by curve 'c' in Figure 2.12.

According to Scott (1968) the induction period results in the formation of preferential flow paths which have their origin in the interfloc void and development of these flow paths takes time and a sufficient quantity of fluid flow. The size of these flow paths is sufficiently small that they do not appear as macro-volcanoes and hence the interface appears homogeneous. Channeling or channel formation can be expected to be favored in tall cylinders (Guadin et al. (1964), Michaels and Bolger (1962) and Coe and Clevenger (1917)). Tests by Scott (1968) have shown that slow stirring (1/2 rev/min) of a suspension is sufficient to prevent the acceleration of the interface. Tests results from two identical suspensions, demonstrated that the interface settling rate of the stirred suspension was linear and did not experience the acceleration that occurred in the suspension, which was not stirred. Similar duplicate testing in dilute slurries caused no change in the settlement behavior, providing evidence that the stirring

did not prevent sedimentation of the free settling flocs and its effects were limited to prevention of channel development.

2.5.2.1.2 Settling Stage

Once the suspension has equilibrated with respect to floc formation or channel development, the permeability of the slurry abruptly increases and the settling begins. During settling, two distinct zones develop concurrently within the deposit. In the upper portion of the deposit, a hindered settling zone develops while in the lower portion a consolidation zone develops. Graphically this was shown in Figure 2.11, where a nonlinear sediment formation line, separates the two aforementioned zones. The sediment formation line separates the upper zone where effective stresses are not present and the lower zone where effective stress are present. The sediment formation line or effective stress wave moves upwards from the base and separates a fluid-like suspension (upper portion) from a traditional soil capable of resisting applied shear stresses (lower portion). Imai (1981) rationalizes the convex shape of the sediment formation line, is a result of the uniform settling taking place above the consolidation zone while at the same time water is being released from the portion undergoing consolidation. He argues that the rate of volume decrease of the underlying consolidation zone provides an increasing contribution from the growing consolidating layer.

Initially, the hindered settling zone dominates the deposit but ultimately vanishes once the effective stress wave has traveled up the entire standpipe and intersects the slurry-water interface. This transitional point between the settling stage and consolidation stage is referred to as the critical settling point (Coe and Clevender, 1951) or the soil formation void ratio, e_m, (Pane and Shiffman, 1997). The soil forming void ratio may be regarded as a fundamental material property of a given clay-water mixture for a given set of chemical and environmental

conditions (Pane and Shiffman, 1997). Beyond this transitional point or e_m, water is expelled via self-weight consolidation.

2.5.2.1.3 Solids Content of Hindered Settling Zone

There appears to some debate in the literature as to the behavior of the upper portion of the deposit experiencing hindered sedimentation. Gaudin and Fuestenau (1960) have proved, using x-ray transviewer data, that during the settling stage, the solid content of the zone above the sediment formation line is constant and equal to the initial solids content. Imai (1980) shows an increase in the solids content of this same zone, as a result of supernatant water released by the self-weight consolidation of the material below the sediment formation line. He argues that an increasing volume of water passes through the hindered settling zone as a result of an increase in the height of the consolidating layer. Since the height of the hindered settling zone decreases, the seepage force increase causing the solids content in the upper zone to increase.

2.5.3 Consolidation Settling Theory

Consolidation is the time dependent reduction in void ratio as a result of a change in effective stress. The process of consolidation continues until the excess pore pressures, which are a direct result of a change in total stress, are completely dissipated. The magnitude of the total settlement is related to the compressibility characteristics of the soil, while the rate is dominated by the hydraulic conductivity.

Suspensions which have transitioned from sedimentation, by definition will enter the consolidation phase with the total stress equal to the pore pressure. The magnitude of the total stress and pore pressure are directly related to the weight of the soil. Under these conditions it is the self-weight of the soil, which drives the process. The theory of self-weight consolidation is very well understood and

can be found in any intermediate soil mechanics textbook and will not be presented herein.

2.5.3.1 General Discussion on Soil Compressibility

Changes in volume are caused by changes in applied stress, chemical and moisture environments and temperature (Mitchell, pg. 293). Changes in stress are generally most important and have been studied in detail compared with the others. In general, the compressibility characteristics of a soil are dependent on physical interactions, physicochemical interactions, chemical and organic environment, mineralogical details, fabric and structure, stress history, temperature, pore water chemistry and stress path (Mitchell, 1993). Additionally, there is a direct link between compressibility and natural water content, as they are both influenced by material composition (particle size) and structure. Both theses two factors influence the void ratio at which a soil will equilibrate and also its compressibility after the soil structure begins to yield.

The compressibility, in increasing order, of the clay minerals is kaolinite < illite < montmorillonite (Mitchell, 1993). The effect of structure in fine grained soils, manifests itself by influencing the arrangement of the particles and interparticle forces. Factors such a flocculation and interparticle bonding, which allow a soil to come into equilibrium at high void ratios, lead to high compression indexes beyond the preconsolidation pressures (Terzaghi et al.,1996). Regardless of the effects of mineralogy and structure, the compression index (Cc) of all soils typically decreases as the void ratio decreases.

Compression index (Cc), is defined as the change in void ratio per 10 fold increase in effective stress. Values of compression index below 0.2 are considered to represent soils of low compressibility, values between 0.2 to 0.4 are for soils of moderate to intermediate compressibility, while compression

indexes beyond 0.4 are highly compressible. The compression index for kaolinite ranges from approximately 0.19 to 0.28, while montmorillonite ranges from 1.0 to 2.6. However, as mentioned earlier the effects of physicochemical interactions, structure and pore water chemistry will alter the overall compressibility of a soil.

2.5.3.1.1 Inclusion of Interparticle Forces to Effective Stress

Section 2.3.2 described several attractive and repulsive intergranular forces that can exist in a given soil environment. Quantitative expression of the interaction of these forces in a soil is beyond the present state of knowledge (Mitchell, 1993). However, a simplified consideration of the intergranular forces can be incorporated into the classic effective stress relationship for saturated soil. The classic definition of effective stress (σ'_n), is the difference between the total applied stress (σ_n) and the pore water pressure (u), and can be modified as follows to account for interparticle or physico-chemical forces.

The average interparticle conditions for a fully saturated clay system can be schematically shown in Figure 13. In this figure, "A" denotes the component of effective due to the summation of the attractive interparticle forces, while "R" denotes the component of effective stress due to the summation of repulsive interparticle forces.

Research by Morgenstern et al., 1989 demonstrated that the classic effective stress equation was inadequate in explaining volume change and shear strength characteristics of an active clay-water system as it excludes the net physico-chemical forces of interaction which are present in such systems. Morgenstern's tests indicated that the volume change and residual shear strength characteristics of a Na-montmorillonite are essentially governed by the true effective stress which is defined as the difference between the total stress and

the summation of pore water pressure and the net physico-chemical forces of repulsion and attraction (R-A). Incorporation of the these two additional components to effective stress, leads to the following definition of the true effective stress

$$\sigma_n^* = \sigma_n - u_w - (R\text{-}A) \qquad 2.7$$

where: σ_n^* = true effective stress
σ_n = total normal stress
u_w = pore pressure
(R-A) = net interparticle stress due to physico-chemical environment

The net (R-A) stress is a function of water content, pore fluid salt content and temperature, which arise from a net charge deficiency in the lattice structure, a high specific surface area and the chemical environment. All other parameters being equal, a higher salt concentration reduces the (R-A) term and results in an increase in effective stress.

2.5.3.1.2 Factors Affecting the Interparticle Pressure

The long-range repulsive forces, which are generated when two double layers interact can be quantified using either the osmotic pressure concept or the water adsorption theory. Of these two theories, the osmotic pressure theory is convenient and most widely used (Mitchell, 1993) and for this reason is the only one presented within. The osmotic theory is based on the presence of the semi permeable membrane, which separates two solutions of unequal electrolyte concentration. Since the semi permeable membrane does not permit the passage of solute, the natural tendency for the concentration difference to be equalized occurs when the solvent passes through the semi permeable membrane. Without external changes, the solvent flow would continue from the

low concentration solution to the high concentration solution, until the electrolyte concentrations are equal. The external pressure, which if applied to the side with the high electrolyte concentration, that would stop the flow of solvent, is termed the osmotic pressure and it can be calculated using van't Hoff's equation. In this equation, the osmotic pressure difference between two solutions separated by a semi-permeable membrane is directly proportional to the concentration difference.

In soils, the presence of a semi permeable membrane is introduced by the influence of the negative clay surface, which results in adsorbed cations (which are not free to diffuse). Although the osmotic pressure within the double layer decreases continuously with distance from the solid surface, it can be proven that the effective osmotic pressure of the system is determined by the concentration of the ions in the central plane. The difference in osmotic pressure between the central plane cation concentration and the equilibrium solution concentration is the interparticle repulsive pressure or swelling pressure.

$$P_s = RT \Sigma (C_{ic} - C_{io}) \qquad 2.8$$

where C_{ic} = midplane cation concentration

C_{io} = equilibrium solution concentration

2.5.3.1.3 Quantifying the Interparticle Pressure

According to Bolt (1956), in order to calculate the interparticle pressure, three relationships are needed:

(1) The actual ion distribution in the double layer.
(2) The swelling pressure as determined as the difference between the osmotic pressure in the central plane and the osmotic pressure in the bulk solution.

(3) The distance between adjacent clay particles

The first two relationships were discussed previously, while the last relationship is a function of the void ratio (e) and the specific surface area of the clay. The distance (d) between adjacent clay particles in a saturated system can be determined as;

$$d = w / A_s \qquad 2.9$$

where w = geotechnical water content as defined in equation 3.3.19.1

A_s = Specific surface (m^2/gm)

Bolt (1956) combined the above three relationships, and tabulated the swelling pressure of a pure clay system as a function of the distance variable (in terms of void ratio) for homoionic solutions. For a given soil, the swelling pressure depends on the relative difference between the concentration within the adsorbed layer and the free solution phase and the distance between adjacent particles (void ratio). Solutions with low valency, low concentration, or low void ratio cause high interparticle repulsion, high interparticle pressures and large physicochemical resistance to compression.

2.5.3.1.4 Application of the Osmotic Pressure Theory

A reasonably clear understanding of the how well the osmotic pressure concept can account for the compression and swelling behavior of fine-grained soils has been developed. (Mitchell, 1993). Numerous laboratory experiments have been conducted to compare the experimental and theoretical relationships between void ratio and pressure as a function of electrolyte concentration and/or type. In general, these tests have been performed using ideal pure clays in equilibrium with homoionic solutions (only one ion present).

2.5.3.1.5 Physico-Chemical Effects

Morgenstern et al (R-A) compared the residual shear strength of five Na-montmorillonite samples before and after leaching with distilled water. Five samples in equilibrium with 33.6 gms/liter of NaCl were consolidated to effective stresses ranging from 17.2 and 103.4 kPa and sheared along a precut plane until the residual shear strength was achieved. Following shearing, the five specimens were leached with distilled water, during which time no volume change was permitted. As a result of the removal of sodium ions, each sample attempted to swell and the corresponding pressure was recorded with the load cells as no volume change was permitted. The increased load due to leaching (physico-chemical change) is the net (R-A) term as discussed in the previous section. After each sample reached equilibrium and no longer had swelling tendencies, the final stress value recorded on the load cells at the end of leaching were applied. Each sample was resheared in the same manner as before, until the residual shear strength was reached. Test results indicated the residual shear strength of the montmorillonite was independent of pore fluid chemistry and is governed by the true effective stress of the system and not the apparent effective stress. Previous results by Kenney (1967) were also reinterpreted by Morgenstern et al. (1989) and these also supported that the residual friction angle calculated in terms of the true effective stress is independent of the pore fluid chemistry.

During the previous mentioned leaching process, the measured change in (R-A) was compared to the theoretical value calculated using the double-layer repulsive stress equation (Bolt, 1956) as discussed in the osmotic pressure concept above. Water content as function of the measured and theoretical values of (R-A) are shown in Figure 2.14. From the figure, it is apparent the measured values of R-A are closely approximated by the double-layer repulsive stress equation providing the surface area of the minerals can be estimated. Also, the magnitude of the

(R-A) pressure varied from approximately 130 kPa to over 300 kPa as the water content decreased from approximately 230 % to 150 %. Conceptually, this make sense as the repulsive force increases as a decrease in water content brings adjacent particles close together, resulting in more double layer interaction and an increase in repulsion. The effect of changes in the pore water chemistry is to change the net (R-A) effective stress and thus bring about a change in the true effective stress and ultimately volume.

2.5.3.2 Measurement of Hydraulic Conductivity

Hydraulic conductivity can be measured in the laboratory using either indirect or direct measurement techniques. The reader is deferred to Suthaker, 1995 to a series of discussions on the limitations, advantages, and disadvantages of several methods for direct determination of hydraulic conductivity in the laboratory. The test procedures to directly measure the hydraulic conductivity within were based on the aforementioned discussions.

2.5.3.2 Hydraulic Conductivity Measurements at High Void Ratios

The transition from hindered settling to consolidation occurs at a void ratio, known as the soil-formation void ratio (e_m). There exists a range of void ratio below e_m in which the direct determination of k by means of standard techniques encounters serious difficulties; among these, the highly non uniform distribution of the void ratio within the sample due to its self-weight, and the necessity of imposing extremely low gradients to minimize the effects of seepage induced consolidation (Pane and Shiffman, 1997). At sufficiently low void ratios, direct measurement of hydraulic conductivity can be made using traditional geotechnical laboratory techniques, while above e_m sedimentation tests provide adequate means to determine the hydraulic conductivity. Other authors including Michaels and Bolger (1962) and Been and Sills (1981) define this region

as a transitional or 'intermediate' behavior between suspensions and soils, where channeling and fabric changes can seriously affect the interpretation of the results.

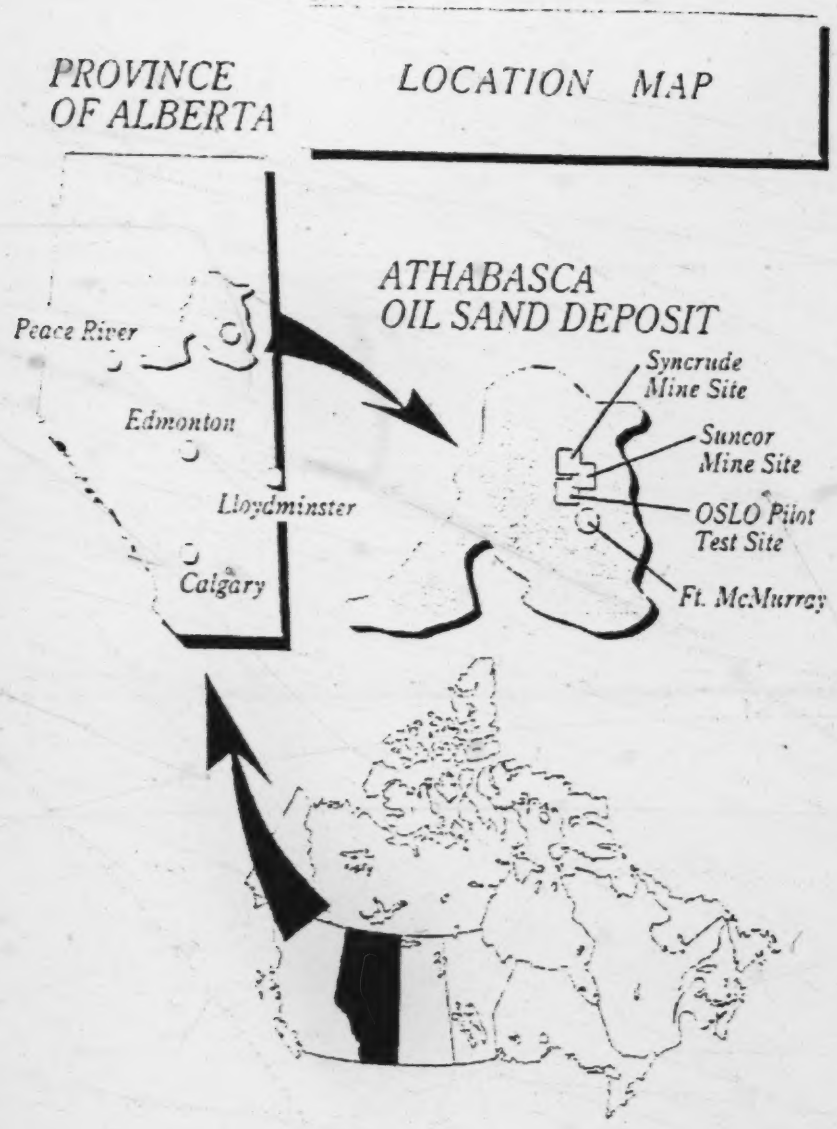

Figure 2.1 Athabasca oil sands deposit

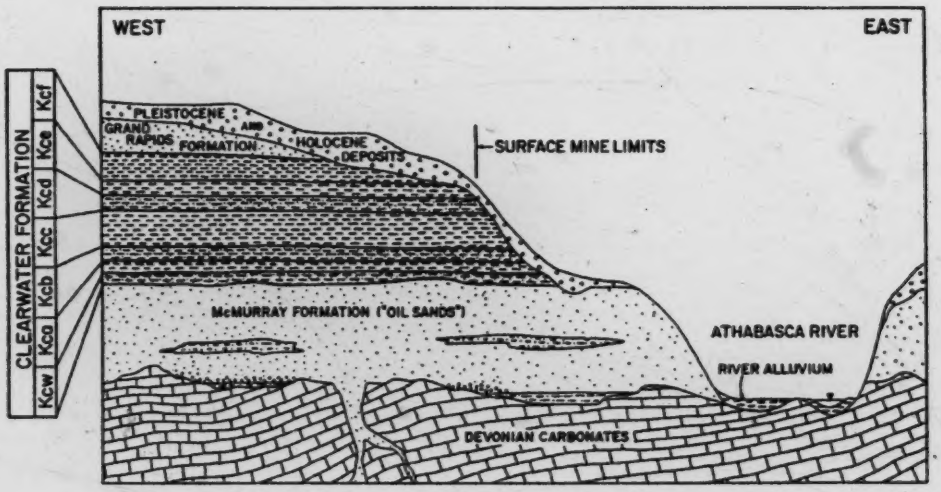

Figure 2.2 Cross-section of Athabasca deposit (modified from Sego, et al. 1994)

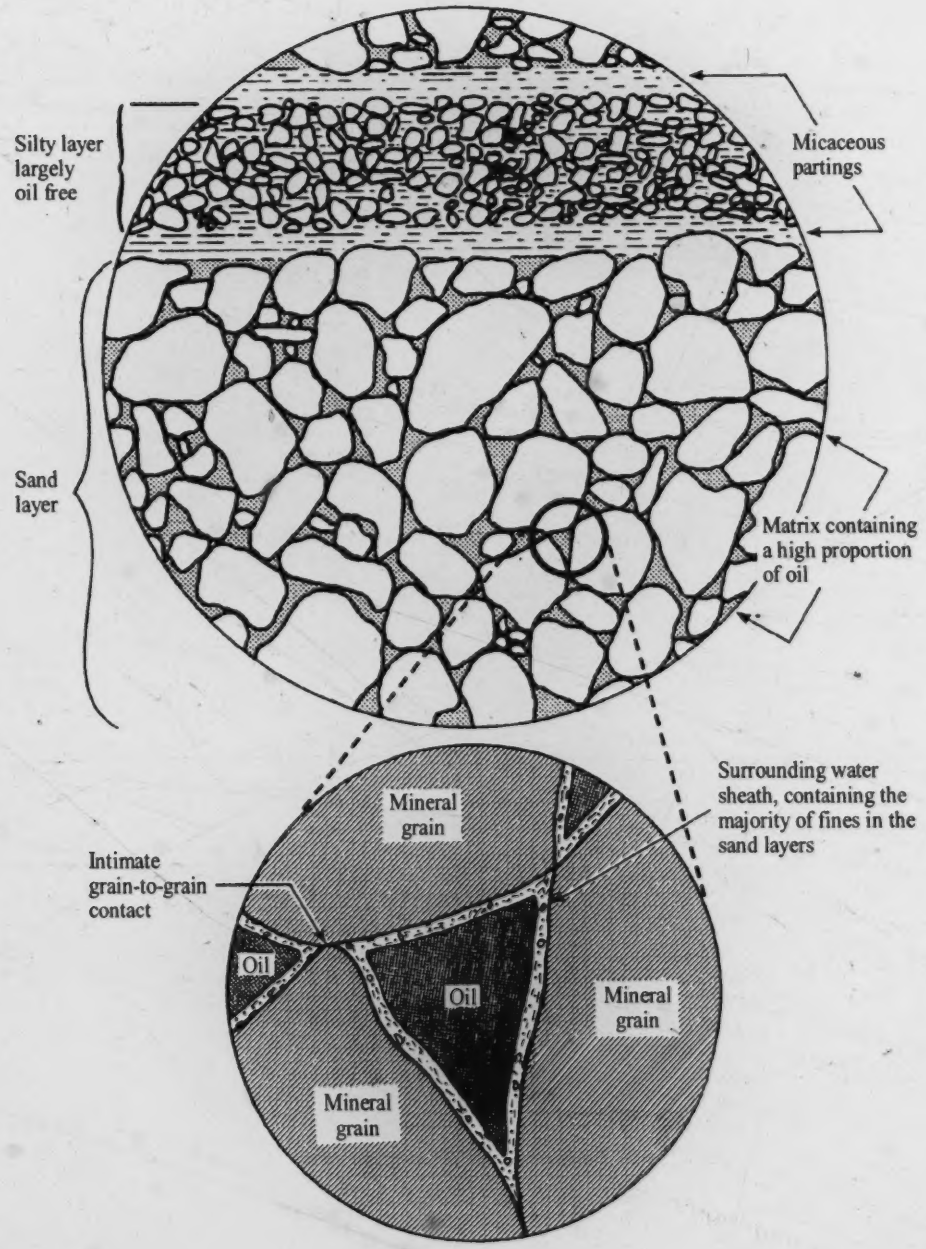

Figure 2.3 Water-wet arrangement of oil sands (modified from Sego, et al. 1994)

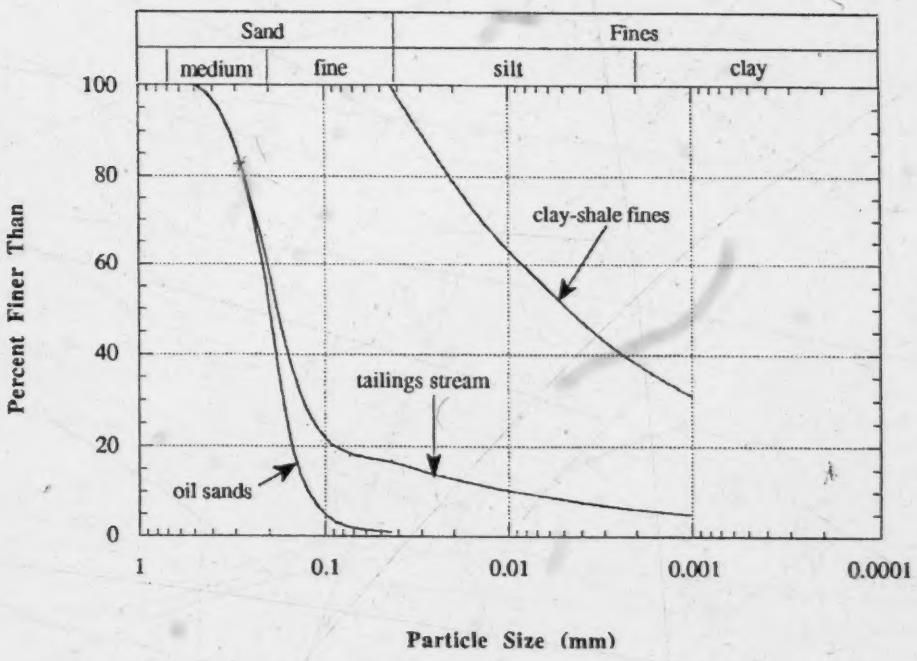

Figure 2.4 Grain size distribution

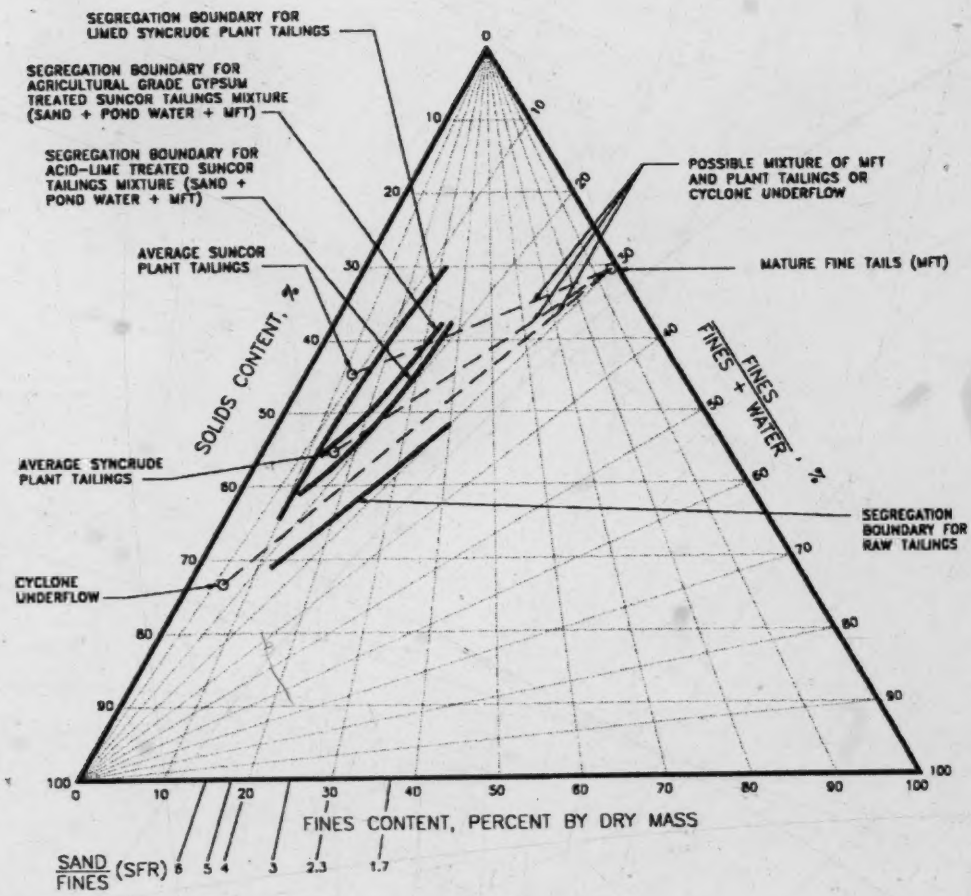
SEGREGATION BOUNDARY FOR LIMED SYNCRUDE PLANT TAILINGS
SEGREGATION BOUNDARY FOR AGRICULTURAL GRADE GYPSUM TREATED SUNCOR TAILINGS MIXTURE (SAND + POND WATER + MFT)
SEGREGATION BOUNDARY FOR ACID-LIME TREATED SUNCOR TAILINGS MIXTURE (SAND + POND WATER + MFT)
AVERAGE SUNCOR PLANT TAILINGS
AVERAGE SYNCRUDE PLANT TAILINGS
CYCLONE UNDERFLOW
POSSIBLE MIXTURE OF MFT AND PLANT TAILINGS OR CYCLONE UNDERFLOW
MATURE FINE TAILS (MFT)
SEGREGATION BOUNDARY FOR RAW TAILINGS
SOLIDS CONTENT, %
FINES + WATER, %
FINES CONTENT, PERCENT BY DRY MASS
SAND/FINES (SFR) 6 5 4 3 2.3 1.7

Figure 2.5 Slurry properties diagram (modified from FTFC, 1995)

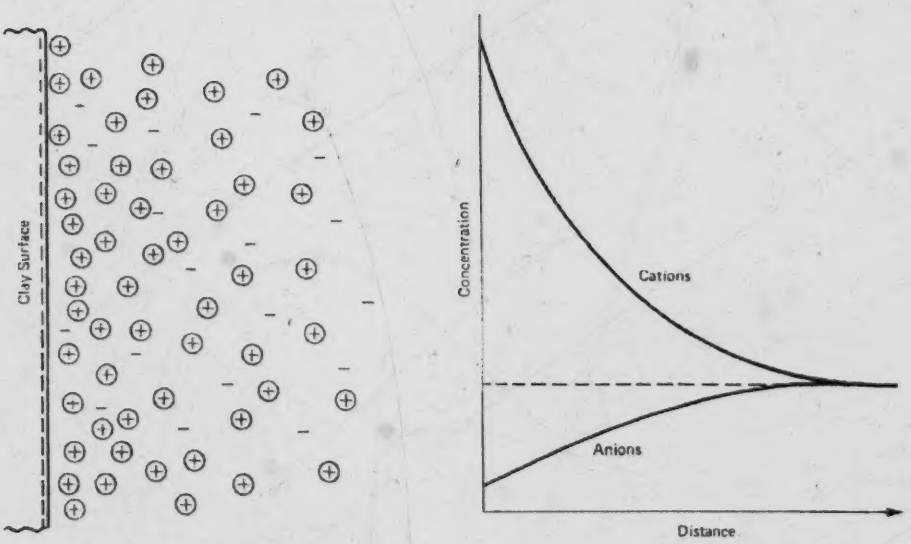

Figure 2.6 Distribution of adsorbed cations according to the diffuse double layer theory (modified from Mitchell, 1993)

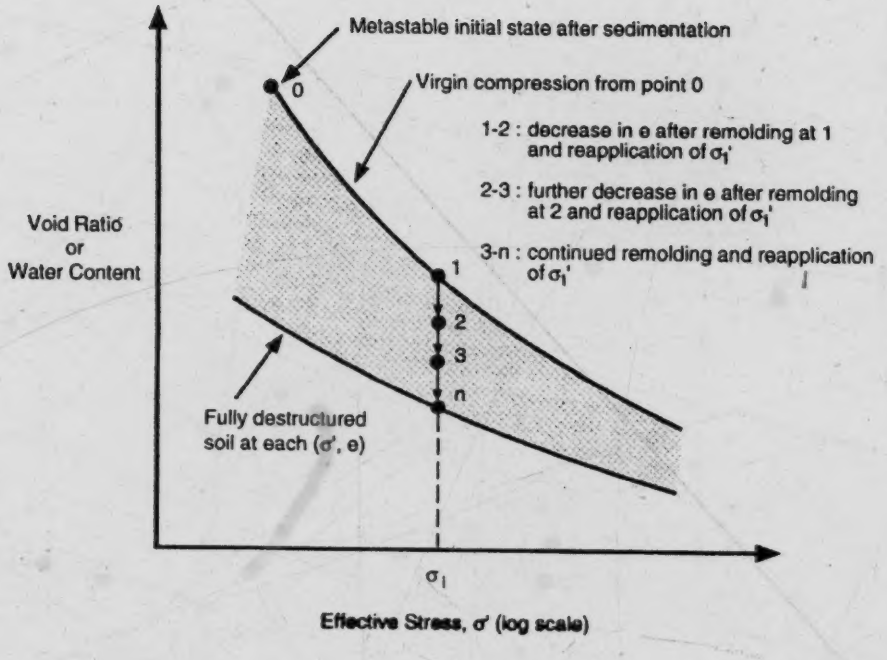
Metastable initial state after sedimentation
0
Virgin compression from point 0
1-2 : decrease in e after remolding at 1 and reapplication of σ_1'
2-3 : further decrease in e after remolding at 2 and reapplication of σ_1'
3-n : continued remolding and reapplication of σ_1'
Void Ratio or Water Content
1
2
3
n
Fully destructured soil at each (σ', e)
σ_1
Effective Stress, σ' (log scale)

Figure 2.7 Influence of metastable fabric on void ratio under an effective consolidation pressure (modified from Mitchell, 1993)

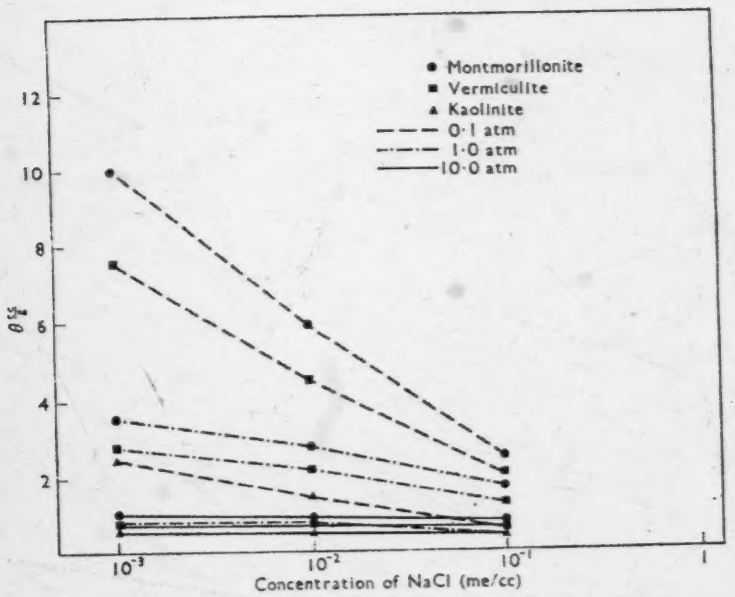

Figure 2.8 Theoretical water-retention curves for Na-clays as a function of NaCl concentration (modified from EL-Swaify and D.W. Henderson, 1967)

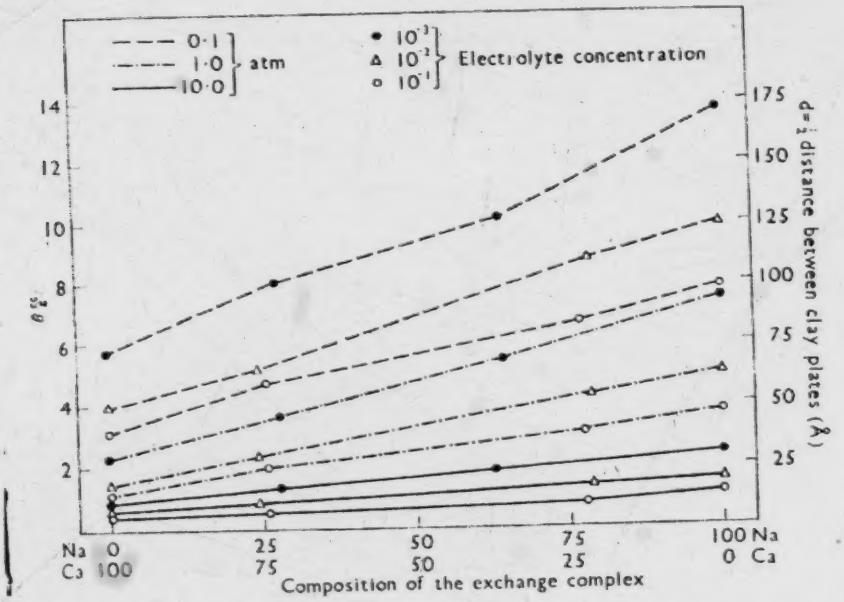

Figure 2.9 Experimental water-rention curves for mixed ion Na-Ca-Montmorillonite system (modified from EL-Swaify and D.W. Henderson, 1967)

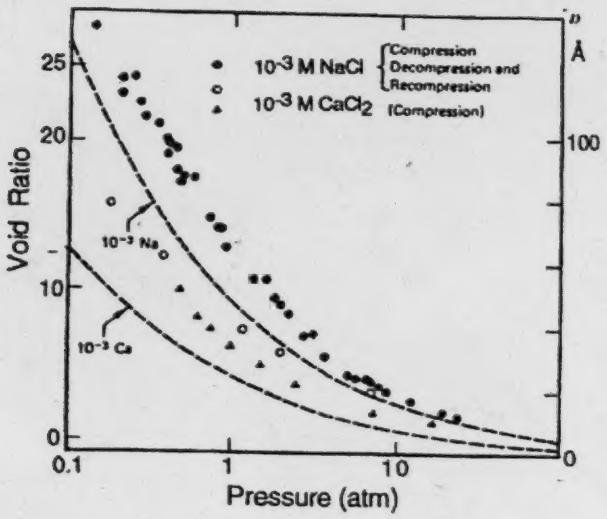

Figure 2.10 Compression curves of Na-montmorillonite and Ca-montmorillonite, fraction < 2μm (modified from Mitchell, 1993)

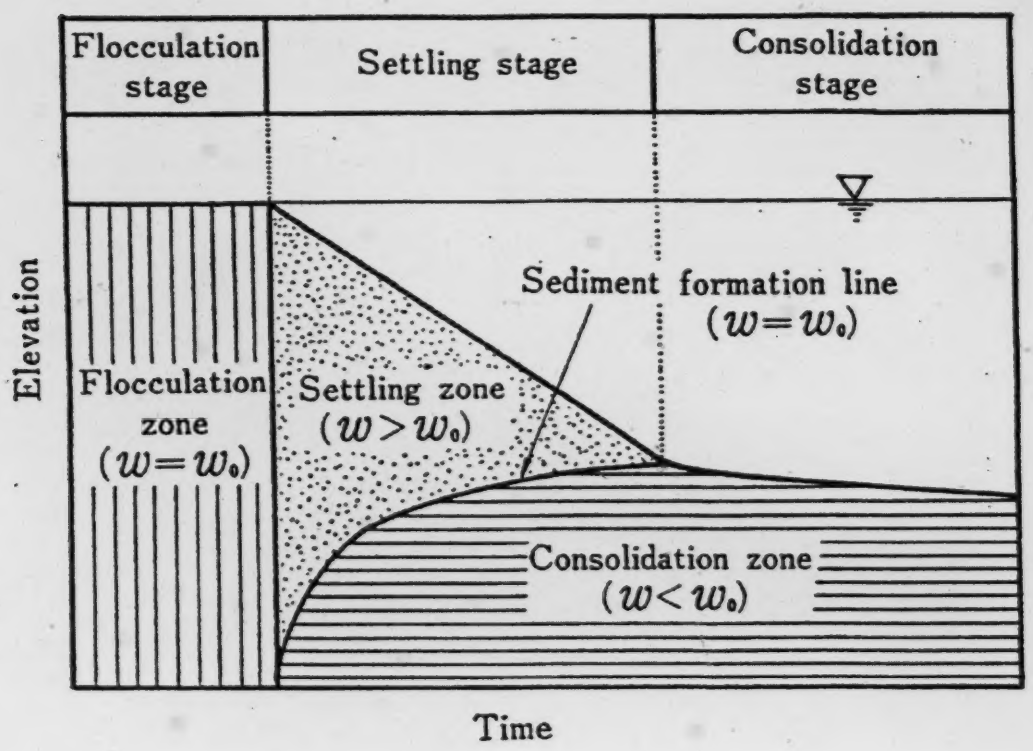

Figure 2.11 General characteristics of sedimentation of clay-water mixture

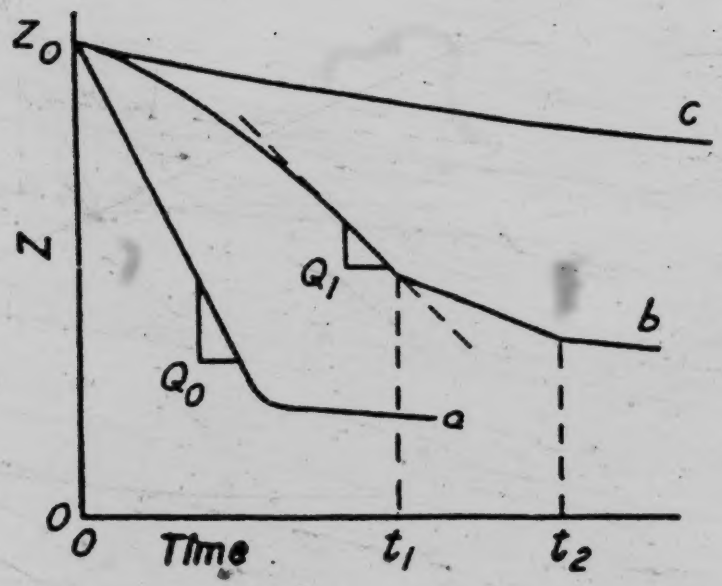

Figure 2.12 Three generalized types of settling plots (modified from Michaels and Bolger, 1962)

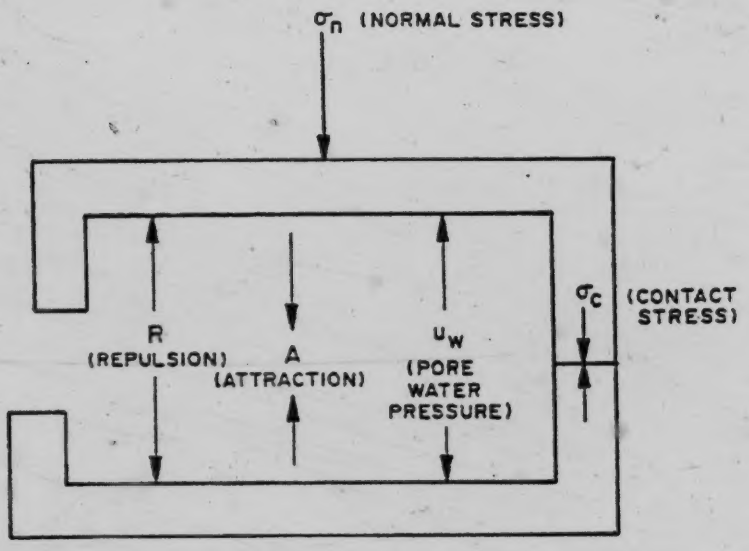

Figure 2.13 Interparticle forces in an active clay-water system

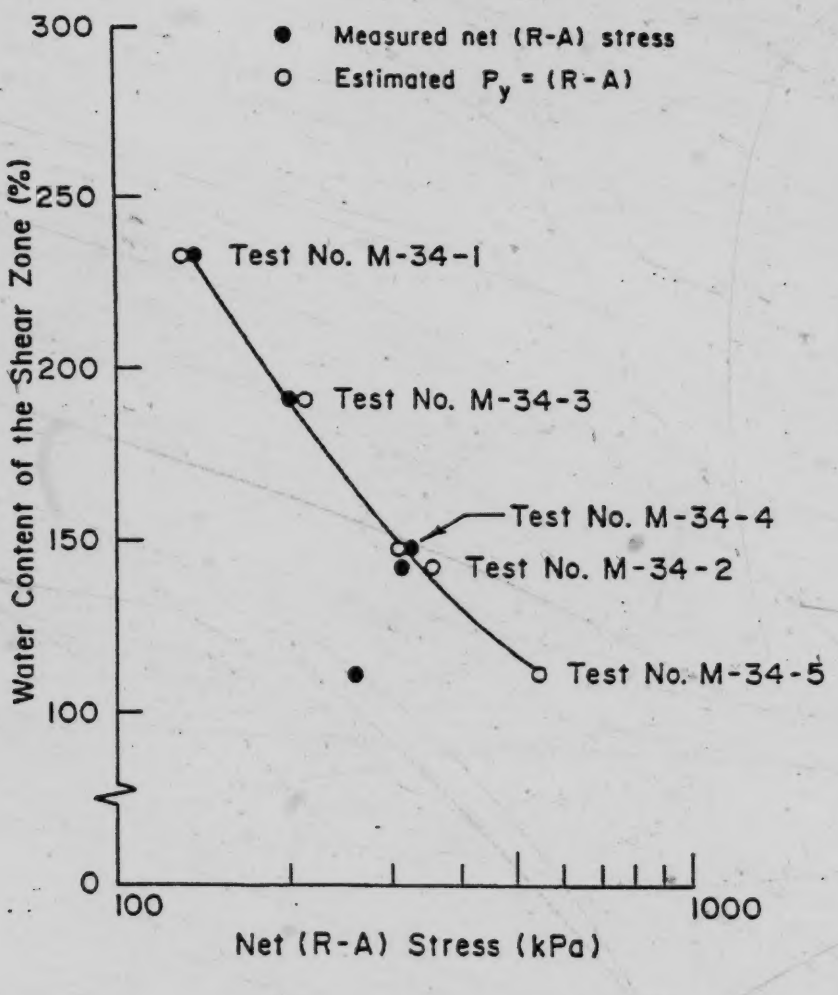

Figure 2.14 Measured vs. estimated net physico-chemical stress (modified from Morgenstern et al, 1989)

3.0 Multiphase Mass-Volume Relationships

This chapter contains the introduction and definition of mass-volume relationships, which are used to index and classify, oil sands tailings. Ordinarily, a phase diagram is constructed to facilitate the calculation of common mass-volume relationships such as void ratio, water content and bulk density. When dealing with traditional soils, the geotechnical engineer typically deals with soils in which two or three phases are present. For simplicity, soils are often assumed to be fully saturated, such that there are only two phases present, namely pore water and mineral grains. Relaxing the assumption of complete saturation, introduces a third phase; pore air or gas.

3.1 Introduction to the Multiphases of Oil Sands Tailings

Oil sands tailings are an unequaled geotechnical material, in that four different phases can be easily identified. These four phases include; mineral grains, water, bitumen and gas, however it is the presence of the bitumen that truly makes oil sands tailings unique. This organic material influences the behavior of the clays contained with the tailings stream and its presence complicates the definition of several mass-volume relationships. Since bitumen is 10^6 times more viscous than water at 20°C (Scott, 2002) its high viscosity prevents it from being

mobile and thus the common geotechnical practice is to assume it's a solid. During the extraction process much of the bitumen becomes bound to the silts and clays and therefore it is assumed that it is associated with the fines. The introduction of a fifth phase occurs when the mineral phase is split in two phases according to grain size. The net result is a five-phase material, as shown on Figure 3.1.

Upon review of oil sands and other tailings literature, it became apparent that in addition to being a five-phase material, there exist several mass-volume relationships, which are unique to the tailings field. These unique mass-volume relationships include but are not limited to fines void ratio, sand void ratio (Lui et. al, 1996), fines water ratio (FWR) and sand fines ratio (SFR) (Scott, 2002). The definition of these new tailings mass-volume relationships came out of a necessity to increase understanding of material behavior through correlation. Previous researchers (Scott and Dusseault (1980), Dusseault and Scott (1982), Scott and Dusseault (1982) and Dusseault and Scott (1983)) often accompanied the introduction of their new mass-volume relationships definition with a series of conversion relationships. Despite the introduction of these new mass-volume relationships into the literature, their use has generally remained localized and sometimes misused.

The need for standardizing the oil sand tailings equations has arisen as different engineering disciplines; geotechnical, mining and chemical in addition to geologic

disciplines often work together on different aspects within the oil sands industry. As a result of this overlapping of disciplines, mass relationships such as water content or fines content of the same sample varied due to a discrepancy in definition. This discrepancy between definitions partially resulted because in geotechnical mass-volume relationships it is common that the numerator and denominator are independent of each other. Whereas mass-volume relationships within the "mining" community do not employ this restriction, as the numerator and denominator often contain the same phase. Since the geotechnical engineering definitions for common mass-volume relationships such as water content and fines content appear to be dominant within the oil sands tailings literature, these definitions have been identified as such while other alternative definitions for common mass-volume relationships have been labeled as "mining".

The following sections contain a five-phase tailings diagram, definitions of oil sands tailings mass-volume relationships (including both traditional geotechnical definitions and "mining" definitions) and a conversion table. It is hoped that this chapter will form the basis for standardizing the usage of the oil sands tailings mass-volume relationships and act as a visual tool to increase the understanding of material behavior.

Please note the definition of geotechnical bitumen content (b), has been changed from a previous definition proposed by Scott and Dusseault (1980). The new

definition presented within, is the ratio of the bitumen mass to the mass of solids, whereas the previous definition was the ratio of the bitumen mass to the mass of mineral grain only.

3.2 Five Phase Oil Sands Tailings Diagram

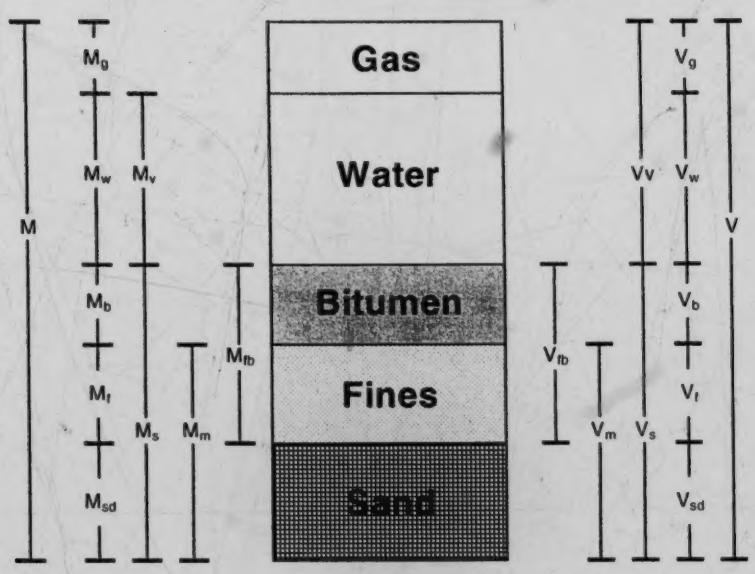

Where:

M = total mass of tailings	V = total volume of tailings
M_g = mass of gas	V_g = volume of gas
M_w = mass of water	V_w = volume of water
M_b = mass of bitumen	V_b = volume of bitumen
M_f = mass of fines	V_f = volume of fines
M_{sd} = mass of sand	V_{sd} = volume of sand
M_v = mass of voids	V_v = volume of voids
M_s = mass of solids	V_s = volume of solids
M_m = mass of mineral	V_m = volume of mineral
M_{fb} = mass of fines & bitumen	V_{fb} = volume of fines & bitumen

Figure 3.1 Five-Phase Tailings Diagram

In Figure 3.1 and throughout the remaining definitions, the mass of gas (M_g) is taken as zero. Therefore, by definition the mass of voids and mass of water are equivalent.

3.3 Definition of Mass-Volume Relationships

The following mass-volume definitions are based on the phase diagram shown on Figure 3.1

3.3.1 Bitumen Content

Bitumen Content – Geotechnical (b)

$$b = \frac{\text{mass of bitumen}}{\text{mass of bitumen, fines and sand}} = \frac{\text{mass of bitumen}}{\text{mass of solids}} = \frac{M_b}{M_s}$$

Bitumen Content – Mining (b_m)

$$b_m = \frac{\text{mass of bitumen}}{\text{total mass of tailings}} = \frac{M_b}{M}$$

3.3.2 Degree of Saturation

$$S_r = \frac{\text{volume of water}}{\text{volume of water + volume of gas}} = \frac{\text{volume of water}}{\text{volume of voids}} = \frac{V_w}{V_v}$$

3.3.3 Density

Bulk Density (ρ)

$$\rho = \frac{\text{total mass of tailings}}{\text{total volume of tailings}} = \frac{M}{V}$$

Bitumen Density (ρ_b)

$$\rho_{bitumen} = \rho_b = \frac{\text{mass of bitumen}}{\text{volume of bitumen}} = \frac{M_b}{V_b}$$

Dry Density (ρ_d)

$$\rho_d = \frac{\text{mass of solids}}{\text{total volume of tailings}} = \frac{M_s}{V}$$

Fines Density (ρ_f)

$$\rho_{fines} = \rho_f = \frac{\text{mass of fines}}{\text{volume of fines}} = \frac{M_f}{V_f}$$

Fines + Bitumen Density (ρ_{fb})

$$\rho_{fines+bitumen} = \rho_{fb} = \frac{\text{mass of fines + mass of bitumen}}{\text{volume of fines + volume of bitumen}} = \frac{M_f + M_b}{V_f + V_b} = \frac{M_{fb}}{V_{fb}}$$

Mineral Density (ρ_m)

$$\rho_{mineral} = \rho_m = \frac{\text{mass of fines + mass of sand}}{\text{volume of fines + volume of sand}} = \frac{M_f + M_{sd}}{V_f + V_{sd}} = \frac{M_m}{V_m}$$

Sand Density (ρ_{sd})

$$\rho_{sand} = \rho_{sd} = \frac{\text{mass of sand}}{\text{volume of sand}} = \frac{M_{sd}}{V_{sd}}$$

Solids Density (ρ_s)

$$\rho_{solids} = \rho_s = \frac{\text{mass of bitumen, fines and sand}}{\text{volume of bitumen, fines and sand}} = \frac{\text{mass of solids}}{\text{volume of solids}} = \frac{M_s}{V_s}$$

Water Density (ρ_w)

$$\rho_{water} = \rho_w = \frac{\text{mass of water}}{\text{volume of water}} = \frac{M_w}{V_w}$$

Standard Water Density (ρ_{sw})

$$\rho_{standardwater} = \rho_{sw} = \frac{\text{mass of standard water}}{\text{volume of standard water}} = \frac{M_{sw}}{V_{sw}}$$

At 1 atmosphere and 4°C, ρ_{sw} = 1000 kg/m^3.

3.3.4 Fines Content

Fines Content – Geotechnical (I) (f)

$$f = \frac{\text{mass of fines}}{\text{mass of bitumen, fines and sand}} = \frac{\text{mass of fines}}{\text{mass of solids}} = \frac{M_f}{M_s}$$

Fines Content – Geotechnical (II) (fb)

$$fb = \frac{\text{mass of fines} + \text{mass of bitumen}}{\text{mass of bitumen, fines and sand}} = \frac{\text{mass of fines + mass of bitumen}}{\text{mass of solids}} = \frac{M_{fb}}{M_s}$$

Fines Content – Mining (f_m)

$$f_m = \frac{\text{mass of fines}}{\text{total mass of tailings}} = \frac{M_f}{M}$$

3.3.5 Fines-Water Ratio

$$FWR = \frac{\text{mass of fines + mass of bitumen}}{\text{mass of fines + mass of bitumen + mass of water}} = \frac{M_f + M_b}{M_f + M_b + M_w} = \frac{M_{fb}}{M_{fb} + M_w}$$

3.3.6 Gas Content

$$A = \frac{\text{volume of gas}}{\text{total volume of tailings}} = \frac{V_g}{V}$$

3.3.7 Porosity

$$n = \frac{\text{volume of water + volume of gas}}{\text{total volume of tailings}} = \frac{\text{volume of voids}}{\text{total volume of tailings}} = \frac{V_v}{V}$$

3.3.8 Sand Content

Sand Content – Geotechnical (sd)

$$sd = \frac{\text{mass of sand}}{\text{mass of bitumen, fines and sand}} = \frac{M_{sd}}{M_s}$$

Sand Content – Mining (sd_m)

$$sd_m = \frac{\text{mass of sand}}{\text{total mass of tailings}} = \frac{M_{sd}}{M}$$

3.3.9 Sand Fines Ratio

$$SFR = \frac{\text{mass of sand}}{\text{mass of fines + mass of bitumen}} = \frac{M_{sd}}{M_f + M_b} = \frac{M_{sd}}{M_{fb}}$$

3.3.10 Solids Concentration

$$\eta = \frac{\text{mass of bitumen, fines and sand}}{\text{total volume of tailings}} = \frac{\text{mass of solids}}{\text{total volume of tailings}} = \frac{M_s}{V}$$

Note: Units of solids concentration are typically kg/m^3 or g/cm^3.

3.3.11 Solids Content

Solids Content – Geotechnical (s)

$$s = \frac{\text{mass of bitumen, fines and sand}}{\text{total mass of tailings}} = \frac{\text{mass of solids}}{\text{total mass of tailings}} = \frac{M_s}{M}$$

Solids Content – Mining (s_m)

$$s_m = \frac{\text{mass of fines + mass of sand}}{\text{total mass of tailings}} = \frac{\text{mass of minerals}}{\text{total mass of tailings}} = \frac{M_m}{M}$$

3.3.12 Specific Gravity

Specific Gravity – Bitumen

$$G_{bitumen} = G_b = \frac{\text{density of bitumen}}{\text{density of standard water}} = \frac{\rho_b}{\rho_{sw}}$$

Specific Gravity – Fines

$$G_{fines} = G_f = \frac{\text{density of fines}}{\text{density of standard water}} = \frac{\rho_f}{\rho_{sw}}$$

Specific Gravity – Fines + Bitumen

$$G_{fines+bitumen} = G_{fb} = \frac{\text{density of (fines + bitumen)}}{\text{density of standard water}} = \frac{\rho_{fb}}{\rho_{sw}}$$

Specific Gravity – Mineral

$$G_{mineral} = G_m = \frac{\text{density of mineral}}{\text{density of standard water}} = \frac{\rho_m}{\rho_{sw}}$$

Specific Gravity – Sand

$$G_{sand} = G_{sd} = \frac{\text{density of sand}}{\text{density of standard water}} = \frac{\rho_{sd}}{\rho_{sw}}$$

Specific Gravity – Solids

$$G_{solids} = G_s = \frac{\text{density of solids}}{\text{density of standard water}} = \frac{\rho_s}{\rho_{sw}}$$

Specific Gravity – Water

$$G_{water} = G_w = \frac{\text{density of water}}{\text{density of standard water}} = \frac{\rho_w}{\rho_{sw}}$$

3.3.13 Unit Weight

Bulk Unit Weight

$$\gamma_{bulk} = \gamma = \rho \times g$$

Bitumen Unit Weight

$$\gamma_{bitumen} = \gamma_b = \rho_b \times g$$

Dry Unit Weight

$$\gamma_{dry} = \rho_{dry} \times g$$

Fines Unit Weight

$$\gamma_{fines} = \gamma_f = \rho_f \times g$$

Fines + Bitumen Unit Weight

$$\gamma_{fines+bitumen} = \gamma_{fb} = \rho_{fb} \times g$$

Mineral Unit Weight

$$\gamma_{mineral} = \gamma_m = \rho_m \times g$$

Sand Unit Weight

$$\gamma_{sand} = \gamma_{sd} = \rho_{sd} \times g$$

Solids Unit Weight

$$\gamma_{solids} = \gamma_s = \rho_s \times g$$

Water Unit Weight

$$\gamma_{water} = \gamma_w = \rho_w \times g$$

Standard Water Unit Weight

$$\gamma_{standardwater} = \gamma_w = \rho_{sw} \times g$$

g is the acceleration due to gravity and is taken as 9.81 m/s^2

3.3.14 Void Ratio

$$e = \frac{\text{volume of water + volume of gas}}{\text{volume of bitumen, fines and sand}} = \frac{\text{volume of voids}}{\text{volume of solids}} = \frac{V_v}{V_s}$$

3.3.15 Fines Void Ratio

$$e_f = \frac{\text{volume of water + volume of gas}}{\text{volume of fines}} = \frac{\text{volume of voids}}{\text{volume of fines}} = \frac{V_v}{V_f}$$

3.3.16 Fines-Bitumen Void Ratio

$$e_{fb} = \frac{\text{volume of water + volume of gas}}{\text{volume of fines + volume of bitumen}} = \frac{\text{volume of voids}}{\text{volume of fines + volume of bitumen}} = \frac{V_v}{V_{fb}}$$

Note: In e_f and e_{fb} the presence of sand is not considered.

3.3.17 Sand Void Ratio

$$e_{sd} = \frac{\text{volume of voids}}{\text{volume of sand}} = \frac{V_v}{V_{sd}}$$

Note: In e_{sd} the presence of fines is not considered.

3.3.18 Volume Concentration

$$\phi_c = \frac{\text{volume of bitumen, fines and sand}}{\text{total volume of tailings}} = \frac{\text{volume of solids}}{\text{total volume of tailings}} = \frac{V_s}{V}$$

3.3.19 Water Content

Water Content – Geotechnical (w)

$$w = \frac{\text{mass of water}}{\text{mass of bitumen, fines and sand}} = \frac{\text{mass of water}}{\text{mass of solids}} = \frac{M_w}{M_s}$$

Water Content – Mining (w_m)

$$w_m = \frac{\text{mass of water}}{\text{total mass of tailings}} = \frac{M_w}{M}$$

3.4 Comparison Between Geotechnical and "Mining" Definitions

As defined in Section 3.3, bitumen content, fines content, solids content and water content each has two or more separate definitions. In the preceding section, a distinction was made between definitions commonly used by the geotechnical and mining communities to omit any ambiguity. In general the usual geotechnical practice is to make the numerator independent of the denominator as it been found that this yields better and more simplified correlations. However, this tradition was not held for geotechnical definitions of bitumen content, fines content and solids content as the numerators and denominator are not independent. In general the "mining" definitions usually represent a ratio of a given mass to the overall total wet mass and thus the numerator and denominator are not independent. As a result of the methodology for defining geotechnical mass-volume relationships a given parameter may be greater than 100 %, while the mining mass-volume relationships are always equal to or less than 100 %. This difference is well illustrated by the two definitions of water content.

To illustrate the visual and mathematical difference between the mining and geotechnical definitions of the aforementioned mass-volume relationships, four phase diagrams are presented within the following section. Given that only mass relationships (no volume relationships) have more than one definition, the gas

component of the phase diagram was omitted as the mass of gas equals zero. In cases where more than one geotechnical definition exists, the more commonly used definition was selected for illustration.

3.4.1 Bitumen Content

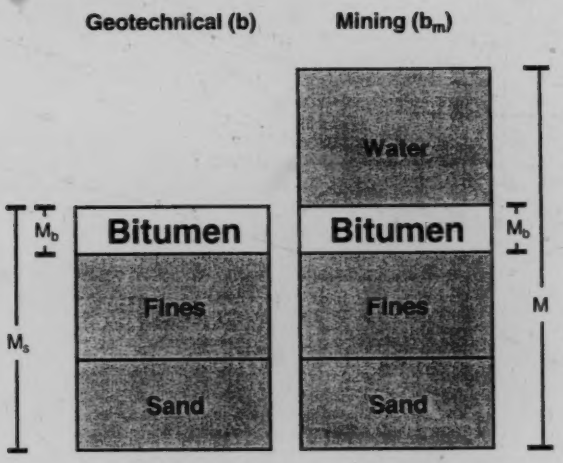

$$b = \frac{M_b}{M_s} \qquad b_m = \frac{M_b}{M}$$

3.4.2 Fines Content

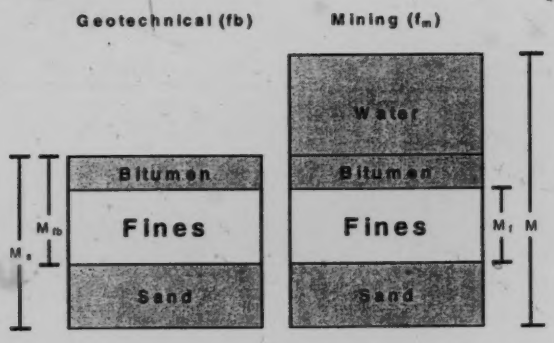

$$f = \frac{M_{fb}}{M_s} \qquad f_m = \frac{M_f}{M}$$

3.4.3 Solids Content

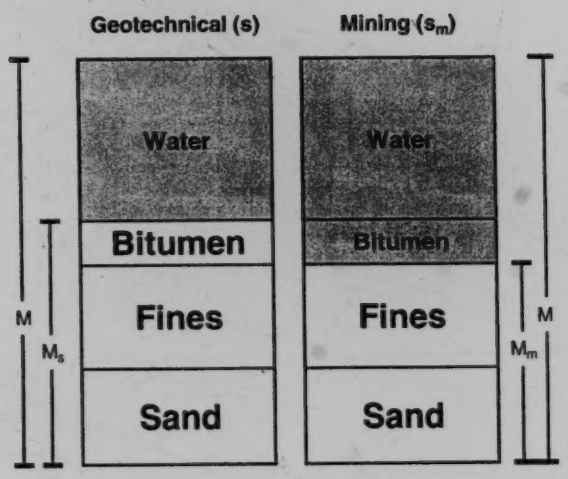

$$s = \frac{M_s}{M} \qquad s_m = \frac{M_m}{M}$$

3.4.4 Water Content

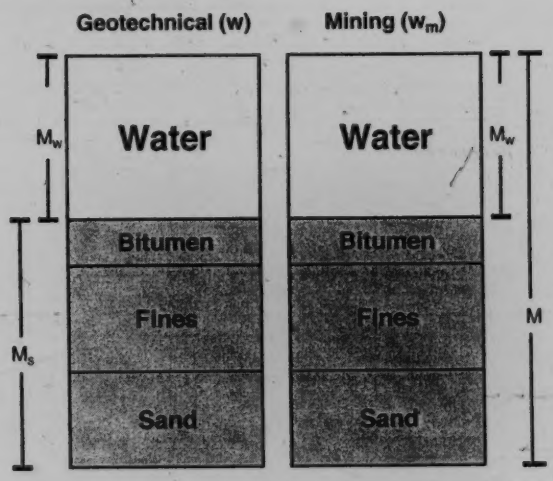

$$w = \frac{M_w}{M_s} \qquad w_m = \frac{M_w}{M}$$

3.5 Conversion Relationships for Mass-Volume Relationships

The following table is a listing of all mass-volume relationships defined in Section 3.3 along with a series of conversion equations. Columns one and two in each row lists the mass-volume relationship symbol and name, respectively, while the remaining columns contain conversion equations, which can be used to calculate the mass-volume relationship of interest. ***Please note, all parameters expressed in the following conversion equations are written as decimals, not percentages. Since many parameters are discussed as percentages, care must be taken when using these conversion relationships.***

Nearly all conversion equations listed in Table 3.1 require that the specific gravity of either the pore water, mineral or solids be known. The conversion relationships shown in Table 3.1 have been derived without any assumptions regarding the density of the water within the pores (ρ_w) or density of standard water (ρ_{sw}) and as such are mathematically and dimensionally correct. As a result of the above and of including G_w throughout Table 3.1, the appearance of the table may appear complicated. However, since ρ_w, ρ_{sw} and G_w can usually be taken as unity, simplifications can be made.

Generally speaking, the variability of the specific gravity for each phase is low compared to the variability of other mass-volume relationships and thus can be estimated for rough calculation purposes. As with any equation, the accuracy of the answer is dependent on the assumptions made and the quality of the input.

For specific gravity of materials tested within, see Section 4.3.1 or Table 4.3.

Table 3.1 Mass-Volume Conversion Relationships

Relationship		Conversion Equations			
b	Bitumen Content - Geotechnical	$b = 1 - \frac{s_m}{s}$	$b = \frac{b_m}{s}$	$b = b_m(1+w)$	
b_m	Bitumen Content - Mining	$b_m = 1 - w_m - s_m$	$b_m = \frac{b}{1+w}$	$b_m = b \times s$	
S_r	Degree of Saturation	$S_r = \frac{w \times G_s}{e \times G_w}$	$S_r = \frac{G_s \times \left(\frac{1}{s} - 1\right)}{e \times G_w}$	$S_r = 1 - \left(\frac{A}{n}\right)$	
ρ	Bulk Density	$\rho = \frac{(1+w) \times \rho_w}{\left(\frac{1}{G_s} + \frac{w}{S_r \times G_w}\right)}$	$\rho = \frac{G_s + (G_w \times S_r \times e)}{1+e} \rho_w$	$\rho = \frac{\rho_w}{\left(\frac{s}{G_s} + \frac{1-s}{S_r \times G_w}\right)}$	
ρ_d	Dry Density	$\rho_d = \frac{\rho_w}{\left(\frac{1}{G_s} + \frac{w}{G_w \times S_r}\right)}$	$\rho_d = \frac{\rho_s}{1-e}$	$\rho_d = \frac{\rho_w}{\left(\frac{1}{G_s} + \frac{\left(\frac{1}{s} - 1\right)}{G_w \times S_r}\right)}$	
f	Fines Content - Geotechnical (I)	$f = \frac{e \times G_f}{e_f \times G_s}$	$f = \frac{w}{\frac{1}{FWR} - 1} - b$		
f_b	Fines Content- Geotechnical (II)	$f_b = \frac{e \times G_{fb}}{e_{fb} \times G_s}$	$f_b = \frac{1}{SRF + 1}$	$f_b = \frac{FWR \times w}{1 - FWR}$	$f_b = \frac{f_m + b_m}{1 - w_m}$
f_m	Fines Content Mining	$f_m = f_b(1 - w_m) - b_m$	$f_m = f_b\left(1 - \frac{w}{1+w}\right) - b_m$		
FWR	Fines-Water Ratio	$FWR = \frac{f_b}{f_b + w}$	$FWR = \frac{f_b}{f_b + \frac{S_r \times e \times G_w}{G_s}}$	$FWR = \frac{f_b}{f_b + \left(\frac{1}{s} - 1\right)}$	$FWR = \frac{1}{1 + e_f\left(\frac{G_w}{G_f}\right)}$

Note: All mass-volume ratios are expressed as decimals, not percentages. See Section 3.3 for definition.

A	**Gas Content**	$A = n \times (1 - S_r)$	$A = \frac{G_s \times w}{(S_r \times G_w) + (G_s \times w)} \times (1 - S_r)$	$A = \frac{G_s \times \left(\frac{1}{s} - 1\right)}{(S_r \times G_w) + G_s \times \left(\frac{1}{s} - 1\right)} \times (1 - S_r)$	$A = \frac{e}{1+e} \times (1 - S_r)$
n	**Porosity**	$n = \frac{e}{1+e}$	$n = \frac{1}{\left(\frac{S_r \times G_w}{w \times G_s} + 1\right)}$	$n = \frac{1}{\left(\frac{S_r \times G_w}{\left(\frac{1}{s} - 1\right) \times G_s} + 1\right)}$	
sd	**Sand Content - Geotechnical**	$sd = 1 - f_b$	$sd = 1 - f - b$		
sd_m	**Sand Content- Mining**	$sd_m = 1 - w_m - f_m - b_m$			
SFR	**Sand-Fines Ratio**	$SFR = \frac{1}{f_b} - 1$			
η	**Solids Concentration**	$\eta = \frac{\rho}{1+w}$	$\eta = \left(1 - \frac{e}{e+1}\right)\rho_s$	$\eta = \rho \times s$	$\eta = (1-n)\rho_s$
s	**Solids Content - Geotechnical**	$s = \frac{1}{1+w}$	$s = \frac{G_s}{G_s + (e \times S_r \times G_w)}$	$s = \frac{1}{\left(\frac{\rho_w}{\rho_d} - \frac{1}{G_s}\right) G_w S_r + 1}$	$s = \frac{1}{1 + \left(\frac{1 - \frac{\rho}{\rho_w G_s}}{\frac{\rho}{G_w S_r \rho_w} - 1}\right)}$
s_m	**Solids Content - Mining**	$s_m = 1 - b_m - w_m$	$s_m = \frac{(1-b)}{(1+w)}$		
G_{fb}	**Specific Gravity of Fines + Bitumen**	$G_{fb} = \frac{f_b}{\left(\frac{1}{G_s} - \frac{(1-f_b)}{G_{sd}}\right)}$	$G_{fb} = \frac{e_{fb} \times G_s \times f_b}{e}$		

Note: All mass-volume ratios are expressed as decimals, not percentages. See Section 3.3 for definition.

G_t	**Specific Gravity of Solids**	$G_s = \frac{S_r \times e \times G_w}{w}$	$G_s = \frac{S_r \times e \times G_w}{\left(\frac{1}{s} - 1\right)}$	$G_s = \frac{e \times G_{fb}}{f_b \times e_{fb}}$	$G_s = \frac{\frac{b}{1-b} + 1}{\left(\frac{b}{G_b(1-b)} + \frac{1}{G_m}\right)}$
γ	**Bulk Unit Weight**	$\gamma = \frac{1+w}{\frac{1}{G_s} + \frac{w}{S_r \times G_w}} \gamma_w$	$\gamma = \frac{G_s + (G_w \times S_r \times e)}{1+e} \gamma_w$	$\gamma = \frac{\gamma_w}{\frac{s}{G_s} + \frac{1-s}{S_r \times G_w}}$	
γ_d	**Dry Unit Weight**	$\gamma_d = \frac{\gamma_w}{\left(\frac{1}{G_s} + \frac{w}{G_w \times S_r}\right)}$	$\gamma_d = \frac{G_s \times \gamma_w}{(1+e) G_w}$	$\gamma_d = \frac{\gamma_w}{\left(\frac{1}{G_s} + \frac{\left(\frac{1}{s} - 1\right)}{G_w \times S_r}\right)}$	
e	**Void Ratio**	$e = \frac{n}{1-n}$	$e = \frac{w \times G_s}{S_r \times G_w}$	$e = \frac{\left(\frac{1}{s} - 1\right) \times G_s}{S_r \times G_w}$	$e = \frac{e_{fb} \times G_s \times f_b}{G_{fb}}$
e_{fb}	**Fines-Bitumen Void Ratio**	$e_{fb} = \frac{w \times G_{fb}}{S_r \times G_w \times f_b}$	$e_{fb} = \frac{e \times G_{fb}}{G_s \times f_b}$	$e_{fb} = \frac{\left(\frac{1}{s} - 1\right) \times G_{fb}}{S_r \times G_w \times f_b}$	
e_f	**Fines Void Ratio**	$e_f = \frac{w \times G_f}{S_r \times G_w \times f}$	$e_f = \frac{e \times G_f}{G_s \times f}$	$e_f = \frac{\left(\frac{1}{s} - 1\right) \times G_f}{S_r \times G_W \times f}$	
e_{sd}	**Sand Void Ratio**	$e_{sd} = \frac{e + \frac{G_s}{G_{fb}} \times f_b}{\frac{G_s}{G_{sd}}(1 - f_b)}$	$e_{sd} = \frac{1 + \frac{G_{fb}}{G_f \times e_{fb}}}{\frac{G_{fb}(1-f_b)}{G_{sd} \times e_{fb} \times f_b}}$	$e_{sd} = \frac{\frac{G_{sd}}{S_r \times G_w}\left(\frac{1}{s} - 1\right) + \frac{G_{sd}}{G_{fb}} \times f_b}{1 - f_b}$	

Note: All mass-volume ratios are expressed as decimals, not percentages. See Section 3.3 for definition.

ϕ_c	**Volume Concentration**	$\phi_C = \frac{\rho}{\rho_s(1+w)}$	$\phi_C = \frac{\rho}{\rho_s\left(1+\frac{S_r \times e \times G_w}{G_s}\right)}$	$\phi_C = \frac{s \times \rho}{\rho_s}$	$\phi_C = \frac{\eta}{\rho_s}$
w	**Water Content - Geotechnical**	$w = \frac{1}{s} - 1$	$w = \frac{S_r \times e \times G_w}{G_s}$	$w = \left(\frac{\rho_w}{\rho_d} - \frac{1}{G_s}\right) G_w S_r$	$w = \frac{\left(1 - \frac{\rho}{\rho_w G_s}\right)}{\left(\frac{\rho}{G_w S_r \rho_w} - 1\right)}$
w_m	**Water Content - Mining**	$w_m = 1 - b_m - s_m$	$w_m = \frac{w}{1+w}$	$w_m = \frac{S_r \times e \times G_w}{G_s + (S_r \times e \times G_w)}$	$w_m = \frac{\left(\frac{1}{s} - 1\right)}{1 + \left(\frac{1}{s} - 1\right)}$

Note: All mass-volume ratios are expressed as decimals, not percentages. See Section 3.3 for definition.

4.0 Experimental Program and Procedures

The experimental testing program undertaken in this research included a series of laboratory tests which sought to determine the effect of experimental procedures and the effect of phosphogypsum on the rate of water release of CT. The following sections review the details associated with field production of CT and the origin of the fines and water which were used in the laboratory testing program. A detailed examination of the field production of CT is necessary in order that laboratory-prepared samples closely resemble the field make-up of CT. Furthermore, this chapter summarizes the sampling and storage procedures used when obtaining field samples for laboratory use and summarizes the geotechnical parameters for each tailings stream. The chapter concludes with a review of the mix designs used in laboratory production of CT and the laboratory procedure used for index tests, large strain oedometers and scanning electron microscopy (SEM) images.

4.1 Field Production of CT

CT is produced in the field using a hydrocylcone to increase the solids content of the whole tailings stream prior to the addition of MFT and gypsum. The cyclones take the incoming whole tailings stream with a solids content of 42 - 57 % and a fines content of 17 % and produces cyclone underflow at approximately 75 % solids and 10 % fines. Cyclone overflow, which flows out the top of the cyclone, is pumped to the tailings ponds where it undergoes dewatering and eventually becomes MFT.

4.1.1 Makeup of Field Produced CT

Prior to conducting any laboratory experiments, it was deemed necessary to examine the makeup of field produced CT. CT is produced in the field by

combining cyclone underflow, MFT, pond water and phosphogypsum. Table 4.1 summarizes the average solids content and fines content of the four input components used to produce CT as taken from Syncrude's 1995 NST Field Demonstrations (Shaw et al, 1996). Additionally, by knowing the average solids and fines content of each input component, it was possible to calculate the mass of each input component required to produce a cubic meter of CT at 62 % solids and 20 % fines (ρ_{bulk} = 1616 kg/m^3). See Table 4.1 for summary and Appendix A (Calculation A1) for detailed calculations of this procedure.

Also included within Table 4.1 is an assigned age designation; either "young" or "age". The assignment of an age designation was done for the purpose of preparing CT in the laboratory with the same portions of "young" and "aged" fines and water, as was in the field produced CT. The designations "young" and "aged" are based on the period of time, which has elapsed since each component left the extraction plant. Since whole tailings comes directly from the extraction plant prior to being hydrocycloned (to produce cyclone underflow), it was designated as "young". MFT and pond water are pumped from tailings ponds, and have undergone physical and possible chemical changes since leaving the extraction plant, were designated "aged". Utilizing the information contained in Table 4.1, the three major phases (fines, sand and water) were analyzed to determine what percentage (on a mass basis) were "young" and "aged". Table 4.2 summarizes the percentage of each phase according to the "young" or "aged" designation. Appendix A (Calculation A2) contains the details of these calculations.

The distributions shown in Table 4.2 were used to ensure that laboratory prepared CT was similar to field produced CT in terms of solids and fines content and also in terms of "young" and "aged". Section 4.4.3 provides details on the laboratory mix design. Previously, laboratory CT was prepared to duplicate the same solids and fines content used in the field, however, the relative proportions

of "young" and "aged" fines and water were generally not considered. That is, the previous method assumed that all sources of fines and water were equivalent with respect to their influence on hydraulic conductivity, fabric and compressibility. If a significant difference in behavior occurs due the differing proportions of young and aged fines, the general applicability of the previous laboratory test results may be affected.

4.2 Collection and Storage of Laboratory Tailings Samples

In addition to laboratory samples having the same breakdown of "young" and "aged" fines and water as field produced CT, laboratory samples must also be prepared from quality field samples. Care needed to be exercised during long term storage of laboratory samples in order to preserve their original physical and chemical properties.

Experience has shown that MFT stored for an extended period of time in metallic containers exhibits segregation characteristics which are different than freshly sampled MFT. Laboratory prepared CT which contained MFT that was stored in metallic drums which began rusting after the emplacement of MFT, did not exhibit behavior consistent with the segregation boundary (Scott, 2002). Laboratory CT which was prepared with freshly sampled MFT, segregated when the phosphogypsum dosage was less than 900 g/m^3. However, a sample with the same solids, fines and phosphogypsum dosage which contained MFT from a rusting drum, did not segregate even when no gypsum was added.

It is surmised that the addition of Fe^{2+} to the MFT pore water as a result of the oxidation process causes an effect similar to the addition of the calcium ions (Ca^{2+}) during phosphogypsum treatment. Thus, storage of tailings in metallic containers may in itself cause the tailings to be nonsegregating.

Given the detrimental long term effects of using tailings which have been stored in metallic containers, fresh samples of whole tailings, MFT and recycled pond water were collected in May 1998 from Syncrude Canada Ltd. and used for all testing conducted in this research. The following section describes the collection and storage details for all tailings used in the research testing.

4.2.1 Mature Fine Tails (MFT) Sampling and Storage

Between April 1-3, 1998 thirty 5 gallon unlined steel pails were filled with MFT from Syncrude's holding pond, located at the toe of the Northwest corner of Mildred Lake Settling Basin (MLSB). The holding pond was filled with MFT taken from the MLSB in 1993. MFT from the holding ponds was pumped from a common depth and placed directly into the 5-gallon pails. Each of the thirty pails were approximately 80 to 90 % of their capacity and were filled consecutively.

Forty-eight hours after the MFT was sampled, the tailings arrived at the University and were transferred from the steel pails into three 220-L plastic drums. Since the pails were not labeled in the order in which they were filled, one-third of each 5-gallon pail was poured into each of the three plastic drums. Each plastic drum was covered with an airtight lid to prevent evaporation. A visual inspection of the interior surface of the unlined steel pails showed that little or no oxidation had occurred during the 48-hour residence time. One of the three plastic drums was randomly selected and was used as the sole source of MFT for the remainder of the testing program.

4.2.2 Recycled Pond Water Sampling and Storage

On May 5, 1998 eight 15-liter plastic pails were sampled by Gord McKenna of Syncrude from MLSB. Each pail was assumed to be representative of typical recycled pond water and blending the eight pails was deemed unnecessary. All

recycled pond water was kept in its original plastic containers and sealed to prevent evaporation.

4.2.3 Whole Tailings Sampling and Storage

The term whole tailings refers to fresh tailings that have come straight from the extraction plant, have not been treated or altered and contain both the coarse and fine mineral fraction. On May 12, 1998 five 45 gallon unlined steel drums of whole tailings were collected at Syncrude's CT pilot plant. At the time of sampling, Syncrude's #2 whole tailings line was being used for the pilot test while the other 3 whole tailings lines were being deposited at the South West Sand Storage. Each of the five drums were filled to approximately 80 % of their capacity and were trucked to the University of Alberta and arrived the following afternoon.

All 5 drums had segregated, leaving the finer fraction, designated as "thin fine tails" (TFT), in the upper portion of each drum and the coarse material, designated as "sand", in the lower portion of the drum. Two drums were randomly selected, and the TFT was siphoned off and combined into a single 220-liter plastic drum. Similarly, the sand fraction was removed from the steel drums and placed into a 220-L plastic drum. Both plastic drums were covered with an airtight lid to prevent evaporation.

4.3 Geotechnical Test Results on Laboratory Tailings Samples

Following the transfer of MFT and whole tailings into plastic drums, a series of standard geotechnical laboratory tests were conducted to determine if the laboratory materials had the same physical properties as the field materials. Section 4.2 provides documents the steps which were taken to ensure that the chemical properties of laboratory samples were preserved.

4.3.1 Index Properties of Laboratory Samples

Representative samples were collected from each tailings stream to determine their geotechnical parameters. Table 4.3 summarizes the average solids content, fines content, specific gravity and age designation (as described in Section 4.1.1) of MFT, whole tailings, TFT, sand and recycled pond water.

As previously mentioned, the whole tailings contained within the two metallic drums had segregated upon arrival. Since it was impossible to re-suspend the coarse fraction and sample the whole tailings in its original state, the overall solids and fines content of each drum was back calculated. The back calculation was based on measuring the depth of TFT and sand within each drum along with the solids and fines content of these two layers. As shown in Table 4.3, the back calculated solids and fines content of the whole tailings was 47.6 % and 19.4 %, respectively. Appendix A (Calculation A3) provides the detailed calculations for this assessment.

All solids contents shown in Table 4.3 were determined using standard gravimetric analysis and represent the average of at least two samples. All samples, except for phosphogypsum, were placed in an aluminum tart dish and dried in an oven at 110 °C overnight or until a constant mass was reached. All solids contents have been calculated according to the geotechnical definition presented in Section 3.3.11.1.

The solids content of the phosphogypsum was measured after drying the sample to a constant weight in an 80 °C oven. This drying technique removes the non-bound water while the chemically bounded water remains behind. This is a standard procedure for determination of the free water content of chemical compounds which contain both free water and bounded water.

4.3.1.1 Summary of Index Properties of Laboratory Samples

According to Syncrude's 1995 NST Field Demonstration the solids content for the whole tailings ranged from 42 to 57 %, while the fines content averaged 17 %, while the solids content of MFT averaged 31 % with an average fines content of 98.4 % (Shaw et al, 1996). Thus, the laboratory samples of whole tailings and MFT, as received from Syncrude, had solids and fines contents consistent with those materials used in the field production of CT.

4.3.2 Gradation of Laboratory MFT

To determine if the gradation characteristics of laboratory MFT were consistent with field MFT, a washed sieve analysis was performed on MFT. The gradation results on MFT are shown in Figure 4.1 along with maximum, minimum and average mean values as determined by Syncrude for MFT used at 1995 NST Field Demonstration. In total, Syncrude conducted over 20 sieve analyses for each tailings stream used during the 5 week operation.

4.4 Laboratory Production of CT

To ensure that laboratory test results are meaningful and can be extrapolated to predict field performance, laboratory CT must be prepared carefully to mimic both the physical and chemical properties of field produced CT. Laboratory CT was produced by combining laboratory manufactured cyclone underflow, MFT, recycled pond water and phosphogypsum. Since we were unable to sample cyclone underflow directly from the field, we simulated the cycloning process by vacuum dewatering the TFT. The following paragraphs summarize how CT was produced in the laboratory and how the physical properties compare with field produced CT.

4.4.1 Production of Laboratory Manufactured Cyclone Underflow

The hydrocyclone used in the 1995 NST Field Demonstration increased the solids content of the incoming whole tailings stream from approximately 42 to 57 % solids and 17 % fines to approximately 75 % solids and 10 % fines. In addition to removing water during the cycloning process, fines were also removed as the cyclone underflow contains a lower percentage of fines than whole tailings. As mentioned previously, direct sampling of the cyclone underflow from Syncrude's 1997/1998 CT field test was not possible. However, knowing the solids and fines content of the cyclone underflow, it was possible to manufacture simulated cyclone underflow.

To manufacture simulated cyclone underflow, the solids content of the TFT (see section 4.2.3. for definition) was increased using a technique known as vacuum dewatering. Tang (1997) provides complete details relating to vacuum dewatering. TFT was vacuum dewatered from a solids content of 10.7 % to 22.8 % solids to simulate the water removal which occurs during cycloning. Vacuum dewatered TFT was then combined with sand such that the ratio (mass basis) of TFT to sand was approximately 0.15. This ratio is based on the solids and fines contents shown in Table 4.3. The grain size distribution for TFT and sand are shown on Figure 4.2 and 4.3, respectively.

4.4.2 Gradation Laboratory Manufactured Cyclone Underflow

Figure 4.4 shows the theoretical gradation of laboratory manufactured cyclone underflow along with maximum, minimum and average mean values of cyclone underflow as determined by Syncrude during their 1995 NST Field Demonstration (Shaw et al, 1996). This theoretical gradation curve was calculated using the gradation characteristics of TFT and sand, the solids contents and the mass proportions used to blend these two material together. Figure 4.4 indicates that laboratory manufactured cyclone underflow had a gradation similar to field produced CT for grain sizes less than 0.1 mm. However, for grain sizes between

0.1 and 0.3 mm the manufactured cyclone underflow is approximately 40 % more coarse than field produced cyclone underflow.

4.4.3 Mix Design for Standard Laboratory CT

Since water and fines in CT originate from different sources, namely MFT, cyclone underflow, and gypsum slurry, it's critical that laboratory prepared CT have the same type of fines and water as in the field. It is important to note that numerous combinations of sand, TFT, MFT, and pond water can be used to produce CT with 62 % solids and 20 % fines. However, only one combination will yield the same breakdown of "young" and "aged" fines and water.

Supporting this concept, there is a belief (Scott, 2002) that the origin of the fines may influence the rate of water release. Two samples of CT, one made from entirely "young" fines (using only TFT) and one made from entirely "aged" fines (using only MFT) are theorized to have different water release rates, despite the fact that the solids and fines contents are identical. The effect may be due to changes in the type of fines or water present and ultimately their impact on the fine fabric.

Table 4.4 summarizes the solids content, fines content and mass of each component required to produce 2.0 liters of standard laboratory CT. Standard laboratory CT is defined as CT with target values of 62 % solids, 20 % fines, of which 48 % of the water is "young" water and 45 % of the fines are "young". Phosphogypsum dosage varied according to the desired dosage.

Laboratory CT prepared according to the proportions shown in Table 4.4 had an average solids content of 62.1 % and fines content of 19.9 % and a specific gravity of the solid portion (sand, fines and bitumen) of 2.59.

4.4.4 Gradation of Standard Laboratory CT

As mentioned previously, the field sampled MFT and the laboratory manufactured cyclone underflow were compared to standard known values in Sections 4.3.2 and 4.4.2, respectively. Although the laboratory components used to produce CT were deemed to be representative of their field counterparts, it was still necessary to demonstrate that CT produced in the laboratory had gradation characteristics consistent with field CT. Figure 4.5 shows the gradation characteristics of standard laboratory CT along with the maximum, minimum and average mean values for CT produced during Syncrude's 1995 NST Field Demonstration. Figure 4.5 shows that the gradation of laboratory prepared CT is approximately 3 to 5 % finer than field CT between grain sizes of 0.1 and 0.0014 mm and approximately 3 % coarser between 0.15 and 0.2 mm. These anomalies are likely due to the MFT which on average was approximately 5 to 10 % finer than field produced CT and manufactured cyclone underflow which was approximately 40 % coarser than field produced CT between grain sizes of 0.1 and 0.2 mm. From Figure 4.5 it is apparent that standard laboratory prepared CT had similar gradation characteristics to field produced CT. Therefore, it has been assumed that differences in the gradation characteristics is not responsible for the anomalies between field and laboratory behavior.

4.5 Water Release Index Test (WRIT)

Early in the laboratory testing program, it was not totally clear whether CT, at a solids content of 62 %, underwent hindered sedimentation or consolidation immediately after deposition. The transition from hindered settling to consolidation occurs at a void ratio, known as the soil-formation void ratio (e_m). There exists a range of void ratios below e_m in which the direct determination of k by means of standard techniques encounters serious difficulties; among these, the highly non-uniform distribution of the void ratio within the sample due to its self-weight, and the necessity of imposing extremely low gradients to minimize the effects of seepage induced consolidation (Pane and Shiffman, 1997). At

sufficiently low void ratios, direct measurement of hydraulic conductivity can be made using traditional geotechnical laboratory techniques, while above e_m, sedimentation tests provide adequate means to determine the hydraulic conductivity. Other authors including Michaels and Bolger (1962) and Been and Sills (1981) define this region as a transitional or 'intermediate' behavior between suspensions and soils, where channeling and fabric changes can seriously affect the interpretation of the results.

4.5.1 Design Consideration for Water Release Index Test (WRIT)

In order to effectively determine the behavioral response of CT and avoid the aforementioned complications, the water release index test (WRIT) was implemented. The WRIT, consisted of filling an acrylic cell with a constant height of CT and measuring the amount of water released after 24 hours. The results of the WRIT do not allow for a direct calculation of the hydraulic conductivity, however they are quick and permit relative comparisons to be made between numerous test results. The WRIT was designed to act as a screening mechanism, to identify those factors which significantly influence the water release rate of CT from those that do not.

Since it was not known whether CT was experiencing consolidation or hindered sedimentation, precautions were taken in the design of the WRIT so that the results were not negatively impacted. If consolidation was occurring during the index test, the height of CT placed in each index cell needed to be constant, as the rate of consolidation is proportional to the length of the drainage path squared. Since placing exactly 5.0 cm of CT in a test cell by eye was not accurate enough for the aforementioned reason, it was decided that each cell would be filled on an electronic scale according to a constant mass. Since the diameter of each cell was identical, placing a constant mass would ensure that the height of CT would be constant.

However, experience showed, that as a result of the mixing process in the laboratory, air was entrained in the specimen and resulting in a measured density that was always slightly less than the target value of 1616 kg/m^3. Since the bulk density varied in response to changes in the degree of saturation (amount of air entrained), placing a constant mass of CT (without knowing the degree of saturation) would result in a variable height of CT in each cell. To account for the variation in bulk density the procedure outlined in Appendix A (Table A1) was developed to ensure that the height of CT remained constant at 5.0 cm. Immediately after mixing, but prior to filling each test cell, the bulk density of the CT was measured and the mass of CT required for a constant height of 5.0 cm was determined from Table A1. See next section.

4.5.2 Test Procedure for Standard Water Release Index Test (WRIT)

To perform a standard WRIT; sand, TFT, MFT and pond water were combined in a plastic 5.0L pail, according the standard laboratory mix design for CT, as shown in Table 4.4. Approximately 10 grams of pond water was combined with the required mass of phosphogypsum (approximately 1.2 to 6.4 g depending on required dosage) in a separate aluminum tart dish. The mixing blade was inserted into the plastic pail containing the sand, TFT, MFT and pond water and the tailings were mixed for approximately 30 second to promote homogeneity. See Caughill (1992) for a detailed description of the mixing blade. After 30 seconds of mixing, the pond water and phosphogypsum slurry (from the aluminum dish) were added to the mixing pail and the CT was mixed continuously for 5 minutes at 540 RPM. Approximately 3 minutes after adding the phosphogypsum slurry, three 100 cm^3 grab samples were taken for analysis of the actual solids and fines content.

At the conclusion of the 5 minute mixing period, a pre-weighed 1000 ml graduated glass standpipe (height = 30 cm and diameter = 5.8 cm) was filled

with CT to approximately the 950 ml mark. This standpipe was weighed and the actual volume was read from the graduated markings. Using the total weight and total volume of CT contained within the standpipe, the bulk density was calculated. Using Table A1 (Appendix A), the mass of CT required for a constant height of 5.0 cm was determined. The 14.55 cm diameter acrylic cell was placed on the electronic scale and filled with the required mass. Finally, the acrylic cell was sealed to prevent evaporation by securing a cellophane wrapper with an elastic band. Exactly twenty-four hours after pouring the CT, the mass of release water that was released by the sample and accumulated on the surface of the deposit was determined. All release water was carefully removed using 0.5 cm diameter plastic tube connected to a vacuum pump. To ensure that only water was removed and not CT, a 0.5 cm high wedge was placed under one corner of the acrylic cell such that the water flowed to the low end. After complete removal of release water, the acrylic cell was reweighed and the total mass of release water was calculated.

4.6 Laboratory Test Procedures

The laboratory testing program was divided into two sections according to their objective, which were:

1. Determination if laboratory scale effects were causing the anomalies between the field and laboratory behavior; and

2. Determination of the effect of phosphogypsum dosage on the behavior of CT.

The objective of the first portion of the laboratory testing program was to determine if techniques used in the laboratory was causing the anomalies between the observed behavior of CT in laboratory and in the field. This portion focused primarily on the effects of scale (boundary conditions) and its effect on

the behavior of CT in the laboratory. The objective of the second portion of the laboratory testing program was to quantify the effects of increasing phosphogypsum dosage on the dewatering characteristics of CT.

4.6.1 Effect of Experimental Procedure

In the field, CT is produced by injecting gypsum into the MFT, prior to combining with cyclone underflow. These three components are combined in a mixing tank and mixing is achieved by means of a recirculating pump at the base of the tank. The total residence time, including post-mixing piping transport is approximately 5 minutes. Laboratory procedures for CT preparation (see section 4.5.2) were arbitrarily determined as it was impossible to recreate the same mixing procedure as used in the field. As a result, laboratory preparation techniques were selected based on the availability of equipment, repeatability and operator ease. Thus, the laboratory preparation technique was appealing from a precision point of view, however since laboratory technique used a blade mixer instead of a recycling pump (different physics) the accuracy of the laboratory tests results may be questionable.

A series of tests were performed to determine the following :

1. Is the laboratory technique influencing the behavior of CT in the laboratory ?;
2. What is the magnitude ? ; and
3. What changes must be made to reduce or eliminate the bias.

This portion of the testing was quantified by the behavior of CT using WRIT's and was designed to eliminate laboratory biases and validate the laboratory procedure used for CT production. Ultimately, these results will help increase the

overall appeal of laboratory test data for prediction of future field CT performance.

The following sections describe modifications that were made to the standard WRIT to determine the sensitivity of the rate of water release to changes in the experimental procedure.

4.6.1.1 Effect of Diameter-to-Height Ratio (DHR)

Field deposition of CT during the 1995 NST Field Demonstration occurred in ponds where the minimum width ranged from 35 to 100 meters while the depth of these cells ranged from 2 to 3 meters deep (Shaw et al., 1996). Due to the large lateral extent of the settling ponds and the rate at which CT was produced, approximately 10 to 15 cm of CT was deposited daily. Thus, the minimum diameter-to-height ratio (DHR) during daily production was approximately 230 times and once the pond reached capacity, the minimum DHR was approximately 12.

Since it was impossible to replicate the field DHR within the laboratory, the effect of DHR was investigated to determine whether laboratory tests were subject to negative biases due to smaller DHR's. To assess the sensitivity of DHR, the standard WRIT was performed in a series of five tests cells where the diameter varied from 5.71 to 20.22 cm while the height of the deposit remained constant at 5.0 cm. These five tests were repeated at both 900 g/m^3 and 2000 g/m^3 dosage to determine if DHR was dependent on dosage. For each dosage, three separate but theoretically identical batches of CT were prepared according to the standard preparation technique. One of the three batches was used to fill the cells with diameters of 5.71 and 14.55 cm, while a second batch was used to fill the cells with diameter of 8.86 and 13.9 cm. The entire third batch was used to fill the 20.22 cm cell. The filling schedule was designed to minimize the effect of

minor deviations in the actual solids content, fines content and degree of saturation, as CT from the same batch was placed into two cells with different diameters.

4.6.2 Effect of Phosphogypsum Dosage

The effect of increasing phosphogypsum dosage was examined using WRIT's, theory of hindered sedimentation, large strain oedometer tests and Scanning Electron Microscopy (SEM). This approach provided both quantitative and qualitative changes in CT as a function of phosphogypsum dosage and help to improve our understanding of the role of PG.

4.6.2.1. Water Release Index Tests (WRIT's)

To quantify the effect of increasing PG dosage on the mass of water released from a standard WRIT, forty-nine standard WRIT's were conducted with dosages ranging from 600 to 3200 g/m^3. Each sample was prepared according to the procedure described in Section 4.5.2. Of the forty-nine WRIT's conducted to determine the effect of increasing PG dosage, sixteen tests were performed at 900 g/m^3 and fourteen were performed at 3200 g/m^3.

4.6.2.2 Capturing Behavior of CT / Water Interface During WRIT

To determine whether CT was experiencing hindered sedimentation and/or consolidation during the index test, a video camera was used to capture the descent of the interface. After preparing, mixing and placing the CT as described in Section 4.5.2, a video camera attached to a lap top computer was placed within several millimeters of the acrylic cell for the entire 24 hour duration of the index test. A scale was attached to the outer wall of the acrylic cylinder and aligned within the field of view, so that changes in height could be determined. Using time lapse photography, a digital image was recorded each minute to track

the position of interface versus time. Upon completion of the index test, a sufficient number of images (which covered the entire duration of the test) were randomly selected and converted to bitmap images. Each bitmap image was enlarged at 20:1, such that the height of the interface could be accurately determined from the attached scale. The theory of hindered sedimentation was then used to analyze the position of the interface versus time.

4.6.2.3 Step Loaded Slurry Consolidometers

To quantify the effects of PG on the compressibility and hydraulic conductivity of CT, four step-loaded slurry consolidometer tests were conducted at PG dosages of 900 g/m^3 and 3200 g/m^3. The following section summarizes the test procedure for the slurry consolidometer. A schematic of the slurry consolidometer is shown in Figure 4.6.

Prior to the placement of the CT within the oedometer, the porous stone at the base of the cell, the horizontal burettes and all plastic tubing were carefully filled with TFT water to ensure no entrapped air. After preparing and mixing the CT it was poured from the mixing pail and the initial height of the sample was recorded according to a scale attached to the outside wall of the acrylic cylinder. A cellophane wrapper was placed over top of the oedometer cell to prevent evaporation and desiccation of the specimen surface. The height of the sample was recorded as a function of time (by eye) until no further change was observed and the sample had reached equilibrium. After reaching equilibrium, additional pond water was tremied down the side of the acrylic cell, until there was approximately 1 cm of surface water. The external horizontal burettes were then adjusted such that the centerline of the burettes had the same elevation as the top of the aforementioned surface water.

To measure the hydraulic conductivity after the specimen had reached self weight equilibrium, a constant upward then downward gradient were applied by raising or lower one of the horizontal burettes above the surface water elevation. The resulting flow rate into or out of the sample was recorded with time by monitoring the position of the meniscus within the horizontal burette. The position of the meniscus was measured every several minutes during the first 15 minutes of the test and less frequently thereafter and was used to calculate the flow rate into and out of the sample. Flow was continued until it was apparent that a constant flow rate had been achieved for a given flow direction. Using the flow rate and applied gradient the hydraulic conductivity was calculated.

Upon completion of determining the hydraulic conductivity under self weight, the loading cap was placed in contact with the surface of the CT and the linear variable displacement transducer (LVDT) was placed atop the loading cap. As the loading cap was released and its full weight was transferred to the CT, the FLUKE data logger began recording the voltage reading of the LVDT. The LVDT was recorded every several minutes for the first 30 minutes and then less frequently thereafter. Upon determining that the height of the sample was no longer changing (constant voltage on LVDT), equilibrium was reached and the hydraulic conductivity was measured using the constant head technique described earlier. This procedure was repeated for all subsequent loading steps up the final load of 700 kPa.

For complete details regarding design of slurry consolidometer, its features and its limitations see Suthaker (1995).

4.6.2.4 Scanning Electronic Microscopy (SEM) Images

To qualitatively assess changes in the fabric of the fines as a function of dosage, eight CT samples ranging in dosage from 900 g/m^3 (ratio of mass of PG to mass

of fines (PGFR) = 4.68) to 3200 g/m^3 (PGFR = 15.72) were examined with a scanning electron microscope (SEM). Five of the eight CT samples were observed using a cryogenic SEM, while the remaining three samples were observed using a variable pressure SEM. All CT specimens for observation with the SEMs were prepared and mixed according to the procedure outlined in Section 4.5.2 and were modified according to the required phosphogypsum dosage. After placing the required mass of CT in the 14.55 cm acrylic cell and obtaining three grab samples (100 ml each) the CT was poured into a glass jar and transported to the SEM laboratory for observation. The following sections briefly describes each the cryogenic and variable pressure SEM setup, the method used to mount the specimen for observation and the collection of images.

4.6.2.4.1 Cryogenic SEM

The SEM used for cryogenic observation was a JEOL model, JSM.6301FXV located in the Earth Science building (University of Alberta) and was operated by George Braybrook.

CT samples for cryogenic observation were transported to the SEM laboratory and allowed to stand undisturbed on the counter top for at least half an hour prior to being sampled. A 5 mm open ended square metal tube was then inserted vertically into the glass jar and held approximately 2 to 3 cm below the surface of the CT until the tube was filled. After covering the upper end of the tube, to create a vacuum, the tube was removed from the CT and submerged immediately in a cup of liquid nitrogen slush. The liquid nitrogen had been cooled to its freezing point by vacuuming with a cryosystem model, Emitech K1200. The metal tube (and CT within) was held in the liquid nitrogen for approximately 20 seconds, however complete freezing of the entire CT sample likely occurred in approximately 2 seconds or less. The metal tube was then

removed from the liquid nitrogen slush and held in the palm of the hand to warm the specimen so that is could be extracted. Upon extraction from the metal tube, the CT specimen was submerged in the liquid nitrogen slush until it was ready to be mounted.

The frozen CT sample was removed from the liquid nitrogen slush and positioned vertically within a copper box (approximately 2 cm long by 0.5 cm wide by 0.3 cm deep), known as the stage. Given the size of the stage with respect to the frozen CT sample, the stage was able to accommodate up to 4 samples at once. Prior to inserting any samples into the stage, it was filled with glue to secure each sample vertically. After securing each specimen to the stage, another cup of liquid nitrogen was reduced to its freezing point using the vacuuming mentioned earlier. The entire stage was then submerged within liquid nitrogen and each CT specimen was fractured (below the surface of the liquid nitrogen) using hand-held pliers to expose a fresh surface. This preparation technique is known as freeze-fracturing.

The stage was removed from the liquid nitrogen cup and placed within optical vacuum chamber to undergo sublimation. The chamber temperature was maintained below -40 $^{\circ}$C, to prevent recrystallization of the ice on exposed surface. Lastly, the samples were bombarded with gold in a process known as sputtering. The samples were then ready for observation at a vacuum pressure and temperature of $6 * 10^{-7}$ torr and -157 °C, respectively. Images or "photographs" were collected at magnifications ranging from 15 to 2000 times.

4.6.2.4.2 Variable Pressure SEM

The SEM used for variable pressure observation was a LEO 438VP temporarily located in the Earth Science Building (University of Alberta) and was operated by George Braybrook. Usage and experience with the variable pressure SEM was

very limited as it was at the University for approximately only two weeks as part of a promotional tour. The variable pressure SEM was capable of magnifications from 15 to 300 000 times, had an accelerating voltage of 300 V to 30 kV, a probe current range of 1pA to 500nA and a variable pressure range of 1Pa to 400 Pa. The specimen stage had full 360° rotation capabilities in addition to been able to move approximately 3 cm in all directions.

CT samples for variable pressure observation were transported to the SEM laboratory and allowed to stand undisturbed on the counter top for at least half an hour prior to being sampled. "Wet" samples of CT were collected using a modified plastic laboratory eye dropper. The eye dropper was modified by cutting an inch off the bottom to increase the diameter to approximately 3 mm and ensure that CT could move freely within. The eye dropper was inserted vertically approximately 2 cm below the surface of the CT and the squeeze ball was slowly released, thereby pulling the CT into the eye dropper. Approximately 1 to 2 ml of CT was released from the eye dropper onto a metallic circular pedestal (diameter approximately 7 mm), known as the stage.

The stage (with CT) was secured in the observation chamber and a vacuum was applied. The pressure within the chamber decreased from atmospheric (approximately 100 kPa) to 400 Pa in approximately one minute. During the first 20 seconds of the vacuuming bubbles (approximately 0.5 mm diameter) appeared on the surface of the CT as the pressure was decreased. Beyond 20 seconds and up to approximately 45 seconds the entire surface of the CT appeared to be "boiling" as the surface fluctuated rapidly up and down. After 45 seconds of vacuuming, the surface of the CT stopped moving and CT surface remained stationary throughout the viewing process. As result of the vacuuming process the CT dried in an irregular hollow dome shape (approximately 0.3 mm high) with numerous cracks and/or fissures. Prior to vacuuming, the CT was medium brown in color, however during vacuuming the color changed to a pale

brown. This color change was very similar to that seen when samples are oven dried to determine their solids content.

Images were collected after the pressure was reduced to 400 Pa, with magnifications ranging from 227 to 2500 times. During imaging of the specimen, the pressure was modified from 400 Pa and the focus length was varied from 7 to 10 mm, in order to produce the clearest image. However, since the CT surface was stationary 45 seconds after being vacuumed, alternating the pressure during observation was thought to have little or effect on the structure observed. Unlike the cryogenic SEM which observes the fracture surface (cross-sectional view), the variable pressure SEM observes the outer surface of the CT (plan view).

4.7 Summary

Given previous experience of long term storage of tailings in metallic containers, every effort was made to preserve the integrity of the laboratory samples. Although no water chemistry parameters were measured upon receipt of the laboratory samples, visual inspection of the steel drums that were used for shipping the tailings revealed little or no oxidation has occurred. Thus, the laboratory samples were assumed to have the same chemical properties as the field samples upon arrival and during subsequent storage within plastic drums. Additionally, comparing the measured values of solids content and fines content for MFT and whole tailings along with gradation results for MFT with values reported during the 1995 NST Field Demonstration, indicate that the field samples obtained for laboratory usage had similar physical properties to those used for field production of CT.

Given that cyclone underflow was not available for direct sampling in the field, it had to be reproduced in the laboratory by simulating the cycloning process.

Sieve analysis indicated that laboratory manufactured cyclone underflow had similar gradation characteristics to field cyclone underflow. Using the mix design presented on Table 4.4 it was possible to prepared CT in the laboratory with a solids content, fines content (including similar age designation for water and fines) and gradation characteristics very similar to field produced CT. The gradation results on the laboratory prepared CT indicate that it is slightly finer than field produced CT. This slight deviation would suggest that the measured value of hydraulic conductivity would be lower (more conservative) in the laboratory compared to the field. Similarly, due an increase in the fines content of CT, one also expect that the laboratory CT would be more compressible than field CT. Given that both these changes are on the conservative side along with the fact that is took approximately one year to obtain fresh tailings samples, we elected to continue the testing program with current laboratory samples.

Table 4.1 - Components Required to Produce 1 m^3 of Field CT at 62 % Solids and 20 % fines

Input Component	Average Solids Content (%)	Average Fines Content (%)	Mass (kg)	Age Designation
Cyclone Underflow	75.0	10.1	1186	"young"
MFT	31.0	98.4	362	"aged"
Pond Water	0	0	67	"aged"
		SUM	1616*	

* Includes approximately 0.9 kg Phosphogypsum (for 900 g/m^3 treatment)

Table 4.2 Breakdown of Age Designations for CT Phases

Phase	% that are "young"	% that are "aged"
Water	48	52
Fines	45	55
Sand	99.8	0.2

Table 4.3: Average Geotechnical Parameters of Laboratory Tailings Samples

Tailings Sample	Solids Content (%)	Fines Content (%)	Specific Gravity	Age Designation
MFT	31.8	97.0	2.55*	"aged"
Whole Tailings +	47.6	19.4	2.59*	"young"
TFT	10.7	97.2	2.69*	"young"
Sand	82.8	6.5	2.66	"young"
Phosphogypsum	na	na	na	na
Recycled Pond Water	na	na	1.00++	"aged"

* Depends on bitumen content

+ As back calculated, see note in Section 4.3.1

++ Assumed.

Table 4.4 Standard Laboratory CT Mix Design (2.0 L)

Tailings Component	Average Solids Content (%)	Average Fines Content (%)	Mass (g)
Sand[+]	82.8	6.5	2062
TFT[+]	22.8	97.2	308
MFT	31.8	97.0	710
Pond Water	0	0	150
		SUM	3232[*]

[*] includes 1.8 g of phosphogypsum, however dosage varies

[+] manufactured cyclone underflow is prepared by adding sand and TFT in the ratio shown above.

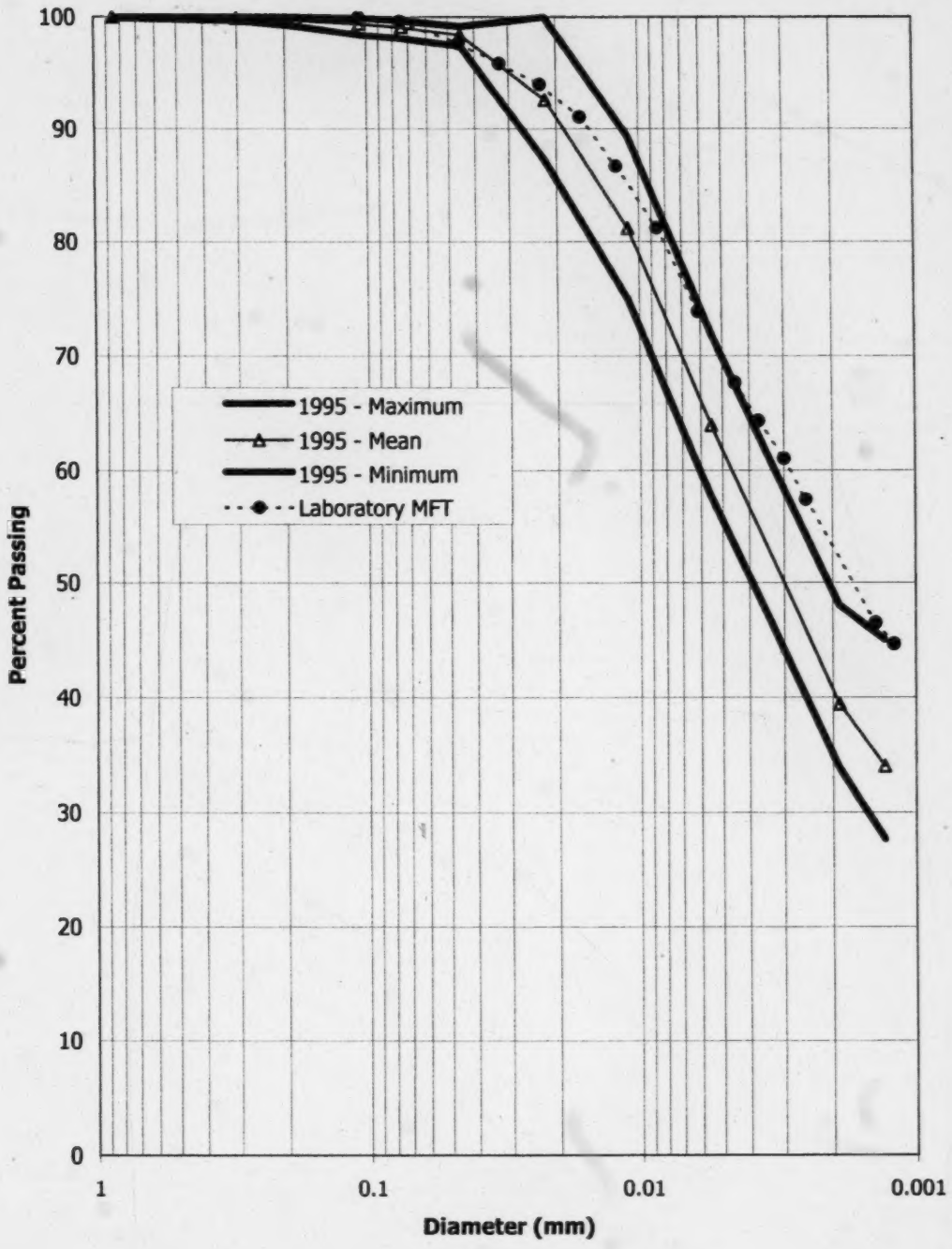

Figure 4.1 Grain size distribution of laboratory MFT compared to MFT used by Syncrude in 1995 Field Trial

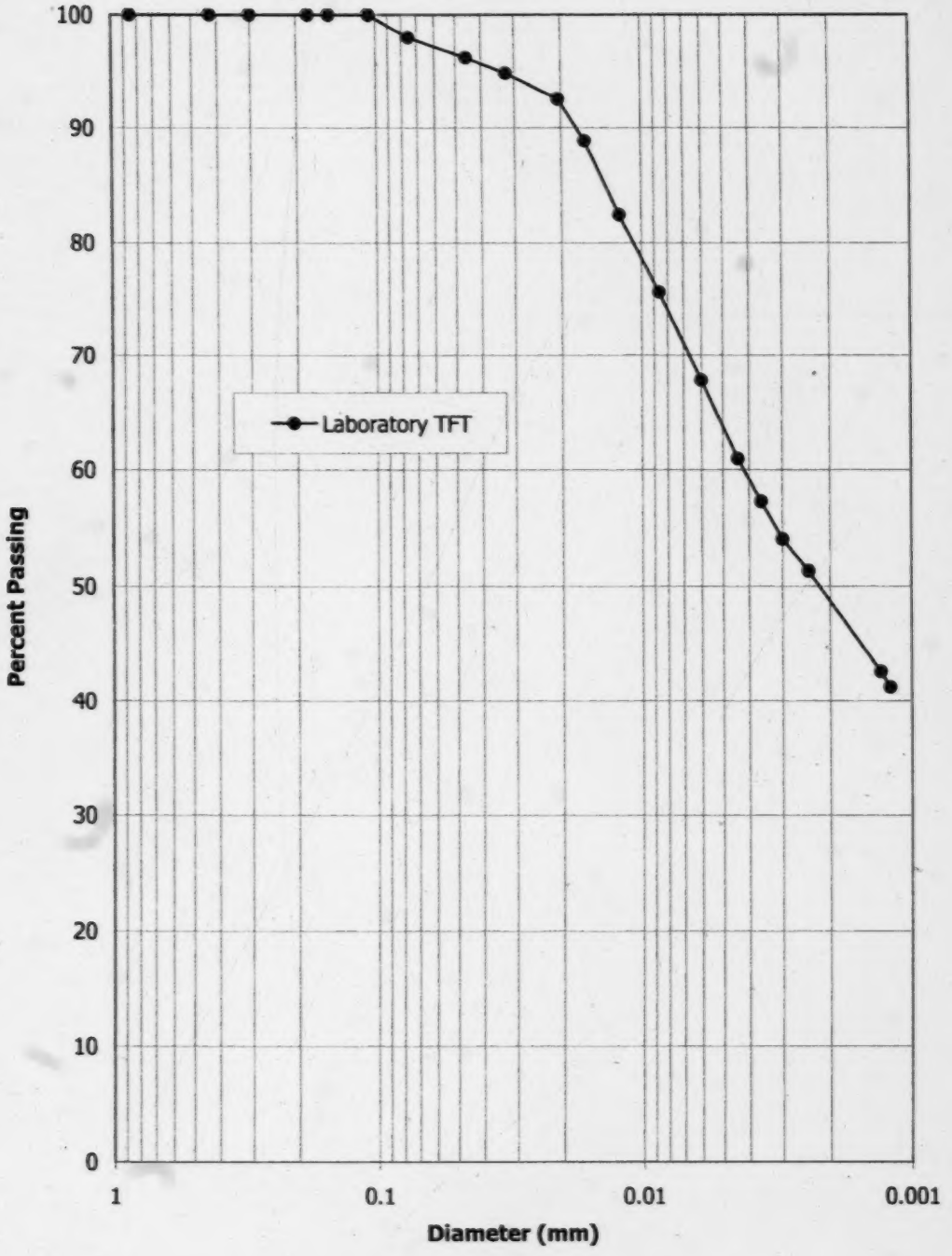

Figure 4.2 Grain size distribution of laboratory TFT

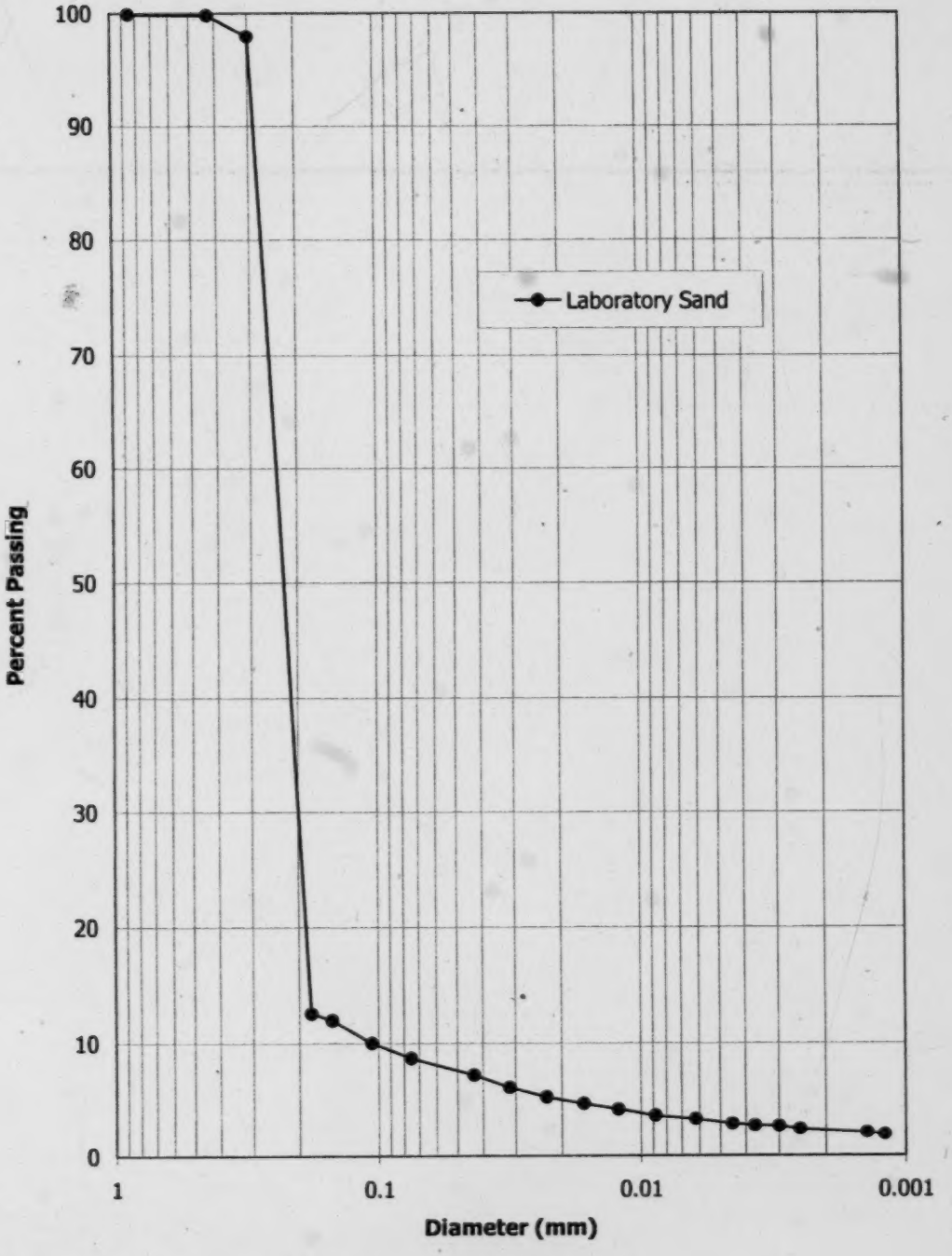

Figure 4.3 Grain size distribution of laboratory sand

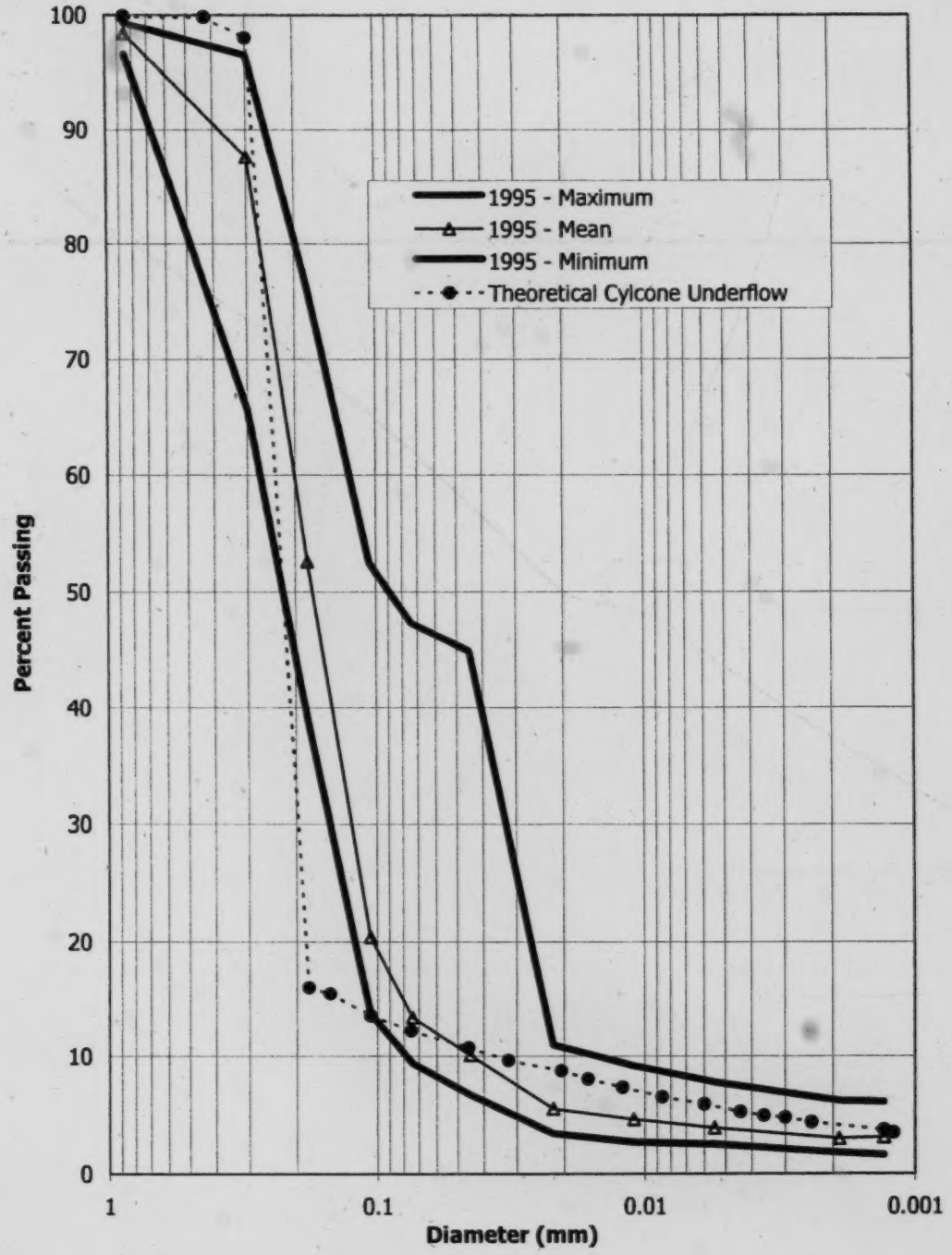

Figure 4.4 Grain size distribution of cyclone underflow used in 1995 Field Trial and laboratory simulated cyclone underflow

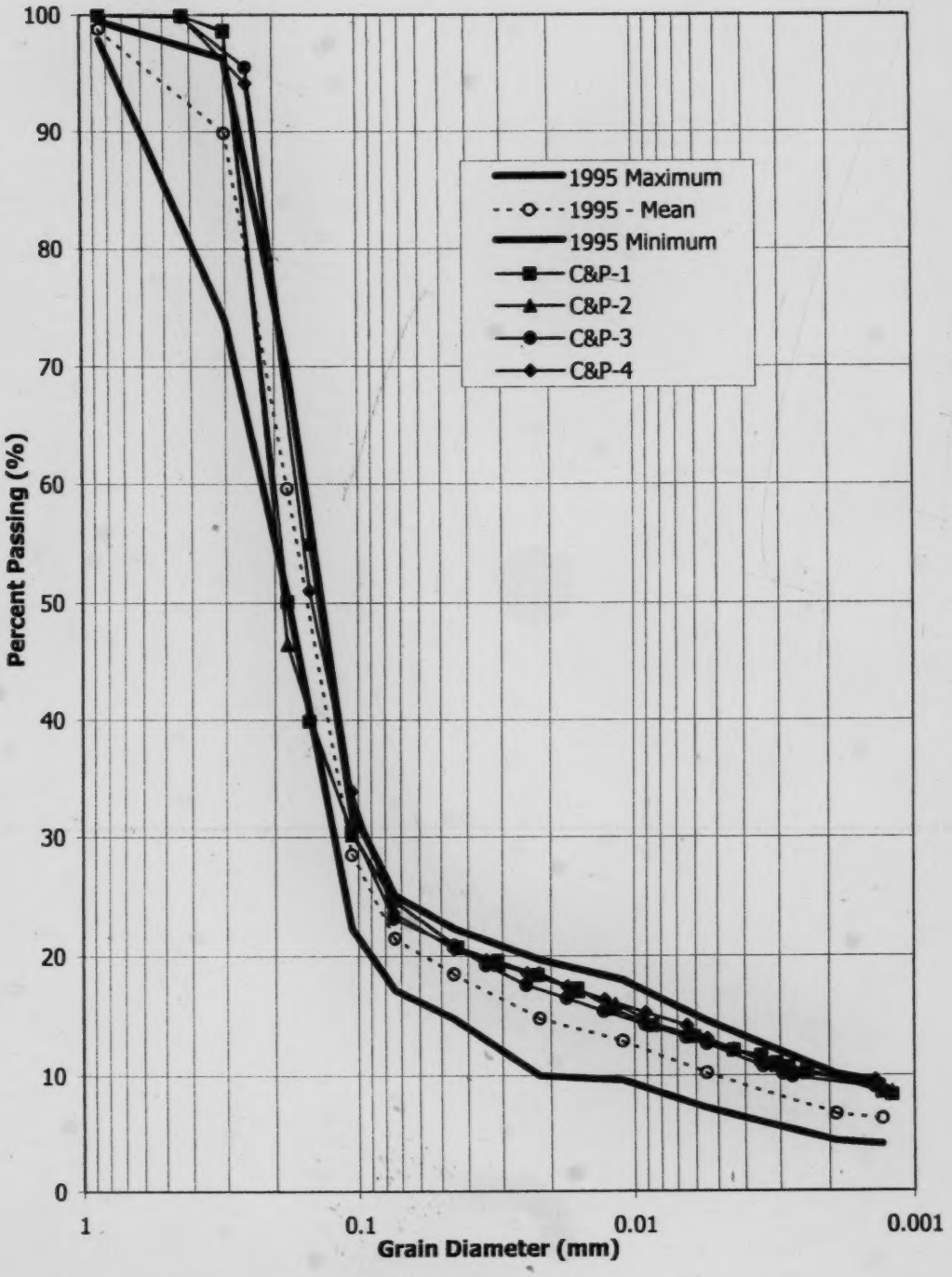

Figure 4.5 Grain size distribution of CT

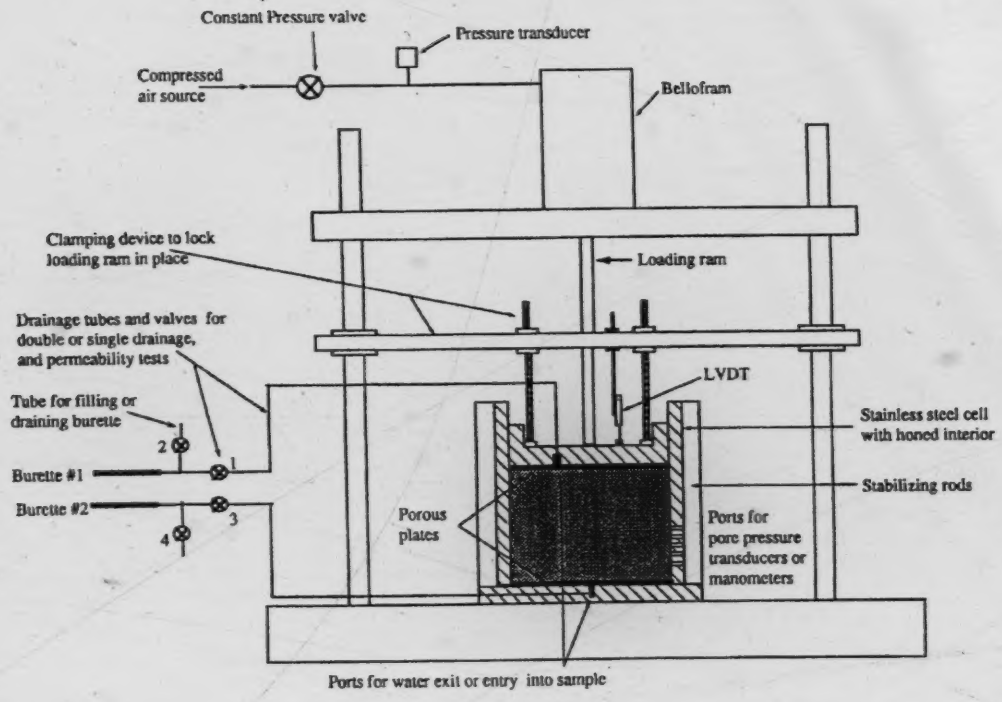

Figure 4.6 Slurry consolidometer

5.0 Results on Effect of Experimental Procedure and Effect of Increasing Phosphogypsum Dosage

5.1 Introduction

The laboratory testing program was divided into two sections; those factors dealing with the experimental procedures and those dealing with the effect of phosphogypsum as it relates to the dewatering behavior of CT. At the onset of the testing program, these two sections appeared independent of each other, however the test results suggested otherwise. Therefore, the results of the testing program are not presented in the same order as the discussion on testing procedure described in Chapter 4, but are presented in an order that will aid in the interpretation of the test results. Discussion and interpretation of all tests results are deferred to Chapter 6, with the exception of a partial discussion on the effect of increasing phosphogypsum dosage as measured with the water release index test (WRIT).

5.1 Diameter to Height Ratio (DHR)

The effect of diameter to height ratio (DHR) was investigated for phosphogypsum dosages of 900 g/m^3 and 2000 g/m^3 by preparing a series of CT samples according to the standard water release index test (WRIT), and then depositing the CT in a series of cells with diameters ranging from 5.71 to 20.22 cm. For each test, the depth of CT was held constant at 5.0 cm (by mass), thus providing a range of DHR's from 1.14 to 4.04. A depth of 5 cm was used in the laboratory to simulate a field test which was conducted just prior to commencing our testing program. Based on limited resources available for purchasing new laboratory equipment, the testing within was limited to a maximum cell diameter of 20.22 cm.

5.1.1 Effect on Grams of Release Water per cm^2

Tables 5.1 and 5.2 summarize the solids content, fines content, cell diameter, DHR, grams of release water, grams of release water per cm^2 of cross-sectional area and normalized grams per cm^2 for each of the five tests conducted at 900 and 2000 g/m^3 of PG, respectively. Intuitively, all other parameters being equal, a test cell with a larger diameter will release a greater mass of water than a test cell with a smaller diameter. Thus, in order to account for variation in cell diameter, the mass of release water (after 24 hours) was divided by the cross sectional area of each individual cell. This is summarized in the second to last column of Tables 5.1 and 5.2, as grams of release water per cm^2 of cross-sectional area. Based on the method by which the water was removed from the surface of the CT deposits, the accuracy of the mass of release contained within is estimated to be on the order of plus or minus 0.50 g.

Figure 5.1 shows a plot of grams of release water per cm^2 versus DHR for phosphogypsum dosages of 900 and 2000 g/m^3 along with their best fit trendlines. The trendlines shown within were generated using the built functions within Excel. From Figure 5.1 it is apparent that the greatest mass of release water per cm^2 occurred in the cell with largest DHR, while the least mass of release water per cm^2 occurred in the cell with the smallest DHR, regardless of dosage level. The test results shown in Table 5.1 and 5.2 indicated that the mass of release water was significantly impacted (> 10 % reduction) for DHR's less than or equal to 2.78, while test results for DHR's above 2.78 were not significantly impacted (< 10 % reduction). The slope of the best fit curve for the 900 g/m^3 series is flatter than the 2000 g/m^3 series, however both curves indicate a decreasing slope as the DHR increases from 1.14 to 4.04 suggesting that an upper limit to this relationship likely exists. Lastly, regardless of the

DHR, all samples with 2000 g/m^3 of PG, released more water than any sample with 900 g/m^3 of PG.

5.1.2 Effect on Normalized Grams of Release Water

To determine whether small DHR were more pronounced at high or lower dosages, the grams of release water per cm^2 was normalized to the amount of release water per cm^2 for the largest DHR within each dosage. As shown in Tables 5.1 and 5.2 and Figure 5.2, at a DHR of 1.14, the sample at 900 g/m^3 of PG experienced a 37 % reduction in mass of release water (compared to a DHR of 4.0), while at 2000 g/m^3 of PG the reduction was 52 %. Similarly, at DHR of 1.77 the sample at 900 g/m^3 of PG experienced a 13 % reduction in mass of release water (compared to a DHR of 4.0), while at 2000 g/m^3 of PG the reduction was 26 %. Clearly, DHR has a greater effect at higher phosphogypsum dosages.

5.2 Effect of Phosphogypsum Dosage

The effect of increasing phosphogypsum dosage on the dewatering characteristics of CT was examined using several different measurement techniques. They include using WRIT's, theory of hindered sedimentation, large strain consolidation tests and Scanning Electron Microscopy (SEM).

5.2.1 Index Test Results

To quantify the effect of increasing PG dosage on the water release characteristics of CT as measured using a standard WRIT, forty-nine standard WRIT's were conducted with dosages ranging from 600 to 3200 g/m^3 using a constant DHR of 2.91. This range of PG dosage was based on the fact that commercial production of CT was occurring with a dosage of 1400 g/m^3. At the time of our testing, the cost associated with transporting PG to the mine site was

a relatively high and therefore dosages beyond 3200 g/m^3 were not considered feasible. Additionally, there were potentially detrimental water quality issues associated with high PG dosages.

Table 5.3 summarizes the solids content, fines content, degree of saturation, PG dosage (g/m^3) and grams of release water as determined at the conclusion of a standard WRIT. All dosage levels with the exception of 1200, 1700, 2300 and 2900 g/m^3 had a minimum of two tests conducted. Of the forty-nine WRIT's, sixteen were performed at 900 g/m^3 and fourteen were performed at 3200 g/m^3.

From Table 5.3 it is apparent that although all forty-nine standard specimens were prepared using the standard laboratory mix design and mixed using the standard technique (see section 4.5.2), there are differences in solids content, fines content and degree of saturation. As shown in Table 5.3, the solids content ranged from 60.1 to 62.9 %, while the fines content and degree of saturation varied from 17.9 to 24.0 % and 89 to 97 %, respectively.

Figure 5.3 plots the grams of release water measured after 24 hours versus phosphogypsum dosage (g/m^3) for all tests shown in Table 5.3 along with a best fit trendline. From Figure 5.3, it is apparent that there is a significant range of water release rates corresponding to dosages ranging from 600 to 3200 g/m^3. Increasing the phosphogypsum dosage from 600 to 3200 g/m^3 causes the mass of release water to vary from a low of 4.3 g to a high of 83.4 g. The best fit trendline emphasizes that increasing the phosphogypsum dosage results in a corresponding increase in the mass of release water. The best fit trendline is steepest between phosphogypsum dosages of 600 and 900 g/m^3, and continuously decreases as the dosage increases up to 3200 g/m^3. The best fit trendline is heavily influenced by the large number of data points at 900 and 3200 g/m^3. This effect is apparent between dosages of 900 and 3200 g/m^3, where the best fit trendline tends to underestimate the observed water release

rate. Despite this, the best fit logarithmic curve has a regression coefficient of 0.89.

5.2.1.1 Partial Discussion of WRIT

The following discussion on the effect of PG dosage on WRIT results is required to place in context the manner in which subsequent test results are presented. See Chapter 6.0 for a full discussion of all research results.

As shown in Table 5.3, at 600 g/m^3 of PG the mass of release water varied from 4.3 to 5.5 g, while at 3200 g/m^3 the mass of release water varies from 52.0 to 83.4 g. This wide range of water release rates at a constant dosage level, would tend to suggest a lack of repeatability of the WRIT. However, as shown in Table 5.3 the fines content and solids content of each test varied slightly from the target value of 62 % solids and 20 % fines. Despite the apparent lack of repeatability of the index, the observed relationship between increasing PG dosage and increasing mass of release water as shown in Figure 5.3 is significant.

However, the wide range of water releases for duplicated tests at a constant phosphogypsum dosage was troublesome. Since the sand and bitumen are considered inert from reacting with the phosphogypsum, the trend observed in Figure 5.3 can be interpreted as increasing the ratio of PG to either fines and/or water. Reconsidering the data in Figure 5.3, and assuming all forty-nine samples had the same solids content and fines content (although they clearly did not) the abscissa of Figure 5.3 shows an increase in the ratio of PG to fines.

The concept of using PG to fines ratio (PGFR), as opposed to phosphogypsum dosage in g/m^3, was further investigated to resolve the apparent lack of repeatability of the WRIT and defend its usage (as an index test) in subsequent tests. Thus, the test results shown in Table 5.3 were re-analyzed to determine

bulk density, mass of fines per m^3, and ultimately, the ratio between the mass of PG (mg) and the mass of fines (kg) (PGFR). Using the solids content measured for each test, the bulk density was calculated using the specific gravity of the solids (G_s) and water (G_w) shown in Table 4.3. Based on this computed bulk density, the mass of fines per m^3 of CT was determined by multiplying the bulk density by both the solids content and fines content. Calculation A4 provides a detailed sample calculation of the bulk density, kilograms of fines per m^3 of CT and the PGFR for Test J199. This calculation results in PGFR being expressed in terms of mg/kg or parts per million (ppm).

Table 5.4 summarizes bulk density, mass of fines per $m^3$of CT, PG dosage (g/m^3), PGFR (ppm) and grams of release water for all test results originally shown in Table 5.3. The bulk density of the CT varied from 1587 to 1628 kg/m^3 and the mass of fines per m^3 of CT varied from 170 to 237 kg. The resulting PGFR's varied from a low of 2823 to a high of 16656 ppm.

Figure 5.4 plots the grams of release water versus PGFR (ppm) for all tests shown in Table 5.4 along with a best fit trendline. From Figure 5.4 it is clear that increasing the PGFR resulted in an increase in the mass of release water. Increasing the PGFR from approximately 4000 to 16000 ppm increases the mass of release water from approximately 10 to 75 grams. The best fit trendline has a slightly better correlation (R^2=0.93) than shown on Figure 5.3, supporting the general trend observed on Figure 5.3.

Graphically speaking, the major difference between the data points shown on Figures 5.3 and 5.4, is the slight spread in the data along the abscissa. Rather than plotting all test results at a pre-determined dosage (as was done on Figure 5.3), the minor deviations in solids content and fines content or actual PG dosage have been considered and all tests have been plotted at a unique value of PGFR.

This method considers the actual conditions which were present during the test and appears better suited to interpret future WRIT results.

To further examine the relationship between the water release rates and PGFR, Figures 5.5 and 5.6 show a close up view of the two large groups of test results at PGFR's of 4300 and 15000 ppm, respectively. From Figure 5.5 it is clear that increasing the PGFR results in a corresponding increase in the mass of release water. Increasing the PGFR from approximately 3700 to 4700, increases the mass of release water from approximately 2 to 14 grams, respectively. Similarly, from Figure 5.6 it is clear that increasing the PGFR from approximately 13500 to 16500 ppm increases the mass of release water from approximately 52 to 82 grams, respectively. The trends shown in Figures 5.5 and 5.6 both support the overall trend shown in Figure 5.4.

5.2.1.2 Summary of Index Test Results

The test results shown on Figures 5.3 through 5.6 all clearly show a relationship between the mass of release water and the amount of phosphogypsum present. Increasing the PG dosage, causes an increase in the mass of release water and the presence of an optimum dosage was not observed. The trend shown on Figure 5.3 resulted from increasing the dosage from 600 to 3200 g/m^3 while keeping the mass of fines relatively constant. However, the results shown on Figures 5.5 and 5.6 were a result of maintaining a constant PG dosage while the mass of fines in each specimen fluctuated from the target value as a result of standard laboratory error. The relationships shown on Figures 5.5 and 5.6 display the same relationship as shown on Figure 5.4 but do so on a much smaller scale. Thus, the wide range of water release rates observed at constant dosages of 900 and 3200 g/m^3 of PG, as shown on Figure 5.3 do not indicate a lack of repeatability in the index, but further emphasize the relationship between PGFR and mass of release water. Comparing Figure 5.4 with 5.3 indicates that

PGFR provides a better correlation than dosage (g/m^3) in terms of predicting the outcome of the WRIT. For this reason all subsequent WRIT results will be presented in this manner.

5.2.2 Behavior of CT / Water Interface During WRIT

To determine whether CT was experiencing hindered sedimentation and/or consolidation or both during the WRIT, the position of the CT / water interface was recorded over the entire 24 hour duration of the test. Figure 5.7 shows a plot of the interface height (cm) versus elapsed (seconds) for index tests at 900 $g/m^3$and 3200 g/m^3 having initial heights of 5.00 and 5.02 cm , respectively.

As shown in Figure 5.7, the movement of the interface in both tests is characterized by an immediate constant rate of downward movement (no induction period) followed by a period in which the rate of interface movement decreases rapidly. For each test a best fit linear line has been drawn through the data points which characterize a constant rate of movement. As shown the constant rate of movement lasted for approximately 25 000 and 29 000 seconds (7-8 hours) for the two tests shown. The slope of the best fit linear lines are $2.0 * 10^{-6}$ and $1.1 * 10^{-5}$ cm/s for the tests prepared with 900 and 3200 g/m^3 of PG, respectively.

Beyond the period of constant interface movement, the behavior of the two curves were significantly different. For the test with a dosage of 900 g/m^3, the interface shows almost no change in height during the remaining 17 hours of the test, as it decreased from 4.95 to 4.94 cm (0.2 % incremental strain). In contrast, the sample with a dosage of 3200 g/m^3 decreased from 4.68 to 4.58 cm (2.0 % incremental strain) over a similar time period. Over the 24 hour time period, the samples with a dosage of 900 and 3200 g/m^3 experienced a total change in height of 0.06 cm (1.2 % total strain) and 0.42 cm (8.4 % total strain), respectively. Note, that the results of the WRIT for these two samples

were previous shown in Tables 5.3 and 5.4 and are denoted as Test VB (900 g/m^3) and VA (3200 g/m^3).

5.2.3 Slurry Consolidometer Test Results

To quantify the effects of PG dosage on the compressibility and hydraulic conductivity of CT, a total of four samples were step loaded in the slurry consolidometers up to maximum vertical stress of 700 kPa. Two separate tests were conducted at dosages of 900 and 3200 g/m^3 of PG.

5.2.3.1 Compressibility Relationship at 900 g/m^3 of PG

Table 5.5 summarizes the vertical effective stress at the center of the sample, solids content and void ratio (at the end of each loading steps) for two samples, C&P-1 and C&P-3, with 900 g/m^3 of PG. The initial solids content, fines content and void of those samples was s=61.8 %, f=19.8 % and e=1.60 and s=63.3, f=20.9 % and e=1.51, respectively.

The vertical effective stress, calculated at the center of the specimen, ranged from a minimum of approximately 0.14 kPa to a maximum of 700 kPa. A vertical effective stress of 0.14 kPa represents the average self-weight stress at the center of the specimen after it equilibrated under its own self weight. The location within the sample where the effective stress was determined was only important when the effective stress was less than approximately 2.5 kPa. Beyond this stress level, the self weight component contributed less than 5 % of the total effective stress, and the external load dominated the stress distribution such that the effective stress was essentially uniform with depth.

The initial solids content (prior to loading) was determined at the start of each test using gravimetric analysis on two grab samples. The void ratio and solids contents shown in Table 5.5 represent the average equilibrium values as

calculated at the end of each loading step. Average void ratio at the end of each loading step was calculated using the total cumulative strain and the initial void ratio.

Figure 5.8 shows the variation in normalized void ratio as a function of average vertical effective stress for two slurry consolidometer samples (C&P-1 and C&P-3) both with 900 g/m^3 of PG. The normalized void ratio of sample C&P-1 decreases from 1.0 to 0.42 while the normalized void ratio of sample C&P-3 decreases from 1.0 to 0.34. Beyond 1.2 kPa the difference between the void ratio continues to decrease and the difference averages approximately 12 %. At the conclusion of test, the void ratios at 631 and 700 kPa were 0.66 and 0.51 for samples C&P-1 and C&P-3, respectively.

5.2.3.2 Compressibility Relationship at 3200 g/m^3 of PG

Table 5.6 summarizes the effective vertical stress at the center of the sample, solids content, and void ratio for two samples with 3200 g/m^3 of PG at the end of eleven loading steps. See section 5.2.3.1 for determination of effective stress, void ratio and solids content. The initial solids content, fines content and void of those samples was s=61.5 %, f= 20.0 % and e=1.62 and s=62.5 %, f= 20.6 % and e=1.56, respectively.

Figure 5.9 shows the variation in normalized void ratio as a function of effective stress for two slurry consolidometer samples (C&P-2 and C&P-4) both with 3200 g/m^3 of PG. The normalized void ratio of sample C&P-2 decreases from 1.0 to 0.28 while the void ratio of sample C&P-4 decreases from 1.0 to 0.33. At the conclusion of the test, the void ratios at 710 and 700 kPa were 0.46 and 0.52 for samples C&P-2 and C&P-4, respectively.

5.2.3.3 Comparison of Compressibility Relationships at 900 and 3200 g/m^3 of PG

As shown in the previous section the void ratios of the two samples at 900 g/m^3 were not unique for a given level of effective stress. This was also the case for the two samples at 3200 g/m^3. Therefore in order to facilitate a comparison between the compressibility characteristic as a function of dosage, the void ratios for the C&P-3 and C&P-4 were compared. It is the author's opinion that the test results obtained for C&P-3 and C&P-4 are more accurate than those for C&P-1 and C&P-2. After performing the first set of tests (C&P-1 and C&P-2) it was felt that due to operator inexperience and potential equipment problems the test results were potentially unreliable. Therefore, a second set of tests were performed by a senior engineering technician and are thought to be more reliable. For this reason, the compressibility (and hydraulic conductivity) result for C&P-1 and C&P-2 are shown for completeness, however only the test results from C&P-3 and C&P-4 will be discussed.

Figure 5.10 shows the variation in normalized void ratio as a function of effective stress for CT with 900 and 3200 g/m^3 of PG. As shown, the normalized void ratio of the sample with 900 g/m^3 of PG was always greater than the 3200 g/m^3 sample for the same level of effective stress. The best fit trendlines suggests that the behavior of the two materials appears similar from self weight up to 10 kPa, and also from 10 kPa up to 100 kPa. That is, up to an effective stress of 10 kPa the slope of the best fit curves are nearly identical. Similarly, between effective stresses of 10 and 100 kPa the trendlines are also parallel. Beyond 100 kPa the curves are convergent and intersect at an effective stress of 700 kPa. The void ratio as a function of time for each load step are shown in Figures C1 through C22 (Appendix C).

5.2.3.4 Hydraulic Conductivity Relationship at 900 g/m^3 of PG

Table 5.7 summarizes the vertical effective stress at the center of the sample, solids content, fines void ratio and average hydraulic conductivity for two

samples with 900 g/m^3 of PG at the end of eleven loading steps. As shown the fines void ratio for sample C&P-1 decreased from approximately 6.7 to 3.0 as the vertical effective stress was increased from 0.14 to 631 kPa, while the fines void ratio of sample C&P-3 decreased from approximately 5.5 to 2.3 as the vertical effective stress was increased from 0.2 to 700 kPa. The hydraulic gradient used to force water upwards or downward through the sample the end of each loading step ranged from 0.3 to 5.0.

The fines void ratios shown in Table 5.7 were based on the definitions presented in Section 3.3.16 and calculated using the void ratio, fines content and specific gravity of fines and bitumen together. As mentioned previously, the flow rate of water into or out of the sample was recorded as a function of elapsed time. The flow rate was calculated in terms of both cumulative and incremental flow rate. Cumulative flow rate was the total amount of flow divided by the total elapsed time, while the incremental flow rate was calculated based only on flow that occurred during a particular increment in time. The variation in flow rate versus time are included on Figures D1 through D11 in Appendix D for each of the eleven loading steps for sample C&P-3. As shown on Figures D1 through D11, the measured flow rates are generally the highest during the first 30 minutes of the test and then decrease until reaching a nearly constant value. The flow of water into or out of sample per loading step was observed for an average of approximately 185 minutes. Flow rate versus elapsed time plots for sample C&P-1 have not been included, as they are similar to those shown for C&P-3.

Figure 5.11 illustrates the relationship between fines void ratio and hydraulic conductivity for the two slurry consolidometer samples (C&P-1 and C&P-3), both with 900 g/m^3 of PG. As shown, the hydraulic conductivity of sample C&P-1 decreases from approximately $1.8 * 10^{-06}$ to $8.2 * 10^{-08}$ cm/s while the hydraulic conductivity of sample C&P-3 decreased from $1.2 * 10^{-06}$ cm/s to $1.03 * 10^{-07}$ cm/s. The data for C&P-1 has more scatter to it than the C&P-3 and the

measured hydraulic conductivity of C&P-1 was always lower than C&P-3, with the exception of the two data points near a fines void ratio of approximately 4.

5.2.3.5 Hydraulic Conductivity Relationship at 3200 g/m^3 of PG

Table 5.8 summarizes the vertical effective stress at the center of the sample, solids content, fines void ratio and average hydraulic conductivity for two samples with 3200 g/m^3 of PG at the end of eleven loading steps. As shown the fines void ratio for sample C&P-2 deceased from approximately 6.4 to 2.0 as the vertical effective stress was increased to 710 kPa, while sample C&P-4 decreased from 5.1 to 2.3 as effective stress increased to 700 kPa.

The fines void ratios shown in Table 5.8 were based on the definition presented in Section 3.3.16 and calculated using the void ratio, fines content and specific gravity of fines and bitumen together. The incremental and cumulative flow rate of water into or out of the sample was recorded as a function of elapsed time and are shown on Figures D12 through D22 in Appendix D for each of the eleven loading steps for sample C&P-4. Flow rate versus elapsed time plots for sample C&P-2 have not been included within, as they have the same shape (but different magnitude) as they are similar to those shown for C&P-4.

Figure 5.12 shows the variation in fines void ratio - hydraulic conductivity relationship for the two slurry consolidometer samples (C&P-2 and C&P-4) both with 3200 g/m^3 of PG. As shown, the hydraulic conductivity of sample C&P-2 decreases from $7.4 * 10^{-06}$ to $1.5 * 10^{-07}$ cm/s while the hydraulic conductivity of sample C&P-4 decreased from $1.9 * 10^{-06}$ cm/s to $2.6 * 10^{-07}$ cm/s. The hydraulic conductivity of sample C&P-2 was consistently greater than C&P-4.

5.2.3.6 Comparison of Hydraulic Conductivity Relationship at 900 and 3200 g/m^3 of PG

Figure 5.13 shows the variation in hydraulic conductivity (cm/s) as a function of fines void ratio for samples C&P-3 and C&P-4 with 900 and 3200 g/m^3 of PG, respectively. For reasons discussed in section 5.2.4.3. C&P-1 and C&P-2 are not included in the comparison discussion. Additionally, the hydraulic conductivity as determined during hindered sedimentation (from the linear portion of Figure 5.7) are included on Figure 5.13. However, these two values were not used to determine the best fit trendline.

From Figure 5.13 it is apparent that the hydraulic conductivity of the sample treated with 900 g/m^3 of PG is always lower than the 3200 g/m^3 sample at the same fines void ratio. The best fit trendlines shown in Figure 5.13 are essentially parallel for the range of fines void ratios tested. The hydraulic conductivity of the 3200 g/m^3 sample is approximately 2.5 times higher than the 900 g/m^3 at the same fines void ratio. For both the 900 and 3200 g/m^3 specimens, the hydraulic conductivity calculated from the theory of hindered sedimentation shows a good correlation with the extrapolated line.

5.2.4 Scanning Electron Microscopy (SEM)

5.2.4.1 Introduction

In order to visually assess the effect of phosphogypsum dosage on the fabric of CT, both cryogenic and variable pressure SEMs were utilized. In preparing a sample for observation with the SEM, standard WRIT was occasionally performed on the same sample. This provided both qualitative (SEM images) and quantitative (WRIT) results for the same sample.

Table 5.9 summarizes SEM type, solids content, fines content, bulk density, PG dosage (g/m^3), PGFR (ppm) and mass of water released during a standard WRIT. Only two of the five CT specimens that were observed with the cryogenic SEM had associated WRIT completed, while all three variable pressure SEMs

specimens had associated WRIT completed. In order to correlate the qualitative observations of the SEM images with the predicted quantitative behavior from the WRIT, Figure 5.14 shows actual test results from 5 WRIT which were performed in conjunction with the SEM work along with the previously developed trendline.

Five CT samples with PG dosages of 900, 1400, 2000, 2600 and 3200 g/m^3 were observed with the cryogenic SEM, while three CT samples with PG dosages of 600, 900 and 3200 g/m^3 were observed with the variable pressure SEM. The following sections outline the qualitative changes observed in the fabric of the fines as the PG dosage was increased from 900 to 3200 g/m^3. In general the fabric of the fines of the CT was observed to have the characteristics card-house structure. It is this card-house arrangement which is believed to explain the high water content capacity of the fines within CT.

5.2.4.2 Cryogenic SEM Images with 900 g/m^3 of PG.

The three images collected for this specimen, prepared with a 900 g/m^3 of PG, are shown in Figures 5.15, 5.16 and 5.17 at magnifications of 15, 100 and 200 times, respectively. Figure 5.15 shows an overview of the entire sample at low magnification and shows sand grains suspended within fines structure. The top and bottom portions of the image are out of focus as a fracture surface slopes away from the bottom of the image towards the top. Thus the central portion of the image is the clearest at this low magnification. As seen in the Figure 5.15 and denoted by arrow "A", the sand grains are easily distinguished and appear to be at the surface of the fracture created during sample preparation. At this magnification the fabric of the fines is very homogeneous and appears to be continuous with no particular pattern or linear structure.

Figure 5.16 shows a close up view of the same sample at a magnification of 100 times in which there is a heavy concentration of sand grains around the perimeter of the left side. Again, the sand grains are easily identifiable and range in diameter from approximately 50 to 185 μm. Most of the sand grains appear to have gap between their outer edge and the adjacent fines, as denoted by arrow "B". The width of the gap is approximately 15 μm. The fines structure, which appeared very homogeneous with no pattern or structure at the previous magnification, now shows the typical card house structure of the fines. Nearly all of the fines which appear parallel to the viewing direction, are oriented parallel to each other and platelets are approximately 3 to 5 μm thick while the alignment spacing is approximately 8 to 15 μm. The presence of cross members make the voids between the fines appear rectangular in shape. As denoted on the figure, there is region in which the voids appear to square like or circular in shape.

Lastly, Figure 5.17 shows a close up of the center of the previous image, now at a magnification of 200 times. This figure clearly illustrates that the sand grains which are at the surface were the fracture occurred are essentially bare and do not have a significant amount of fines adhered to the surface of the sand grain. This figures shows in more detail the predominately rectangular shape of the fines structure (although some square/circular structure is shown in the upper right corner) as well as the gap between sand grains and the adjacent fines.

In accordance with double layer theory the electric double layer of kaolinite clays is expected to be on the order of 10 Angstroms. Given that the alignment spacing of the card house structure is on the order to 80,000 to 150,000 angstroms (8 to 15 μm) the alignment spacings seen with this set of SEM images are not to be construed as the electric double layer thickness.

5.2.4.2.1 Cryogenic SEM Images with 1400 g/m^3 of PG.

The images collected for the specimen prepared with 1400 g/m^3 of PG are shown in Figures 5.18 and 5.19 at magnifications of 100 and 500 times, respectively. Figure 5.18 shows the card house structure of the fines and is very similar in appearance to the previous SEMs with a dosage of 900 g/m^3. That is the gap around the perimeter of the sand grains and the typical rectangular shape of the fines structure. However, as denoted by arrow "A", some fines are adhered to the surface of the sand grains. Figure 5.19 is dominated by the presence of two sand grains in the lower portion of the image, which have a "diameter" of approximately 110 μm. This figure illustrates the semi-rectangular shape of the fines, however voids with square like or circular shapes are also present.

5.2.4.2.2 Cryogenic SEM Images with 2000 g/m^3 of PG.

The images collected for the specimen prepared with 2000 g/m^3 of PG are shown in Figures 5.20 and 5.21 at a magnifications of 15 and 200 times. Figure 5.21 shows the distribution of sand grains within the fines. Figure 5.21 is dominated by the presence of a sand grain approximately 280 μm in diameter. Along the bottom edge of this sand grain there is gap approximately 3 μm wide, while the remaining edges of the sand grain appear to be in direct contact with the adjacent fines. This images clearly illustrates the presence of fines adhered to the face of a sand grain. Finally, this image shows the typical card house structure of the fines.

5.2.4.2.3 Cryogenic SEM Images with 2600 g/m^3 of PG.

The two images collected for the specimen prepared with 2600 g/m^3 of PG are shown in Figures 5.22 and 5.23 at a magnification of 15 and 100 times. Figure 5.22 shows an overview of the entire sample at low magnification. As seen in

Figure 5.22 , the sand grains are easily distinguished, are well distributed within the fines matrix which appears to have an irregular porous structure.

Lastly, Figure 5.23 shows a close up view (100X) of the fines matrix. This image shows that the majority of the sand grain are in direct contact with the adjacent fines matrix and the fine matrix has a generally square or circular shape, rather than the rectangular structure observed previously.

5.2.4.2.4 Cryogenic SEM Images with 3200 g/m^3 of PG.

The three images collected for the specimen prepared with 3200 g/m^3 of PG are shown in Figures 5.24, 5.25 and 5.26 at magnifications of 15, 100 and 200 times, respectively. Figure 5.24 shows an overview of the entire sample at low magnification. As seen in Figure 5.24 , the sand grains are not as easily distinguished and structure of the fines appears to appears to have a porous or honeycomb type structure. Additionally, as denoted by arrow "A" there are three dark irregularly shaped features which are up to 0.25 mm in size. These are most likely air pockets as a result of entertainment during mixing, or "cavities" left behind after fracturing occurred. These voids are not anticipated to be continuous with depth. Figure 5.25 at a magnification of 100 times show the generally porous nature and circular shape of the fines matrix. As denoted by arrow "A", regions of the sample have a very parallel orientation, with an alignment spacing of approximately 10 μm. This portion of the image is similar to the fines matrix shown in Figure 5.17 with 900 g/m^3 of PG. However, the upper portion of the image shows are series of circular, square or rectangular voids which are on the order of 30 to 80 um in size. Additionally, as denoted by arrow "B", sand grains are completely covered with fines and are difficult to delineate.

Lastly, Figure 5.23 shows a close up view now at a magnification of 200 times. This image shows a fines structure in which appears to be dominated by the presence of square like or circular void shapes. Additionally, at the center of the image it shows a sand grain which is essentially covered by fines.

5.2.4.2.5 Variable Pressure SEM Images with 600 g/m^3 of PG.

The two variable pressure SEM (VPSEM) images collected for the specimen prepared with 600 g/m^3 of PG are shown in Figures 5.27 and 5.28 at magnifications of 266 and 690 times, respectively. Figure 5.27 shows an overview of the entire sample at low magnification and shows the spherical shape of the sample. Figure 5.27 is dominated by the presence of a large crack which formed on the surface of the CT during the vacuuming procedure. Approximately 80 % of the surface for the CT, appears to be very homogeneous with no particular pattern and sand grains are not easily discerned. The remaining 20 % of the surface displays an apparent rectangular structure, as identified by the clouded region.

Figure 5.28 shows a close up view (690X) of linear structure inside the clouded region shown in the previous image. In the central portion of the image, the fines appear parallel to the viewing direction, are oriented parallel to each other with an alignment spacing of approximately 10 to 17 μm. The thickness of the platelets are approximately 3 to 10 μm and they have cross members which make the voids between the fines appear rectangular in shape. Additionally, there appears to be an absence of sand grains within the area where the fines are orientated parallel to each other. The fines around the exterior portion of the image appear to be orientated perpendicular to the viewing direction and as such do not appear to have the linear structure as observed in the central portion.

Within the exterior portion of the image, sand grains are moderately discernible are in intimate contact with the surrounding fines matrix.

5.2.4.2.6 Variable Pressure SEM Images with 900 g/m^3 of PG.

The two VPSEM images collected for the specimen prepared with 900 g/m^3 of PG are shown in Figures 5.29 and 5.30 at magnifications of 286 and 690 times, respectively. Figure 5.29 shows an overview of the entire sample at low magnification and shows the spherical shape of the sample. Figure 5.29 is dominated by the presence of a single large crack that formed on the surface of the CT during the vacuuming procedure. The region on either side of the crack appears to have a porous texture while the remainder of the surface appears to be very homogeneous with no particular pattern and sand grains are not easily discerned.

Figure 5.30 shows a close up view of linear structure now at a magnification of 690 times. Fines which are orientated parallel to the viewing direction cover approximately 50 % of total area shown in Figure 5.30. The fines structure which is parallel to the viewing direction is characterized by a rectangular shape with an alignment spacing of approximately 10 to 17 μm.

5.2.4.3 Variable Pressure SEM Images with 3200 g/m^3 of PG

The two VPSEM images collected for the specimen prepared with 3200 g/m^3 of PG are shown in Figures 5.31 and 5.32 at magnifications of 227 and 690 times, respectively. Figure 5.31 shows an overview of the entire sample at low magnification and shows the spherical shape of the sample. Figure 5.31 is dominated by the presence of the two ellipsoidally shaped regions. The remainder of the image contains an irregular porous structure in which sand grains are not easily discerned.

Figure 5.32 shows a close up view (690 X) of the upper of the two ellipsoidally shaped regions. The fines in the central portion of the image are oriented parallel to each other with an alignment spacing of approximately 10 to 17 μm in length. The remainder of the fines which are parallel to the viewing direction have irregularly shaped void spaces.

Table 5.1 Effect of Diameter-to-Height Ratio (DHR) at 900 g/m^3

Test	Solids Content	Fines Content	PGFR (ppm)	Diameter (cm)	DHR	Release Water (g)	Release Water per cm^2	Normalized Grams per cm^2 +
J14	61.6%	19.1%	4748	5.71	1.14	1.7	0.066	0.63
J15	61.9%	19.0%	4760	8.86	1.77	5.6	0.091	0.87
J16	61.9%	19.0%	4760	13.9	2.78	13.4	0.088	0.84
J17	61.6%	19.1%	4748	14.55	2.91	16.6	0.100	0.95
J18	61.6%	18.8%	4832	20.22	4.04	33.6	0.105	1.00

+ Ratio of Grams of Release Water per cm^2 as compared to Test J18.

Table 5.2 Effect of Diameter-to-Height Ratio (DHR) at 2000 g/m^3

Test	Solids Content	Fines Content	PGFR (ppm)	Diamter (cm)	DHR	Release Water (g)	Release Water per cm^2	Normalized Grams per cm^2 [+]
J9	60.9%	19.8%	10408	5.71	1.14	5.0	0.195	0.48
J10	61.7%	19.1%	10544	8.86	1.77	18.5	0.300	0.74
J11	61.7%	19.1%	10544	13.9	2.78	51.4	0.339	0.84
J12	60.9%	19.8%	10408	14.55	2.91	64.1	0.386	0.96
J13	61.1%	19.7%	10412	20.22	4.04	129.5	0.403	1.00

[+] Ratio of Grams of Release Water per cm^2 as compared to Test J13.

Table 5.3 Water Release Index Test (WRIT) Results for PG dosages from 600 to 3200 g/m^3

Test	Solids Content	Fines Content	S_r	PG Dosage (g/m^3)	Grams of Release Water
J199	62.5%	19.8%	91%	600	4.9
J200	62.3%	20.4%	92%	600	4.9
VP3	62.9%	20.8%	94%	600	5.5
VP10	62.1%	20.1%	95%	600	4.3
J1	60.5%	19.8%	n.m.	900	15.2
J2	60.5%	20.0%	n.m.	900	15.4
J17	61.6%	19.1%	96%	900	16.6
VB	61.3%	19.6%	97%	900	14.9
S-5	61.2%	21.5%	92%	900	10.1
S-7	61.1%	21.0%	91%	900	5.2
S-9	61.3%	21.6%	92%	900	8.6
S-11	61.3%	22.2%	90%	900	8.0
M-1	61.3%	21.4%	93%	900	6.8
AS-3	62.2%	22.8%	95%	900	5.7
E1	62.7%	23.3%	93%	900	4.2
VP4	62.5%	20.3%	97%	900	8.3
VP7	62.3%	21.1%	90%	900	7.7
VP11	61.8%	20.9%	94%	900	10.7
C&P-1	61.8%	19.8%	95%	900	14.0
C&P-1B	62.7%	19.8%	95%	900	12.6
J3	61.1%	19.0%	n.m.	1200	39.3
J4	60.3%	19.3%	n.m.	1400	31.9
J5	61.2%	20.4%	n.m.	1400	46.9
J23	61.2%	20.0%	n.m.	1400	32.6
SEM100	62.2%	19.2%	n.m.	1400	30.6
J6	61.6%	19.8%	n.m.	1700	59.5
J7	61.1%	20.6%	n.m.	2000	69.9
J8	60.9%	21.0%	n.m.	2000	64.7
J12	60.9%	19.8%	n.m.	2000	64.1
M-2	61.0%	21.8%	94%	2000	46.1
SEM200	61.9%	19.8%	n.m.	2000	59.6
J19	61.3%	20.4%	n.m.	2300	67.6
J20	60.1%	17.9%	n.m.	2600	76.1
SEM300	62.0%	20.2%	n.m.	2600	69.0
J21	61.0%	19.7%	n.m.	2900	82.7
J22	60.8%	20.3%	n.m.	3200	83.1
VA	61.1%	19.7%	97%	3200	77.2
S-6	60.7%	21.4%	93%	3200	74.2
S-8	60.9%	21.4%	89%	3200	69.1
S-10	61.1%	22.1%	92%	3200	65.6
S-12	61.1%	22.0%	93%	3200	62.4
M-3	61.0%	21.9%	94%	3200	64.2
E3	62.4%	22.6%	98%	3200	58.6
E4	61.4%	24.0%	94%	3200	52.0
E5	62.2%	22.9%	94%	3200	56.0
VP5	61.6%	21.2%	97%	3200	71.9
VP12	62.8%	20.5%	96%	3200	65.4
C&P-2	61.5%	20.0%	94%	3200	83.4
SEM400	61.6%	20.0%	n.m.	3200	77.6

n.m. = not measured

Table 5.4 Re-evaluating WRIT Results for PG dosages from 600 to 3200 g/m^3

Test	ρ_{bulk} (kg/m^3)	Mass of Fines per m^3 (kg)	PG Dosage (g/m^3)	PGFR (ppm)	Grams of Release Water
J199	1622	201	600	2984	4.9
J200	1620	206	600	2911	4.9
VP3	1628	213	600	2823	5.5
VP10	1615	201	600	2978	4.3
J1	1592	191	900	4706	15.2
J2	1590	192	900	4683	15.4
J17	1608	190	900	4748	16.6
VB	1603	192	900	4676	14.9
S-5	1602	211	900	4256	10.1
S-7	1600	205	900	4394	5.2
S-9	1603	213	900	4230	8.6
S-11	1603	218	900	4124	8.0
M-1	1604	211	900	4269	6.8
AS-3	1617	229	900	3928	5.7
E1	1625	237	900	3794	4.2
VP4	1623	206	900	4366	8.3
VP7	1619	213	900	4231	7.7
VP11	1611	208	900	4322	10.7
C&P-1	1611	197	900	4559	14.0
C&P-1B	1625	202	900	4461	12.6
J3	1600	186	1200	6448	39.3
J4	1587	185	1400	7587	31.9
J5	1602	200	1400	7005	46.9
J23	1602	196	1400	7141	32.6
SEM100	1618	193	1400	7254	30.6
J6	1608	196	1700	8665	59.5
J7	1600	201	2000	9953	69.9
J8	1598	205	2000	9770	64.7
J12	1597	192	2000	10408	64.1
M-2	1599	213	2000	9398	46.1
SEM200	1614	198	2000	10107	59.6
J19	1603	201	2300	11467	67.6
J20	1584	170	2600	15289	76.1
SEM300	1615	202	2600	12877	69.0
J21	1598	192	2900	15133	82.7
J22	1596	197	3200	16275	83.1
VA	1599	192	3200	16656	77.2
S-6	1594	207	3200	15476	74.2
S-8	1597	209	3200	15344	69.1
S-10	1600	216	3200	14806	65.6
S-12	1600	215	3200	14906	62.4
M-3	1599	213	3200	14992	64.2
E3	1621	228	3200	14020	58.6
E4	1605	236	3200	13536	52.0
E5	1617	230	3200	13894	56.0
VP5	1609	210	3200	15227	71.9
VP12	1628	210	3200	15228	65.4
C&P-2	1606	197	3200	16227	83.4
SEM400	1608	198	3200	16172	77.6

Table 5.5 Summary of Compressibility Test Results at 900 g/m^3

Test	σ_v' at Center (kPa)	Solids Content (%)	Fines Content (%)	Void Ratio
C&P-1	start	61.8	19.8	1.60
C&P-1	0.14	63.1	19.8	1.51
C&P-1	0.86	67.9	19.8	1.22
C&P-1	2.65	72.5	19.8	0.98
C&P-1	4.99	73.5	19.8	0.94
C&P-1	10.1	74.9	19.8	0.87
C&P-1	20.3	75.8	19.8	0.83
C&P-1	19.1	75.8	19.8	0.83
C&P-1	46.0	77.1	19.8	0.77
C&P-1	91.6	78.2	19.8	0.72
C&P-1	631.0	79.6	19.8	0.66
C&P-3	start	63.3	20.9	1.51
C&P-3	0.2	67.7	20.9	1.23
C&P-3	1.2	72.0	20.9	1.01
C&P-3	2.6	74.3	20.9	0.90
C&P-3	5	75.3	20.9	0.85
C&P-3	10	76.7	20.9	0.79
C&P-3	20	77.5	20.9	0.75
C&P-3	40	78.4	20.9	0.71
C&P-3	80	79.2	20.9	0.68
C&P-3	160	80.6	20.9	0.62
C&P-3	277	82.0	20.9	0.57
C&P-3	700	83.4	20.9	0.51

Table 5.6 Summary of Compressibility Test Results at 3200 g/m^3

Test	σ_v' at Center (kPa)	Solids Content (%)	Fines Content (%)	Void Ratio
C&P-2	start	61.5	20.0	1.62
C&P-2	0.13	64.3	20.0	1.44
C&P-2	0.92	69.2	20.0	1.15
C&P-2	1.88	72.3	20.0	0.99
C&P-2	3.04	73.4	20.0	0.94
C&P-2	4.92	74.6	20.0	0.88
C&P-2	10.0	76.1	20.0	0.81
C&P-2	20.0	77.0	20.0	0.77
C&P-2	46.0	78.7	20.0	0.70
C&P-2	91.6	79.9	20.0	0.65
C&P-2	710.9	84.9	20.0	0.46
C&P-2	710.9	84.9	20.0	0.46
C&P-4	start	62.5	20.6	1.56
C&P-4	0.2	69.2	20.6	1.15
C&P-4	1.2	73.6	20.6	0.93
C&P-4	2.6	76.2	20.6	0.81
C&P-4	5	77.4	20.6	0.76
C&P-4	10	79.1	20.6	0.69
C&P-4	20	80.2	20.6	0.64
C&P-4	40	80.8	20.6	0.62
C&P-4	80	81.4	20.6	0.59
C&P-4	160	81.9	20.6	0.57
C&P-4	293	82.5	20.6	0.55
C&P-4	700	83.3	20.6	0.52

Table 5.7 Summary of Hydraulic Conductivity Test Results at 900 g/m^3

Test	σ_v' at Center (kPa)	Solids Content (%)	Fines Content (%)	Fines Void Ratio (efb)	Hydraulic Conductivity (cm/s)
C&P-1	start	61.8	19.8	7.33	1.99E-06
C&P-1	0.14	63.1	19.8	6.72	1.80E-06
C&P-1	0.86	67.9	19.8	5.43	3.85E-07
C&P-1	2.65	72.5	19.8	4.37	5.98E-07
C&P-1	4.99	73.5	19.8	4.15	1.94E-07
C&P-1	10.1	74.9	19.8	3.86	6.12E-07
C&P-1	20.3	75.8	19.8	3.66	2.43E-07
C&P-1	19.1	75.8	19.8	3.66	2.16E-07
C&P-1	46.0	77.1	19.8	3.42	1.73E-07
C&P-1	91.6	78.2	19.8	3.21	1.49E-07
C&P-1	631.0	79.6	19.8	2.95	8.78E-08
C&P-1	631.0	79.6	19.8	2.95	8.22E-08
C&P-3	start	63.3	20.9	6.69	n/a
C&P-3	0.2	67.7	20.9	5.47	1.22E-06
C&P-3	1.2	72.0	20.9	4.46	4.42E-07
C&P-3	2.6	74.3	20.9	3.97	4.06E-07
C&P-3	5	75.3	20.9	3.78	3.04E-07
C&P-3	10	76.7	20.9	3.50	3.09E-07
C&P-3	20	77.5	20.9	3.33	3.05E-07
C&P-3	40	78.4	20.9	3.17	2.45E-07
C&P-3	80	79.2	20.9	3.02	2.11E-07
C&P-3	160	80.6	20.9	2.77	1.73E-07
C&P-3	277	82.0	20.9	2.52	1.61E-07
C&P-3	700	83.4	20.9	2.28	1.03E-07

Table 5.8 Summary of Hydraulic Conductivity Test Results at 3200 g/m^3

Test	σ_v' at Center (kPa)	Solids Content (%)	Fines Content (%)	Fines Void Ratio (efb)	Hydraulic Conductivity (cm/s)
C&P-2	start	61.5	20	7.37	1.13E-05
C&P-2	0.13	64.3	20	6.39	7.42E-06
C&P-2	0.92	69.2	20	5.12	1.15E-06
C&P-2	1.88	72.3	20	4.41	6.25E-07
C&P-2	3.04	73.4	20	4.16	4.71E-07
C&P-2	4.9	74.6	20	3.91	1.72E-07
C&P-2	10.0	76.1	20	3.62	6.58E-07
C&P-2	20.0	77.0	20	3.44	2.98E-07
C&P-2	46.0	78.7	20	3.11	4.77E-07
C&P-2	91.6	79.9	20	2.89	3.75E-07
C&P-2	710.9	84.9	20	2.04	1.27E-07
C&P-2	710.9	84.9	20	2.04	1.47E-07
C&P-4	start	62.5	20.6	6.91	n/a
C&P-4	0.2	69.2	20.6	5.11	1.92E-06
C&P-4	1.2	73.6	20.6	4.13	1.23E-06
C&P-4	2.6	76.2	20.6	3.60	1.21E-06
C&P-4	5	77.4	20.6	3.36	1.08E-06
C&P-4	10	79.1	20.6	3.05	7.01E-07
C&P-4	20	80.2	20.6	2.84	6.85E-07
C&P-4	40	80.8	20.6	2.74	5.87E-07
C&P-4	80	81.4	20.6	2.62	5.31E-07
C&P-4	160	81.9	20.6	2.54	3.95E-07
C&P-4	293	82.5	20.6	2.45	3.46E-07
C&P-4	700	83.3	20.6	2.30	2.55E-07

Table 5.9 Summary of SEM Samples

Test	SEM Type	Solids	Fines	Dosage (g/m^3)	PGFR (ppm)	Mass of Release Water (g)
VP10	V.P.	62.1%	20.1%	600	2977	4.3
SEM1	Cryogenic	61.9%	21.2%	900	4256	na
VP11	V.P.	61.8%	20.9%	900	4321	10.7
SEM3	Cryogenic	61.8%	21.0%	1400	6687	na
SEM200	Cryogenic	61.9%	19.8%	2000	10107	59.6
SEM5	Cryogenic	61.8%	22.2%	2600	11748	na
VP12	V.P.	62.8%	20.5%	3200	15228	65.4
SEM400	Cryogenic	61.6%	20.0%	3200	16172	77.6

V.P. - Variable Pressure

na = no WRIT performed in conjunction with SEM work.

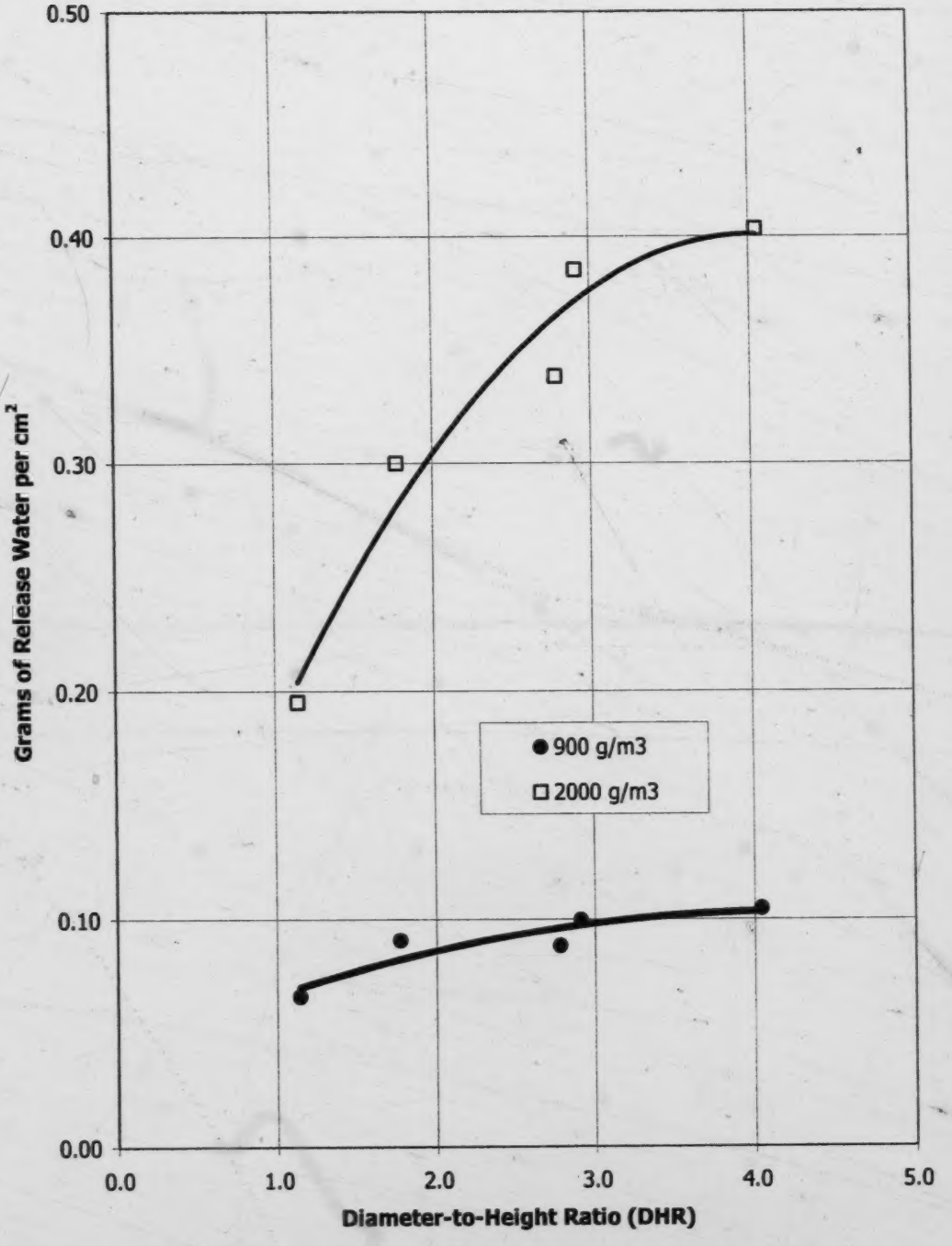

Figure 5.1 Effect of Diameter-to-Height Ratio (DHR) on grams of release water per cm^2

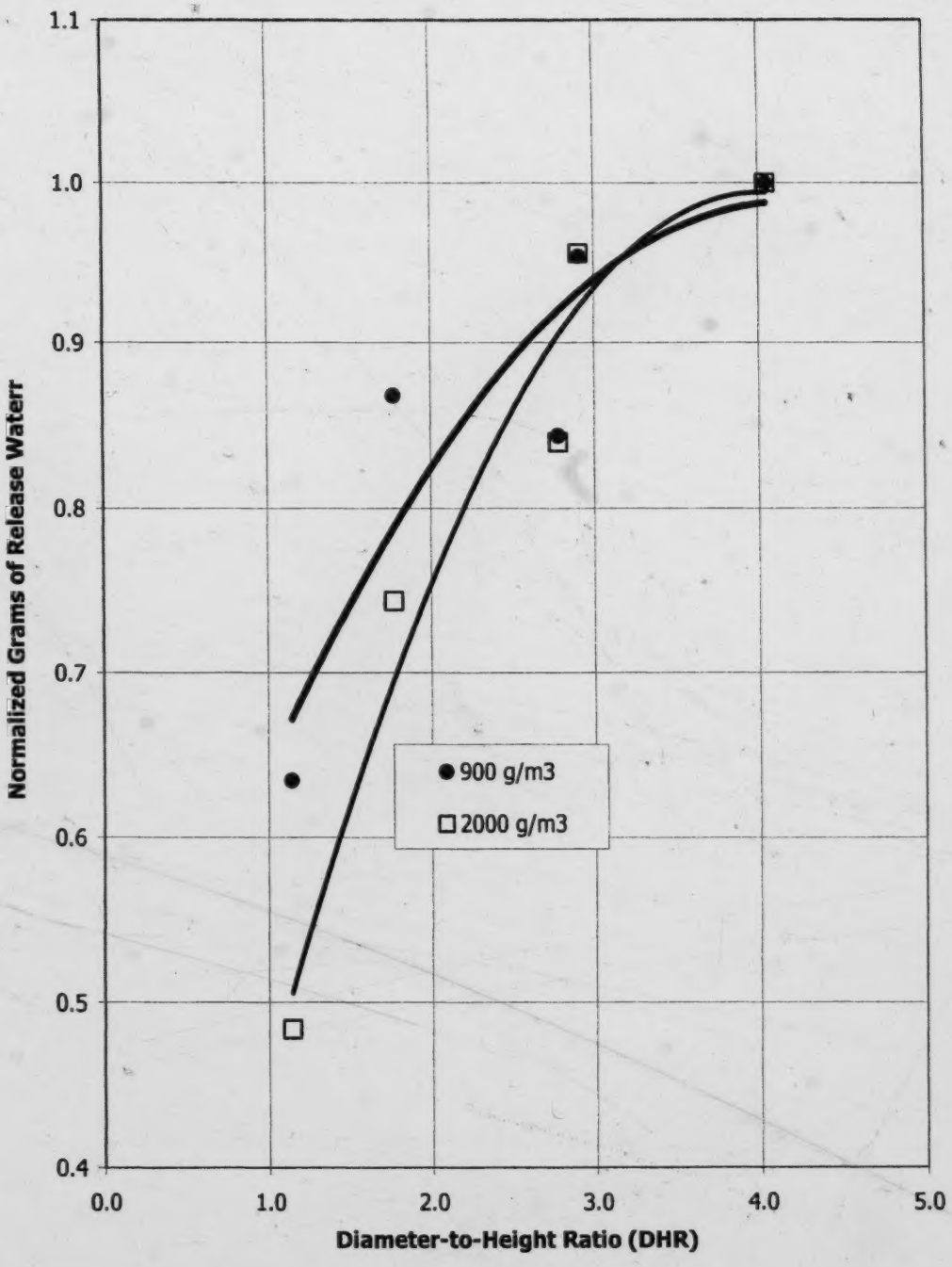

Figure 5.2 Effect of Diameter-to-Height Ratio (DHR) on normalized grams of release water

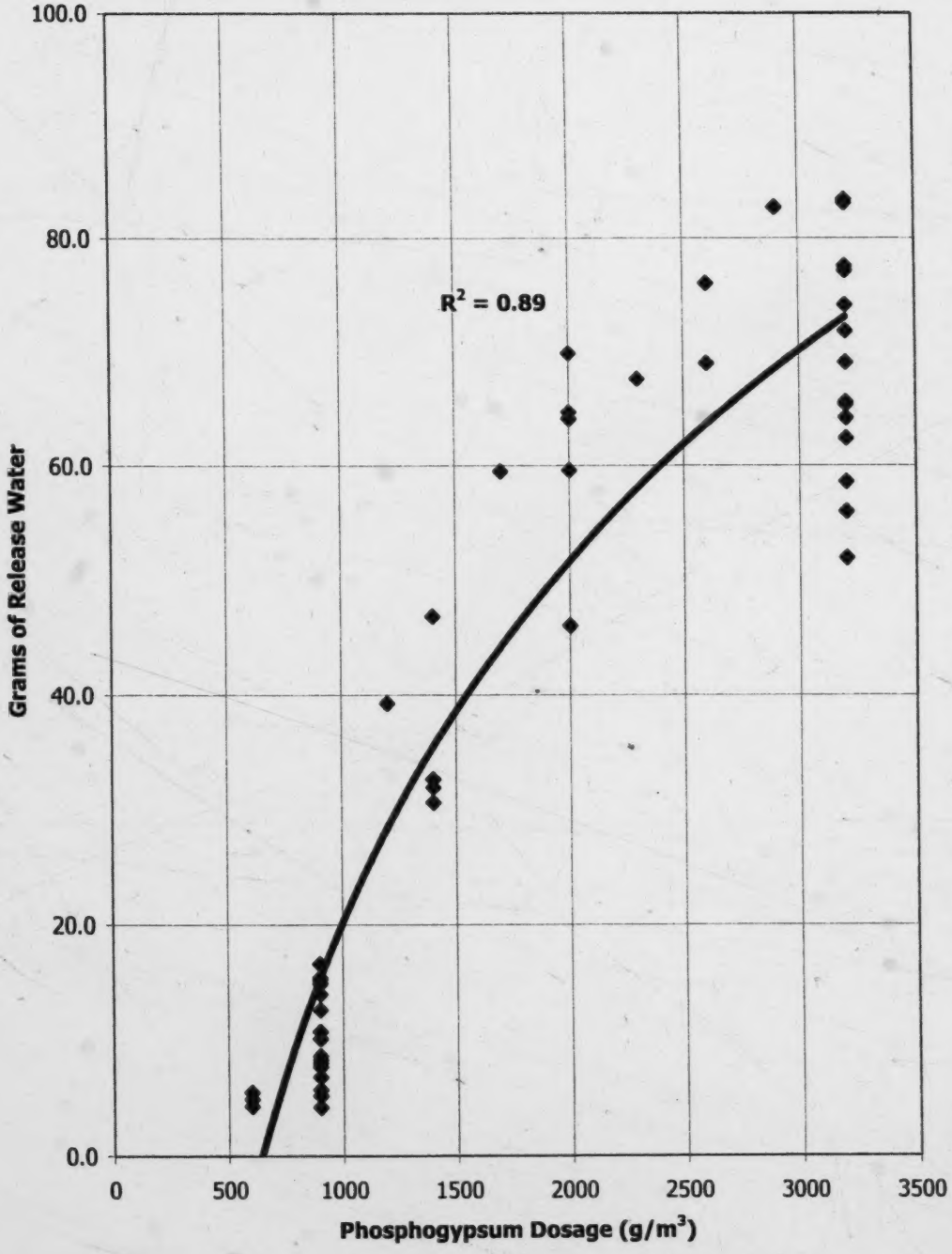

Figure 5.3 Effect of increasing PG dosage (g/m^3) on WRIT results

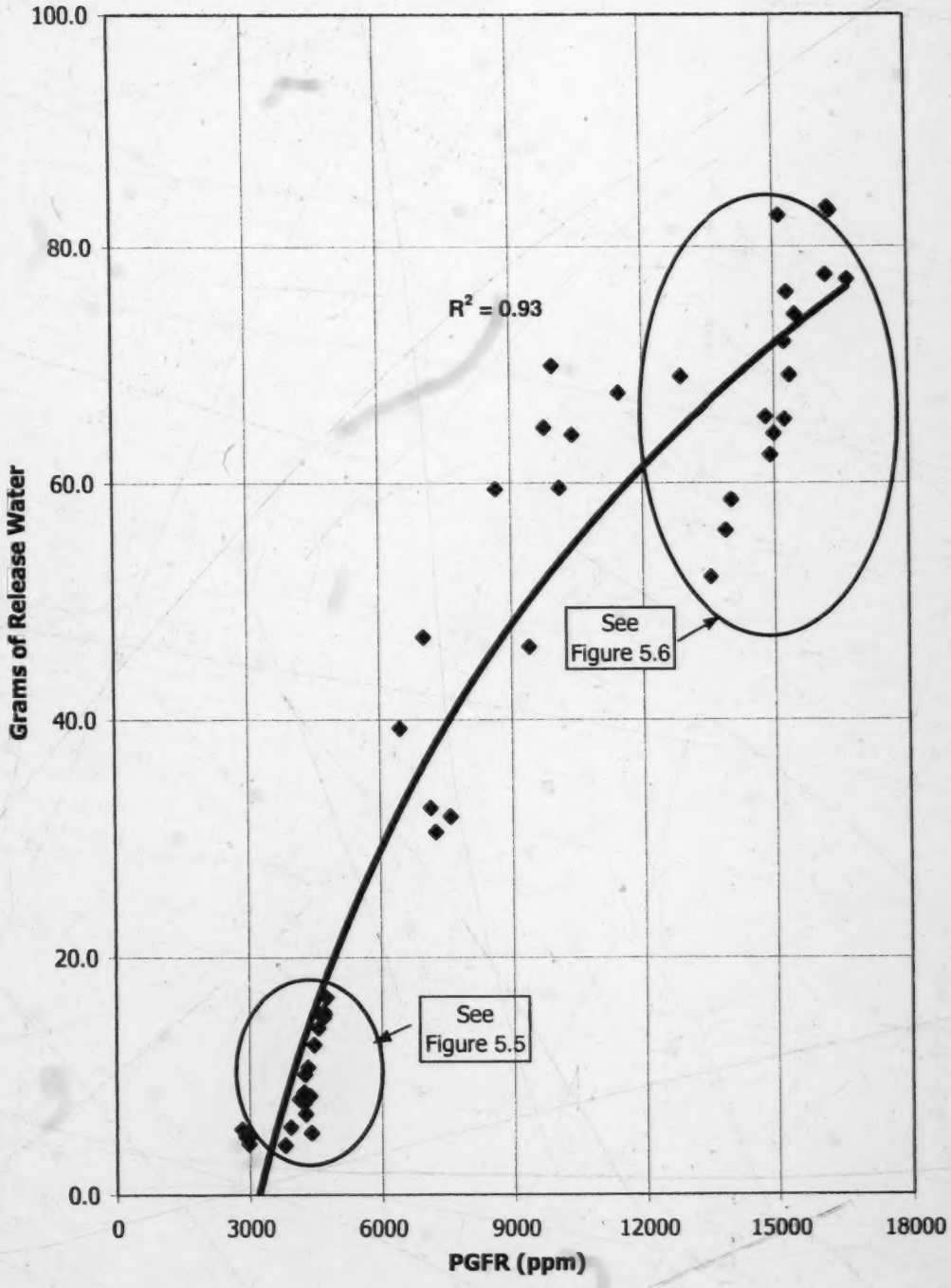

Figure 5.4 Effect of increasing PGFR on WRIT results

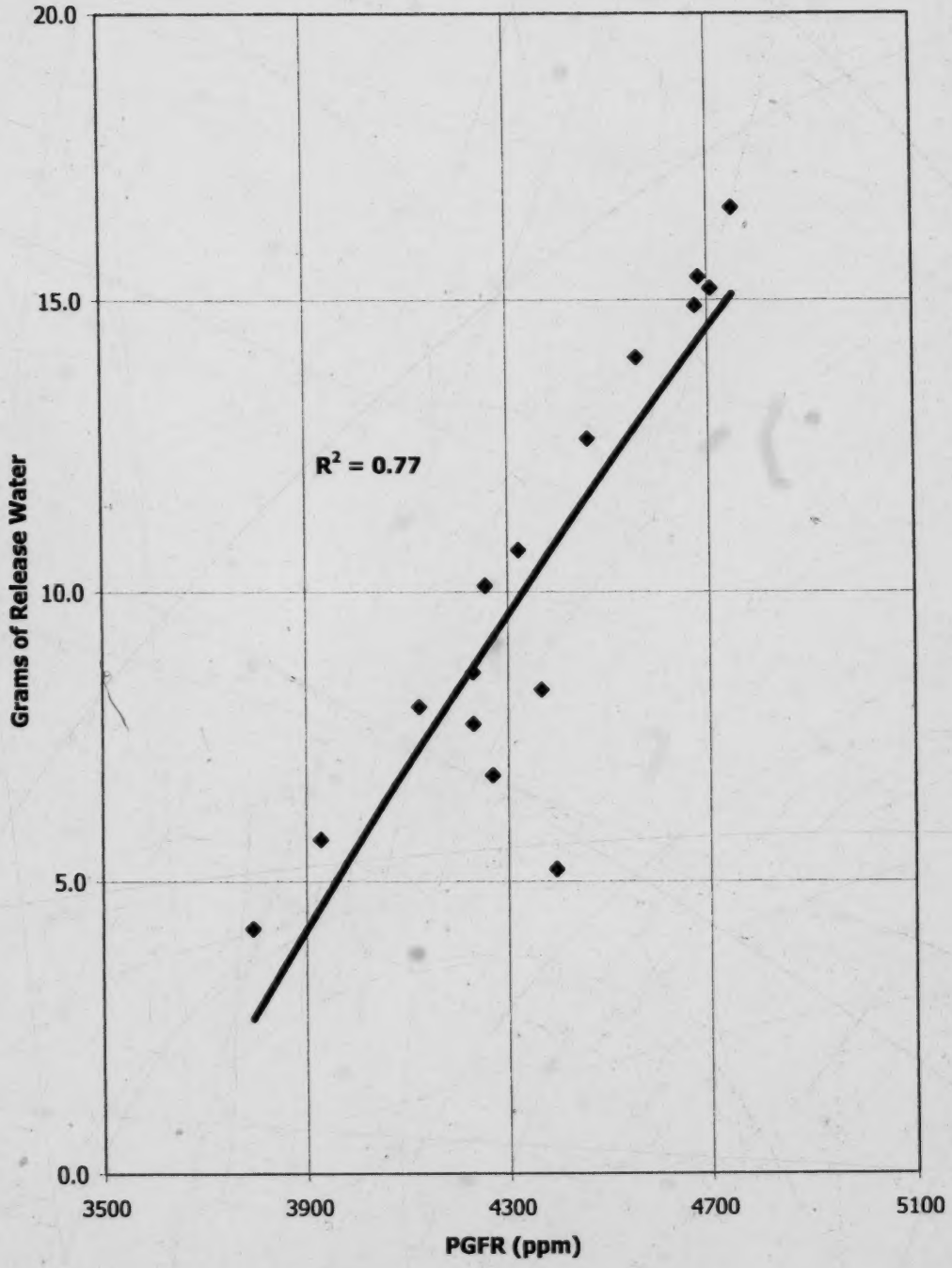

Figure 5.5 Effect of low PGFR's on WRIT results

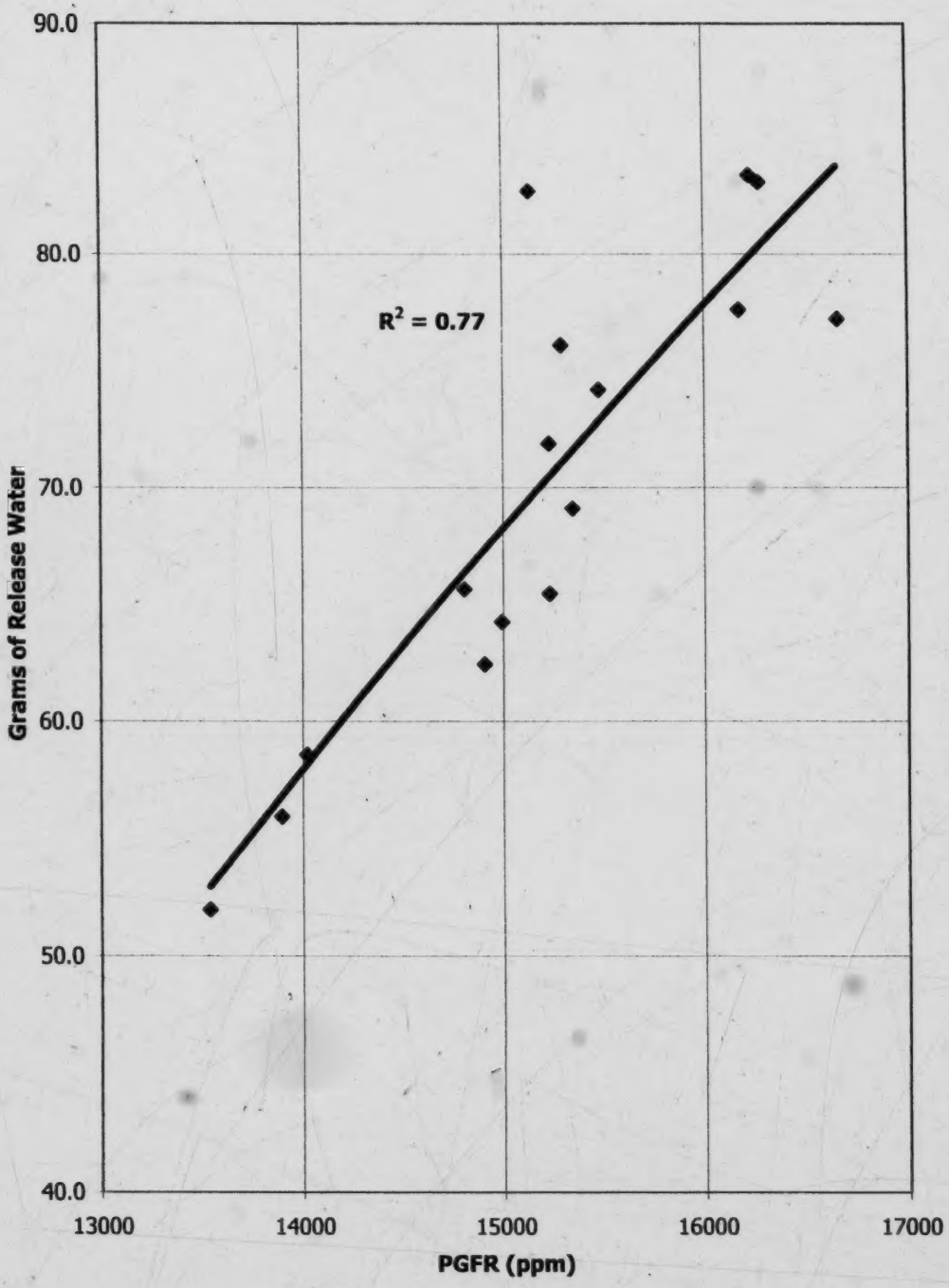

Figure 5.6 Effect of high PGFR's on WRIT results

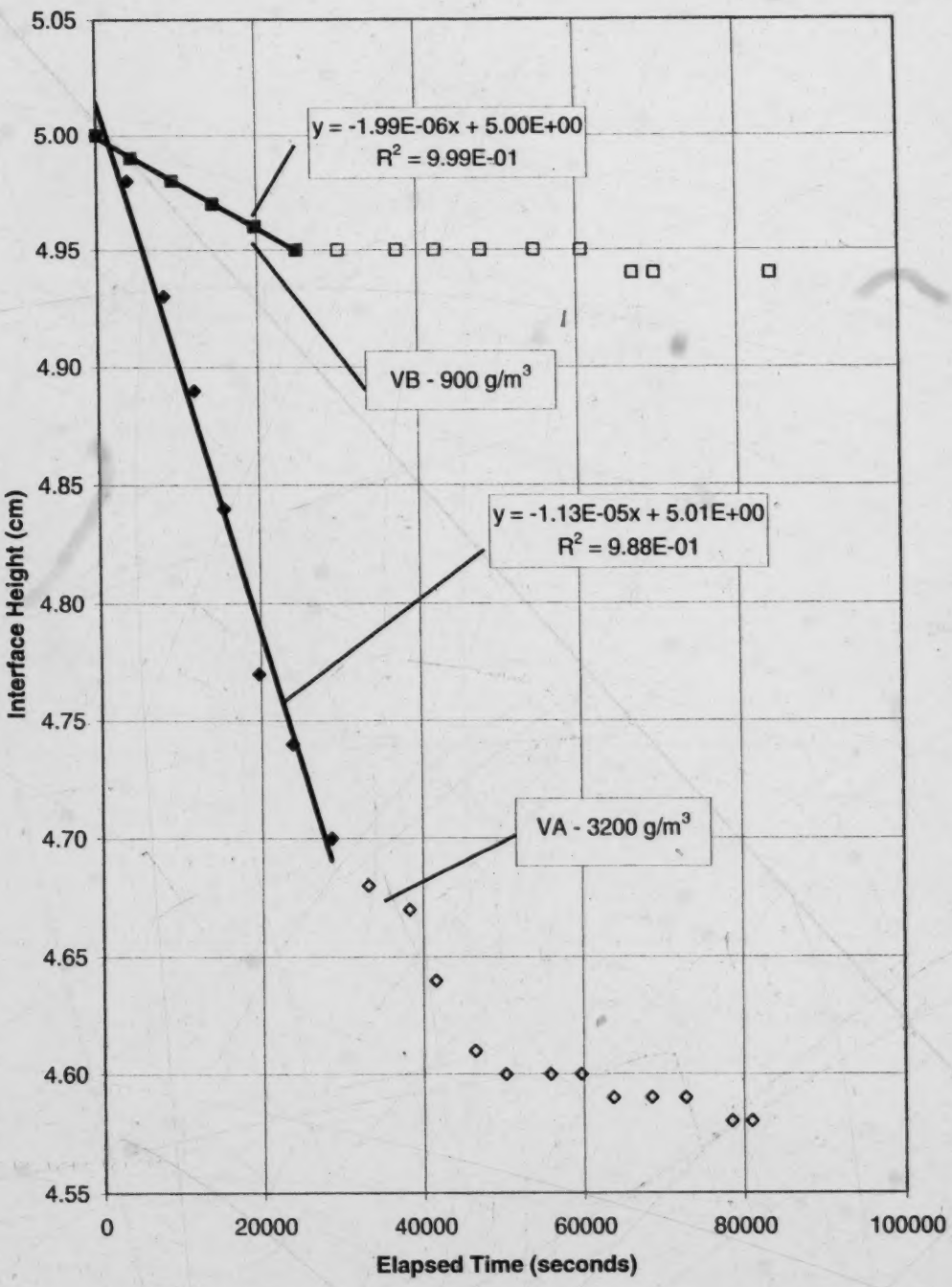

Figure 5.7 Behavior of interface during WRIT at 900 and 3200 g/m^3 of PG

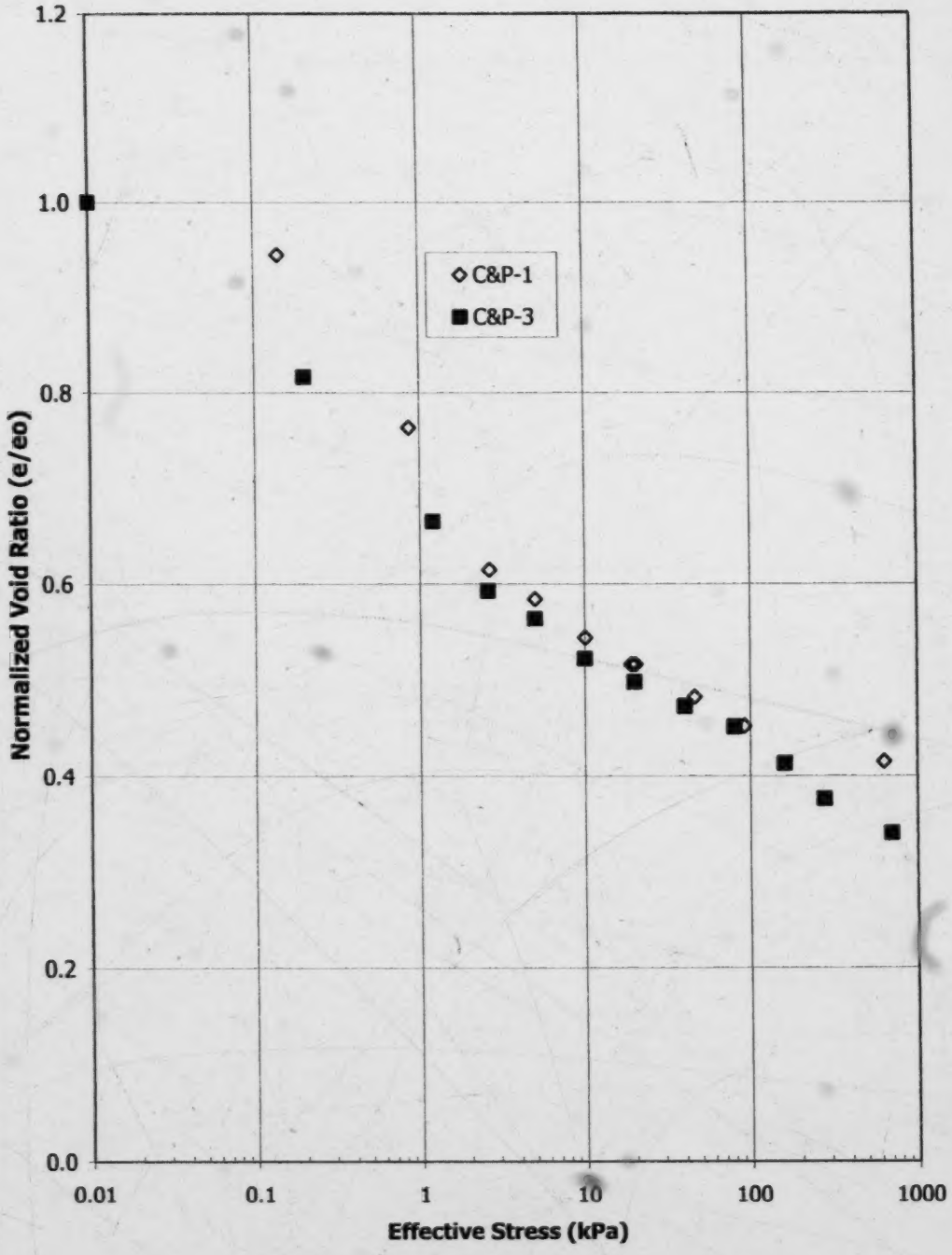

Figure 5.8 Compressibility relationship for CT with 900 g/m^3 of PG

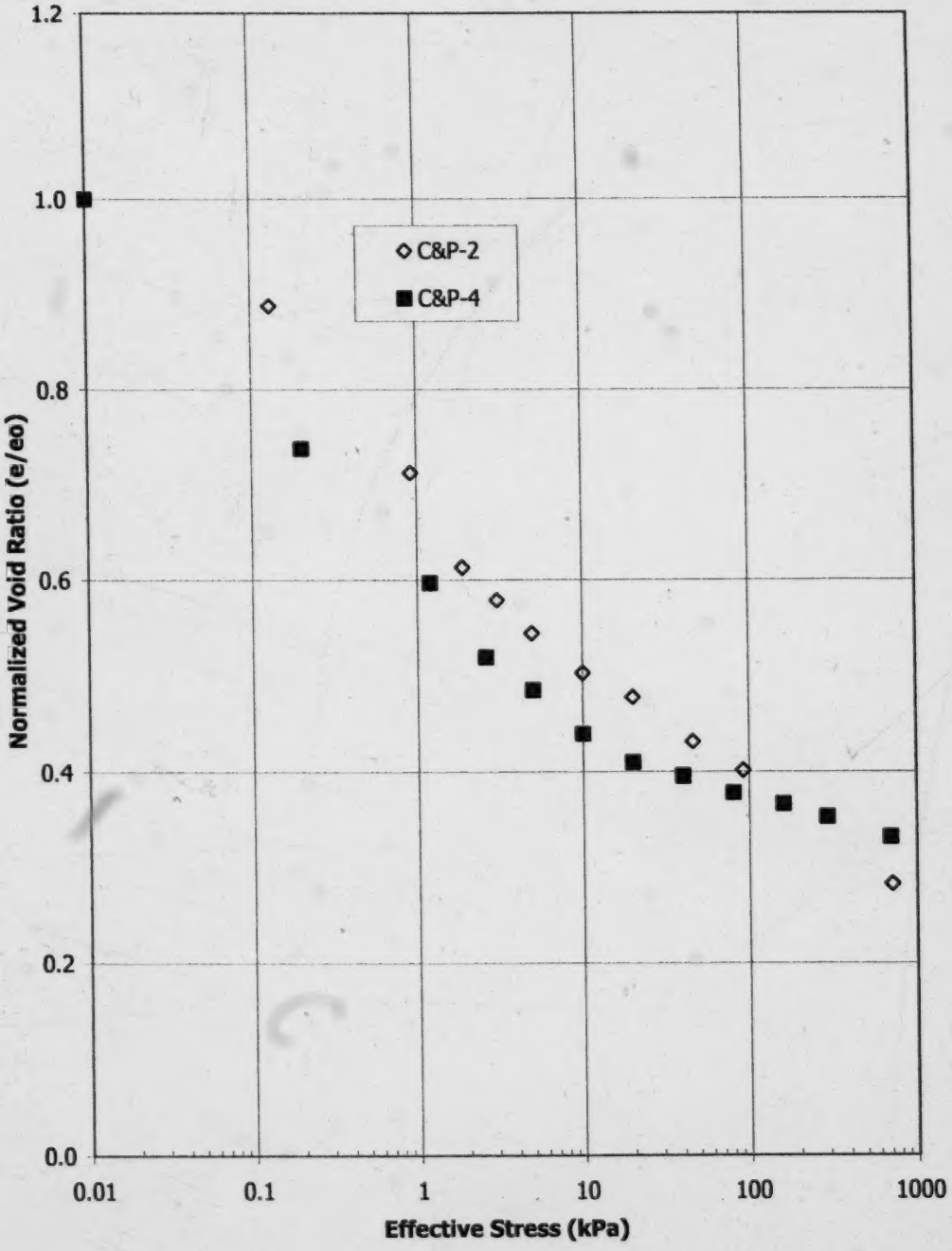

Figure 5.9 Compressibility relationship for CT with 3200 g/m^3 of PG

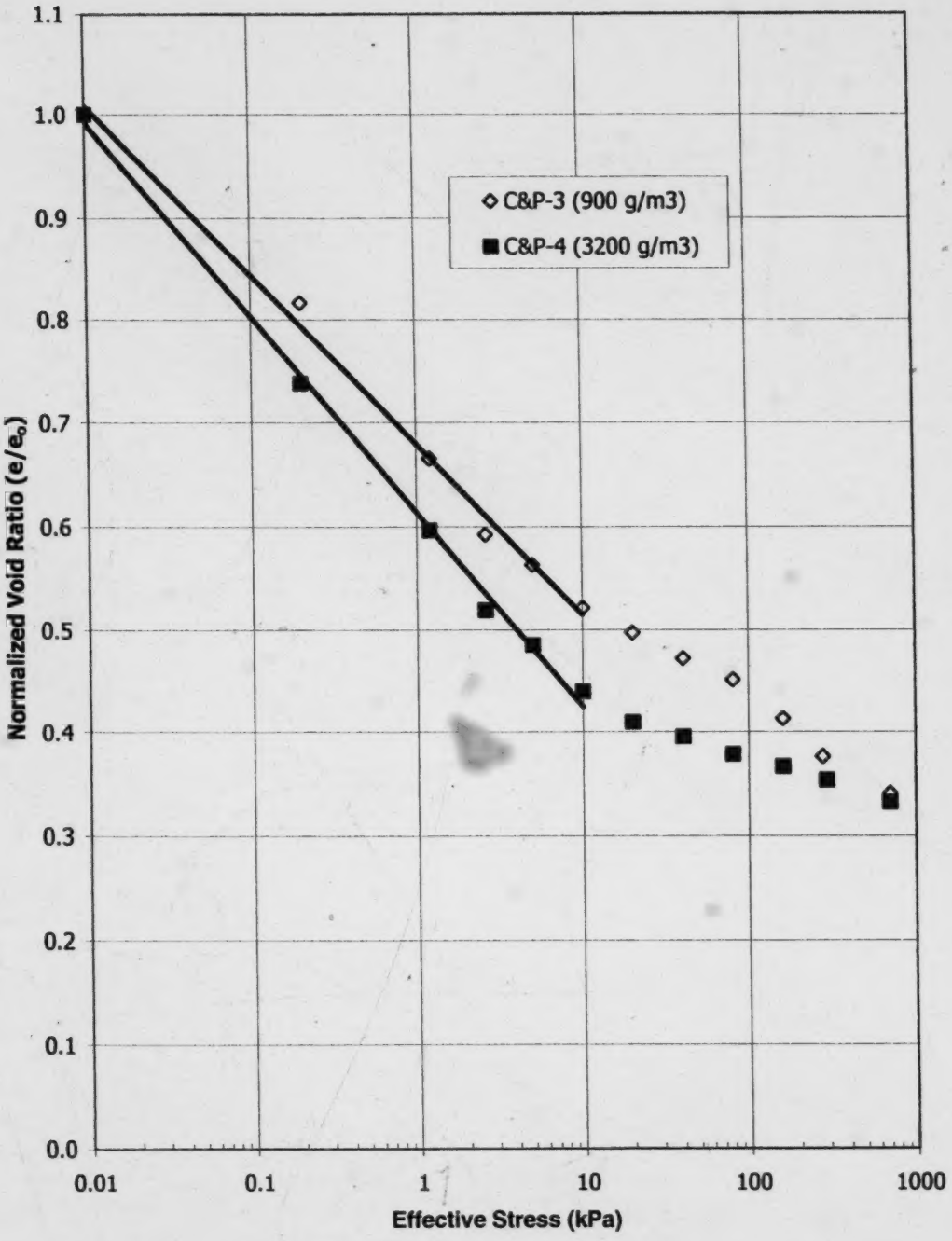

Figure 5.10 Comparison of compressibility relationship for CT at 900 and 3200 g/m^3 of PG

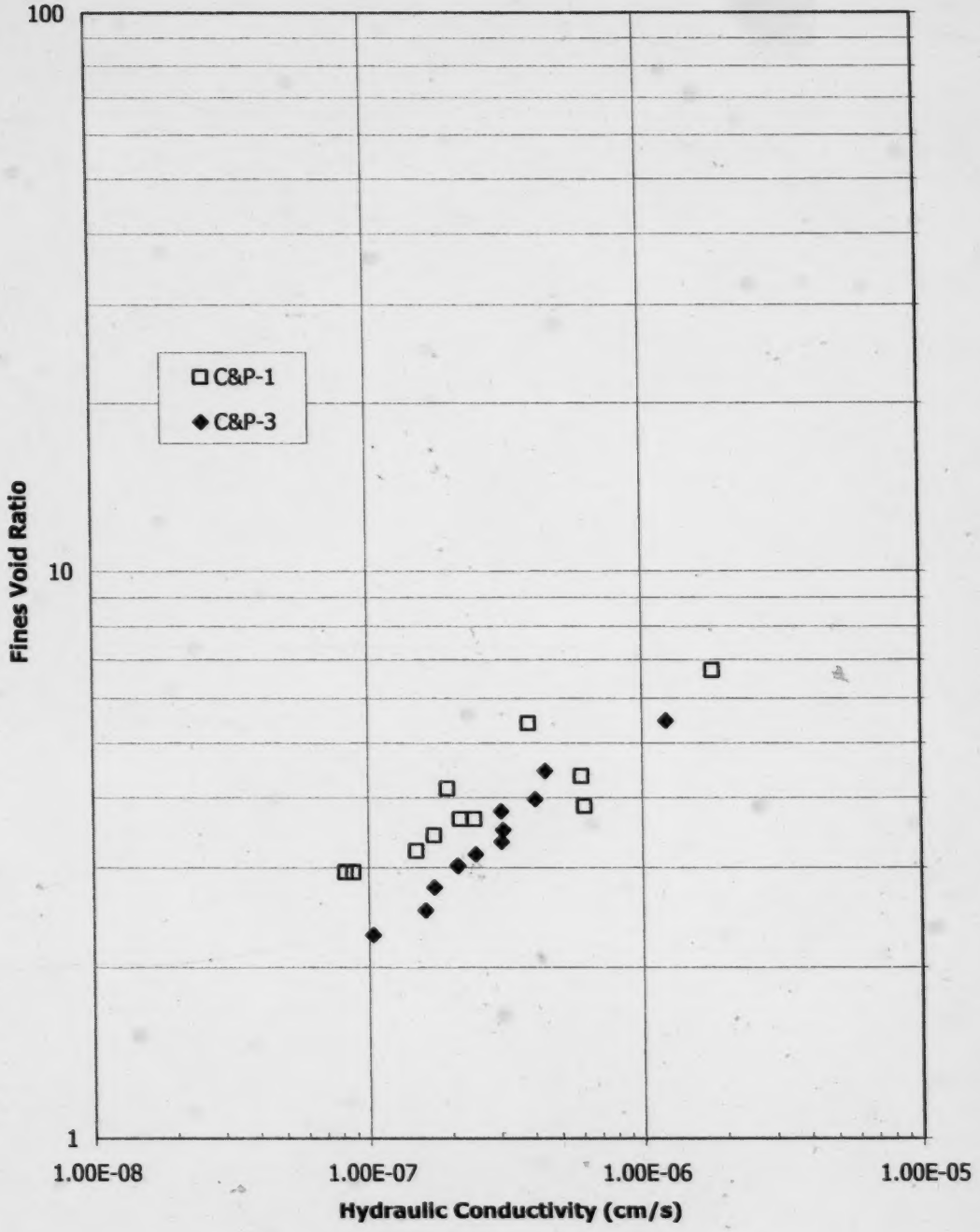

Figure 5.11 Fines void ratio-hydraulic conductivity relationship for CT with 900 g/m^3 of PG

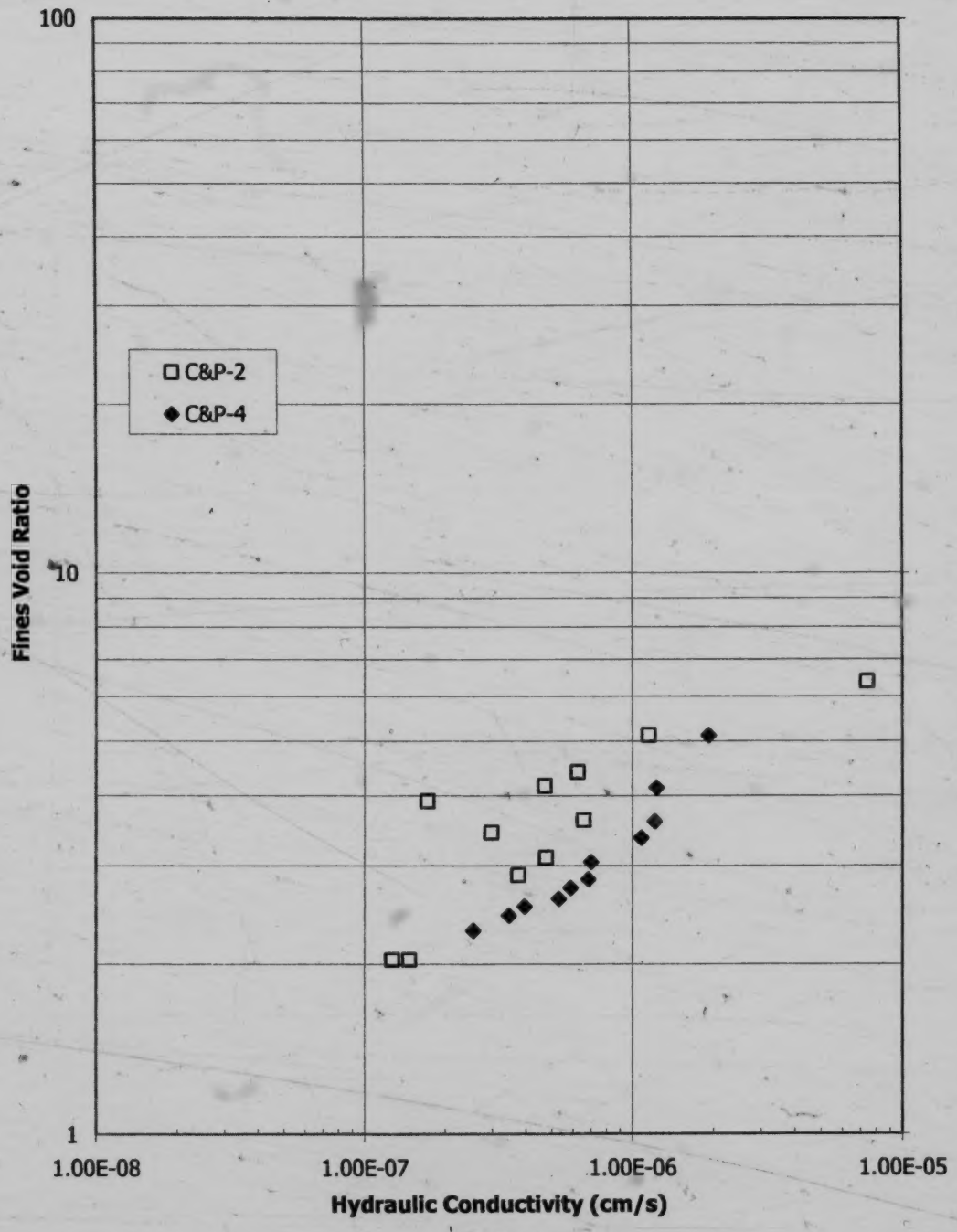

Figure 5.12 Fines void ratio-hydraulic conductivity relationship for CT with 3200 g/m^3 of PG

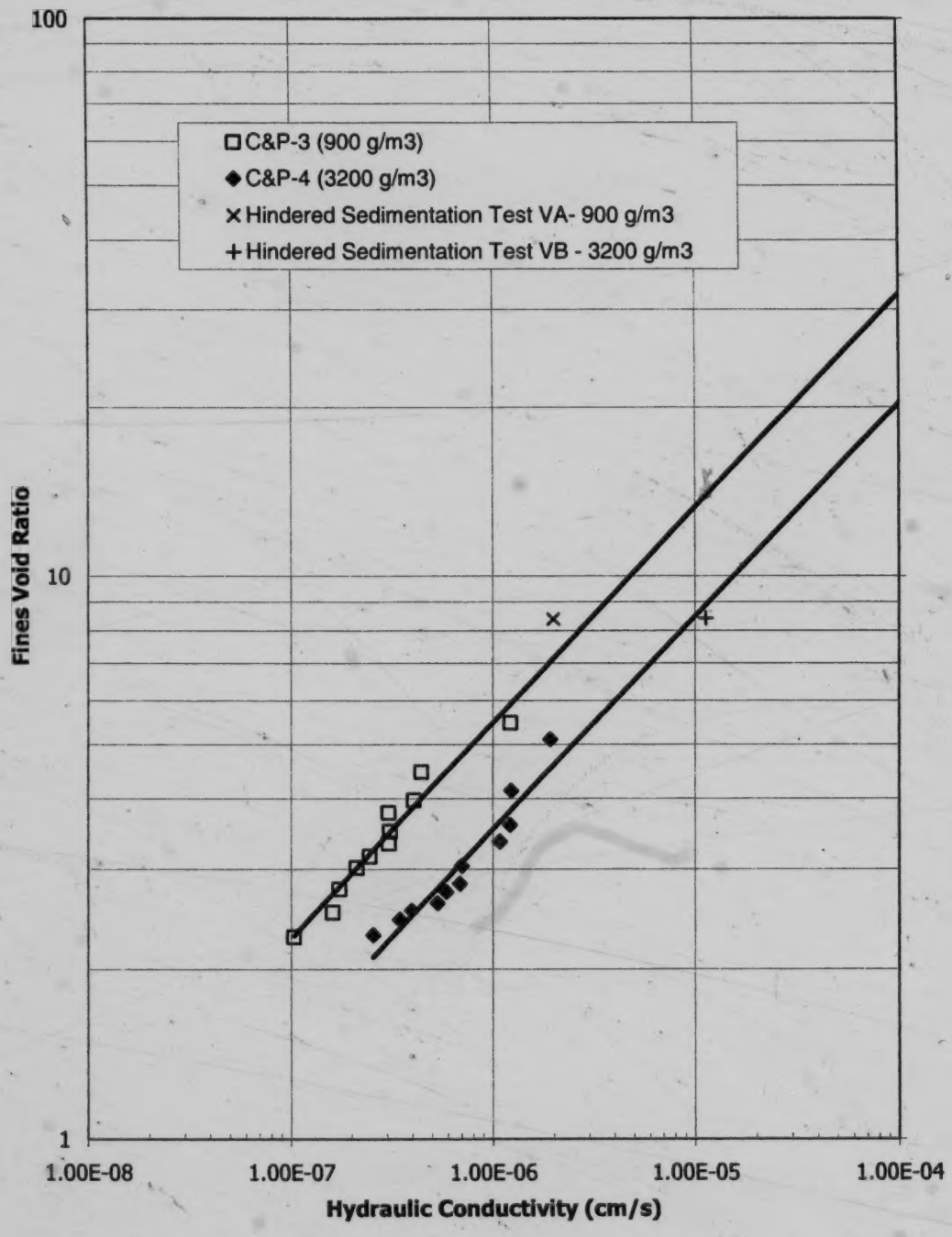

Figure 5.13 Comparison of fines void ratio-hydraulic conductivity relationship for CT with 900 and 3200 g/m^3 of PG

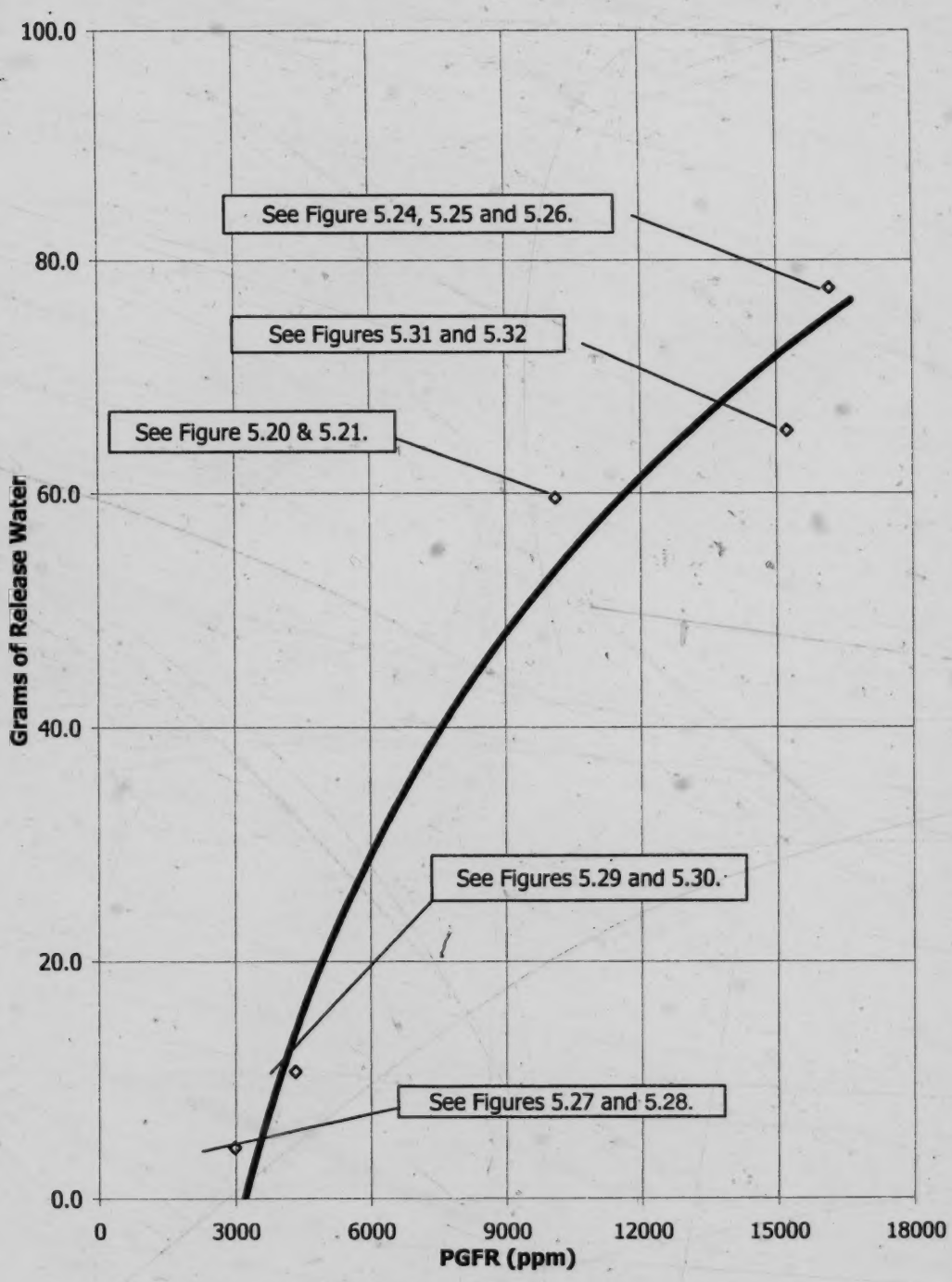

Figure 5.14 Mass of release water vs. PGFR for all SEM images

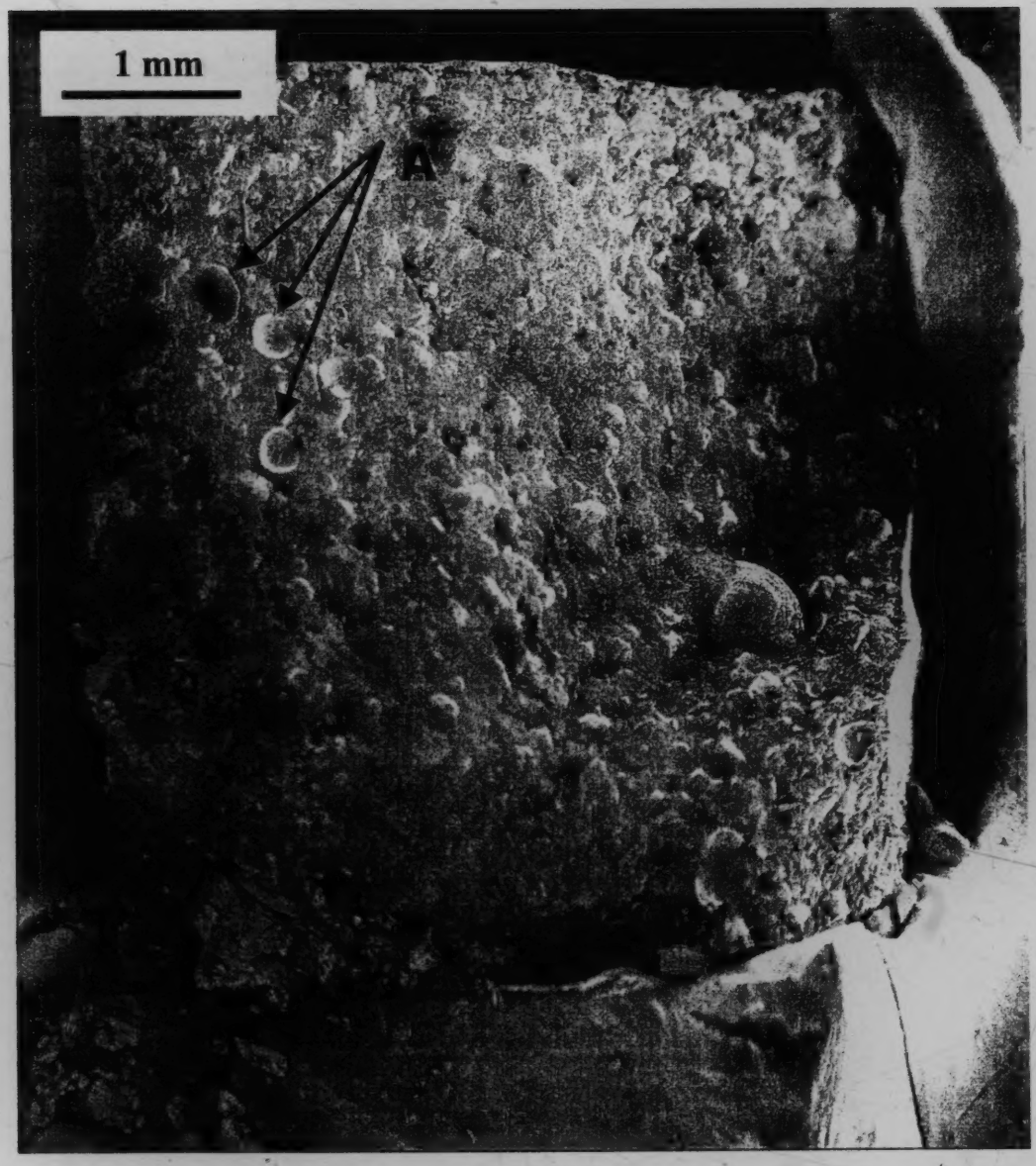

Figure 5.15 Cryogenic SEM for CT at 61.9 % Solids, 21.2 % Fines with 900 g/m^3 of PG (Magnification X 15)

Figure 5.16 Cryogenic SEM for CT at 61.9 % Solids, 21.2 % Fines with 900 g/m^3 of PG (Magnification X 100)

Figure 5.17 Cryogenic SEM for CT at 61.9 % Solids, 21.2 % Fines with 900 g/m^3 of PG (Magnification X 200)

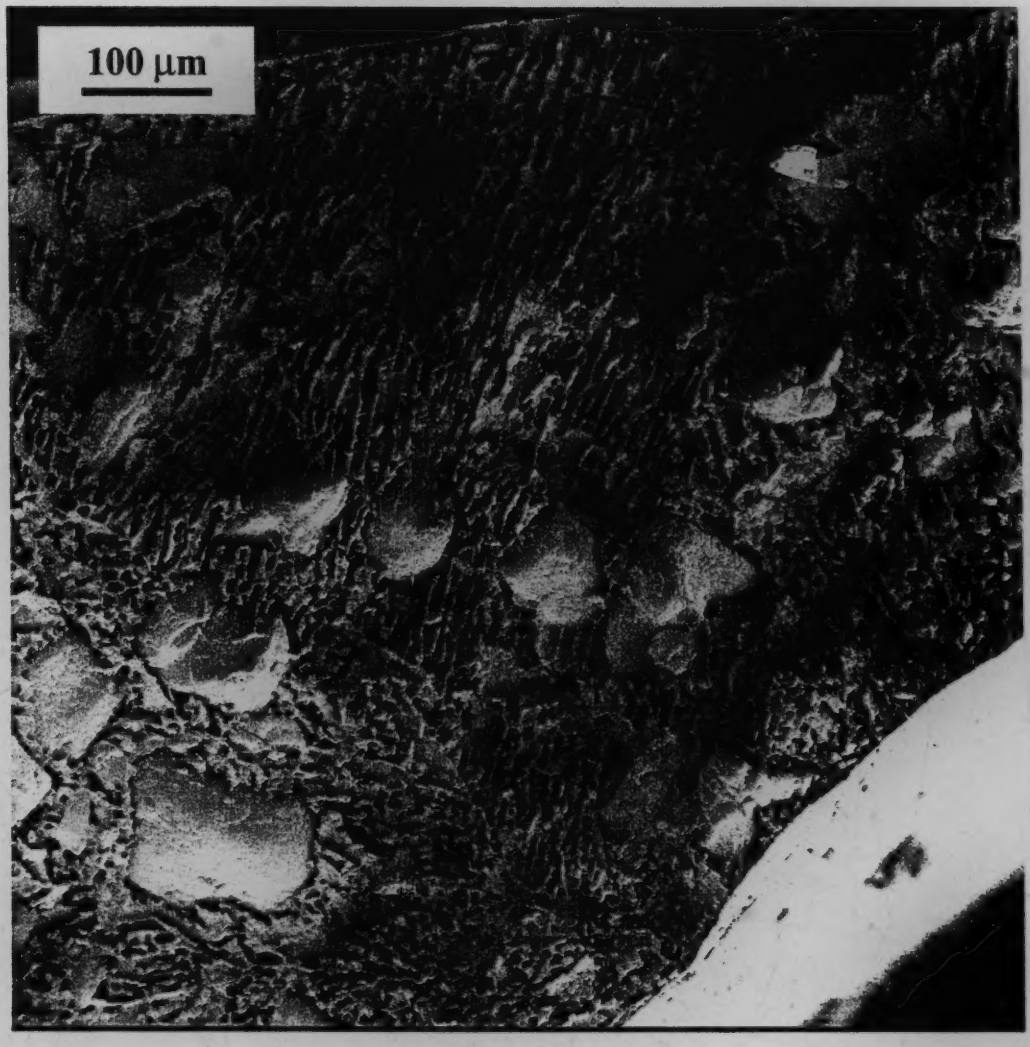

Figure 5.18 Cryogenic SEM for CT at 61.8 % Solids, 21.0 % Fines with 1400 g/m^3 of PG (Magnification X 100)

Figure 5.19 Cryogenic SEM for CT at 61.8 % Solids, 21.0 % Fines with 1400 g/m^3 of PG (Magnification X 500)

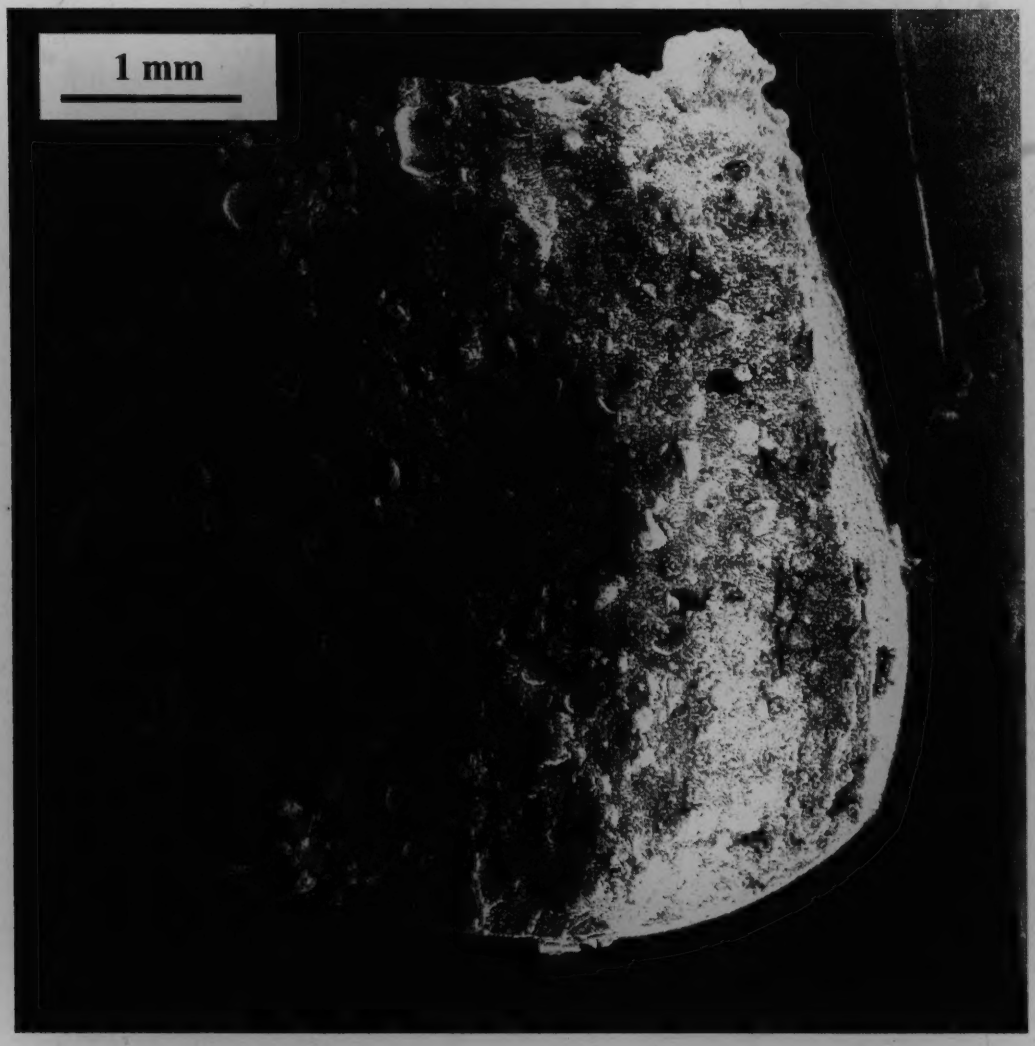

Figure 5.20 Cryogenic SEM for CT at 61.9 % Solids, 19.8 % Fines with 2000 g/m^3 of PG (Magnification X 15)

Figure 5.21 Cryogenic SEM for CT at 61.9 % Solids, 19.8 % Fines with 2000 g/m^3 of PG (Magnification X 200)

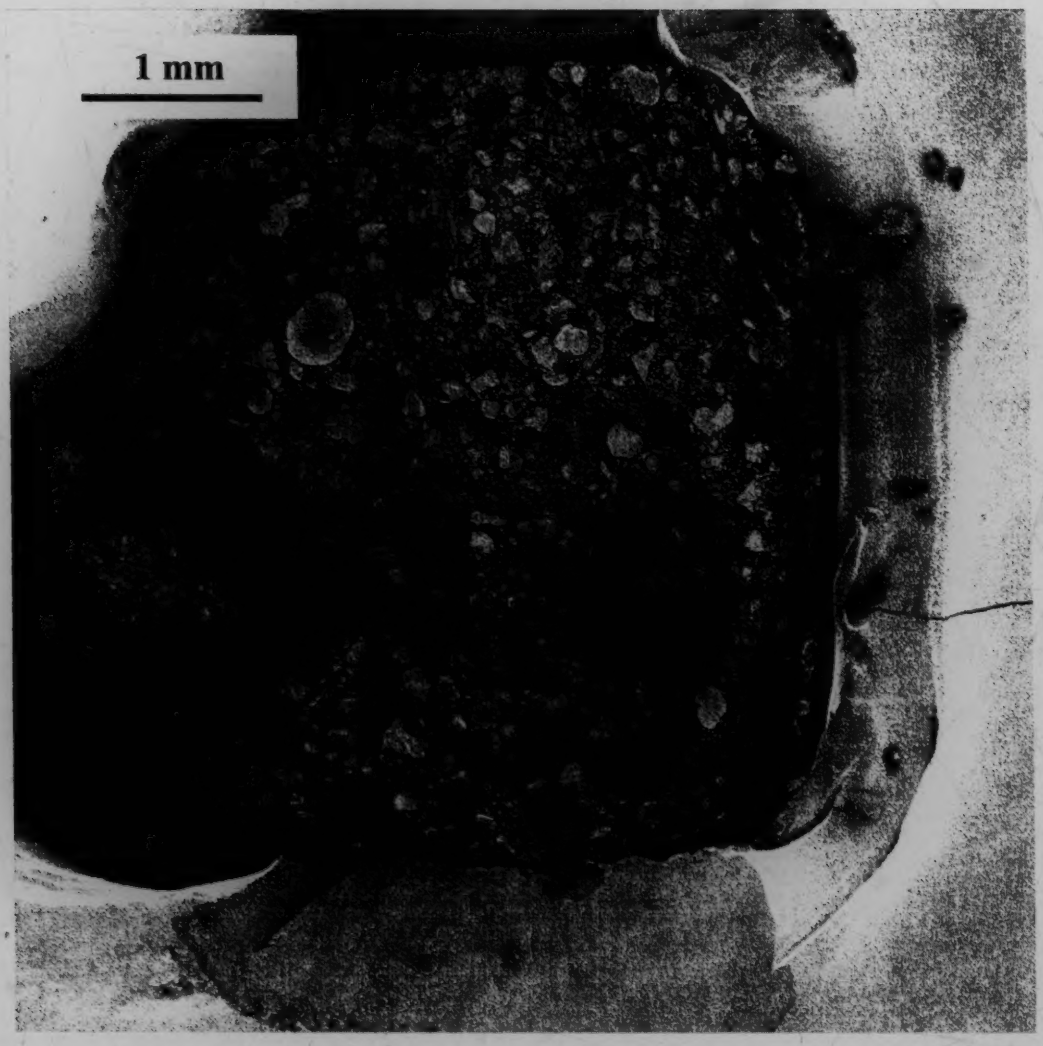

Figure 5.22 Cryogenic SEM for CT at 61.8 % Solids, 22.2 % Fines with 2600 g/m^3 of PG (Magnification X 15)

Figure 5.23 Cryogenic SEM for CT at 61.8 % Solids, 22.2 % Fines with 2600 g/m^3 of PG (Magnification X 100)

Figure 5.24 Cryogenic SEM for CT at 61.6 % Solids, 20.0 % Fines with 3200 g/m^3 of PG (Magnification X 15)

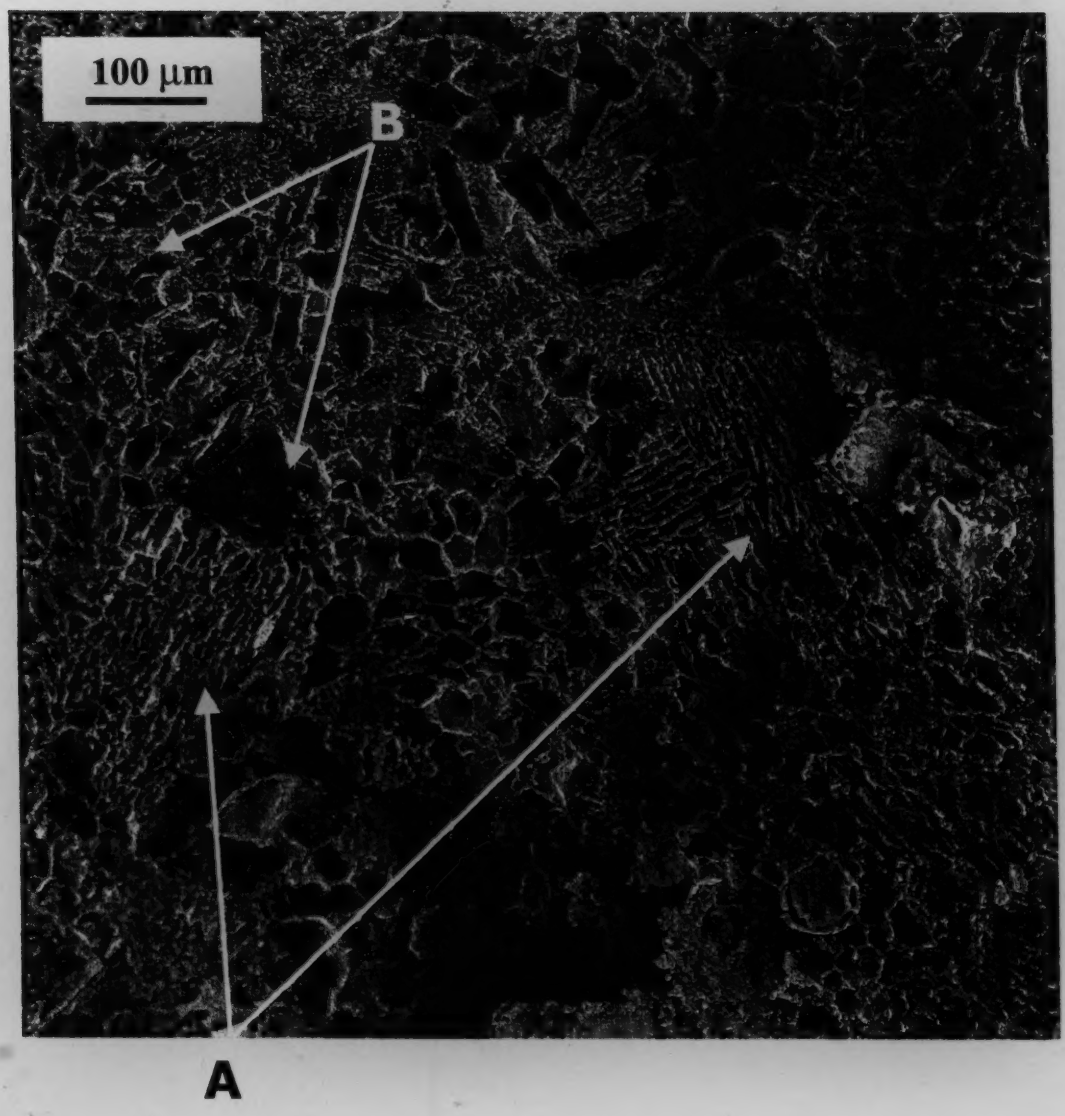

Figure 5.25 Cryogenic SEM for CT at 61.6 % Solids, 20.0 % Fines with 3200 g/m^3 of PG (Magnification X 100)

Figure 5.26 Cryogenic SEM for CT at 61.6 % Solids, 20.0 % Fines with 3200 g/m^3 of PG (Magnification X 200)

Figure 5.27 Variable Pressure SEM for CT at 62.1 % Solids, 20.1 % Fines with 600 g/m^3 of PG (Magnification X 266)

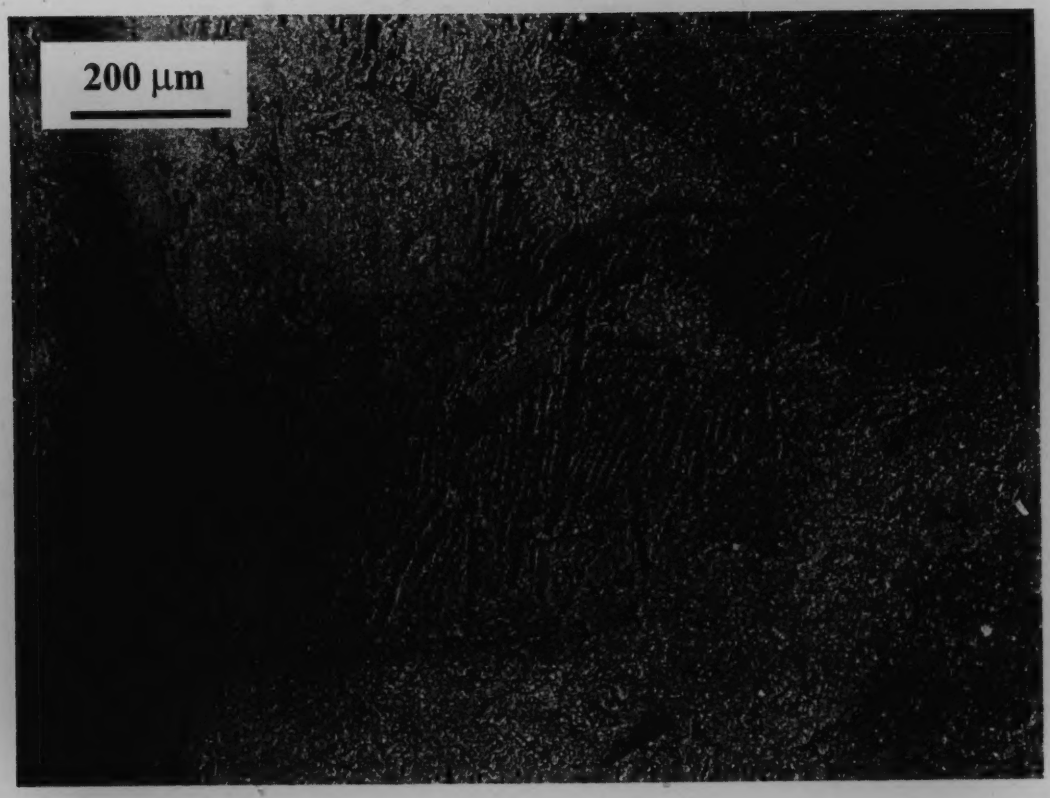

Figure 5.28 Variable Pressure SEM for CT at 62.1 % Solids, 20.1 % Fines with 600 g/m^3 of PG (Magnification X 690)

Figure 5.29 Variable Pressure SEM for CT at 61.8 % Solids, 20.9 % Fines with 900 g/m^3 of PG (Magnification X 286)

Figure 5.30 Variable Pressure SEM for CT at 61.8 % Solids, 20.9 % Fines with 900 g/m^3 of PG (Magnification X 690)

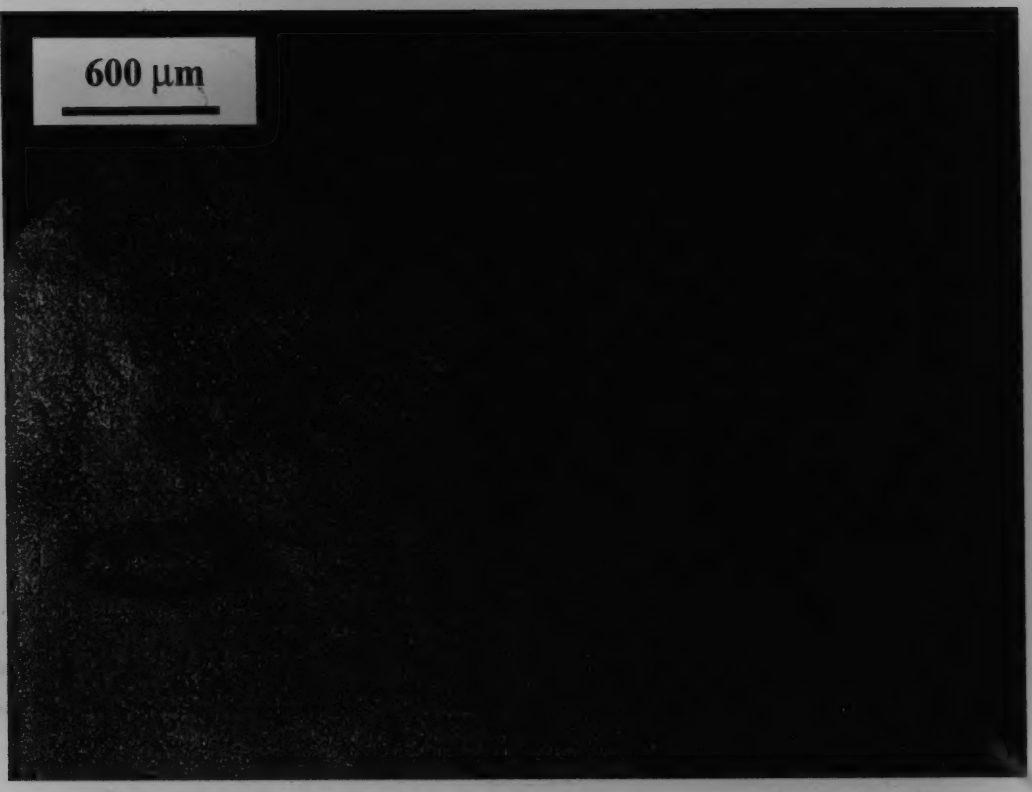

Figure 5.31 Variable Pressure SEM for CT at 62.8 % Solids, 20.5 % Fines with 3200 g/m^3 of PG (Magnification X 227)

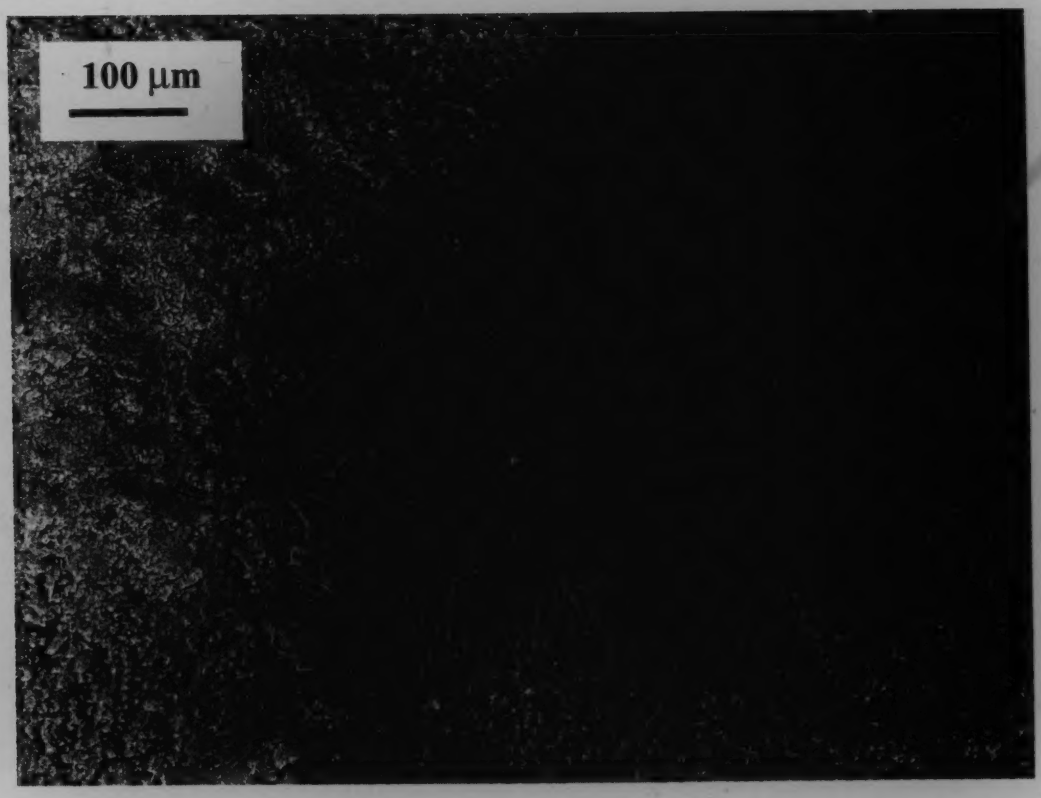

Figure 5.32 Variable Pressure SEM for CT at 62.8 % Solids, 20.5 % Fines with 3200 g/m^3 of PG (Magnification X 690)

6.0 Discussion

6.1 Diameter-to-Height Ratio (DHR)

From the test results shown in Figures 5.1 and 5.2 the following three observations can be made; (1) the mass of release water per cm^2 of cross-sectional area increases as the PG dosage increases from 900 g/m^3 to 2000 g/m^3, (2) increasing the DHR increases the mass of water release per cm^2 of cross-sectional area, and (3) the effect of small DHR's is more pronounced at higher PG dosages. The discussion of the effect of increase PG dosage is deferred to Sections 6.2.2 and 6.2.3, while observation (2) and (3), which are related to DHR are discussed below.

As shown in Figure 5.1, the effect of small DHR's can be significant and must be acknowledged and dealt with, in order that WRIT results are meaningful and can continue to provide a quick screening tool for the water release behavior of CT. In geotechnical engineering the concept of a minimum DHR has long been recognized in traditional consolidation tests, where the American Society for Testing and Materials (ASTM) requires a minimum DHR of 2.5. Additionally, Michaels and Bolger (1962) identified the concept of a yield diameter or minimum standpipe diameter which must be maintained in order ensure that a slurry deposit initially experiences hindered sedimentation followed by consolidation. They discuss the concept of a minimum yield diameter, based on the diameter of aggregated soil particles being small compared to the inside diameter of the settling vessel in order to avoid scale effects. They also note that aggregate size is not a fundamental property of a slurry, but depends on mixing strength and intensity. According to their research, both the yield diameter and yield height can be calculated based on the solids content, yield stress (measured with a concentric cylinder viscometer) and specific gravity of pore water and mineral grains. A failure to reach these minimum criteria results

in the deposit experiencing no hindered sedimentation and all water release is due to consolidation settlement.

Since the isolation of the mechanisms, which are responsible the effect of small DHR's was beyond the scope of this study and is not fundamentally necessary for an index test, no further testing was performed in regard to this matter. However, based on previous experience, the author offers the following geotechnical explanation in regards to what may be causing the DHR effect and why this effect is more pronounced at higher dosages.

As shown in Figure 5.7, the interface of both samples experienced an immediate and constant rate of descent immediately after deposition. Hindered sedimentation was observed to last for approximately 7 to 8 hours in both the sample with 900 g/m^3 and 3200 g/m^3, and therefore changes in PG dosage were not observed to cause a shift in the transition point between hindered sedimentation and consolidation. By definition, during hindered sedimentation no effective stress is present and the velocity of the interface is directly proportional to the hydraulic conductivity of the slurry. Beyond the hindered sedimentation stage, effective stresses are present and further water release is governed by consolidation theory. From Figure 5.7, the sample with 900 g/m^3 of PG, hindered sedimentation accounted for approximately 90 % of the water release during the WRIT, while hindered sedimentation only accounted for 50 % of the total mass of release water for the sample with 3200 g/m^3 of PG. The remaining 10 % and 50 % occurred due to consolidation settlement.

The effect of small DHR's is due to boundary shear forces between the sidewall of the cylinder and the slurry. Boundary shear forces depend on the adhesion characteristics between soils grains and the cylinder wall, effective stress, the frictional characteristics between the mineral grains and the cylinder wall. Since no effective stresses are present during hindered sedimentation, the origin of the

boundary shear forces are not constant throughout the WRIT. That is, during hindered sedimentation adhesion is the only boundary shear force, while during consolidation both adhesion and friction are present.

Irrespective of whether a slurry is undergoing hindered sedimentation or consolidation, one can examine how the magnitude of the driving force and resisting force (boundary shear force) vary as the depth of a CT deposit is held constant and the diameter of the cylinder is tripled from a DHR of 1 to 3 (i.e. Tests J9 and J11) for a constant PG dosage. Firstly, the total mass of the slurry varies with the square of the diameter. Therefore increasing the diameter by a factor of three increases the total slurry mass by a factor of nine. Meanwhile, the change in resisting forces is proportional to a factor of three, as the contact area between the slurry and the cylinder wall varies linearly with the diameter. Thus, as DHR is increased the magnitude of the driving force increases exponentially while the resisting force increases only linearly. As the DHR is increased, a point is reached where the boundary forces becomes insignificant relative to the driving forces.

Regardless of the whether the boundary force is a result of adhesion during hindered sedimentation or adhesion and friction during consolidation; it appears as though the effect of increased dosage can be explained. As shown in Table 5.1 and 5.2, the performance was reduced by 37 % when the DHR was reduced from 4.04 to 1.14 at 900 g/m^3 versus a 52 % reduction in performance over the same DHR for a dosage of 2000 g/m^3. Since an increase in PG dosage would increase the degree of flocculation and ultimately the floc size relative to the diameter of the test cell, higher dosages would be expected to cause more of a negative effect during hindered sedimentation. Similarly, during consolidation the effect of higher PG dosages would increase the effective stress as the repulsion-attraction component of particle interaction would be reduced. This increase in effective stress would produce larger boundary forces and more of a

negative effect for higher dosages. Therefore, the boundary forces would be greater for higher PG dosage during both hindered sedimentation and consolidation.

Due to the limited testing performed within this research program, other factors including but not limited to thixotropy or bridging could also be contributing to the reduction in water release as observed using the WRIT at small DHR's. Irrespective of the physical mechanisms, which are responsible for the negative effects of small DHR's, the objective of this series of tests was to determine if DHR was an influence and what minimum DHR was necessary to effectively eliminate it during subsequent WRIT's. Based on the test results, a DHR of 2.91 causes less than a 10 % reduction in water release of CT at 62 % solids and 20 % fines for dosage up to 3200 g/m^3. Thus, all subsequent tests performed in the experimental program were conducted with a DHR of 2.9. From this series of tests DHR could be removed as a potential significant source of the anomalies between initial water release rates of field and laboratory produced CT.

Due to limited resources, the maximum cell diameter utilized was 20.22 cm. It is suggested that further research be performed using larger diameters and a 5 cm high deposit (or other combinations) to confirm the findings above. Also the type of chemical additive and composition of the test cell (plastic, glass, etc.) will likely influence the effect of DHR.

6.2 Fines and phosphogypsum Interaction

The effect of PG dosage on the dewatering characteristics of CT (62 % solids and 20 % fines) was determined by increasing the PG dosage from 600 to 3600 g/m^3, and observing changes in behavior of the WRIT, slurry consolidometer and SEM images. Quantitatively, the addition of PG is known to have four effects in CT (1) addition of calcium ions and (2) increase in sodium concentration in pore

water due to exchange for calcium (3) an approximately 0.5 decrease in pH (4) decrease in bicarbonate ion concentration. Qualitatively the addition of the PG causes an immediate increase in the viscosity of the CT.

Upon the dissolution of the gypsum in tailings pore water, the sinks for soluble calcium include complexation, uptake by the clay particles through adsorption and precipitation with carbonate. Research by Mikula (1996) has shown that approximately 0.05 % calcium (by weight) will be taken up by a given mass of pure kaolinite in equilibrium with tap water. Also, his test results have shown that at low gypsum dosages, uptake by the fines occurs before precipitation indicating that the favored sink for soluble calcium is the clay particles. This is likely due to the fact that cation exchange rates are nearly instantaneous with kaolinite and precipitation with carbonate is a slow process, due to the low levels of carbonate at a pH of approximately 8. The precipitation of calcium with carbonate causes a decrease in bicarbonate concentration and causes a corresponding decrease in pH. Due to the highly buffered nature of the tailings pore water (due to bicarbonate), a large change in pH does not occur. The following sections discuss the effect of adsorption by the clays and precipitation of calcium as it relates the dewatering characteristics of CT.

Prior to the addition of PG, monovalent sodium cations are preferentially adsorbed and are electrostatically held near the surface of the kaolinite. Upon the addition and dissolution of gypsum, the concentration of the divalent calcium ions in the pore water is dramatically increased. Due to the lyotrophic series for kaolinite, calcium replaces sodium as the preferred adsorbed cation. The increase in the sodium concentration after PG dosage is well documented by Syncrude's 1995 field trial (Shaw et al, 1996). In accordance with the double layer theory, the addition of divalent cations or an increase in electrolyte concentration causes the electric double layer (EDL) to be compressed and allows adjacent particles to approach closer and increase the potential for

flocculation. The approximately 0.5 decrease in pH, which occurs upon gypsum addition, decreases the tendency for H^+ ions (on the clays) to go into solution and therefore reduces the net negative charge on the clay particles. The dramatic increase in the calcium ion concentration combined with the decrease in pH, combines to produce an environment, which destabilizes the clay particles and favors flocculation or agglomeration of clay particles. The compression of the EDL and reduction in repulsive forces allows adjacent clay particles to approach one another more closely than without PG treatment. The net effect is that van der Waals attractive forces begin to dominate and flocculation or agglomeration of adjacent clay particles occurs. The degree of clay flocculation is related to how much the EDL is compressed due to the addition of calcium ions or reduction in the net negative charge due to a decrease in pH, or the reduction in bicarbonate concentration. The relative effect of calcium as it relates to electrostatic attraction, reduction in pH, interaction with surfactants, surface charge effects or reduction in bicarbonate concentration are not clear. Also the presence of the bitumen as it related to soil fabric is unclear. Further research into the specific role of calcium as it relates to the fundamental properties of CT is required.

The following sections discuss the effect of increasing PG dosage on the observed geotechnical behavior of CT.

6.2.1 Behavior of Interface during WRIT

6.2.1.1 Prevention of Segregation

Visual observation of all CT samples prepared within this research project indicated that they were nonsegregating. However, based on the test results it is not clear exactly what mechanism is responsible for preventing segregation. It is not clear whether it is the change in grain size characteristics of the fines or

the apparent increase in strength as a result of more bonding within the fines. However, based on the mechanics of segregation as discussed by Chapuis, distribution of grains as observed in SEMs for CT at 62 % solids and 20 % fines, and test results by Tang (1997) it would appear that the role of PG as it relates to preventing segregation is related to an increase in strength.

The mechanics of the changing a slurry from segregating to nonsegregating are described by Chapuis, in terms of the ability to capture the fines within the sand matrix. Based on the visual examination of the SEMs presented in Chapter 5, at a solids content of 62 % the sands grains are floating within the fines matrix. Therefore, it would seem as though the segregation potential of CT is better described in terms of the ability of the fines matrix to hold sand grains within rather than the ability of the sand matrix to trap the fines. Cavity expansion results by Tang (1997) on two day old MFT treated with gypsum show a thixotropic strength of 420 Pa versus a strength of 165 Pa for untreated MFT. This increase in strength is presumably related to a reduction in repulsion-attraction forces and corresponding increases in true effective stress. However, isolation of the role of PG with respect to preventing segregation requires additional research.

6.2.1.2 Flocculation or Induction Period

As mentioned in Section 2.5.2.1.1, research by others indicates the presence of a time period immediately after a slurry is deposited, when the interface is stagnant and flocculation or formation of optimum shaped flow channels occurs. However, neither of the two samples shown in Figure 5.7 experienced an induction period or flocculation stage during which the interface was stationary. Rather the interface showed an immediate downward descent at a relatively constant rate.

It should be noted that the test results presented in Figure C1 (Appendix C) tend to suggest that an induction or flocculation period existed immediately after deposition of the specimen with 900 g/m^3 of PG. Although the intermediate position of the interface during self weight loading was not the focus of the consolidation test, it was recorded for each of the two slurry consolidometer tests (C&P-3 and C&P-4). These tests consisted of placing a total depth of CT of 5.35 cm (900 g/m^3) and 5.50 cm (3200 g/m^3) in a 13.9 cm diameter slurry oedometer test cell. The specimen treated with 900 g/m^3 of PG (PGFR of approximately 4150 ppm) remained stationary as observed with the naked eye and appeared not to release any water for the first 35 hours of the test (See Figure C1 in Appendix C). From Figure 5.5, CT with 62 % solids and 20 % fines, with a PGFR of 4150 ppm should release approximately 7.5 grams of water in 24 hours. Had this occurred, the interface would have moved downward approximately 0.05 cm. Since readings by the naked eye are accurate to approximately 0.5 mm (or 0.05 cm), the interface appears to be stationary although release water was clearly present on the surface of the deposit. This issue regarding the limited accuracy of naked eye measurements is one of the reasons why the WRIT used total mass of release water as a measure of performance. When the position of the interface as a function of time was required to characterize the settling behavior, time-lapse photography with a video camera placed directly against the exterior cell wall was performed. Post processing enabled the images to be enlarged and examined at a larger scale to determine the movement of the interface in more detail. The naked eye measurements shown in Figure C1 are not conclusive enough to suggest the presence of an induction or flocculation stage for CT with 900 g/m^3 of PG. Despite the limited accuracy of the naked eye measurements, the data shown in Figure C12 shows no lengthy induction or flocculation period exists for CT with 3200 g/m^3. As observed with the naked eye, discernable movement was recorded shortly after deposition.

Given that cation exchange reactions rates for kaolinite are known to be essentially instantaneous, these test results suggest that flocculation began immediately after the addition of PG and sufficient time elapsed during the 5 minute mixing period that equilibrium was reached with respect to flocculation prior to deposition. Therefore, CT treated with PG in excess of 900 g/m^3 and placed in approximately 5 cm thick deposits with a minimum DHR of 2.9 appears not to be subject to a lengthy induction period immediately after deposition.

The intermediate position of the interface during self weight loading of the specimen with 3200 g/m^3 of PG is shown in Figure C12 (Appendix C). The behavior of the 3200 g/m^3 sample indicates a period of interface acceleration as the slope of line between adjacent data points in Figure C12 gradually increased between 0.1 to 3 hours. After 3 hours the rate of descent is constant for approximately 20 hours and is greater than the rate of descent observed from 0.1 to 3 hours. An accelerating interface is consistent with the findings of Michaels and Bolger (1962), who suggest that during the initial stage of settling, flow channels begin to line up into vertical rows, contractions and sharp bends are smoothed out, and the flow path straightens out. However, given the lack of readings between the 3 and 20 hour mark on Figure C12, and the accuracy of naked eye readings, there is not enough data to conclude that the interface experienced an acceleration period.

6.2.1.3 Yield Diameter and Yield Height

Michaels and Bolger (1962) indicate that interface acceleration will only occur if the diameter of the standpipe exceeds the "yield diameter" and the height of the standpipe exceeds the "yield height". If these criteria are not met, hindered sedimentation does not occur and the interface will only subside at an ever decreasing rate, in accordance with the theory of consolidation. Since the two samples shown in Figure 5.7 did not experience a settling rate that continuously

decreased from the beginning of the test, but rather experienced hindered sedimentation (constant rate of interface descent), it is apparent that both the yield diameter and yield height were exceeded. This concept of a yield diameter and yield height was likely addressed when the minimum DHR was determined and a height of 5 cm was selected.

6.2.1.4 Uniqueness of Soil Forming Void Ratio

Pane and Shiffman (1997) have identified the concept of the "soil forming void ratio" with respect to slurries. According to their research, a soil forming void ratio marks the transition from hindered sedimentation to consolidation for a given soil, depending on the chemical and environmental conditions and is independent of the initial void ratio. Their results show a soil forming void ratio of approximately 30 for a speswhite kaolin slurry which began with an initial solids content of approximately 5 %. The two test results shown in Figure 5.7 transitioned from hindered sedimentation to consolidation at total void ratio of 1.61 and 1.49, respectively. The void ratio which signified the transition were not the same for our two samples, since the environmental conditions (a prerequisite according to Pane and Schiffman) were different due to different level of PG dosage. Given that the speswhite kaolin used by Pane and Schiffman has a clay fraction of 75 %, the soil forming total void ratio and soil forming clay void ratio would be equal to 30 and 40, respectively. However, since CT is not a uniform material but has only 20 % fines (50 % of which are clay sized), the clay void ratio at which the CT samples transitioned from hindered sedimentation to consolidation are 16.1 and 14.9, respectively. Since CT is drastically different than the material Pane and Shiffman used, it is not surprising that the soil forming clay void ratios of CT and speswhite kaolin are different. From the test results, CT transitions from hindered sedimentation to consolidation at a much

lower soil forming clay void ratio than speswhite kaolin. This is likely due to the uniqueness of CT with respect to grain size and the environmental conditions.

Since the soil forming void ratio is specific to a given set of chemical and environmental conditions (i.e. constant PGFR) additional testing would be required to verify the applicability of a constant soil forming clay void ratio of CT.

6.2.2 Effect of PG on Compressibility Characteristics

The effect of increasing PG dosage on the compressibility of the CT is shown on Figures 5.8 through 5.10. As mentioned previously only the test results for samples C&P-3 and C&P-4 will be discussed, as the test results from samples C&P-1 and C&P-2 are thought to contain experimental inaccuracies.

6.2.2.1 Overall Compressibility of CT

From Figures 5.8 through 5.10, the compressibility characteristics of the samples treated with 900 and 3200 g/m^3 of PG indicate that CT is normally consolidated and as a result undergoes virgin compression. CT with varying dosages of PG does not have a unique relationship between void ratio and consolidation pressure as would be expected for samples with nearly identical composition and the same stress history. From the test results, the void ratio of the sample treated with 3200 g/m^3 of PG is always less than the void ratio of the sample with 900 g/m^3 for all applied stress levels. The compression indexes (Cc) calculated over the stress range of 0.14 (self weight) to 10 kPa were 0.265 and 0.287 for the sample with 900 and 3200 g/m^3 of PG, respectively. Over this stress range CT displays moderate to intermediate compressibility characteristics (Mitchell, 1993), and has a compression index consistent the upper limit of pure kaolinite (Mitchell, 1993). Laboratory testing (ASTM D4242-91 Test Method C) of the oil sand from the Aurora mine has determined that the sand structure boundary, or solids content at which the sand grains just begin to touch one

another, corresponds to a total void ratio of approximately 1.01 (Scott, 2002). Since 80 % of the solids contained within CT are sand, it can be inferred that up to a stress of 10 kPa the sand is acting as an inert filler as it has no appreciable effect on the compressibility characteristics of CT. For stresses up to 10 kPa, the effect of the sand as it relates to the deformation characteristics of CT is to increase the self weight of the material, thereby driving the dewatering process.

Beyond a void ratio of approximately 0.7 to 0.8 or an effective stress of 10 kPa, the compressibility of CT as measured in the 900 and 3200 g/m^3 samples, showed a significant decrease. From 10 kPa up to approximately 100 kPa the compression indices are approximately half of what they were over the previous stress range. A decrease in the compression index as result of a lower void ratio is typical behavior in soils, however the change in compression index is usually gradual. Over the stress range of 10 to 100 kPa CT displayed low compressibility characteristics and reflects the presence of the sand grains. Therefore, at some stress level near 10 kPa, CT transitions from behaving as soft moderately compressible clay to behaving like clayey sand with low compressibility. Therefore, the convergence of the two compression curves at a void ratio of 0.51 is expected and no further significant deformation is expected.

6.2.2.2 Effect of Increased PG Dosage on Compressibility of CT

A discussed in section 2.4.4, forces of repulsion occur whenever double layers of adjacent particles overlap. The magnitude of the swelling pressure depends on void ratio, electrolyte strength, valency and dielectric constant of the pore water. That is, soil containing low electrolyte concentrations with low valency will have high swelling pressures and large physicochemical resistance to compression, while high valency or high electrolyte concentrations will increase the susceptibility to compression.

The test results from Figure 5.10 confirm that from self weight up to 10 kPa, the compression index of the 3200 g/m^3 sample was only slightly higher than the 900 g/m^3 sample (Cc of 0.278 vs. 0.265). Similarly, from 10 to 100 kPa, the 3200 g/m^3 sample was again only slightly more compressible (Cc of 0.11 vs. 0.09) and beyond 100 kPa the two curves converge. Although the difference in compressibility characteristics is small, it supports the theory that a soil with a more flocculated fabric is more open and has a more compressible structure at stresses beyond its preconsolidation pressure. An increase in the openness of the fines structure at higher PG dosages was observed in the SEM.

Therefore the net effect of increasing PG dosage was an increase in electrolyte concentration and a decrease in pH both of which result in a reduction in the interparticle repulsion and a subsequent increase in the susceptibility to compression. The observed compressibility characteristics for CT with varying PG dosage are consistent with the findings of Bolt (1956) where separate curves for void ratio versus consolidation stress were observed for samples of illite with different concentration of sodium. The compressibility characteristics of the two CT samples shown in Figure 5.8 through 5.10 are consistent with the osmotic pressure theory for interacting double layers where increasing electrolyte concentrations result in a decreased void ratio for a given pressure.

In summary, CT with 62 % solids, 20 % fines and 3200 g/m^3 of PG has a compression index slightly greater than CT with 900 g/m^3 of PG. Due to the increase in PG dosage the sample with 3200 g/m^3 had a higher degree of flocculation, a more porous structure and was slightly more compressible over the given stress range. For a given applied load, the sample with 3200 g/m^3 of PG was always less than the sample with 900 g/m^3 due to the reduced interparticle repulsion and therefore a corresponding increase in susceptibility to compression. However, the influence of a decrease in pH and/or a

corresponding decrease in bicarbonate concentration could also be partially responsible for this effect.

6.2.2.3 CT Compressibility Results of Others

It should be noted that results by Mitchell (1960) identified a series of void ratio vs. pressure relationships which indicated that higher void ratios (for a given pressure) when the electrolyte concentration was increased. This apparent contradiction from the theory was interpreted to be as a result of coarser particles being present and the physical interactions between particles controlling the behavior rather than the osmotic repulsive forces.

The results discussed in the previous section contrast slightly with the results reported by Caughill (1992) where CT treated with varying dosages of lime, showed an optimum dosage in terms of settling and self weight consolidation. Caughill's test results for standpipes with a diameter of 31.5 cm and height of 51.5 cm showed that the average void ratio of a sample with 880 ppm of lime released more water than the sample with 600 ppm. However, samples with lime dosages of 1200 and 1600 ppm released less water than the sample with 800 ppm. However, given that the DHR ratio of these tests was 0.59 (31.5 cm diameter 51.5 cm height) the effect of lower repulsive forces caused by the higher dosages may have been overshadowed by boundary effects which were found be more pronounced at higher dosages. Had the DHR of these tests been larger (on the order of 2-4), it is theorized that the lowest void ratio under settling and self weight consolidation would have been achieved in the sample with the highest dosage and the anomaly of the 1200 and 1600 ppm samples may have been prevented. This is supported by the osmotic pressure concept, which identifies no optimum relationship between increased dosages as it relates to reduction in interparticle repulsion. Therefore, higher dosages should result in a lower void ratio for a given consolidation pressure. However, since lime is

known to increase the pH (rather than decrease it) the concept of an optimum dosage may indeed exist for lime.

6.2.3 Effect of PG on Hydraulic Conductivity

6.2.3.1 Quantitative Measurement of Hydraulic Conductivity

The hydraulic conductivity as measured during hindered sedimentation along with direct measurements after each loading step of the consolidometer, are shown in Figure 5.13 and define the relationship between the hydraulic conductivity and fines void ratio for two PG dosages. The measured hydraulic conductivity spanned two orders of magnitude and decreased from a maximum of approximately $1 * 10^{-5}$ cm/s under hindered sedimentation at 3200 g/m^3 to a low of $1 * 10^{-7}$ cm/s under 700 kPa with 900 g/m^3 of PG. For fines void ratio ranges between 2 and 9, the hydraulic conductivity of the sample with 3200 g/m^3 of PG was approximately 2.5 times greater than the sample with 900 g/m^3. The range of hydraulic conductivities is consistent with sodium kaolinite which has a hydraulic conductivity between 10^{-6} and 10^{-8} cm/s for total void ratios between 0.8 and 2 (Mesri and Olsen, 1971). The range of hydraulic conductivities tested within correspond to soils which have poor drainage characteristics.

Increased PG dosage causes destabilization of the clay particles, thus favoring flocculation and larger particle sizes. The effect of increased PG dosage on the hydraulic conductivity is a result of changes in the fines structure. The corresponding change in structure creates two effects which influence the hydraulic conductivity of the slurry. The first change is related to the tortuosity of the flow paths. The more flocculated a suspension is, the less likely that the particles are parallel to each other and therefore the flow path is more direct and less tortuous. The second change, and the major factor, is the increase in

average pore diameter and the presence of relatively large channels available for flow. The flow rate through soil depends mainly on the cross sectional area and is theoretically proportional to the fourth power of the radius of the pore. Therefore, flow through one large channel will be much greater than flow through numerous flow channels with the same total cross-sectional area. Thus the sample with 3200 g/m^3 was less dispersed and contained an increased average pore diameter and increased pore range and therefore was more permeable than the sample with 900 g/m^3 of PG.

As shown on Figure 5.13, the test results obtained from the slurry oedometer show a straight line correlation exists between the log of hydraulic conductivity and log of fines void ratio. When extrapolated to higher fines void ratios, this relationship predicts with reasonable accuracy the hydraulic conductivity measured during hindered sedimentation. Therefore during hindered sedimentation the interface and all particles within CT regardless of size, are moving at a rate proportional to their hydraulic conductivity and are not being significantly held up by boundary forces. This further supports the previous opinion that the negative effects of boundary shear forces during hindered sedimentation are not significant when the DHR was 2.9.

6.2.3.2 Qualitative Measurement of Hydraulic Conductivity

All SEM images (both variable pressure and cryogenic) provided in Chapter 5 show the typical card house structure of the fines, which features an edge to edge orientation. However, the rectangular shape of the void ratio was observed to transition to circular void shapes as the PG dosage increased. Figures 5.15 and Figure 5.24 show a low magnification view of two cryogenic SEM samples with 900 and 3200 g/m^3 of PG. Since the void ratio of all SEM samples was nearly constant and no significant settling occurred prior to sampling, the void space should be constant in all samples. At low magnifications, increased PG

resulted in the fines fabric appearing more flocculated and open and less continuous than at 900 g/m^3. Therefore, from the SEM images it appears that the increase in hydraulic conductivity due to increased PG dosage is directly related to the increase in average pore diameter and range of pore sizes.

It is interesting to note that the plane upon which the cryogenic samples failed, appears to be dependant on the PG dosage. At low dosages, the fracture surface contains sand grains which are clean and have no fines adhered to them. As the PG dosage is increased the amount of fines adhered to the sand grains increased. At the highest PG dosage, the sand grains are completely covered with fines and were often difficult to discern. This is believed to occur because at low dosages the sample fractured along the gap created between the sand and fines as this was presumably the weakest plane since no soil particles are present to act as "reinforcement" along this plane. As the dosage is increased and the EDL is further compressed clay particles can approach the sand grains much closer such that the gap is eliminated. Therefore, this weak plane is eliminated and at very high dosages the failure occurs through the "middle" of the fines structure adjacent to a sand grain, rather than along a weak "water plane"

Lastly, as noted in Figure 5.25 there are regions within the fines structure in which the pores shapes and sizes are not consistent with the rest of the image. The fines structure in these regions is more consistent with a dosage of 900 g/m^3 rather than 3200 g/m^3. It is believed that these dead zones are a result of incomplete mixing between the fines and PG and therefore these zones appear to be untreated with respect to PG.

6.2.3.2.1. Effect of Minor Fluctuations in PGFR on Hydraulic Conductivity

Given the discussion in the previous sections, the results of Figure 5.4 indicate that increasing the PG dosage (increasing the PGFR) increased the amount of

water which was released during the WRIT. Given the method by which the test specimens were prepared, minor fluctuations in PGFR at constant PG dosage were either a result of (1) minor fluctuations in the amount of PG actually added to each test (2) minor fluctuations in the fines content. These "errors" were likely introduced due to standard laboratory error (ability to measure small amounts of the PG with an electronic scale) or minor variations in the fines contents of the input components used to make CT. A discussion of each type of "error" is presented below.

Since the results of the WRIT incorporate water released during both hindered sedimentation and consolidation, it is difficult to isolate the effect certain variables may have. For example, the effect of minor changes in PGFR during self-weight consolidation could be impacting both the compressibility and hydraulic conductivity which both affect the amount of release water. However, an increase in PG dosage causes a higher hydraulic conductivity and an increased susceptibility to compression, both of which increase the amount of release water. Therefore, since the change in the hydraulic conductivity for samples with 900 and 3200 g/m^3 is more pronounced than the change in compressibility, the following discussion of the effect of minor PGFR's is based on the assumption that the effect is more likely to be related to changes in hydraulic conductivity than compressibility.

Assuming that the actual amount of PG which was added for a given dosage, was exactly the same in each test at the same dosage, then minor fluctuations in PGFR were a result of fluctuations in the solids and fines content of the input components. PGFR which were above the target PGFR, were a result of a decrease in the fines content and vice versa. Thus a logical explanation for the relationship between PGFR and water release rates is a result of changes in the amount of fines which are present in each test. As the fines content increases, PGFR decreases and less water is released during a WRIT. From Figures 5.5 and

5.6, the slope of the curve between PGFR and water release is much steeper at PGFR's near 4500 ppm than at 15000 ppm and indicates a large change in mass of release water for small changes in PGFR. At high PGFR's the curve is flatter and indicates that the mass of release water is less sensitive to PGFR. Therefore it is possible that the shape of these curves can be understood by comparing the type of fabric which is present at these two PGFR's. It was seen that at PGFR's near 15000 ppm the fabric is dominated by the presence of large pores versus a continuous fines network at 4500 ppm. Therefore a slight increase in fines content has less effect for PGFR's near 15000 ppm as the "additional fines" are less likely to clog the relatively large pores. Where as, for PGFR's near 4500 ppm the "additional fines" are more likely to have a clogging effect and therefore reduce the hydraulic conductivity and reduce the amount of release water.

Alternately, assuming that the fines content in each test was constant, the minor fluctuations in PGFR were a result of fluctuations in the amount of PG which was actually added to each test. This would reinforce the major relationship shown on Figure 5.4 between PG dosage and water release rate but on a very small scale. Therefore the change in the slope of the curves at the upper and lower ends could then be related to effectiveness of PG to compressing the EDL, reducing the pH, or reduction in bicarbonate concentration. That is, at high PG dosages, the slope decreases suggesting that an incremental increase in PG cause less compression of the electric double layer or less of a pH change than at low PG dosage. That is, at high PGFR's there are diminishing returns for PG dosage. The presence of an upper limit in terms of pH change is confirmed by the fact that oil sands tailings water is highly buffered and therefore large pH changes are not expected. Similarly, the increase in EDL compression is proportional to the square root of the concentration, which verifies that an upper limit exists for the amount of EDL compression which can occur. The decrease in

the slope of the curve at higher dosage would suggest an upper limit to the effectiveness of compressing the EDL.

It is the authors opinion that changes in the slope of the curves are related to changes in PG dosage on the small scale rather than increases in the amount of fines present. This is based on the large scale trend demonstrated in Figure 5.4 and the disbelief that very minor changes in the fines content would cause such an impact. However, additional research is required to isolate the factor responsible for this behavior.

7.0 CONCLUSIONS and RECOMMENDATIONS

7.1 Conclusions

In order to improve the numerical efficiency in computing multi-phase mass-volume relationships for oil sands tailings slurry, mathematical definitions and conversion equations were developed. It is hoped that these definitions along with the conversion equations will form the basis for standardizing usage of oil sands tailings parameters and act as an analytical tool to increase the understanding of material behavior.

Laboratory testing focused on examining the hindered sedimentation, consolidation, compressibility, hydraulic conductivity and structural characteristics of CT to assess the chemical and physical processes influencing the rapid dewatering of CT. Based on the results of this experimental research, the following conclusions can be made:

- a Diameter to Height Ratio (DHR) equal to or greater than 2.9 is sufficient to prevent a significant reduction (< 10 %) in the water release rate of CT as observed in a Standard Water Release Index Test (WRIT). The negative effects of small DHR's (< 2.9) are thought to be more pronounced at higher PG dosages due to an increase in boundary shear forces as a result of increased adhesion during hindered sedimentation or increased effective stress during consolidation. The minimum DHR is specific to the type of chemical addition and also the composition of the test cell;

- during a standard WRIT with a DHR of 2.9, CT undergoes hindered sedimentation followed by self-weight consolidation;

- hindered sedimentation was observed to last for approximately 7 to 8 hours in both the sample with 900 g/m^3 and 3200 g/m^3, and therefore changes in

PG dosage were not observed to cause a shift in the transition point between hindered sedimentation and consolidation;

- CT with a DHR's > 2.9 and treated with 900 and 3200 g/m^3 of PG and placed in 5 cm high deposits experience an immediate downward movement of the interface after deposition and are not subject to a lengthy induction period or flocculation period;

- WRIT's provide a suitable screening tool to quickly assess the impact of isolated changes (PG dosage, etc.) on dewatering characteristics of CT;

- due to the different PG dosages (physicochemical environment) the clay void ratio at which the CT samples with 900 and 3200 g/m^3 of PG transitioned from hindered sedimentation to consolidation are 16.1 and 14.9, respectively;

- the void ratio of the sample treated with 3200 g/m^3 of PG is always less than the void ratio of the sample with 900 g/m^3 for a given consolidation pressure. Increasing the PG dosage, causes an increase in the mass of release water and the presence of an optimum dosage was not observed;

- from self-weight and up to 10 kPa, CT displays moderate to intermediate compressibility characteristics and has a compression index consistent the upper limit of with pure kaolinite;

- for stresses up to 10 kPa, the effect of the sand as it relates to the deformation characteristics of CT is to increase the self-weight of the material, thereby driving the dewatering processes;

- the net effect of increasing PG dosage is an increase in electrolyte concentration and valency which causes a decrease in pH, a decrease in bicarbonate concentration and a net reduction in the interparticle repulsion. The role of bitumen as it relates to PG dosage and ultimately soil fabric is

unclear. Additional research is required to assess the relative importance of these factors.

- the measured hydraulic conductivity of CT spanned two orders of magnitude and decreased from a high of approximately $1 * 10^{-5}$ cm/s under hindered sedimentation with 3200 g/m^3 to a low of $1 * 10^{-7}$ cm/s under 700 kPa with 900 g/m^3 of PG;

- for fines void ratios ranges between 2 and 9, the hydraulic conductivity of the sample with 3200 g/m^3 of PG was approximately 2.5 times greater than the sample with 900 g/m^3;

- a straight-line correlation exists between the log of hydraulic conductivity and log of fines void ratio. This relationships obtained from the slurry oedometer predicts with reasonable accuracy the hydraulic conductivity measured during hindered sedimentation;

- from the SEM images it appears that the increase in hydraulic conductivity due to increased PG dosage is directly related to the increase in average pore diameter and range of pore sizes as a result of changes in fabric, and

- the presence of the card house structure does not appear to be an artifact of freezing as cryogenic and variable pressure SEMs both showed the typical card house structure.

7.1 Recommendations for Further Research

As elucidated in the discussion of the research results, many additional factors were identified that may have an influence in the rapid dewatering mechanisms of CT. While many of these factors were outside the scope of this research project, they represent components of the fundamental behavior of CT and

should be investigated. The following sections provide brief summaries of suggested recommendations for future research on the dewatering characteristics of CT:

- measure specific surface area and cation exchange capacity of CT to enhance the understanding of physicochemical changes;
- measure repulsion-attraction forces by leaching CT in oedometer with distilled water and preventing volume change;
- closely measure the change in pH as a function of increase PG dosage to determine the relative contribution of calcium ions to the compression of the EDL, decrease in pH and reduction in bicarbonate ion concentration;
- due to the relationship between fines void ratio and hydraulic conductivity; perform a series of test on CT without the sand. Adjust the dosage such that the water chemistry parameters are consistent and measure the hydraulic conductivity and compare to CT with sand and same fines void ratio;
- determine effect of inline mixing and flow regime in the field as it relates to floc formation. Tests by other indicate that high-speed shearing produces a more random structure in MFT and others report that the rectangular fines structure can be disrupted by shaking. Field shearing may produce a more random structure or prevent the formation of the rectangular structure, which ultimately enhances dewatering characteristics as observed in the field;
- use pixel tracking software to better determine the behavior of the soil/water interface during hindered sedimentation; and
- perform image analysis on SEM and obtain quantitative results for size and shape of pores, void ratio, texture, etc.

References

Bennett, R.H., and Hurlbut, M.H. 1986. Clay Microstructure, International Human Resource Development Corporation, Boston / Houston / London, 161 pp.

Bohn, H.L., McNeal, B.L., and O'Connor, G.A., 1985 "Soil Chemistry", 2nd Edition, John Wiley & Sons, Inc., N.Y.

Bolt, G.H. 1956. "Physico-chemical analysis of the compressibility of pure clays", Geotechnique, Vol. 6, No. 2, pp. 86-93.

Camp, F.W., 1976. Processing Athabasca Tar Sands: tailings Disposal, Symposium on Tar Sands, Proceedings 26th Canadian Chemical Engineering Conference, Toronto, 47p.

Been, K. and Sills, G.C., 1981. Self-weight Consolidations of Soft Soils, An Experimental and Theoretical Study, Geotechnique, Vol 31, December 1981, pp. 519-535.

Caughill, D.L, 1992. "Geotechnics of Non-segregating Tailings", M.Sc thesis, University of Alberta, Edmonton, Alberta, Canada.

Caughill, D.L., 1992 "Geotechnics of Non-segregating Oil Sand Tailings", M.Sc., University of Alberta, Edmonton, Alberta, Canada

Chatterji, P.K. and Morgenstern, N.R., 1989. "A Modified Shear Strength Formulation for Swelling Clay Soils", Symposium on Physico-Chemical Aspects of Soil, Rock and Related Minerals, St. Louis, Missouri, June 29, 1989.

Chatterji, P.K. and Morgenstern, N.R., 1989. A Modified Shear Strength Formulation For Swelling Clay Soils. Symposium on Physico-Chemical

Aspects of Soil, Rock and Related Materials, St. Louis, Missouri, June 29, 1989.

Chen, Y. and Banin, A., 1974. Scanning Electron Microscope (SEM) Observations of Soil Structure Changes Induced by Sodium-Calcium Exchange in Relation to Hydraulic Conductivity. Soil Science, Vol. 120, No. 6, pp. 428-436.

Chen, Y., Banin, A and Borochovitch, A., 1983. Effect of Potassium on Soil Structure in Relation to Hydraulic Conductivity. Geoderma, 30 (1983) pp. 135-147.

Coe, H.S. and Clevenger, P.A., 1916. Methods for Determining the Capacities of Slime-Settling Tanks, from Transactions of the American Institute of Mining Engineers, Vol. 55, pp. 356-384.

Collis-George, N. and Bozeman, J.M. 1970 "A double layer theory for mixed ion systems as applied to the moisture content of clays under restrain", Australian Journal of Soil Research, Vol. 8, No. 3, pp. 239-258.

Collis-George, N. and Bozeman, J.M., 1970. A Double Layer Theory for Mixed Ion Systems as Applied to the Moisture Content of Clays Under Restraint. Australian Journal Roils Res., 8: 239-258.

Dusseault, M.B., and Scott, J.D. 1982. "Characterization of Oil Sands Tailings Sludge", Presented at Short Course on Consolidation Behavior of Fine-Grained Waster Materials, Denver, Colorado, October 7, 1982. A

Dusseault, M.B., and Scott, J.D. 1983. "Tailings Pond Behavior and Characterization of Oil Sand Tailings Sludge", Particulate Science and Technology, Vol. 1, pp. 295-309.

El-Swaify, S.A. and Henderson, D.W., 1967. Water Retention by Osmotic Swelling of Certain Colloidal Clays with Varying Ionic Composition. Journal of Science, Vol. 18, No. 2.pp. 223-232.

Fitch, E.B., 1966. Current Theory and thickener Design. Industrial and Engineering Chemistry Fundamentals, 58, 18-28.

Thomas, D.G. 1963. Non-Newtonian suspensions, Industrial and Engineering Chemistry Fundamentals, 55, 27-35.

Shannon, P.T. and Tory, E.M., 1965. Settling of Slurries, Industrial and Engineering Chemistry Fundamentals, 57, 18-25.

Scott, K.J., 1968. Theory of thickening : factors affecting settling rate of solids in flocculated pulps. Transactions/Section C of the Institution of Mining and Metallurgy, volume 77, pages C85 to C97.

FTFC (Fine Tailings Fundamentals Consortium), 1995. "Vol., Title," In: Advances in Oil Sands Tailings Research, Alberta Department of Energy, Oil Sands and Research Division, Publisher.

Volume 1 – Clark Hot Water Extraction Fine Tailings
Volume II – Fine Tails and Process Water Reclamation
Volume III – Volume Reduction of Clark Hot Water Extraction Fine Tailings
Volume IV- Non-Clark Extraction Processes and Their Tailings Characteristics.

Gaudin, A.M. and Fuerstenau, M.C. 1960. On the Mechanism of Thickening. Group II: Paper No. 6, pp. 115-127.

Gaudin, A.M., Fuerstenau, M.C. and Mitchell, S.R., 1959. Effect of Pulp Depth and Initial Pulp Density in Batch Thickening. Mining Engineering, June 1959, pp. 613-616.

Huang, P.M., Senesi, N., and Buffle, J., 1998 "Structure and Surface Reactions of Soil Particles:, Volume 4, John Wiley & Sons, Inc., N.Y.

Imai, G., Experimental Studies on Sedimentation Mechanism and Sediment Formation of Clay Materials, 1981. Soils and Foundation, Japanese Society of Soil Mechanics and Foundation Engineering, Vol. 21, No. 1, March 1981.

Imai, G., Settling Behavior of Clay Suspension, 1980. Soils and Foundation, Japanese Society of Soil Mechanics and Foundation Engineering, Vol. 20, No. 2, June 1980.

Kasperski, K.L., 1992. A Review of Properties and Treatment of Oil Sands Tailings. AOSTRA Journal of Research, 8 (1992) 11, TN 873 A12, 53 p.

Kenney, T.C., "The influence of Mineral Composition of the Residual Strength of Natural Soils". Proceedings of Geotechnical Conference, Oslo, Norway, Vol.1, pp. 123-129, 1967.

Kynch, G.J., 1952. A Theory of Sedimentation. Transactions of Faraday Society, 48: 166-176.

Lambe, T.W. and Whitman, R.V. 1969, *Soil Mechanics*, J. Wiley, New York, 553p.

Leroueil, S., and Vaughan, P.R. 1990. The general and congruent effects of structure in natural soils and weak rocks, Geotechnique, Vol. 40, No. 3, pp. 467-488.

Lui, Y.B., Lord, E. and Scott, J.D., 1996. "Geotechnical Aspects of Two Innovative Disposal Technologies For Oil Sands Tailings"

McBride, M.B., 1994 "Environmental Chemistry of Soils", Oxford University Press, Inc., N.Y.

McNeal, B.L. and Coleman, N.T. 1966. "The Effect of Solution of Soil hydraulic conductivity", Proceedings of the Soil Science Society of America, Vol. 30, No. 2, pp. 308-312.

Mesri, G. and Olson, R.E., "Mechanisms controlling the permeability of clays", Clays and Clay Minerals, 19, No. 3, pp. 151-158.

Michaels, A.S., and Bolger, J.C. 1962. "Settling rates and sediment volumes of flocculated kaolin suspensions". Industrial and Engineering Chemistry Fundamentals, 1:24-33.

Mikula, R.J., Kasperski, K.L. and Burns, R.D. 1996 "Consolidated tailings release water chemistry", Tailings and Mine Waste'96. Vol No. , pg. 459-468. GG

Mitchell, J.K. 1960. "Fundamental aspects of thixotropy in soils", Journal of Soil Mechanics and Foundations Division, A.S.C.E., Vol. 86, No. SM 3, pp. 19-52.

Mitchell, J.K., 1993. Fundamentals of soil behavior. 2nd edition, John Wiley and Sons, Inc., New York.

Morgenstern, N.R., and Balasubramonian, B.I., 1980. Effects of Pore Fluid on the Swelling of Clay-Shale. Proceedings of the 4th International Conference on Expansive Soils, ASCE, pp. 190-205.

Olsen , H.W. 1962. Hydraulic flow through saturated clay, Proceedings of the Ninth National Conference on Clays and Clay Minerals, pp. 131-161.

Pane, V. and Schiffman, R.L., 1997. The permeability of clay suspensions. Geotechnique, 47: 273-288.

Quirk, J.P. and Schofield, R.K., 1955. The Effect of Electrolyte Concentration on Soil Permeability. Journal of Science, Vol. 6, No. 2, 1955, pp. 153-178.

Riech, I. And Robert, D.V. 1957. Floccualtion-Deflocculation in agitated suspensions. Journal of Physical Chemistry, 63, pg. 1497-1501.

Roberts, J.O.L., Yong, R.N. and Erskine, H.L. 1980. Surveys of some tar sand sludge ponds; results and interpretations. Proceedings of Applied Oil sands Geoscience 1980 Conference, Edmonton, Alberta June 11-3. Pg. 46.

Sego, D.C. et al., 1993, Dewatering of Fine Tails Utilizing Freeze-Thaw Process, Edmonton Alberta, Canada, F17-1 to F17-25.

Scott, K.J., 1968, Theory of Thickening. Factors affecting settling rates of solids in flocculated pulps. Transactions of the Institution of Mining and Metallurgy, Volume 77, pg. C85-C97.

Scott, J.D. and Cymerman, G.J., 1984. Prediction of viable tailings disposable methods. Proceedings, Sedimentation/Consolidation Models-Predictions and Validation, San Francisco, California, October 1, 1984, pp. 522-544.

Scott, J.D. and Dusseault, M.B. 1980. "Behavior of oil Sands Tailings", 33rd Canadian Geotechnical Conference, Calgary, Alberta, September 24-26, 1980, 16 pp.

Scott, J.D. and Dusseault, M.B. 1982. "Behavior of Oil Sand Tailings Sludge", 33rd Annual Technical Meeting of the Petroleum Society of CIM Held Jointly with the 6th Symposium of Engineering Applications of Mechanics, Calgary, Alberta, June 6-9, 1982, 19 pp. H

Scott, J.D. and Hemstock, R.A., 1981. Winning of Oil Sands Paper. SeaTech Conference, March 2-6, 1981, Singapore, 38 p.

Scott, J.D. Dusseault, M.B. and Carrier III, W.D., 1986. Large-scale self-weight consolidation testing. Consolidation of Soils: Testing and Evaluation, ASTM SPT 892, pp. 500-515.

Scott, J.D., Liu, Y. and Caughill, D.L., 1993. "Fine Tails Disposal Utilizing Nonsegregation Mixes. Proceeding, Oil Sands – Our Petroleum Future Conference, Edmonton, Alberta, April 4-7, 1993. F18. 19p.

Scott, J.D., 2002 personal communication

Shainberg, I., Bresler, E. and Klausner, Y., 1970. Studies on N_A/C_A Montmorillonite Systems, 1. The Swelling Pressure, 1970. Soil Science, Vol. III, No. 4, pp. 214-219.

Shainberg, I., Caiserman, A. 1971. Studies on N_A/C_A Montmorillonite Systems, 2. The Hydraulic Conductivity, Soil Science, Vol. III, No. 4, pp. 276-281.

Shaw, B., Cuddy, G., McKenna, G. and MacKinnon, M., 1996. "Non-segregating Tailings: 1995 NST Field Demonstration Summary Report"

Sposito, G., 1989 "The Chemistry of Soils", Oxford University Press, Inc., N.Y.

Suthaker, N.N., 1995 "Geotechnics of Oil Sand Fine Tailings", Ph.D., University of Alberta, Edmonton, Alberta, Canada

Syncrude, (1996). "Nonsegregating Tailings: 1995 NST Field Demonstration Summary Report", Syncrude Canada Ltd. Research and Development

Tan, K.H. 1993. Principals of Soil Chemistry, 2nd Edition. Marcel Dekker Inc. 362p.

Tang, J., 1997 "Fundamental Behavior of Composite Tailings", M.Sc., University of Alberta, Edmonton, Alberta, Canada

Tiller, F.M., and Khatib, Z., 1984. The theory of sediment volumes of compressible, particulate structures. Journal of Colloid and Interface Science, 100: 55-67.

Van Olphen, H., 1977. An Introduction to Clay Colloid Chemistry. John Wiley and Sons, New York, NY.

Wild, A., 1993, 'Soils and the Environment", *Cambridge University Press, N.Y.*

APPENDIX A

CT Mix Design and Selected Sample Calculations

A1. Components Used to Produce 1 m^3 of Field CT. See Table 4.1. (Target 62 % Solids and 20 % Fines)

1. 1186 kg of Cyclone Underflow at 75.0 % Solids and 10.1 % Fines contains:

Sand
= 1186 * (0.75) * (1-0.101)
= 799.7
Fines (including bitumen)
= 1186 * (0.75) * (0.101)
= 89.8
Water
= 1186 * (1-0.75)
= 296.5

2. 362 kg of MFT at 31.0 % Solids and 98.4 % Fines contains:

Sand
= 362 * (0.31) * (1-0.984)
= 1.8
Fines (including bitumen)
= 362 * (0.31) * (0.984)
= 110.4
Water
= 362 * (1-0.31)
= 249.8

3. 67 kg of Pond Water contains:

Sand
= 0
Fines (including bitumen)
= 0
Water
= 67 * (1)
= 67.0

Summary

1. Total Sand
= 799.7 + 1.8
= 801.5

2. Total Fines (including bitumen)
= 89.8 + 110.4
= 200.2

3. Total Water
= 296.5 + 249.8 + 67.0
= 614.3

A1. continued

Therefore, actual CT Composition

(see 3.3.4.2 and 3.3.11.1 for parameter definition)

1. Solids Content - Geotechnical (s)

= mass of solids / total mass of tailings

= (801.5 + 200.2) / (801.5 + 200.2 + 614.3)

= **62.0%**

2. Fines Content - Geotechnical (II) (fb)

= (mass of fines + mass of bitumen) / mass of solids

= (200.2) / (801.5 + 200.2)

= **20.0%**

A2. Breakdown of Age Designations for CT Components.
(see A1 for mass of each input component)

1. 1186 kg of Cyclone Underflow contains:

296.5	kg of "young" water
89.8	kg of "young" fines
799.7	kg of "young" sand
1186.0	

2. 362 kg of MFT contains:

249.8	kg of "aged" water
110.4	kg of "aged" fines
1.8	kg of "aged" sand
362.0	

3. 67 kg of Pond Water (and Gypsum) contains:

67.0	kg of "aged" water
67.0	

Summary of Water

1. "Young" Water
   = 296.5
2. "Aged" Water
   = 249.8 + 67.0
   = 316.8
3. **Percent "Young" Water**
   = 296.5 / (296.5 + 316.8)
   = **48.3%**

Summary of Fines

1. "Young" Fines
   = 89.8
2. "Aged" Fines
   = 110.4
3. **Percent "Young" Fines**
   = 89.8 / (89.8 + 110.4)
   = **44.9%**

Summary of Sand

1. "Young" Sand
   = 799.7
2. "Aged" Sand
   = 1.8
3. **Percent "Young" Sand**
   = 799.7 / (799.7 + 1.8)
   = **99.8%**

A3. Backcalculated Solids Content and Fines Content of Whole Tailings.

1. Cross Section of Drum #1

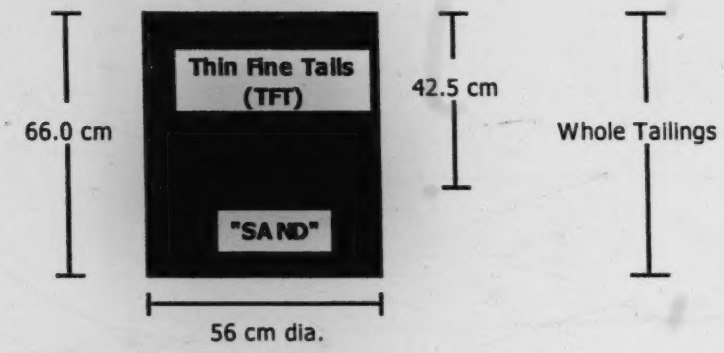

2. Cross Section of Drum #2

3. a) Bulk Denisty of Thin Fine Tails (TFT) at 10.7 % Solids and 97.2 % Fines.

$$\rho = \frac{\rho_{sw}}{\left(\frac{s}{Gfb} + \frac{1-s}{S_r \times G_w}\right)} \text{ OR } \rho = \frac{1000}{\left(\frac{0.107}{2.30} + \frac{1-0.107}{1.0 \times 1.0}\right)} \qquad \rho = 1064 \text{ kg/m}^3$$

b) Average Volume of Thin Fine Tails (TFT)

$$V = \frac{\pi \times \text{dia}^2 \times \text{avg. height}}{4} \text{ OR } V = \frac{3.14 \times 0.56^2 \times 0.445}{4} \qquad V = 0.1095 \text{ m}^3$$

c) Mass of TFT (kg)

Mass = ρ x volume
= 1064 * (0.1095)
= 116.5

A3. continued

d) 116.5 kg of TFT contains

Sand
= 116.5 * (0.107) * (1-0.972)
= 0.3

Fines (including bitumen)
= 116.5 * (0.107) * (0.972)
= 12.1

Water
= 116.5 * (1-0.107)
= 104.0

4. a) Bulk Density of "SAND" 82.8 % Solids and 6.5 % Fines

$$\rho = \frac{\rho_{sw}}{\left(\frac{s}{G_{sd}} + \frac{1-s}{S_r \times G_w}\right)} \quad \text{OR} \quad \rho = \frac{1000}{\left(\frac{0.828}{2.66} + \frac{1-0.828}{1.0 \times 1.0}\right)} \quad \rho = 1064 \text{ kg/m}^3$$

b) Average Volume of Sand

$$V = \frac{\pi \times \text{dia}^2 \times \text{avg. } height}{4} \quad \text{OR} \quad V = \frac{3.14 \times 0.56^2 \times 0.215}{4} \quad V = 0.053 \text{ m}^3$$

c) Mass of Sand

Mass = ρ x volume
= 2069 * (0.053)
= 109.7

c) 109.5 kg of sand contains:

Sand
= 109.7* (0.828) * (1-0.065)
= 84.9

Fines (including bitumen)
= 109.7 * (0.828) * (0.065)
= 5.9

Water
= 109.7* (1-0.828)
= 18.9

A3. continued

7. Summary

a) Total Sand

= 0.3 + 84.9

= 85.2

b) Total Fines

= 12.1 + 5.9

= 18.0

c) Total Water

= 104.0 + 18.9

= 122.9

8. Backcalculated composition of Whole Tailings

(see 3.3.4.2 and 3.3.11.1 for parameter definition)

1. Solids Content - Geotechnical (s)

= mass of solids / total mass of tailings

= (85.2 + 18) / (85.2 + 18 + 122.9)

= 45.6%

2. Fines Content - Geotechnical (II) (fb)

= (mass of fines + mass of bitumen) / mass of solids

= (18.0) / (18.0 + 85.1)

= 17.5%

A4. Determination of Bulk Density, kilograms of fines per m^3 of CT and for Test J199. See Table 5.4.

1. Test J199 = CT 62.48 % Solids and 19.84 % Fines with (600 g/m^3 PG

a) Bulk Density

$$\rho = \frac{\rho_{sw}}{\left(\frac{s}{G_s} + \frac{1-s}{S_r \times G_w}\right)} = \frac{1000}{\left(\frac{0.6248}{2.59} + \frac{1-0.6248}{1.0 \times 1.0}\right)} \qquad \rho = 1622 \text{ kg/m}^3$$

b) Kilograms of Fines per m^3

= Kilograms per m^3 * (% Solids) * (% Fines)
= 1622 * (0.6248) * (0.1984)
= 201.1

c) Ratio of PG Dosage in mg/m^3 to mass of fines in kilograms per m^3 of
= (600 g/m^3) * (1000 mg/g) / 201.1 kg

PGFR = 2984 mg/kg
or
PGFR = 2984 ppm

A5. What changes in the solids or fines content are actually shown in Figures 5.5 and 5.6 ?

1. Figure 5.5 with 900 g/m^3 PG

A.For a **Fines Content of 20 %**, what range of solids content is being shown ?

Ranges in Figure 5.5	PGFR (ppm)	Fines	Required Solids Content to Produce desired PGFR
Low	3800	20.0%	68.6%
High	4700	20.0%	60.3%

Since our grab samples are accurate enough to determine the difference between 60.3 and 68.6 solids %, the variations shown in Figure 5.5 are real.

B. For a **Solids Content of 62 %**, what range of fines content is being shown ?

Ranges in Figure 5.5	PGFR (ppm)	Solids	Required Fines Content to Produce desired PGFR
Low	3800	62.0%	23.7%
High	4700	62.0%	19.1%

Since our grab samples are accurate enough to determine the difference between 19.1and 23.7 % fines, the variations shown in Figure 5.5 are real.

2. Figure 5.6 with 3200 g/m^3 PG

A. For a **Fines Content of 20 %**, what range of solids content is being shown ?

Ranges in Figure 5.6	PGFR (ppm)	Fines	Required Solids Content to Produce desired PGFR
Low	13500	20.0%	68.61%
High	16500	20.0%	60.78%

Since our grab samples are accurate enough to determine the difference between 60.8 and 68.6 % solids, the variations shown in Figure 5.6 are real.

B. For a **Solids Content of 62 %**, what range of fines content is being shown ?

Ranges in Figure 5.6	PGFR (ppm)	Solids	Required Fines Content to Produce desired PGFR
Low	13500	62.0%	23.68%
High	16500	62.0%	19.38%

Since our grab samples are accurate enough to determine the difference between 19.4 and 23.7 % fines, the variations shown in Figure 5.6 are real.

Table A1
Mass of CT required to be added to a 14.55 cm diameter acrylic cell to produce a deposit 5.0 cm high.

Sr	Measured Density (kg/m^3)	Mass of CT to Be Added to Cell (g)	Height if no correction Made (cm)
100%	1615	1342.2	5.00
99%	1605	1334.0	5.03
98%	1595	1325.6	5.06
97%	1584	1317.2	5.09
96%	1574	1308.8	5.13
95%	1564	1300.2	5.16
94%	1554	1291.6	5.20
93%	1543	1283.0	5.23
92%	1533	1274.3	5.27
91%	1522	1265.4	5.30
90%	1511	1256.6	5.34
89%	1501	1247.6	5.38
88%	1490	1238.6	5.42
87%	1479	1229.5	5.46
86%	1468	1220.3	5.50
85%	1457	1211.1	5.54
84%	1446	1201.8	5.58
83%	1434	1192.4	5.63
82%	1423	1182.9	5.67
81%	1411	1173.4	5.72
80%	1400	1163.7	5.77
79%	1388	1154.0	5.82
78%	1376	1144.2	5.87
77%	1364	1134.4	5.92
76%	1352	1124.4	5.97
75%	1340	1114.3	6.02

Assuming:

G_s =	2.59
Solids	62%
Fines	20%

APPENDIX B

Manufacturer's Specification Sheet for

LEO 438 Variable Pressure SEM

LEO 438VP

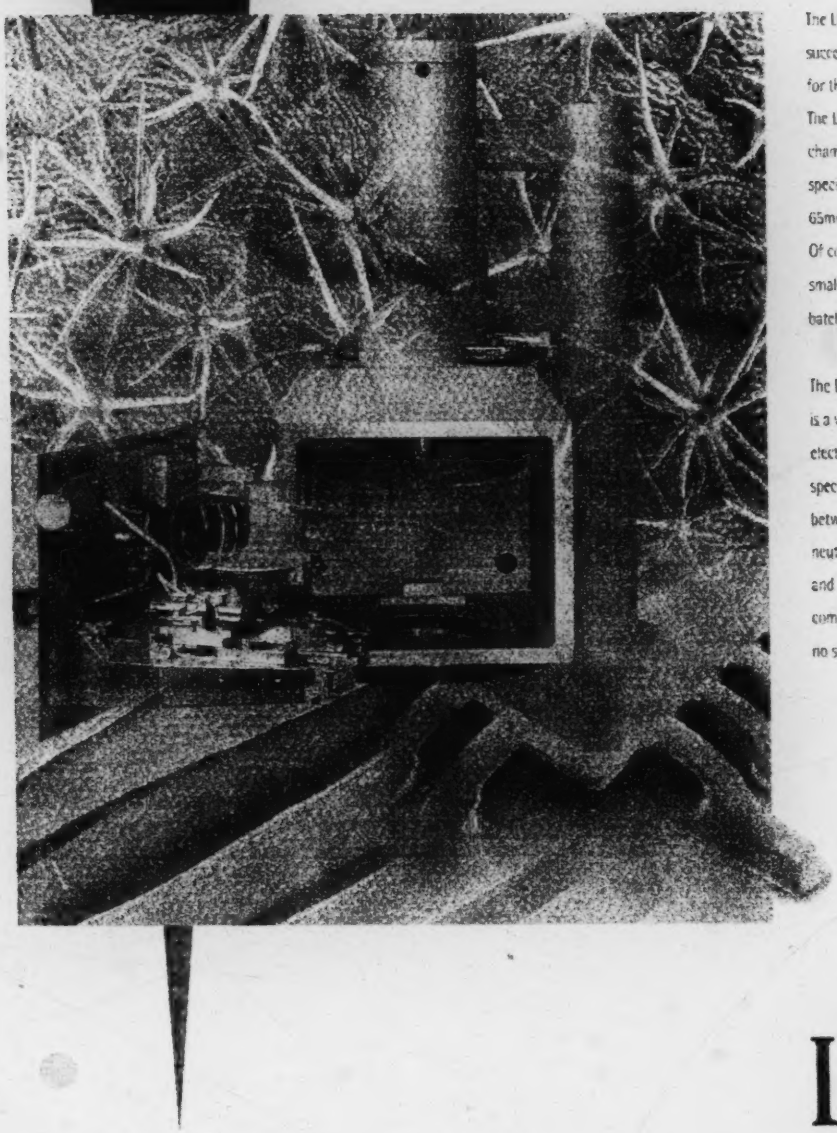

The LEO 438VP, based on the highly successful LEO 435VP is designed for the analysis of large samples. The LEO 438VP's specially designed chamber is capable of holding specimens up to an incredible 65mm thick and 200mm diameter. Of course it can still accommodate small specimens or even a whole batch of specimens together.

The LEO 438VP, like the LEO 435VP, is a variable pressure scanning electron microscope, which uses specimen chamber pressure control between 1Pa and 400Pa to neutralise any specimen charging and allows high kV analysis of complete insulators - with little or no sample preparation.

LEO

The power to resolve

Essential Specifications...

Resolution:

High Vacuum Mode:
SE Resolution 4.0nm

Variable Pressure Mode:
BSD Resolution 6.0nm

Magnification:

15x to 300,000x

Accelerating Voltage:

300V to 30kV

Variable Pressure Range:

Range: 1Pa to 400Pa

Probe Current:

Range: 1pA to 500nA
Adjustment: Continuous

Optibeam:

For smallest spot size/
highest probe current

Detectors:

Everhart-Thornley SE with
VPSE (Variable Pressure
Secondary Electron) or BSD

Specimen Stage:

Type: 5 axis motorised
cartesian

Mounting: Hinged door

Movements:
X = 100mm (± 50mm)
Y = 125mm (+75mm,
-50mm)
Z = 60mm (34mm
motorised)
Tilt = 0° to 90°

Rotation: 360° continuous

Image Display:

17" XVGA monitor

Image Recording:

Video Printer or Optional
HRRU (High Resolution
Record Unit)

Image Processing:

Resolution: 1024 x 768 pixels.
Frame averaging, frame
integration, line averaging
and line integration

Site Services:

AC supply only

Finished integrated circuit, uncoated, in VP mode.

Total user satisfaction...

LEO combines the very best of two leading electron microscope manufacturers, Zeiss and Leica. LEO, with its unique knowledge of innovative techniques and a deep understanding of customer applications, will guarantee a consistent and sustained programme in the advancement of electron microscopy.

The creation of LEO heralds a new era in the development, manufacture, sales and service of scanning and transmission electron microscopes.

LEO - committed to delivering excellent value to electron microscopists around the globe.

LEO

LEO Electron Microscopy Customer Response Centres:

Australia: Sydney Tel (61) 2 9482 1149 Fax (61) 2 9482 1196
E-mail sbwisbey@ozemail.com.au
Czech Republic: Brno Tel (42) 05 47 220 760 Fax (42) 05 47 220 016
E-mail leo_em@mbox.vol.cz
France: Rueil-Malmaison Tel (33) 1 41 39 92 10 Fax (33) 1 41 39 92 29
E-mail LEO_France@compuserve.com
Germany: Oberkochen Tel (49) 73 64 94 6137 Fax (49) 73 64 94 4851
E-mail info@leo.de
India: New Delhi Tel (91) 11 572 3240 Fax (91) 11 681 4181
E-mail leoindia@giasd101.vsnl.net.in
Scandinavia: Sweden Tel (46) 158 13090 Fax (46) 158 13095
E-mail michael.andersson@leo-em.d.se
Singapore: Tel (65) 741 9158 Fax (65) 741 4809
E-mail leospore@singnet.com.sg
UK: Cambridge Tel (44) 1223 414166 Fax (44) 1223 412776
E-mail info@leo-em.co.uk
USA: New York Tel (1) 914 747 7700 Fax (1) 914 681 7443
E-mail 70142.604@compuserve.com
Website: www.leo-em.co.uk

Plus a worldwide network of dealers

Due to [illegible] of continuous development, we reserve the right to change specifications without notice © by LEO [illegible] Microscopy Ltd Cambridge England 1998 LEO/SMP/REV/A1 Printed in the UK on Chlorine free p

APPENDIX C

Large Strain Consolidation Test Results:

Void Ratio vs. Time for Each Loading Step

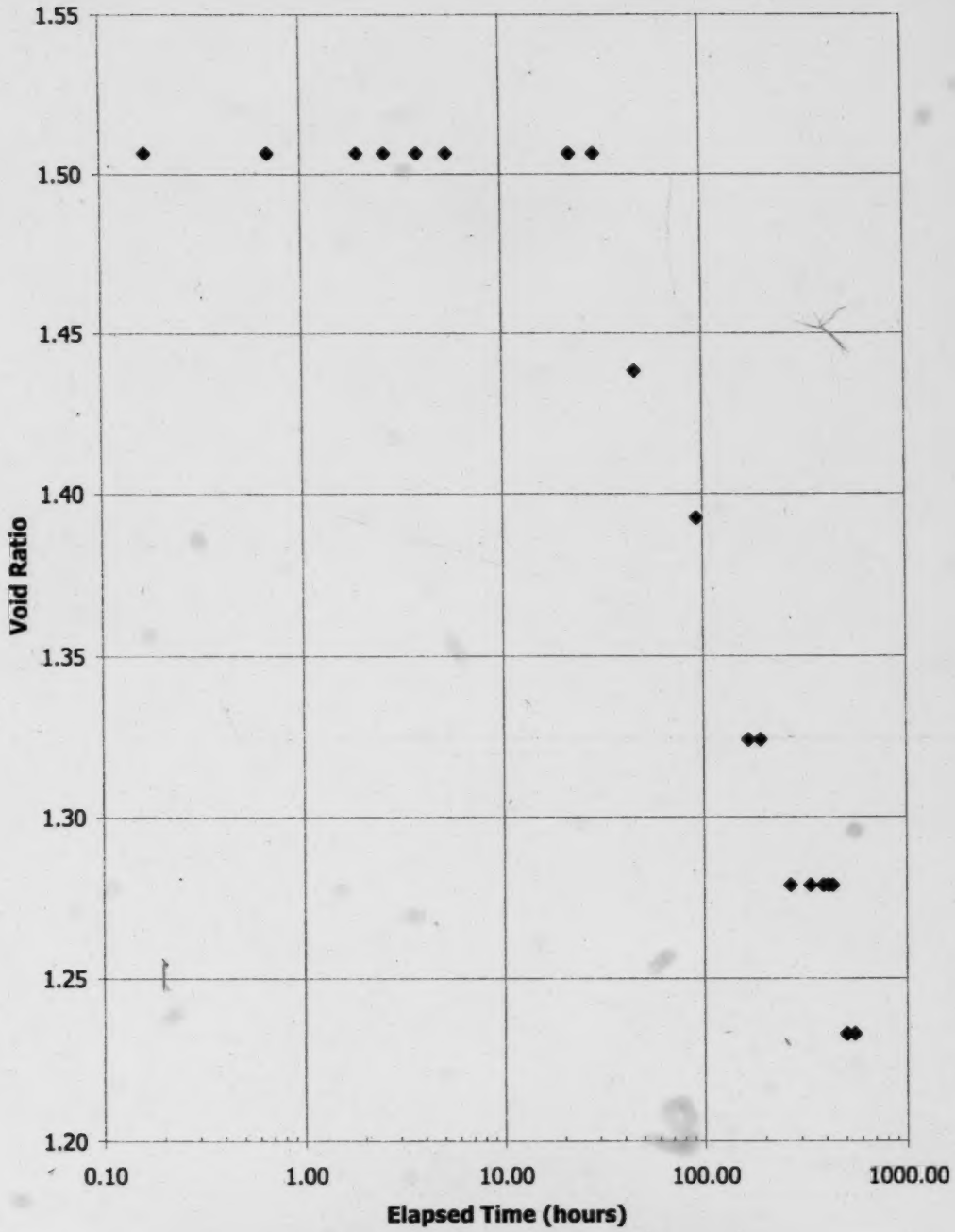

Figure C1: Void Ratio vs. Elapsed Time for C&P - 3
Initially 63.3 % Solids, 20.9 % Fines, 900 g/m^3 PG
Self Weight Loading

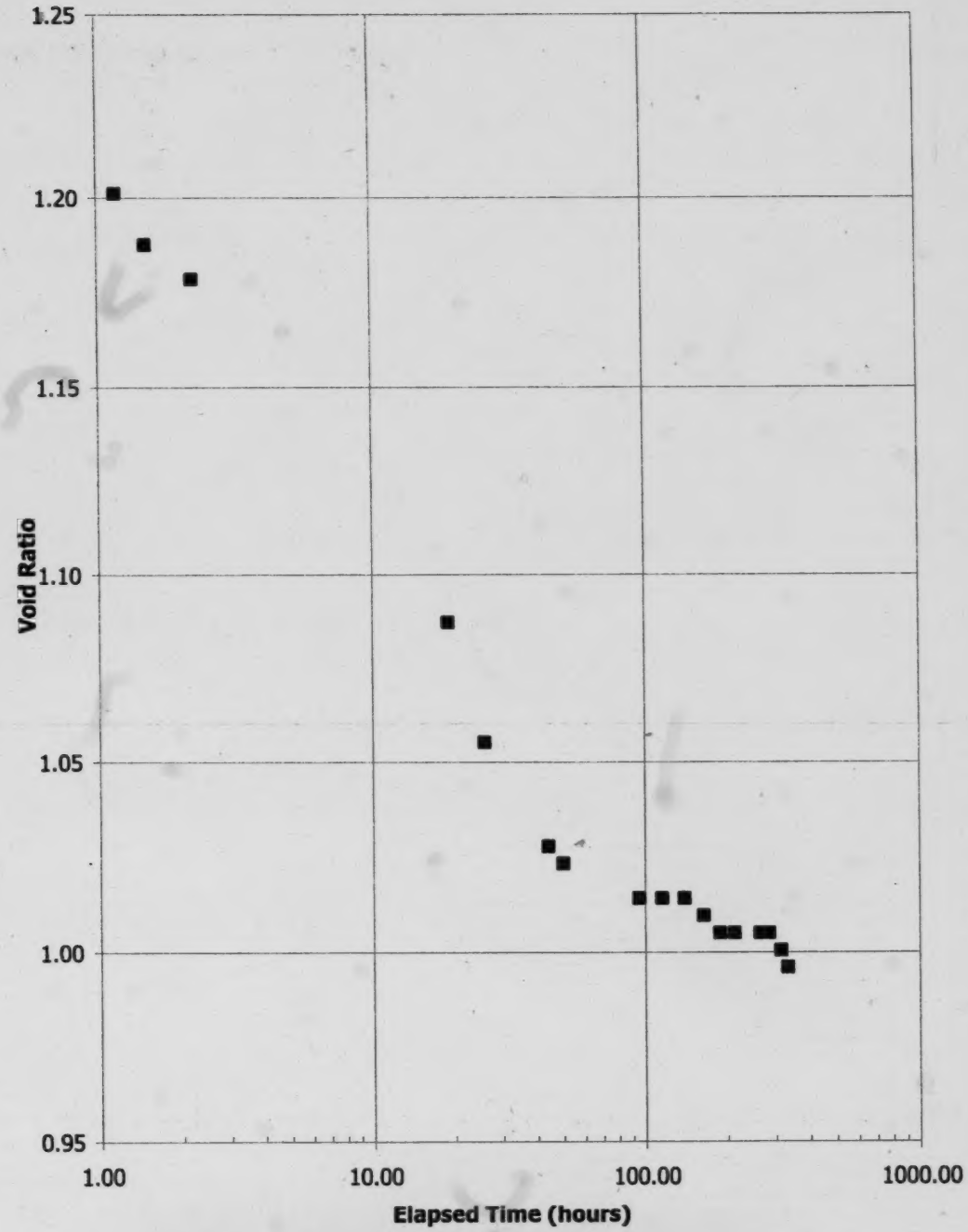

Figure C2: Void Ratio vs. Elapsed Time for C&P - 3
Initially 63.3 % Solids, 20.9 % Fines, 900 g/m^3 PG
Loading from 0.14 kPa (self weight) to 1.2 kPa

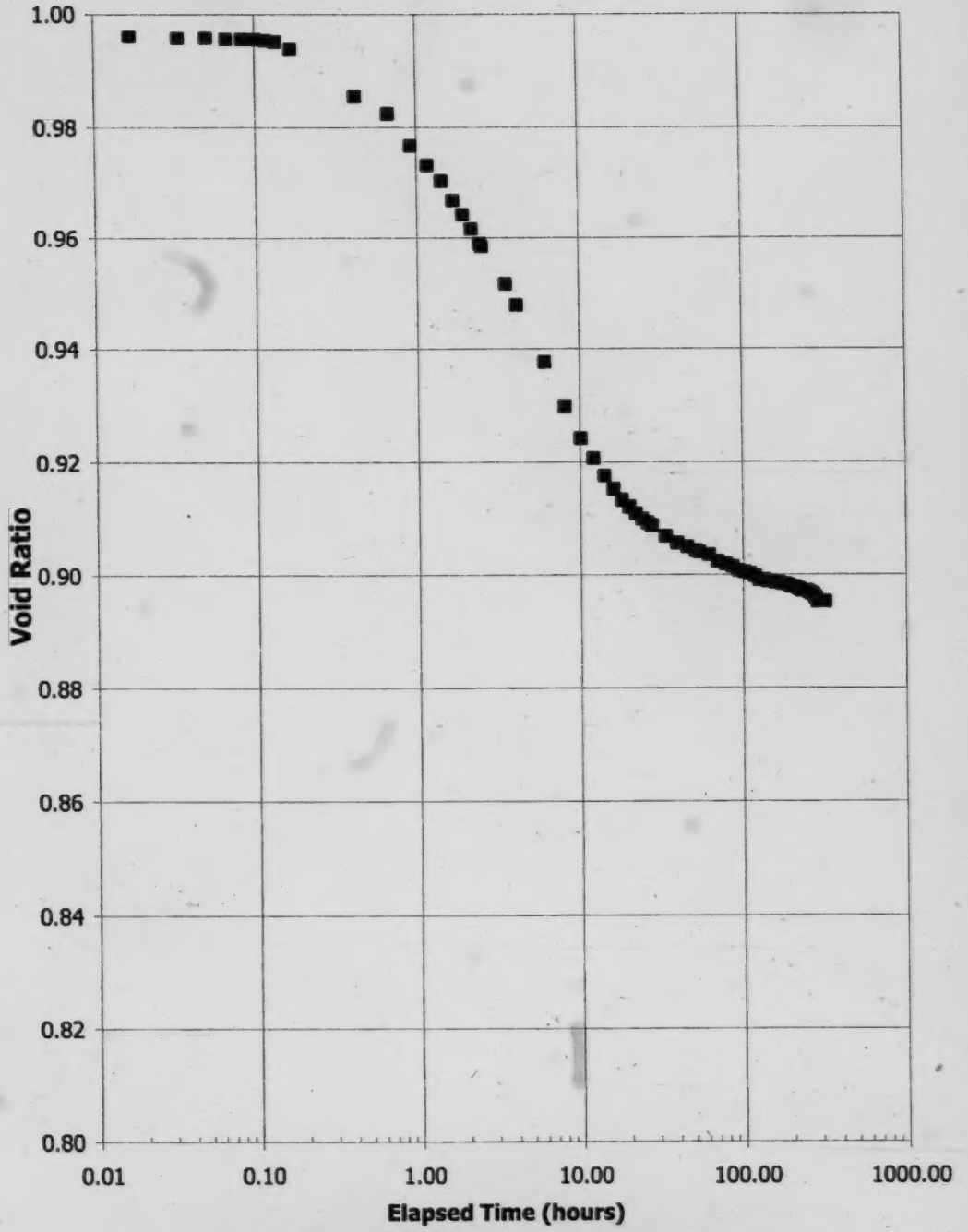

Figure C3: Void Ratio vs. Elapsed Time for C&P - 3
Initially 63.3 % Solids, 20.9 % Fines, 900 g/m^3 PG
Loading from 1.2 kPa to 2.6 kPa

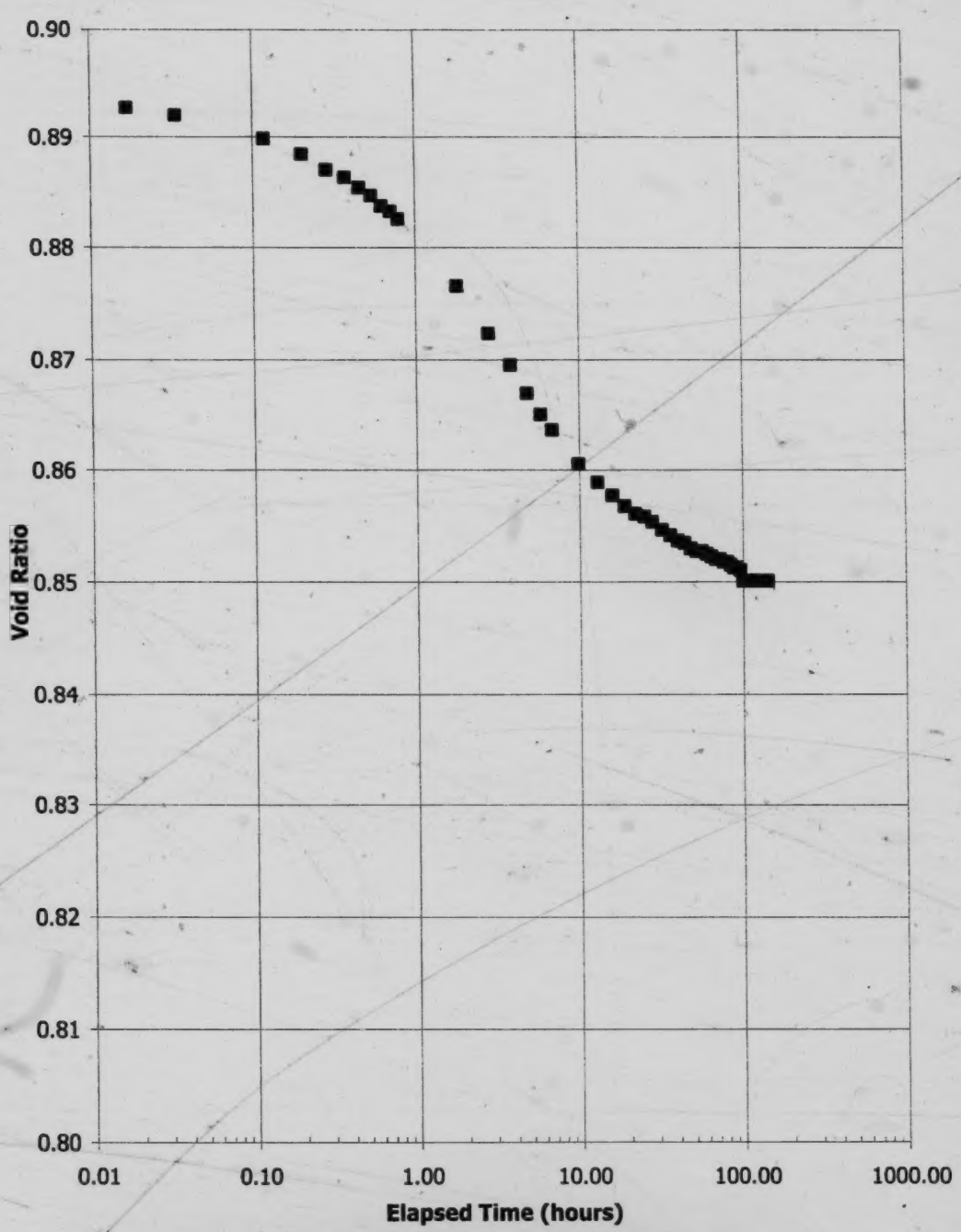

Figure C4: Void Ratio vs. Elapsed Time for C&P - 3
Initially 63.3 % Solids, 20.9 % Fines, 900 g/m^3 PG
Loading from 2.6 kPa to 5 kPa

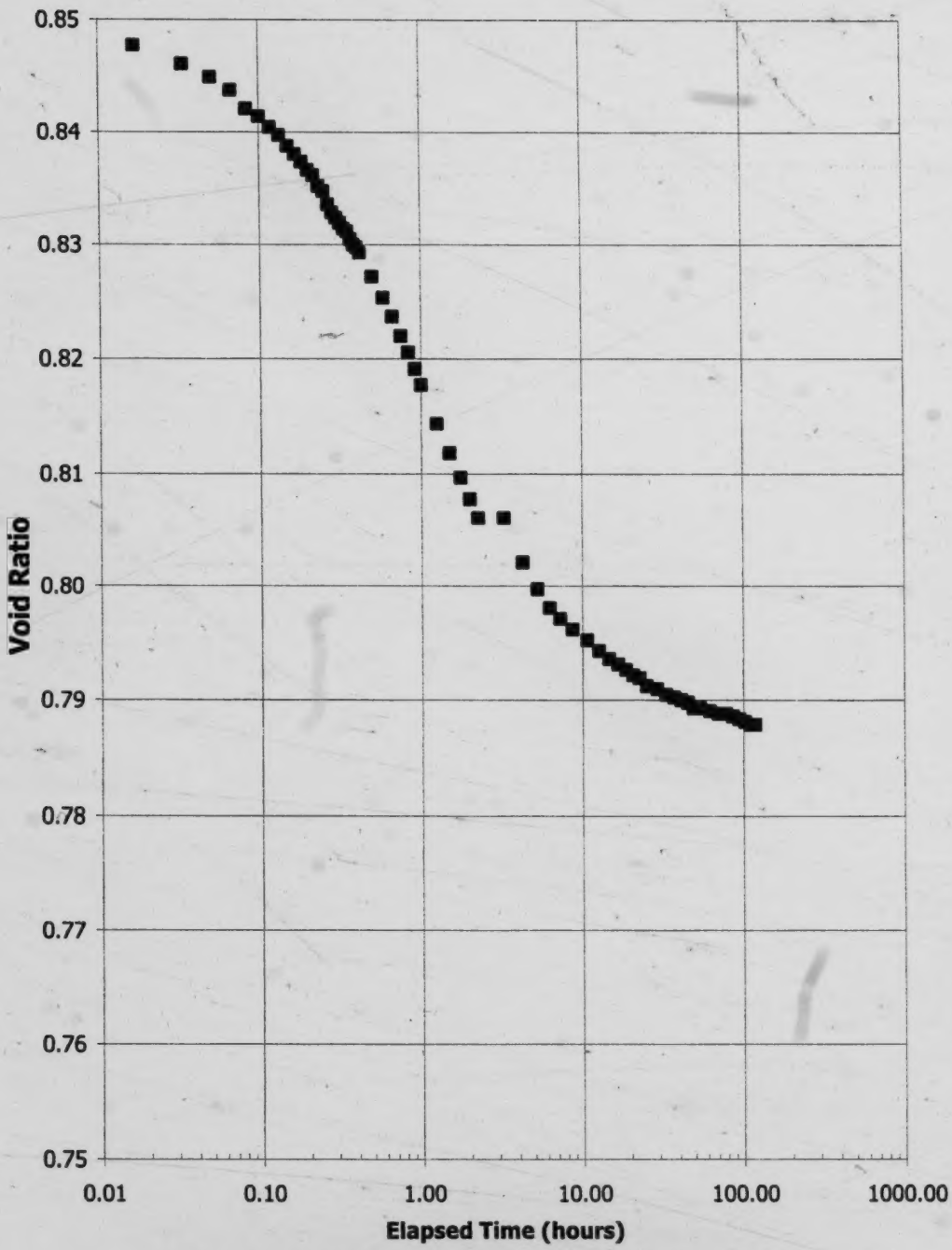

Figure C5: Void Ratio vs. Elapsed Time for C&P - 3
Initially 63.3 % Solids, 20.9 % Fines, 900 g/m^3 PG
Loading from 5 kPa to 10 kPa

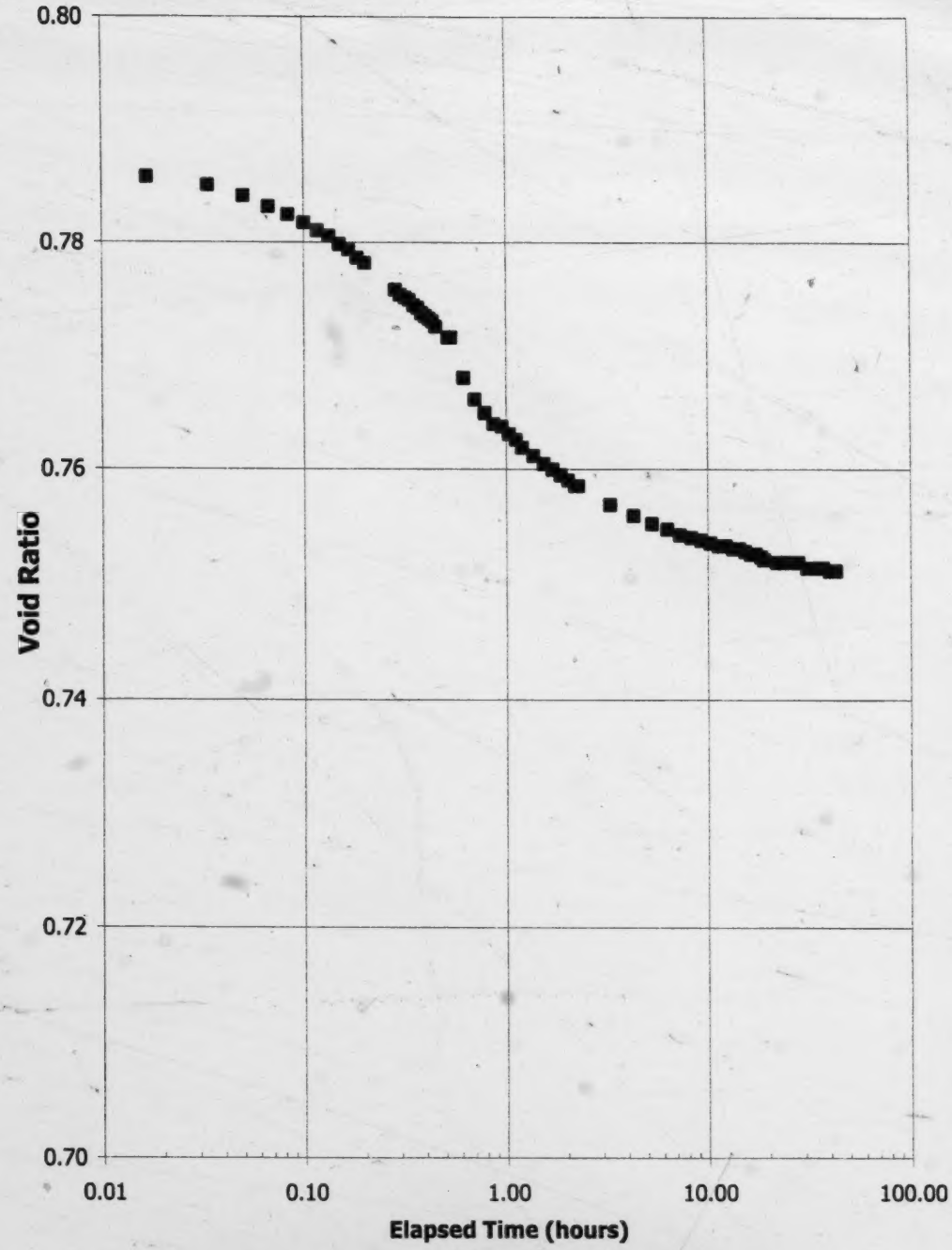

Figure C6: Void Ratio vs. Elapsed Time for C&P - 3
Initially 63.3 % Solids, 20.9 % Fines, 900 g/m^3 PG
Loading from 10 kPa to 20 kPa

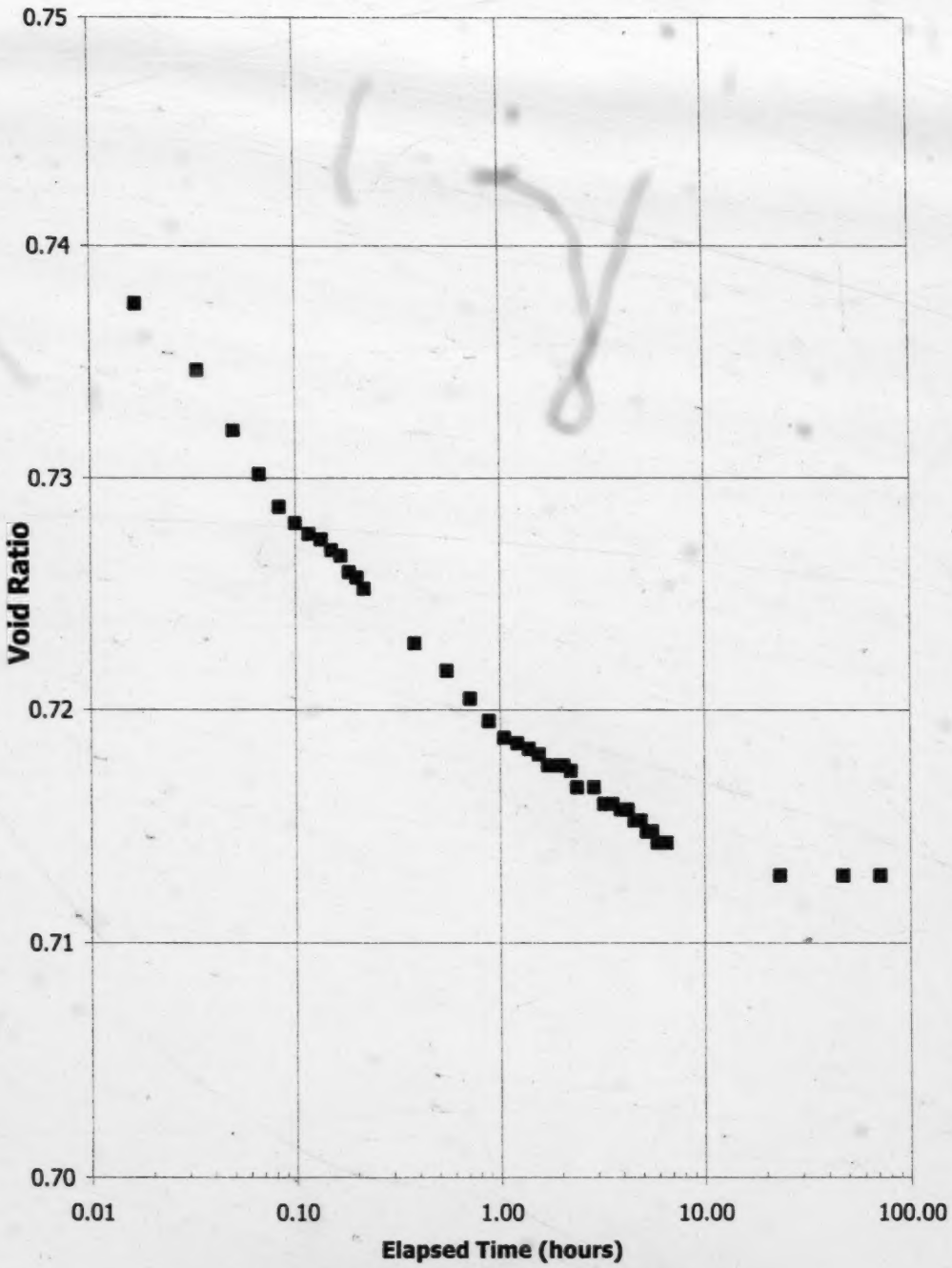

Figure C7: Void Ratio vs. Elapsed Time for C&P - 3
Initially 63.3 % Solids, 20.9 % Fines, 900 g/m^3 PG
Loading from 20 kPa to 40 kPa

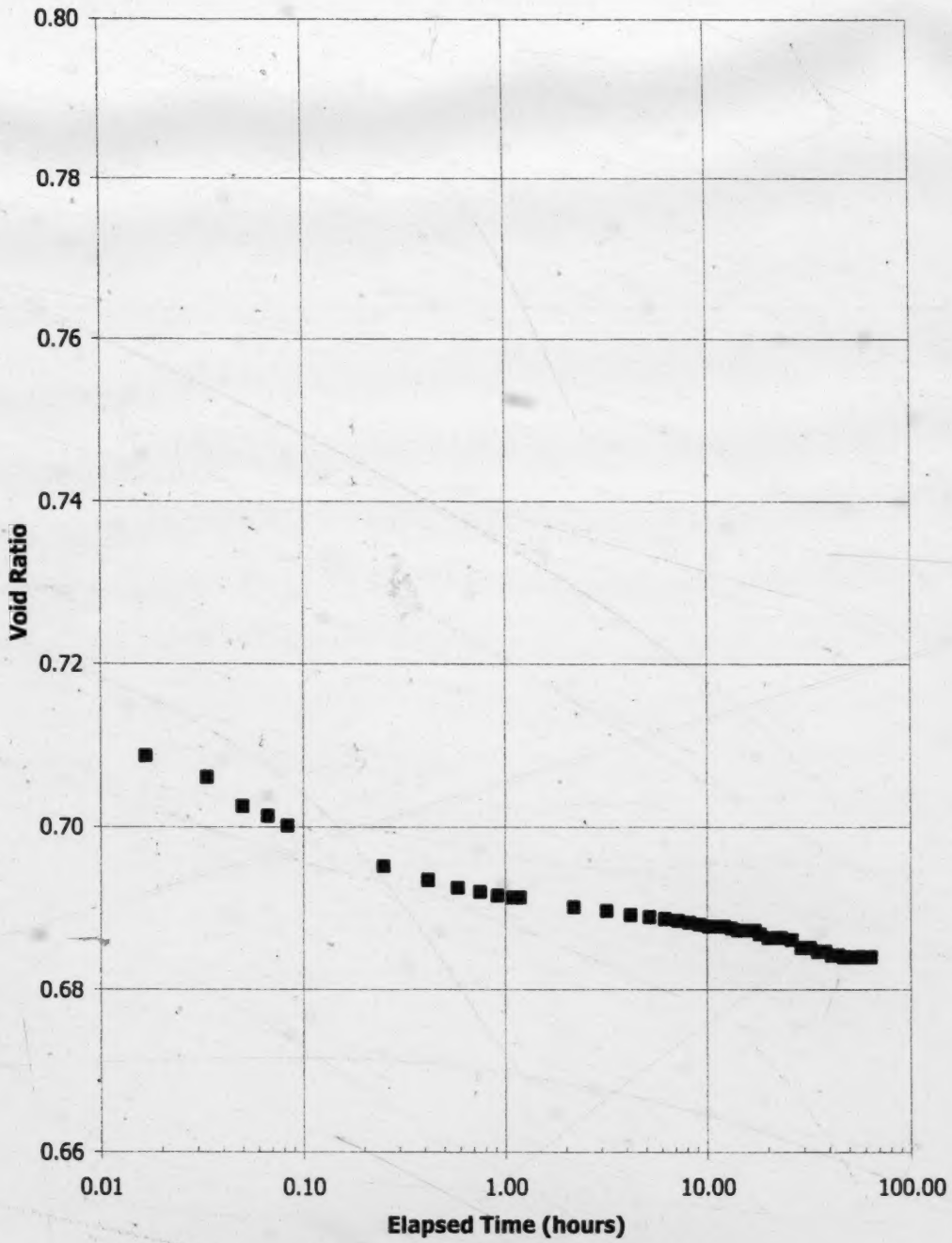

Figure C8: Void Ratio vs. Elapsed Time for C&P - 3
Initially 63.3 % Solids, 20.9 % Fines, 900 g/m^3 PG
Loading from 40 kPa to 80 kPa

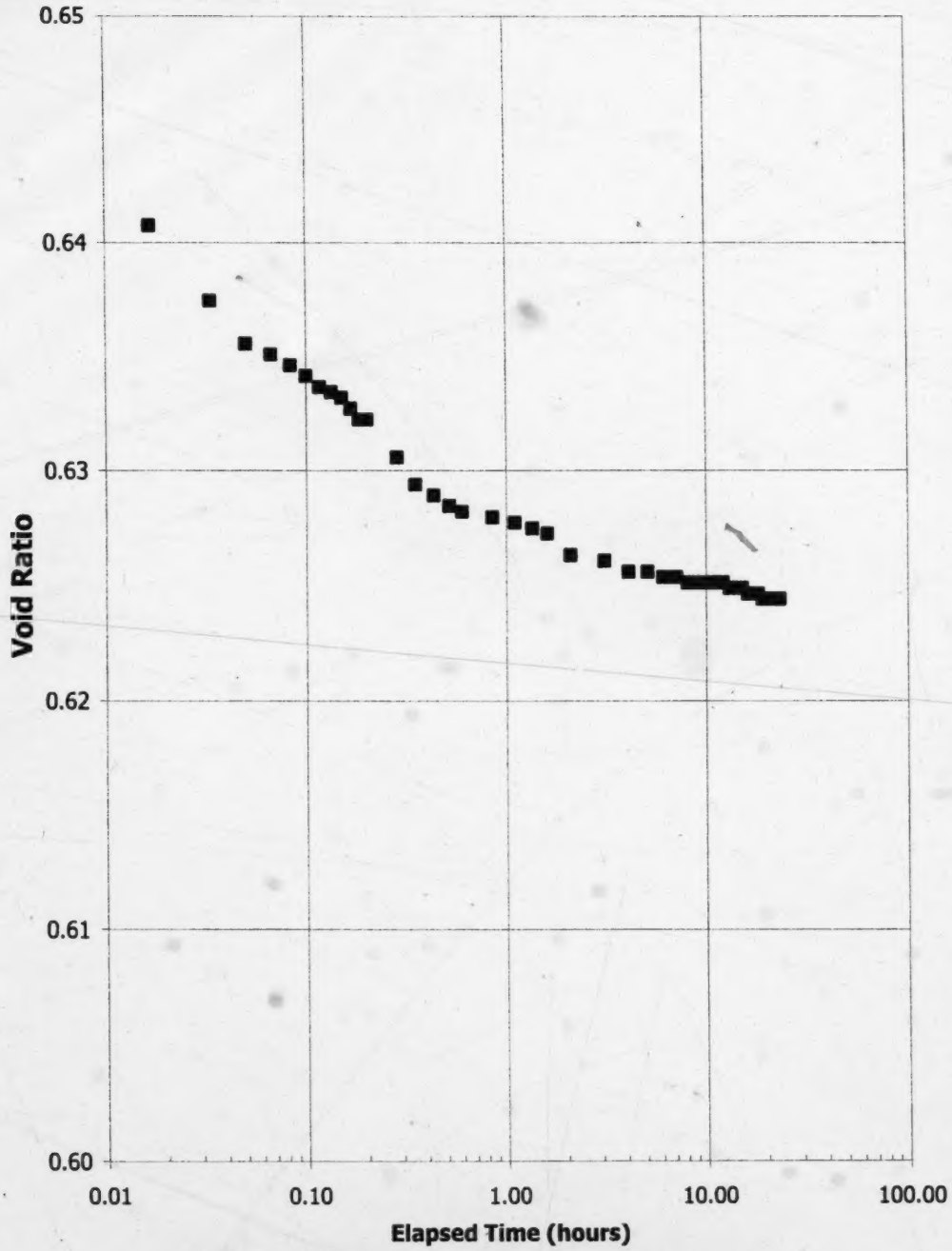

Figure C9: Void Ratio vs. Elapsed Time for C&P - 3
Initially 63.3 % Solids, 20.9 % Fines, 900 g/m^3 PG
Loading from 80 kPa to 160 kPa

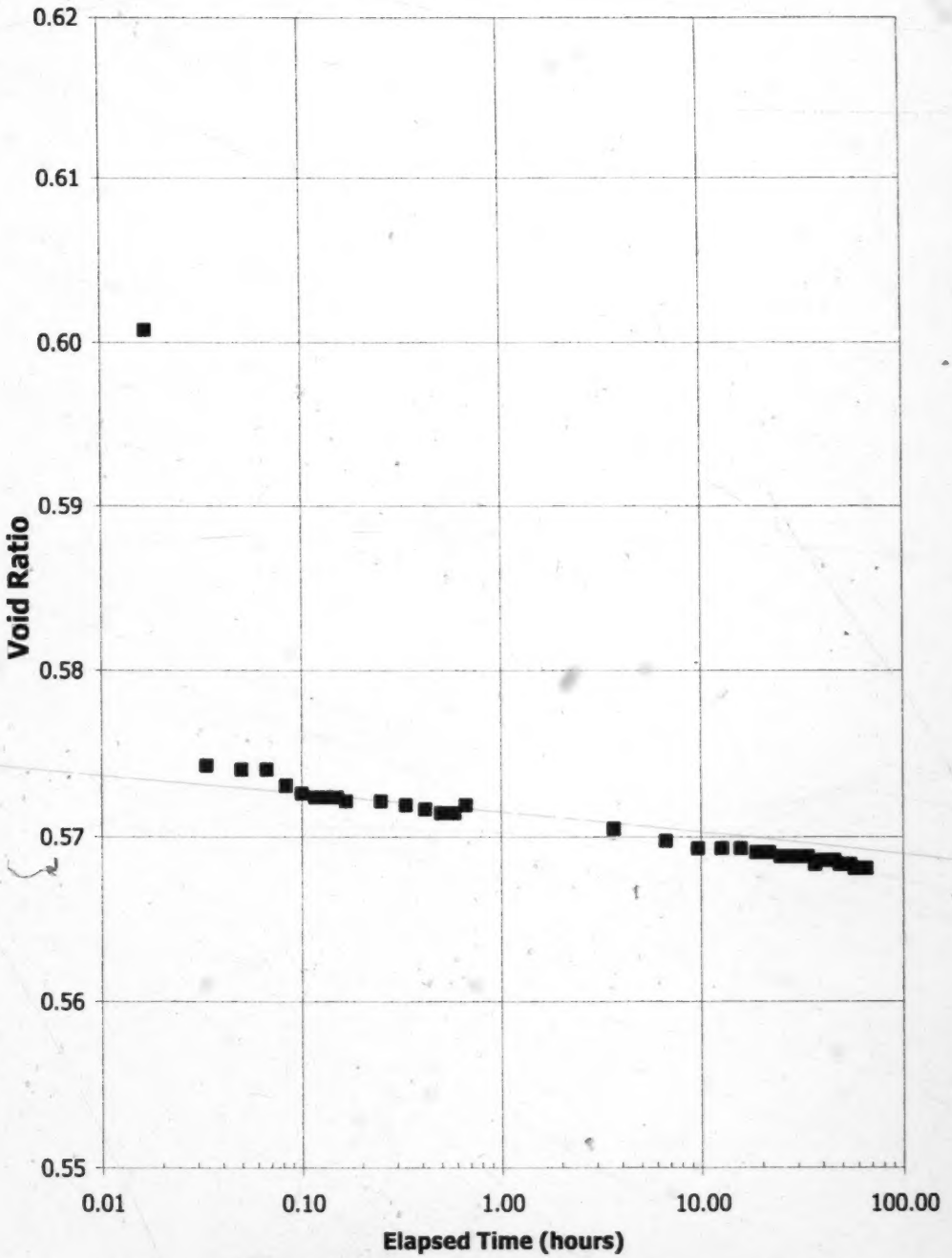

Figure C10: Void Ratio vs. Elapsed Time for C&P - 3
Initially 63.3 % Solids, 20.9 % Fines, 900 g/m^3 PG
Loading from 160 kPa to 277 kPa

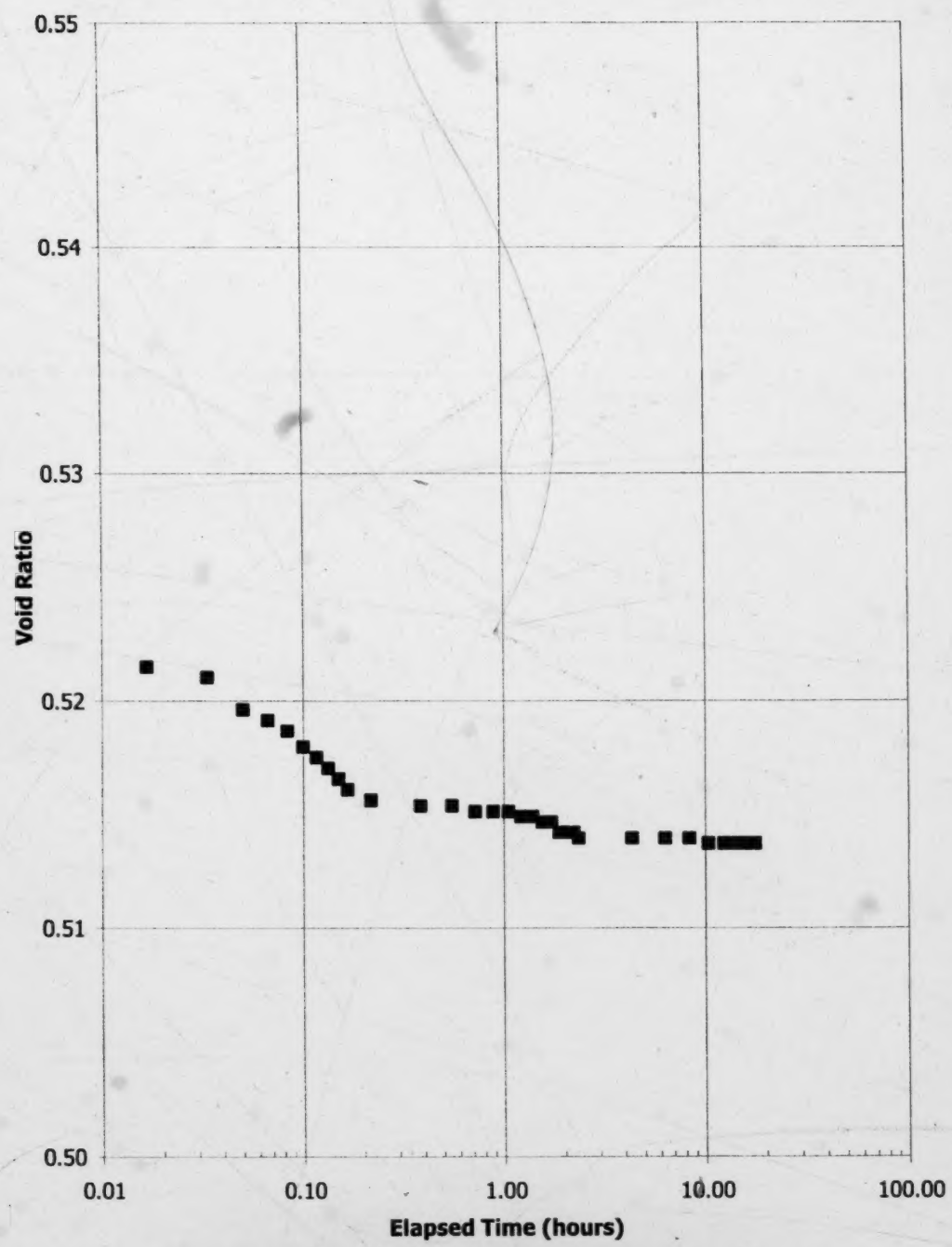

Figure C11: Void Ratio vs. Elapsed Time for C&P - 3
Initially 63.3 % Solids, 20.9 % Fines, 900 g/m^3 PG
Loading from 277 kPa to 700 kPa

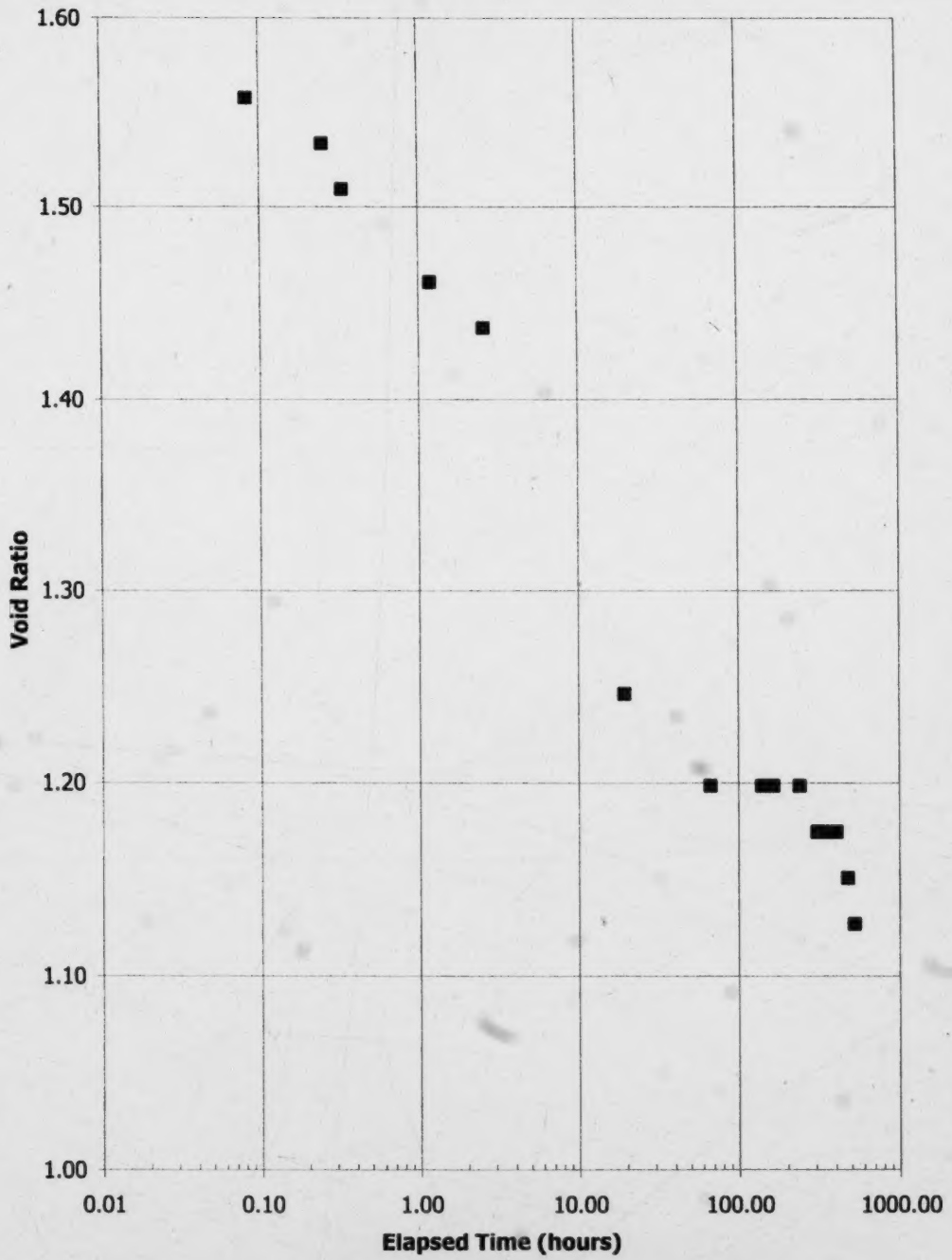

Figure C12: Void Ratio vs. Elapsed Time for C&P - 4
Initially 62.5 % Solids, 20.6 % Fines, 3200 g/m^3 PG
Self Weight Loading

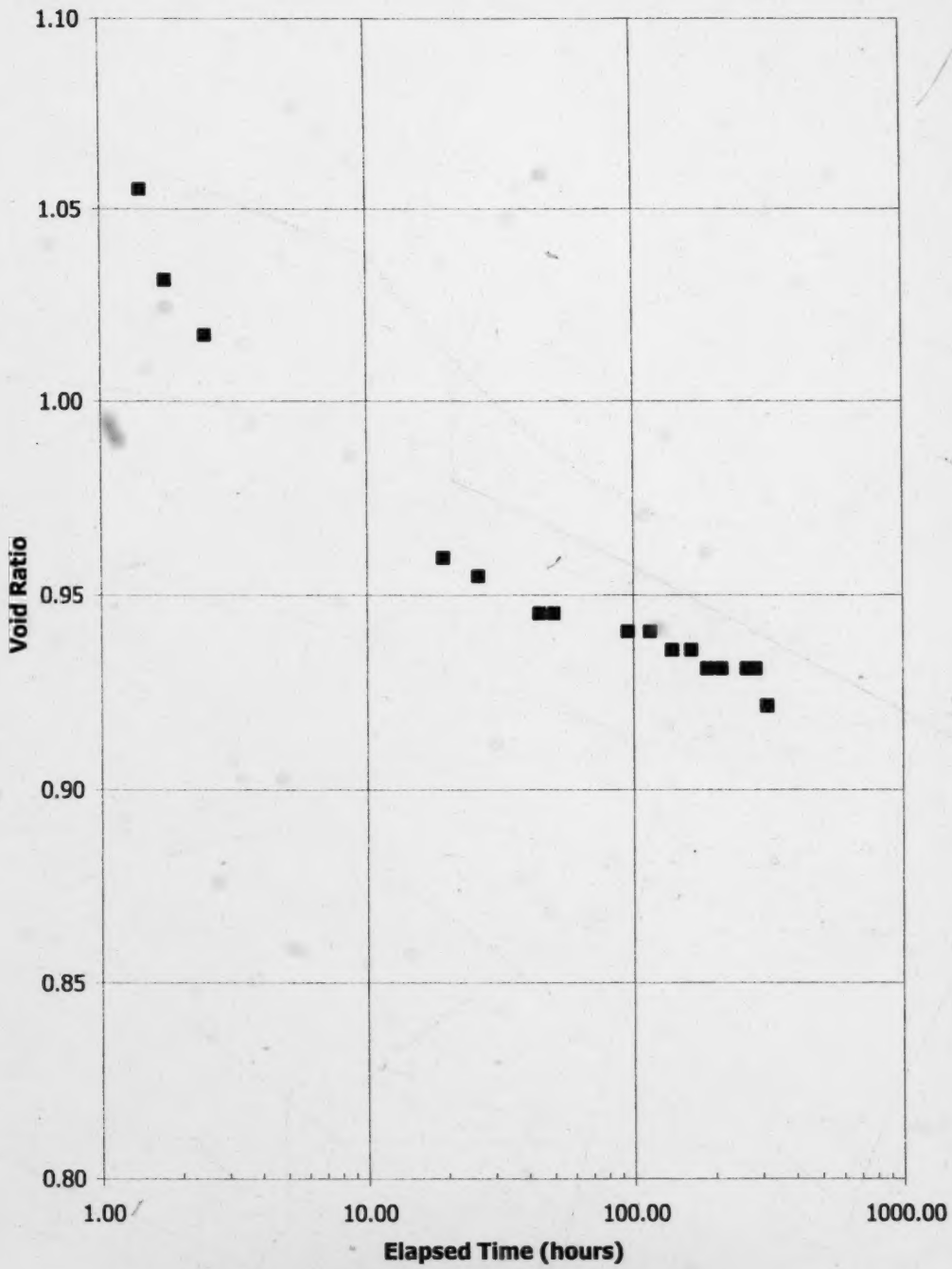

Figure C13: Void Ratio vs. Elapsed Time for C&P - 4
Initially 62.5 % Solids, 20.6 % Fines, 3200 g/m3 PG
Loading from 0.14 kPa (self weight) to 1.2 kP

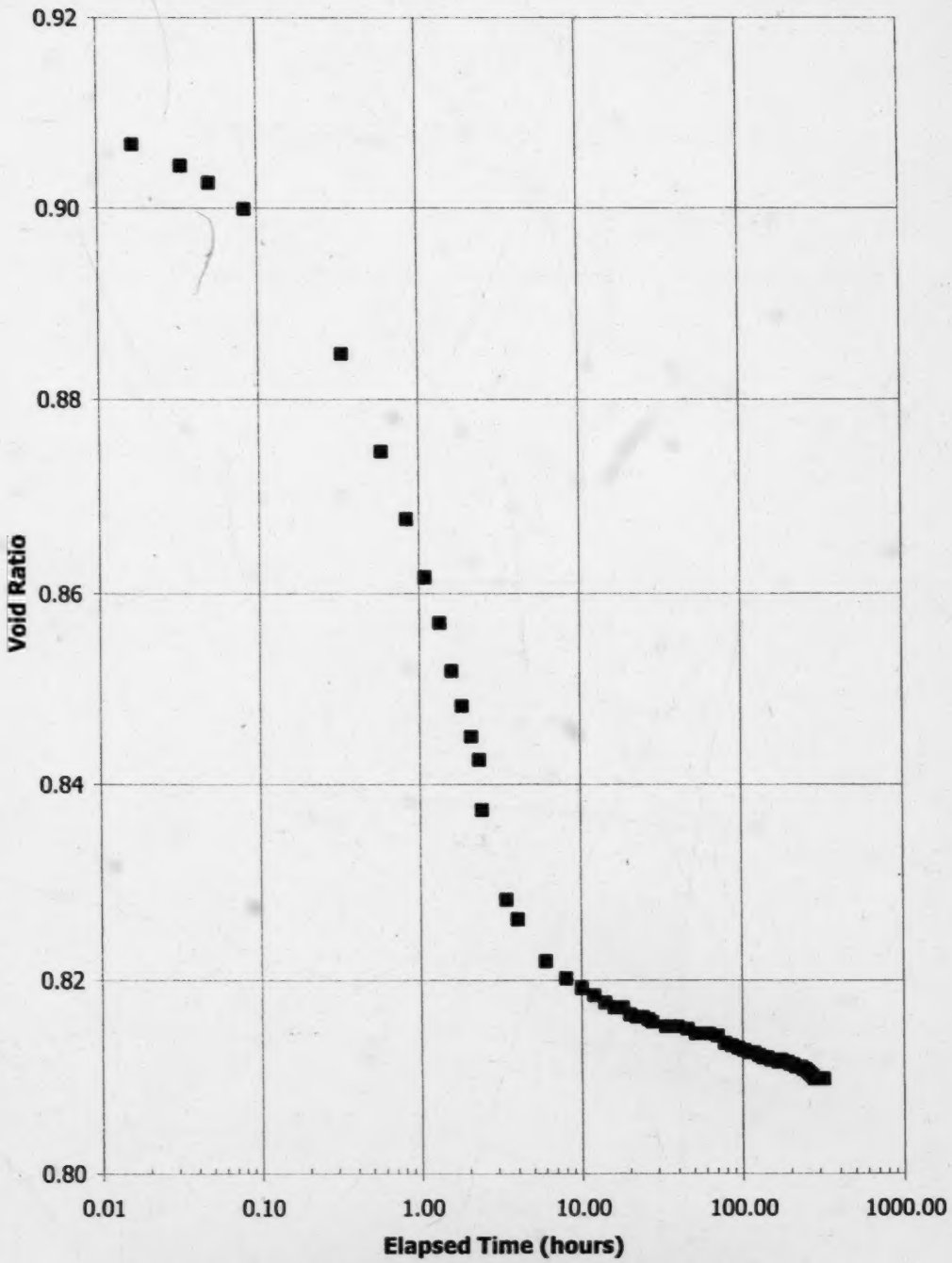

Figure C14: Void Ratio vs. Elapsed Time for C&P - 4
Initially 62.5 % Solids, 20.6 % Fines, 3200 g/m^3 PG
Loading from 1.2 kPa to 2.61 kPa

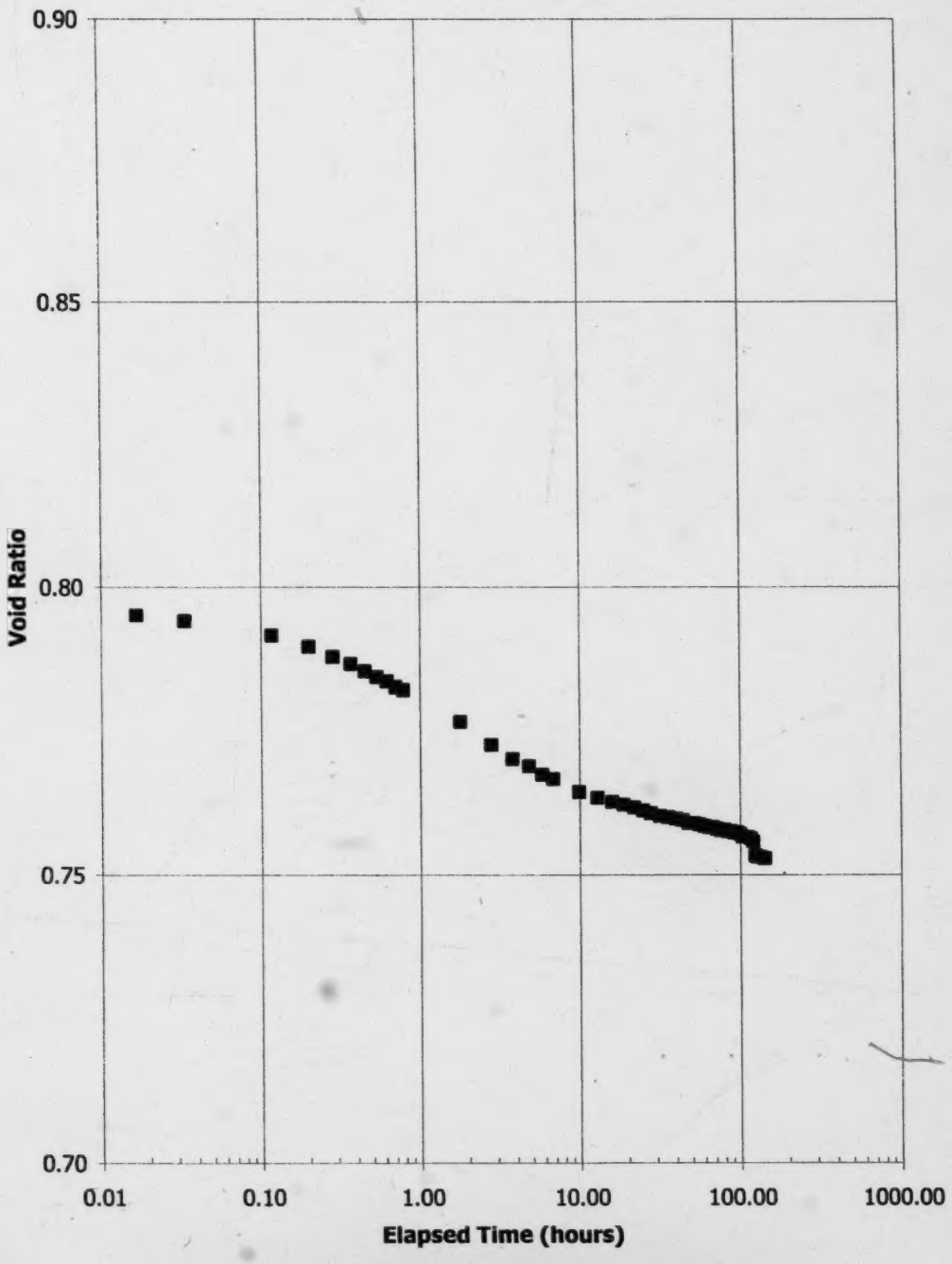

Figure C15: Void Ratio vs. Elapsed Time for C&P - 4
Initially 62.5 % Solids, 20.6 % Fines, 3200 g/m^3 PG
Loading from 2.61 kPa to 5 kPa

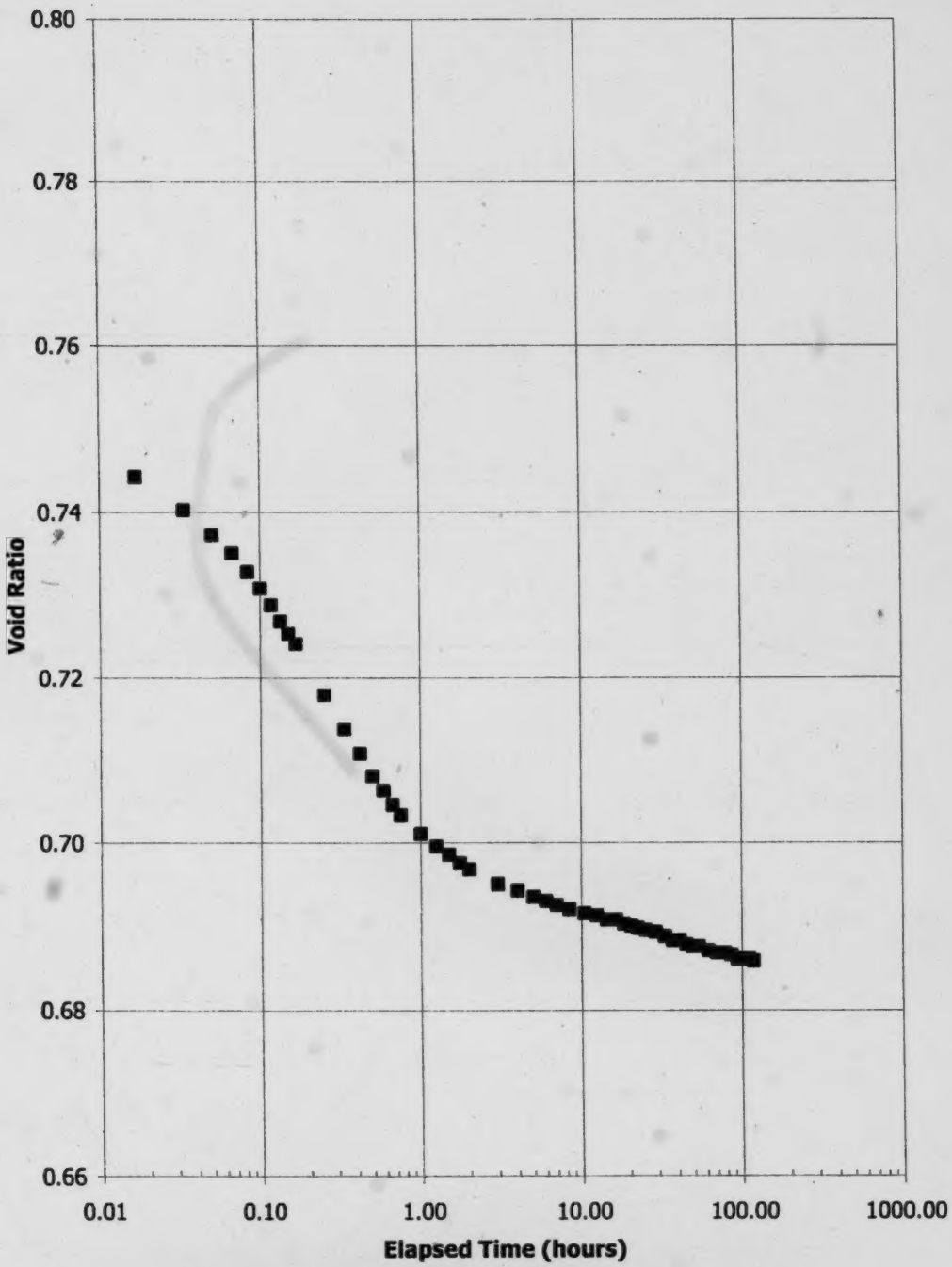

Figure C16: Void Ratio vs. Elapsed Time for C&P - 4
Initially 62.5 % Solids, 20.6 % Fines, 3200 g/m^3 PG
Loading from 5 kPa to 10 kPa

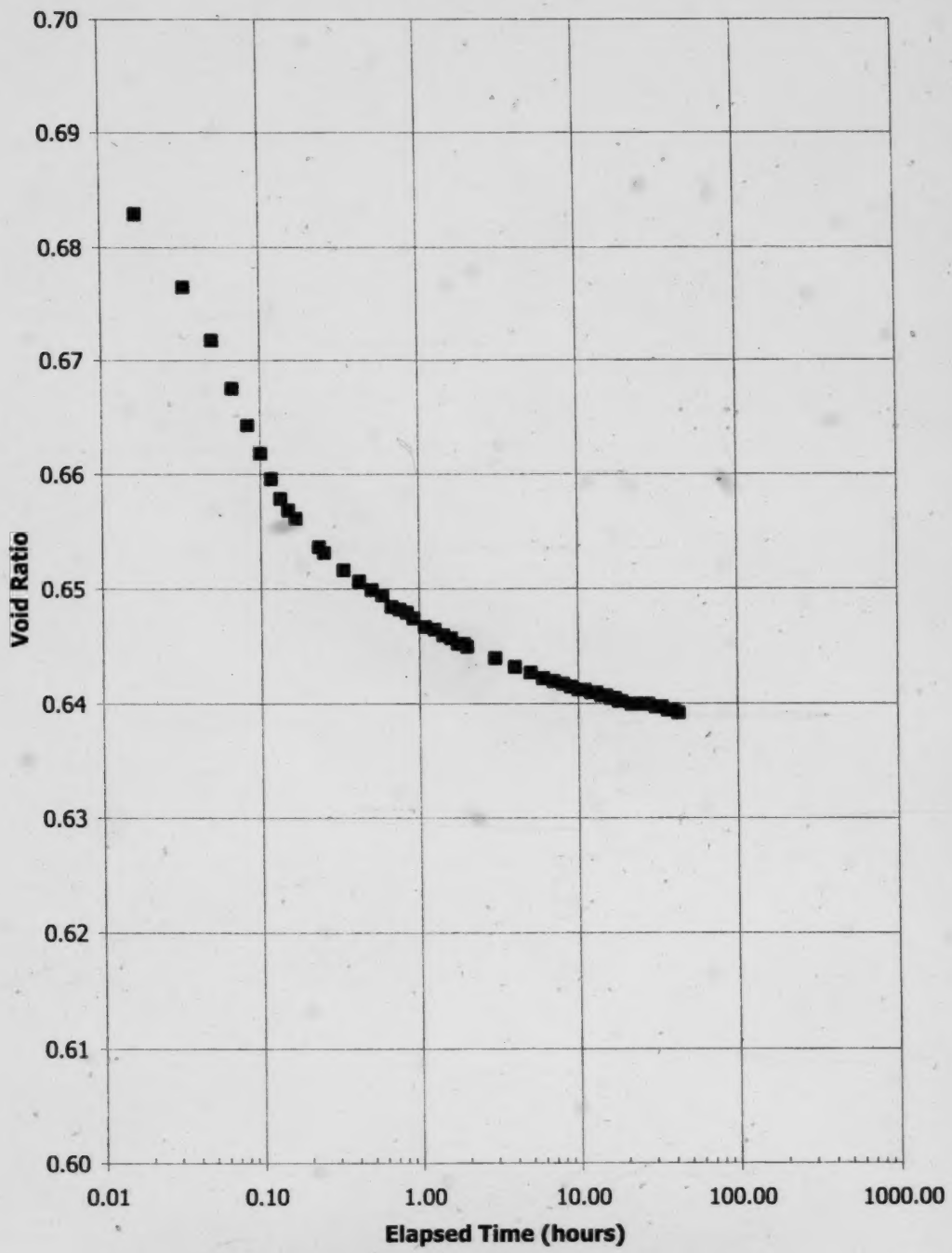

Figure C17: Void Ratio vs. Elapsed Time for C&P - 4
Initially 62.5 % Solids, 20.6 % Fines, 3200 g/m^3 PG
Loading from 10 kPa to 20 kPa

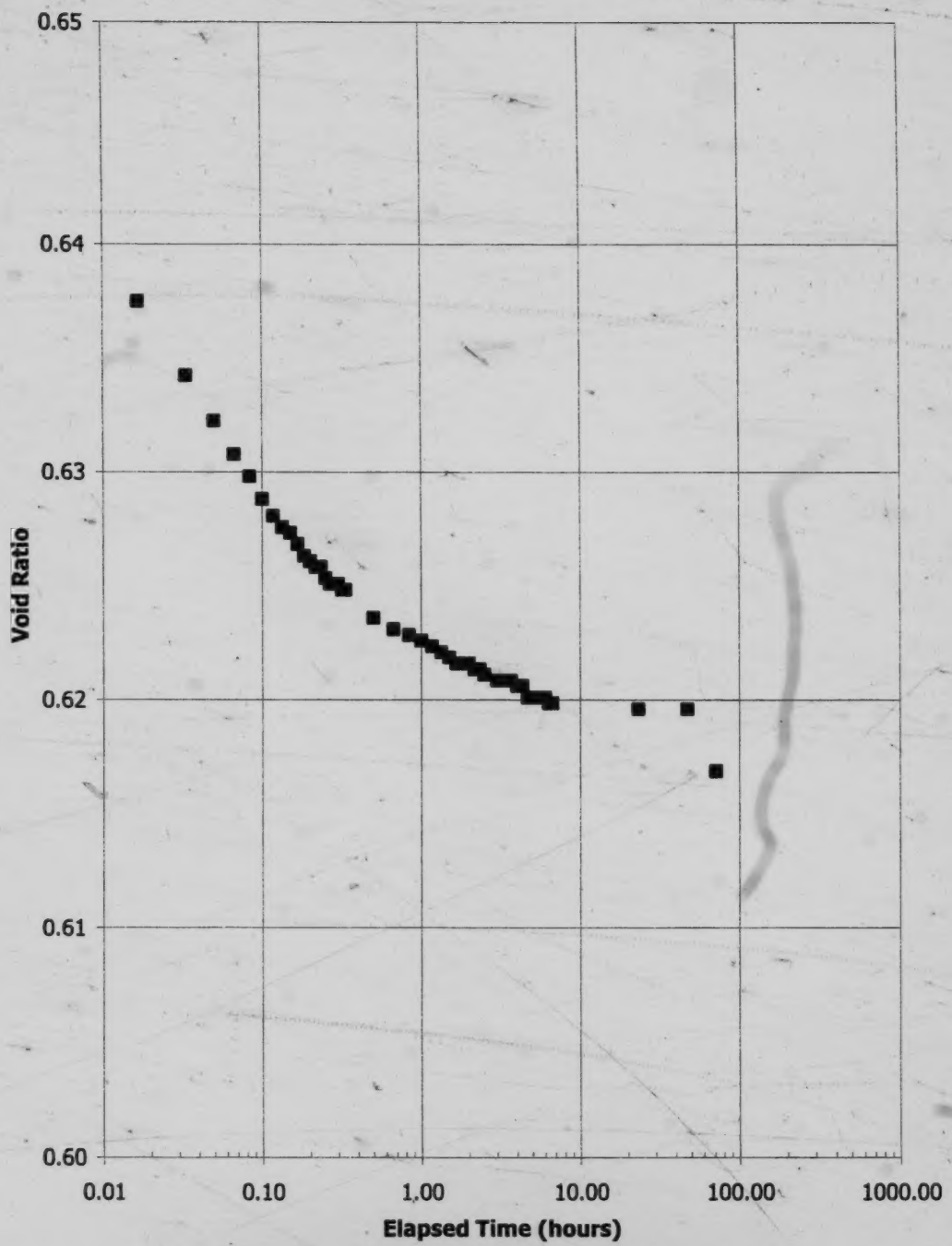

Figure C18: Void Ratio vs. Elapsed Time for C&P - 4
Initially 62.5 % Solids, 20.6 % Fines, 3200 g/m^3 PG
Loading from 20 kPa to 40 kPa

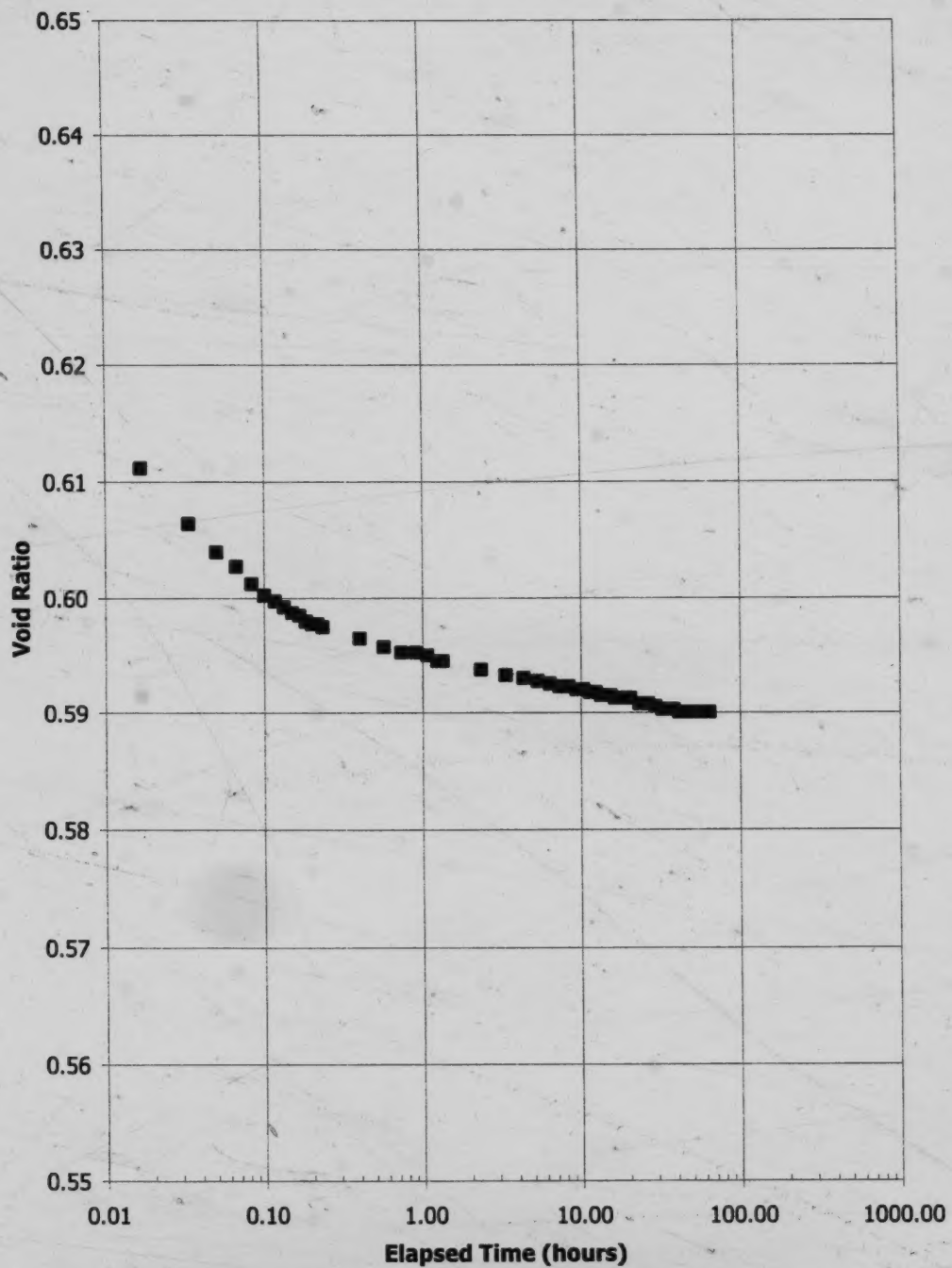

Figure C19: Void Ratio vs. Elapsed Time for C&P - 4
Initially 62.5 % Solids, 20.6 % Fines, 3200 g/m^3 PG
Loading from 40 kPa to 80 kPa

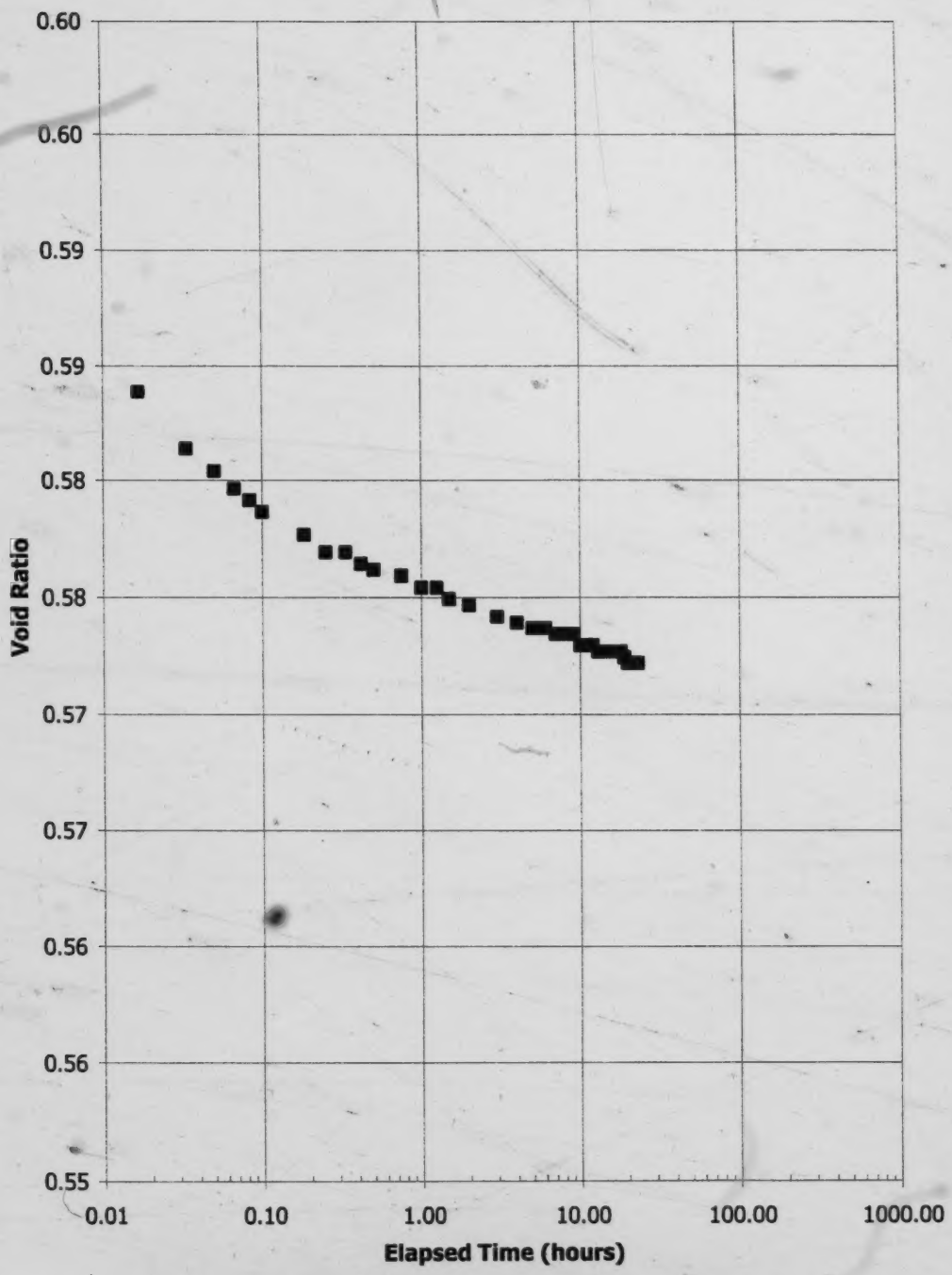

Figure C20: Void Ratio vs. Elapsed Time for C&P - 4
Initially 62.5 % Solids, 20.6 % Fines, 3200 g/m^3 PG
Loading from 80 kPa to 160 kPa

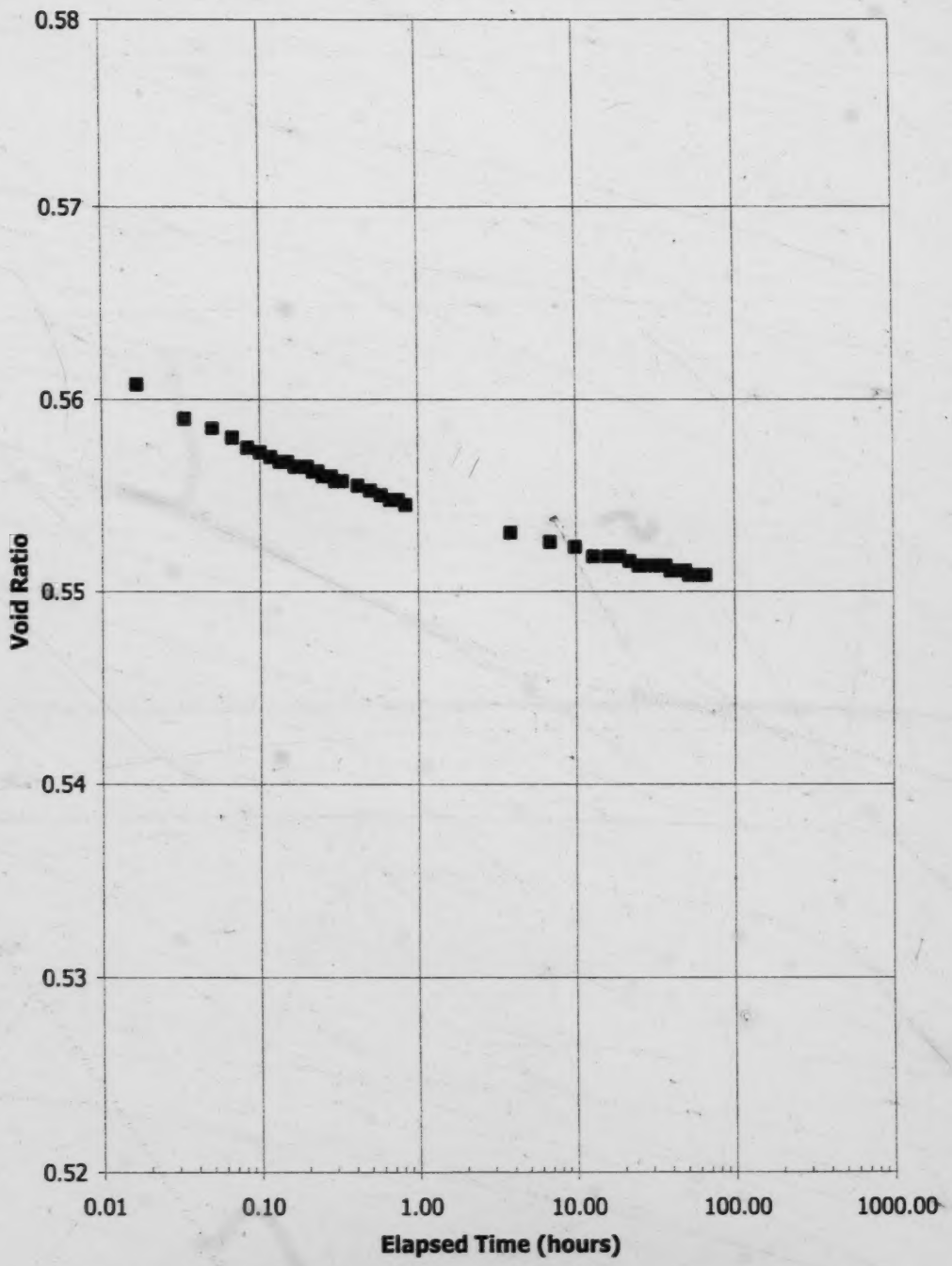

Figure C21: Void Ratio vs. Elapsed Time for C&P - 4
Initially 62.5 % Solids, 20.6 % Fines, 3200 g/m^3 PG
Loading from 160 kPa to 293 kPa

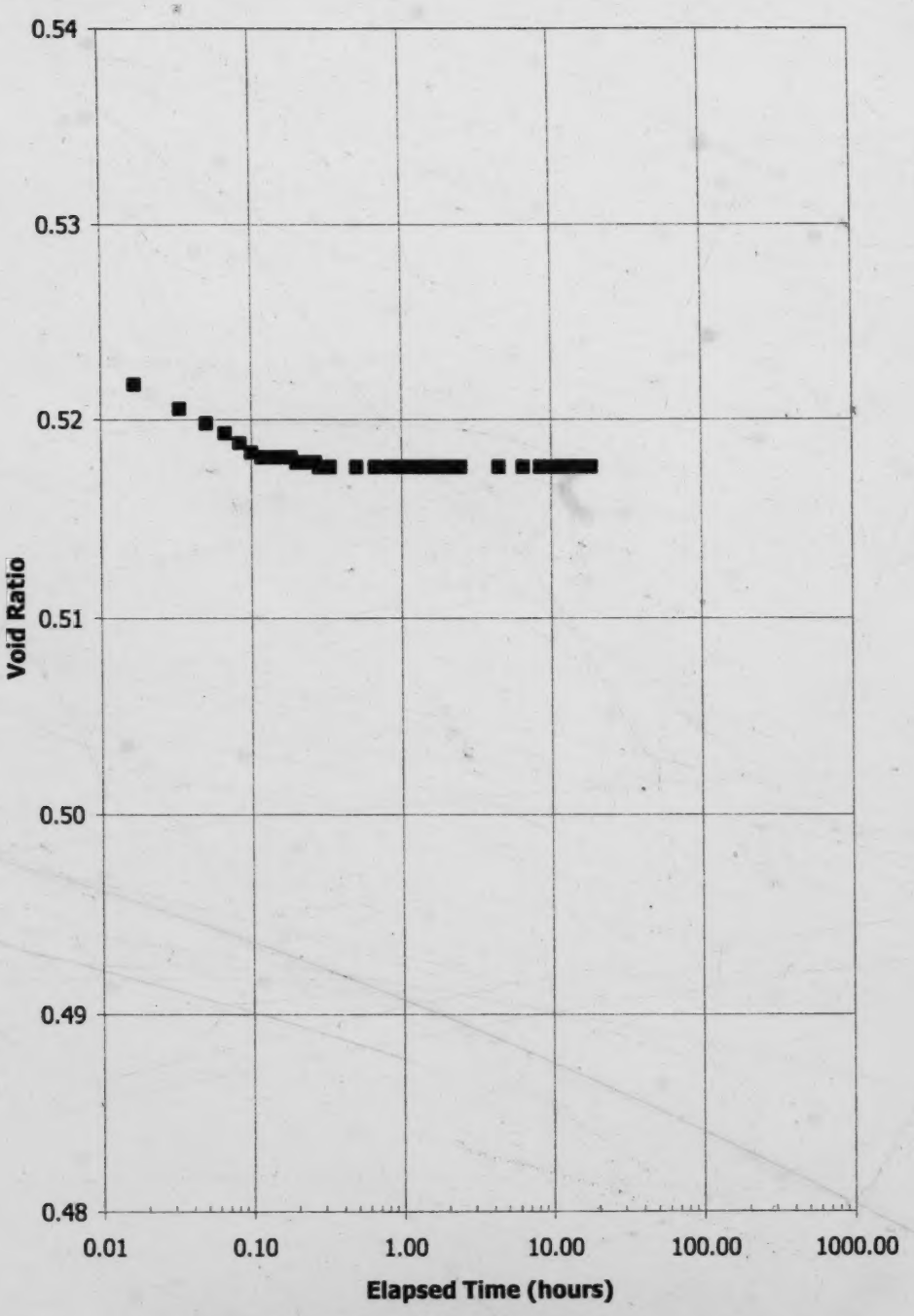

Figure C22: Void Ratio vs. Elapsed Time for C&P - 4
Initially 62.5 % Solids, 20.6 % Fines, 3200 g/m^3 PG
Loading from 293 kPa to 700 kPa

APPENDIX D

Large Strain Consolidation Test Results:

Void Ratio vs. Time for Each Loading Step

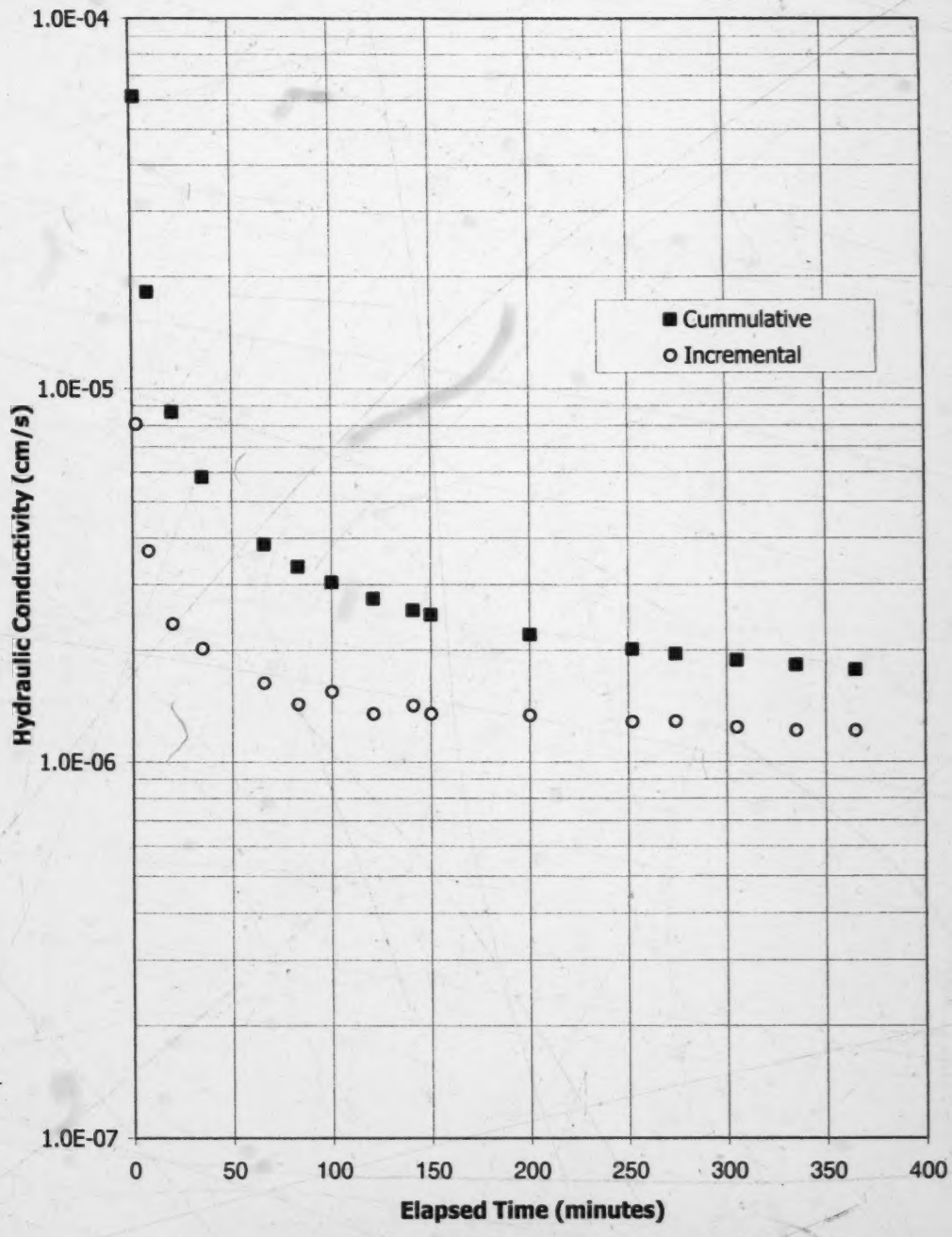

Figure D1: Hydraulic Conductivity vs. Time for C&P-3
Intially 63.3 % Solids, 20.9 % Fines, 900 g/m^3 PG
After Self Weight Load
Upward Flow

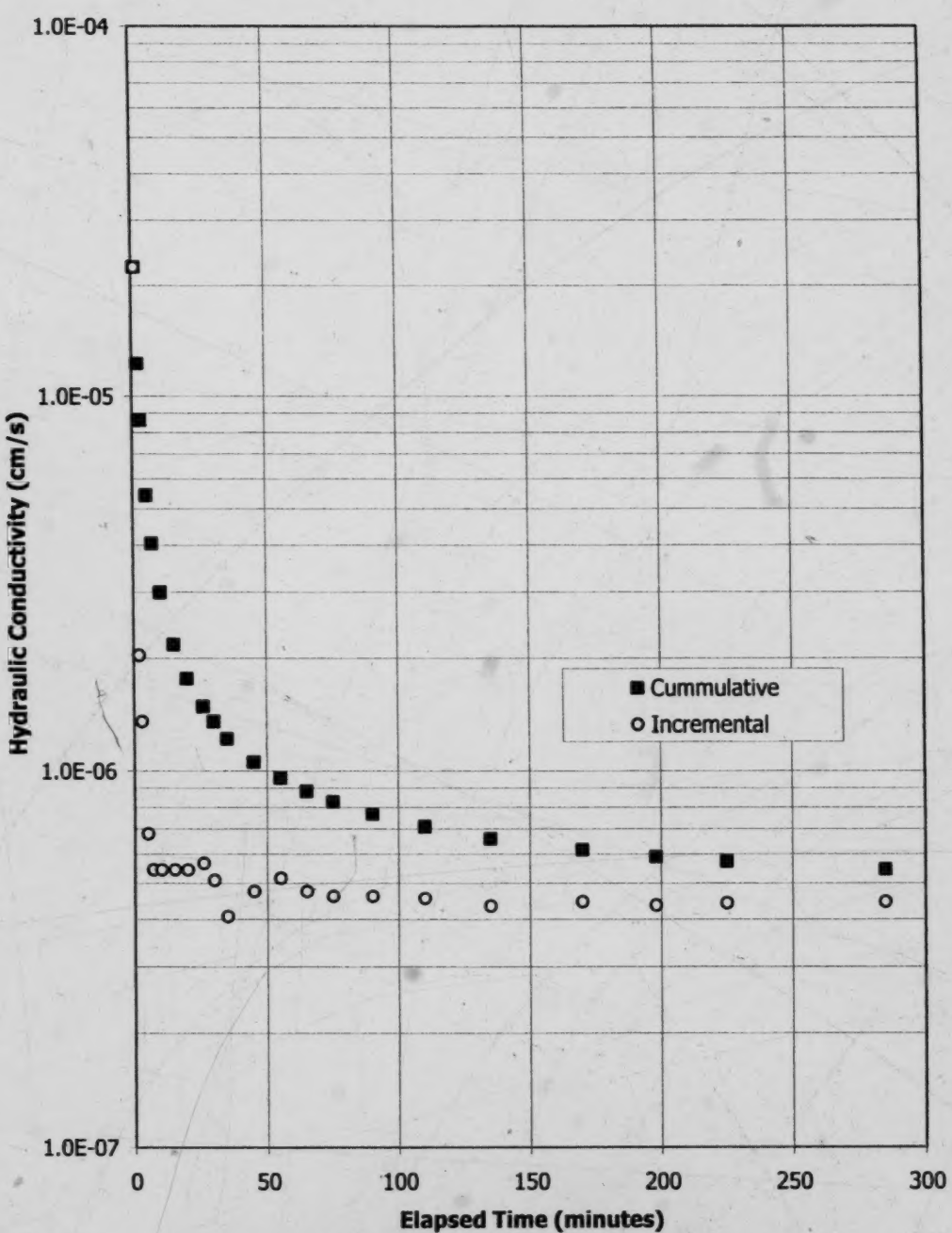

Figure D2: Hydraulic Conductivity vs. Time for C&P-3
Intially 63.3 % Solids, 20.9 % Fines, 900 g/m^3 PG
After 1.2 kPa
Upward Flow

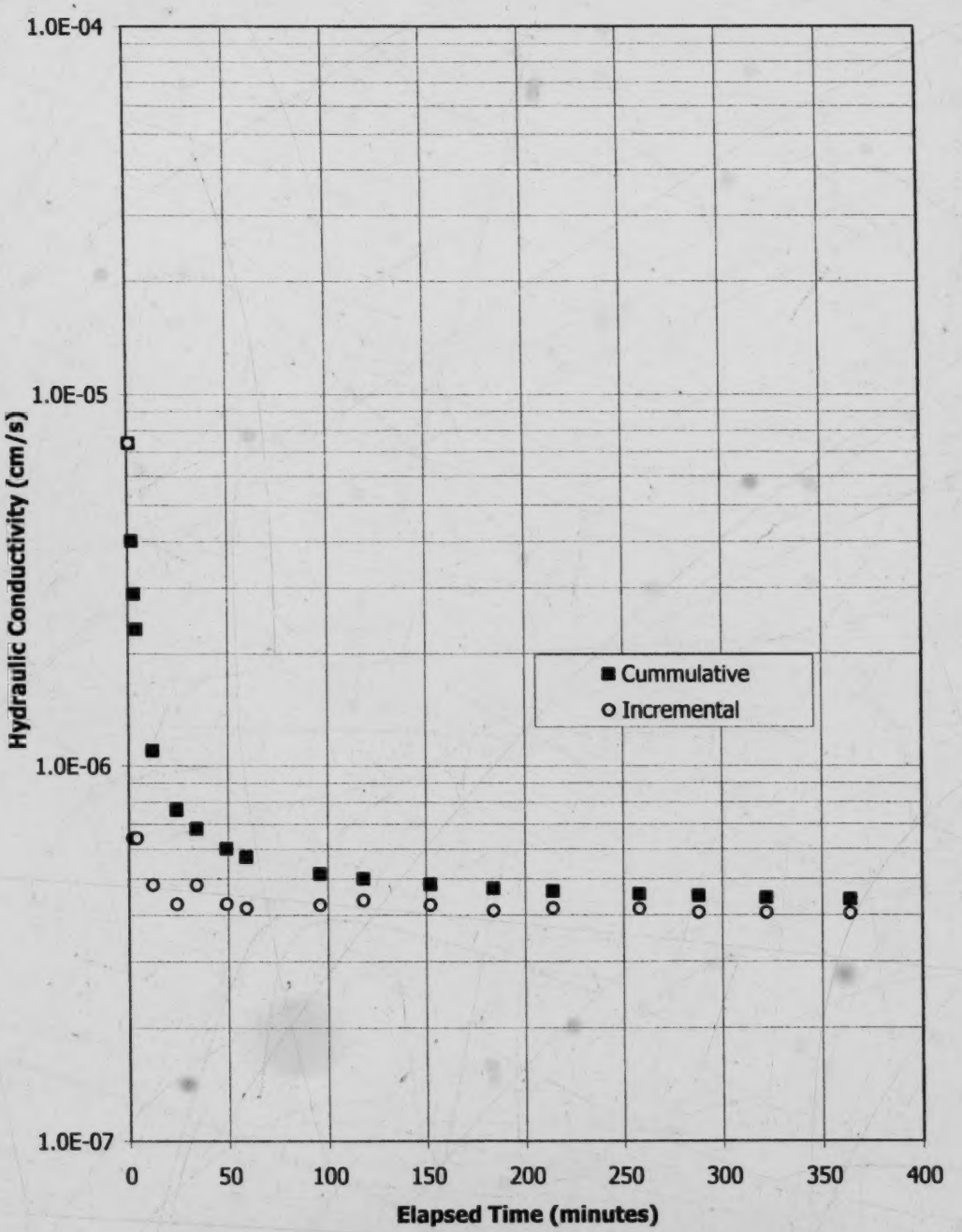

Figure D3: Hydraulic Conductivity vs. Time for C&P-3
Intially 63.3 % Solids, 20.9 % Fines, 900 g/m^3 PG
After 2.6 kPa
Upward Flow

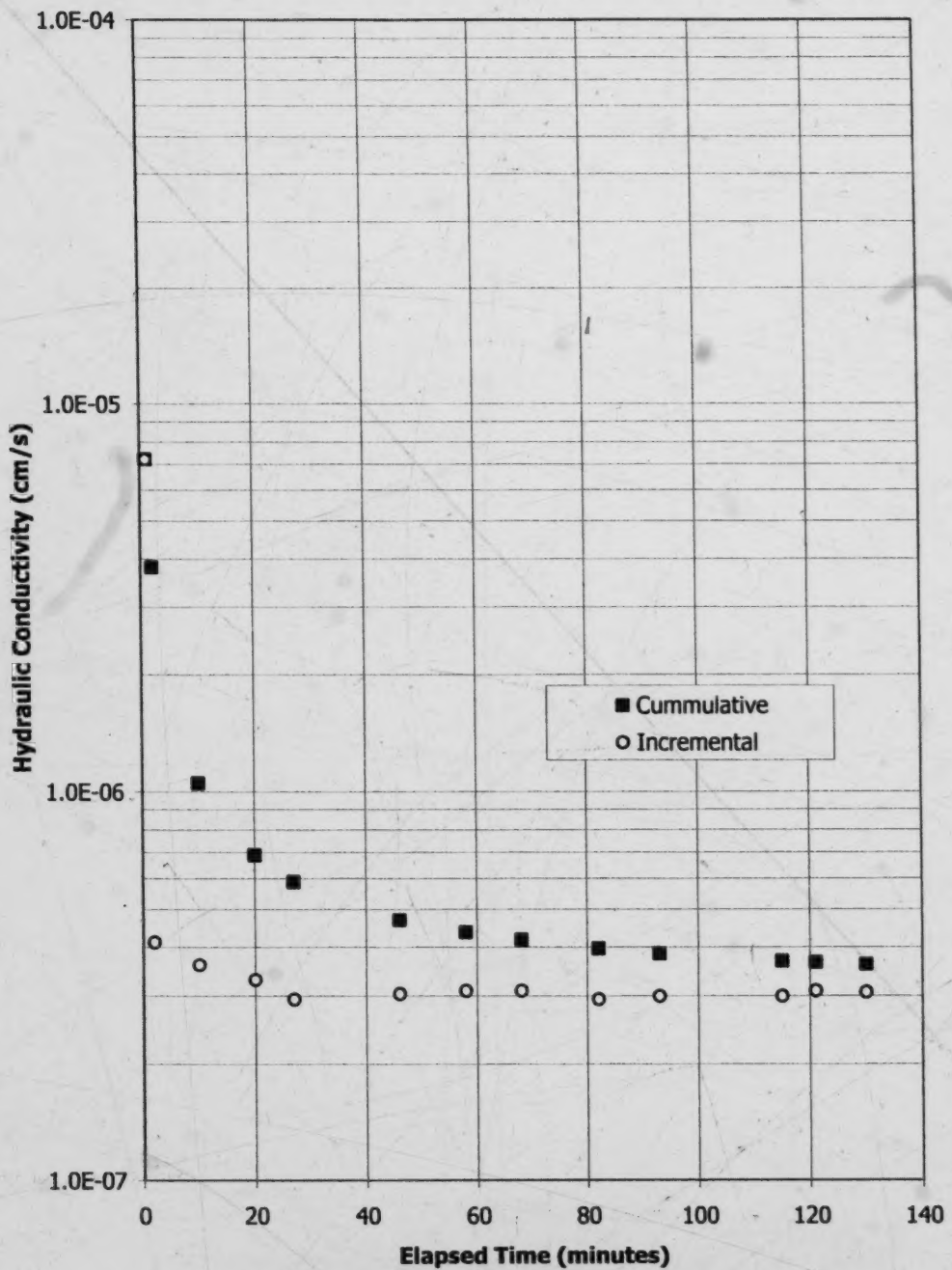

Figure D4: Hydraulic Conductivity vs. Time for C&P-3
Intially 63.3 % Solids, 20.9 % Fines, 900 g/m^3 PG
After 5.0 kPa
Upward Flow

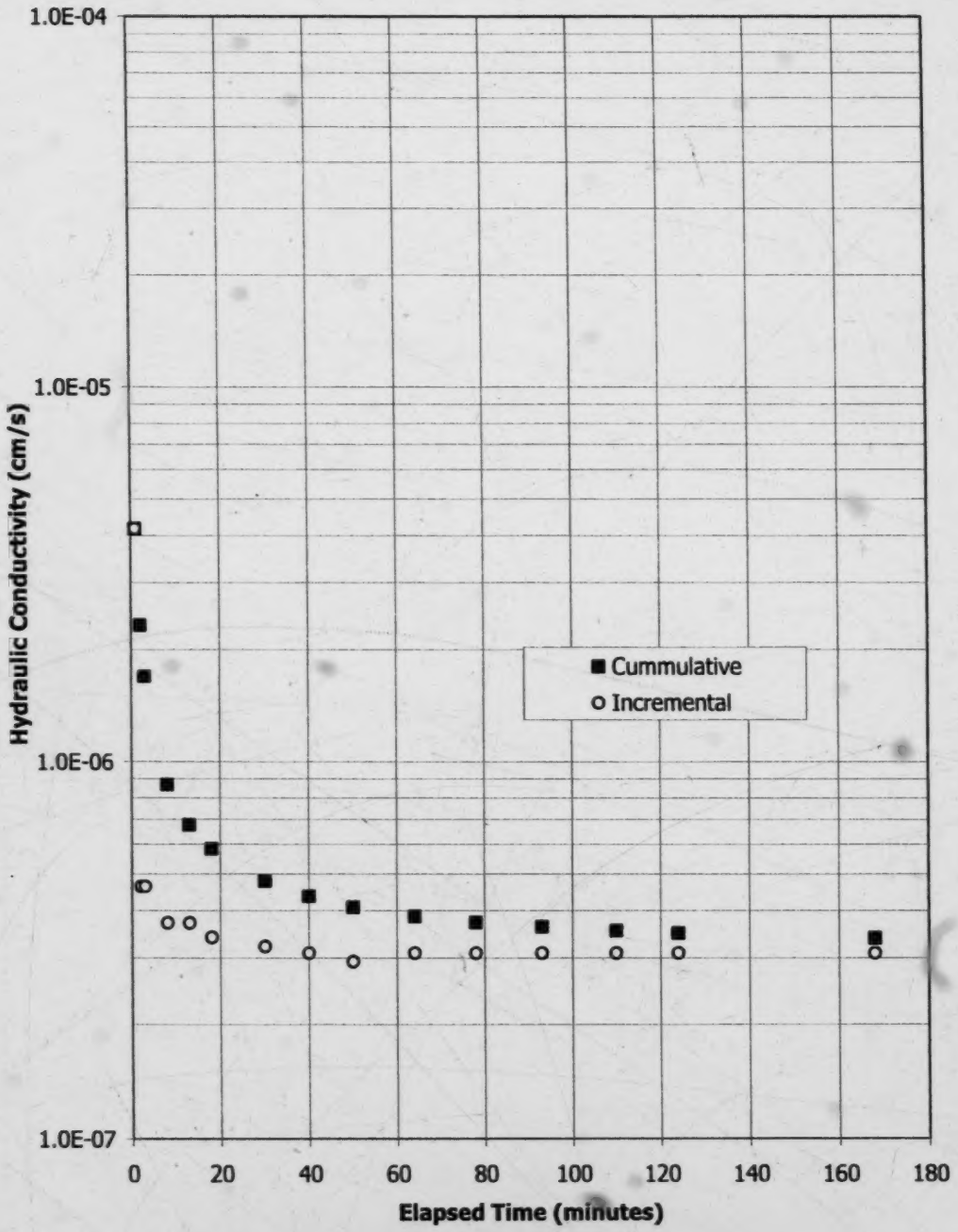

Figure D5: Hydraulic Conductivity vs. Time for C&P-3
Intially 63.3 % Solids, 20.9 % Fines, 900 g/m^3 PG
After 10 kPa
Upward Flow

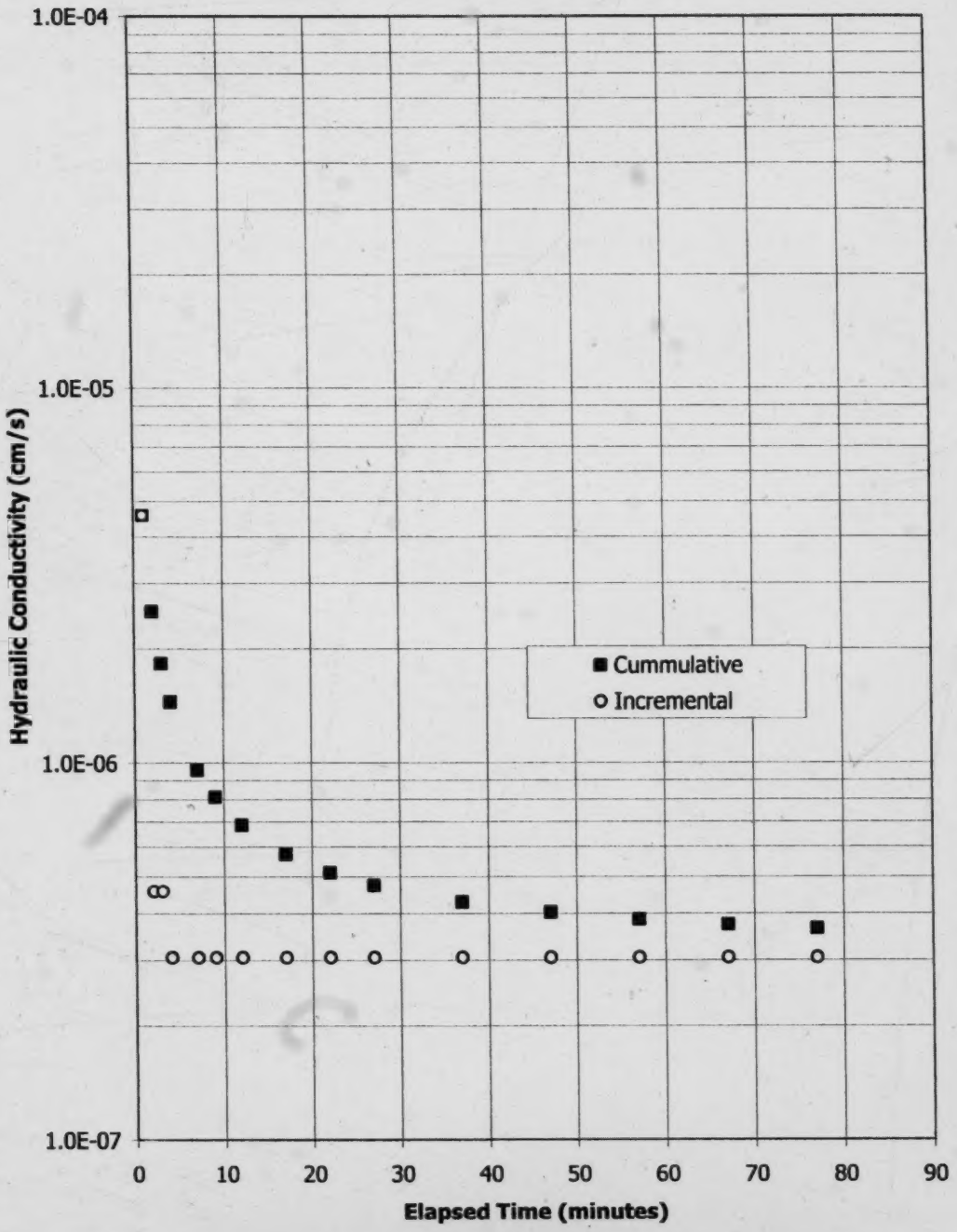

Figure D6: Hydraulic Conductivity vs. Time for C&P-3
Intially 63.3 % Solids, 20.9 % Fines, 900 g/m^3 PG
After 20 kPa
Upward Flow

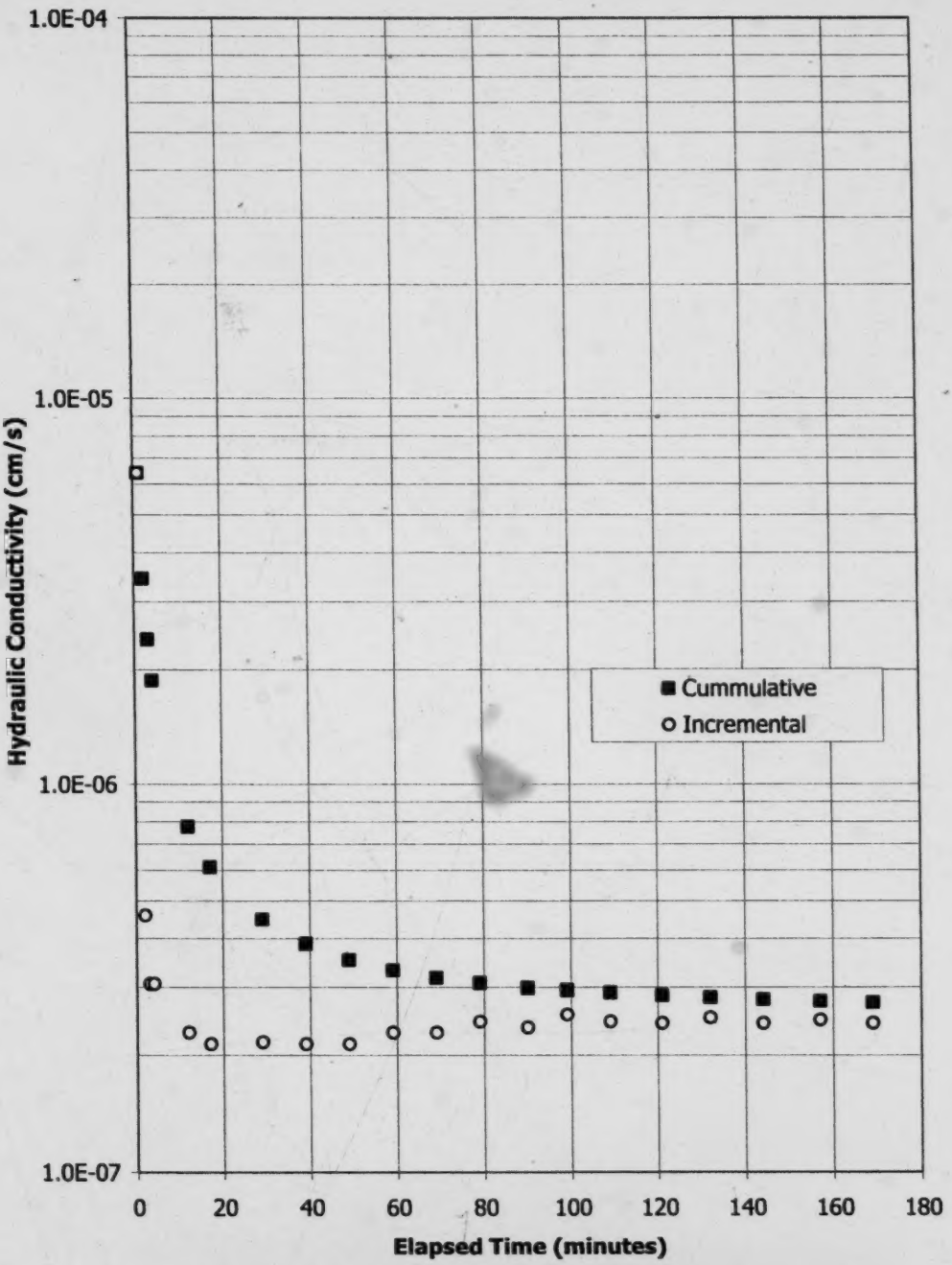

Figure D7: Hydraulic Conductivity vs. Time for C&P-3
Intially 63.3 % Solids, 20.9 % Fines, 900 g/m^3 PG
After 40.2 kPa
Upward Flow

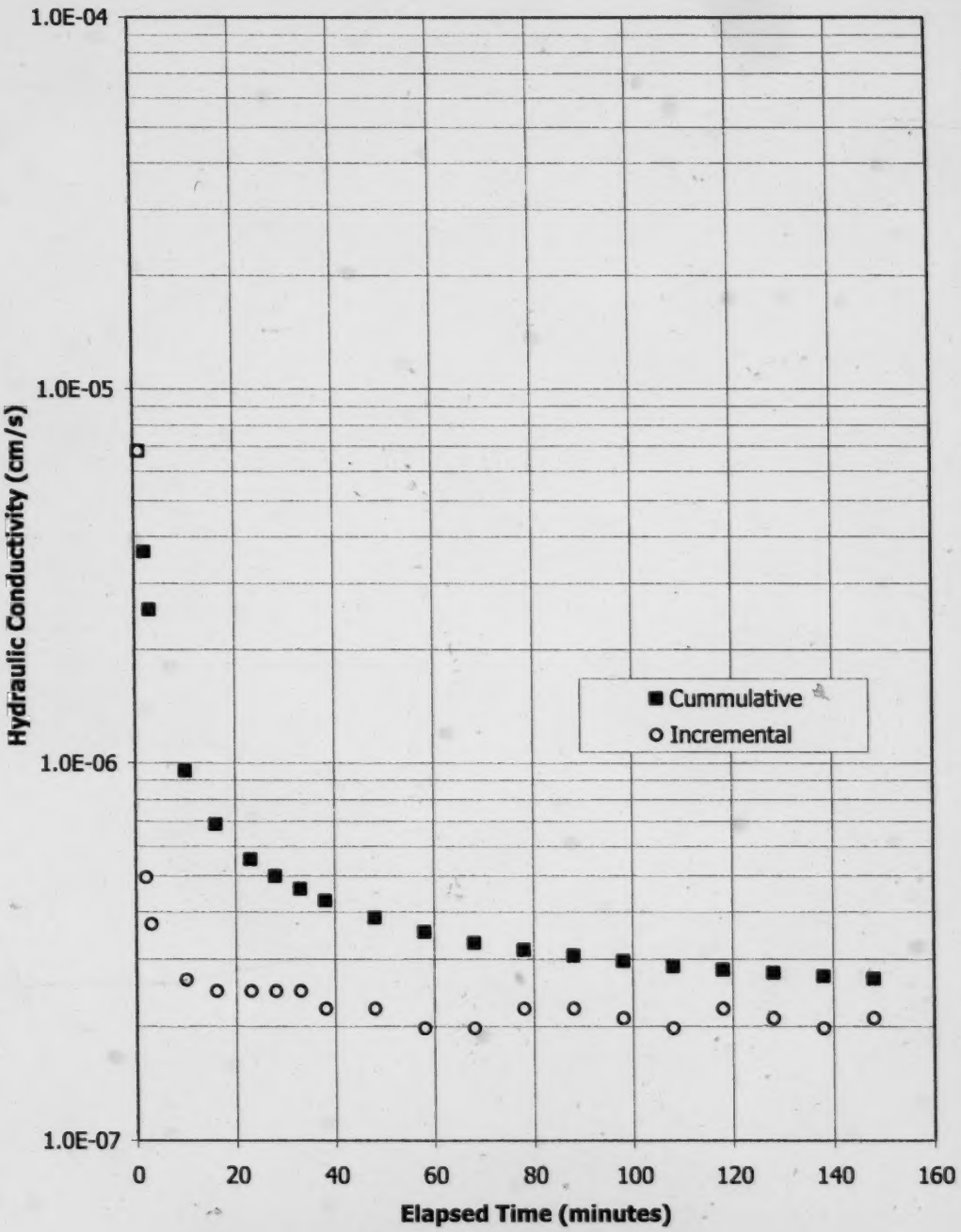

Figure D8: Hydraulic Conductivity vs. Time for C&P-3
Intially 63.3 % Solids, 20.9 % Fines, 900 g/m^3 PG
After 80.2 kPa
Upward Flow

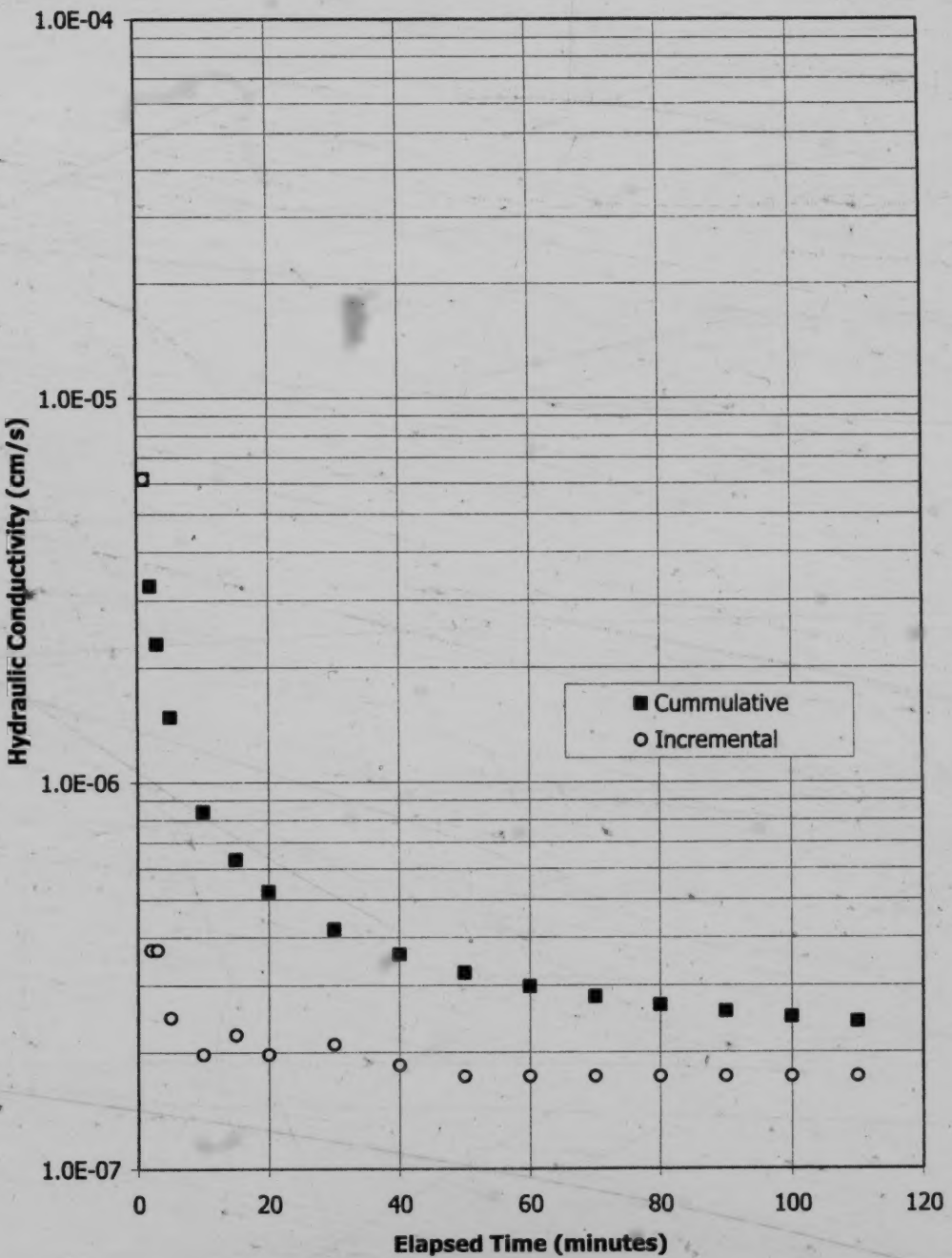

Figure D9: Hydraulic Conductivity vs. Time for C&P-3
Intially 63.3 % Solids, 20.9 % Fines, 900 g/m^3 PG
After 160 kPa
Upward Flow

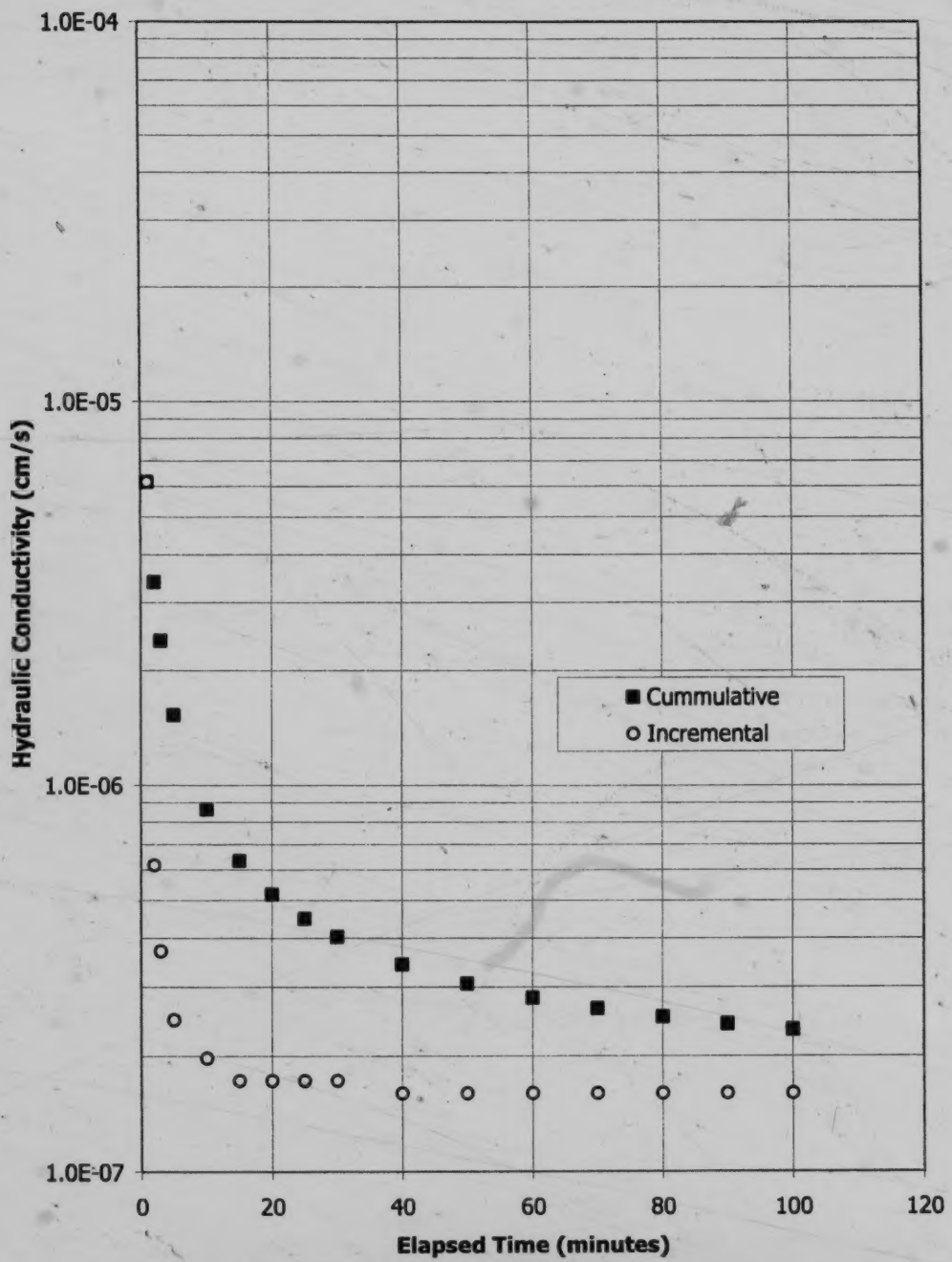

Figure D10: Hydraulic Conductivity vs. Time for C&P-3
Intially 63.3 % Solids, 20.9 % Fines, 900 g/m^3 PG
After 277 kPa
Upward Flow

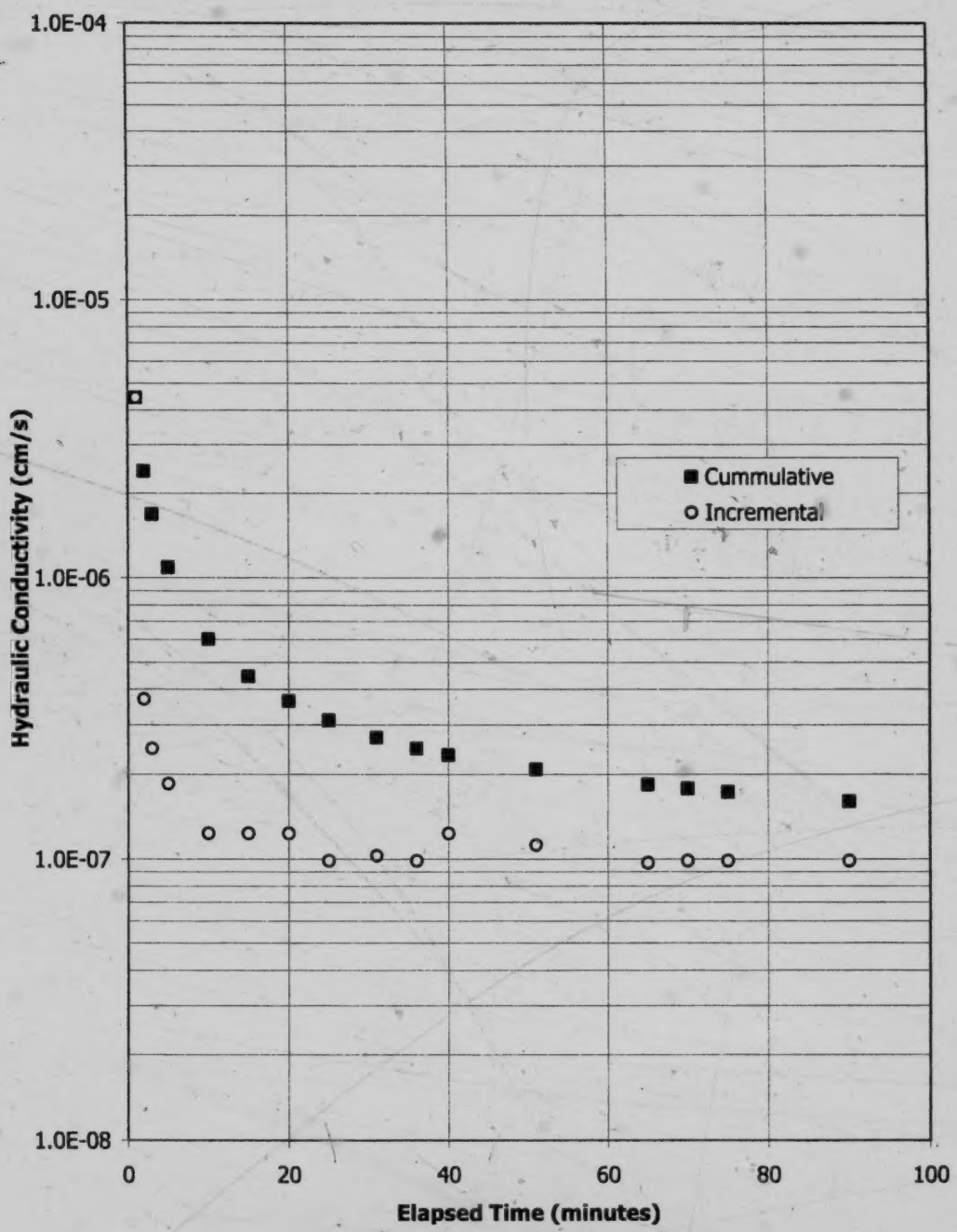

Figure D11: Hydraulic Conductivity vs. Time for C&P-3
Intially 63.3 % Solids, 20.9 % Fines, 900 g/m^3 PG
After 700 kPa
Upward Flow

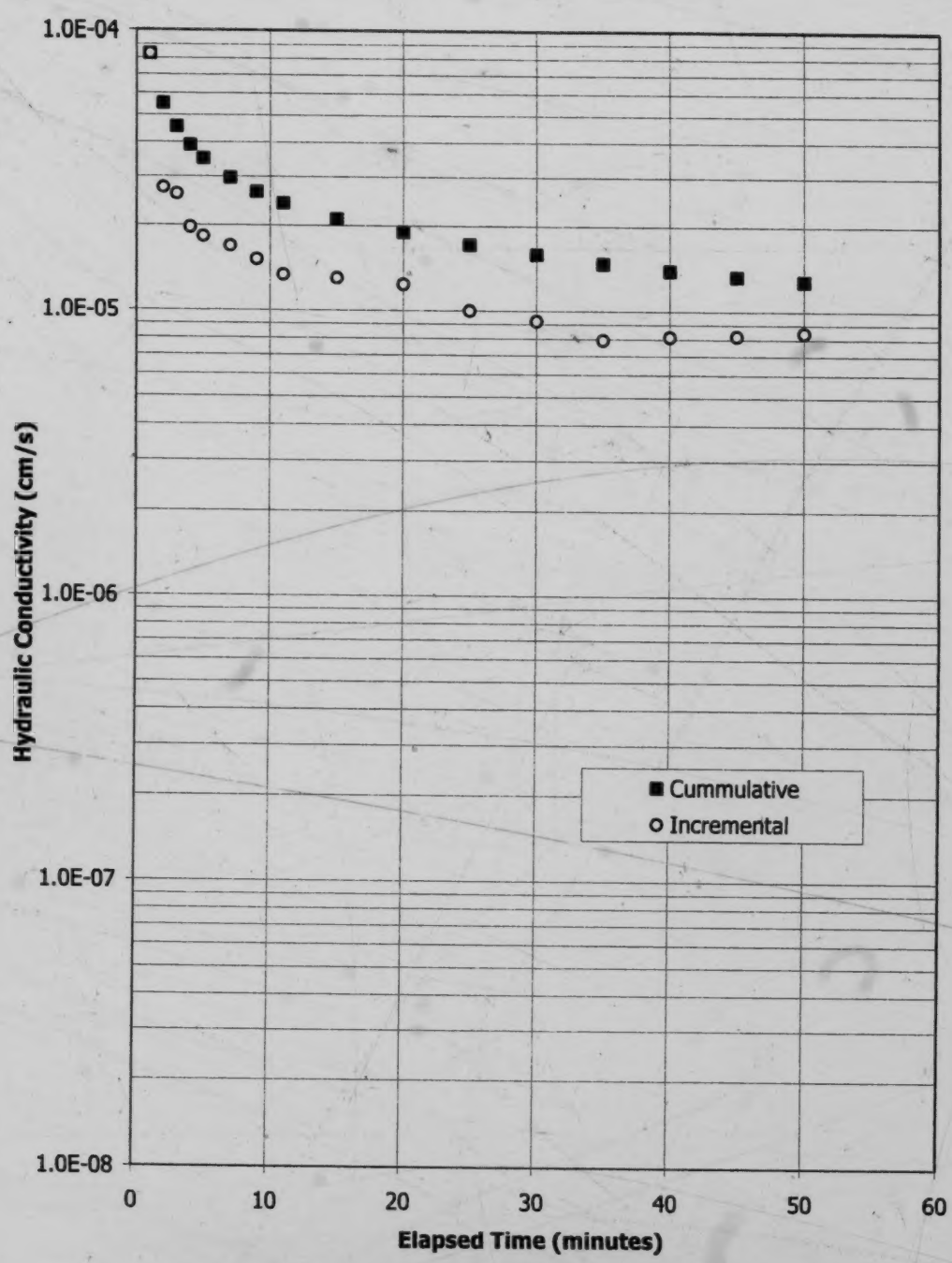

Figure D12: Hydraulic Conductivity vs. Time for C&P-4
Intially 62.5 % Solids, 20.6 % Fines, 3200 g/m^3 PG
After Self Weight Load
Upward Flow

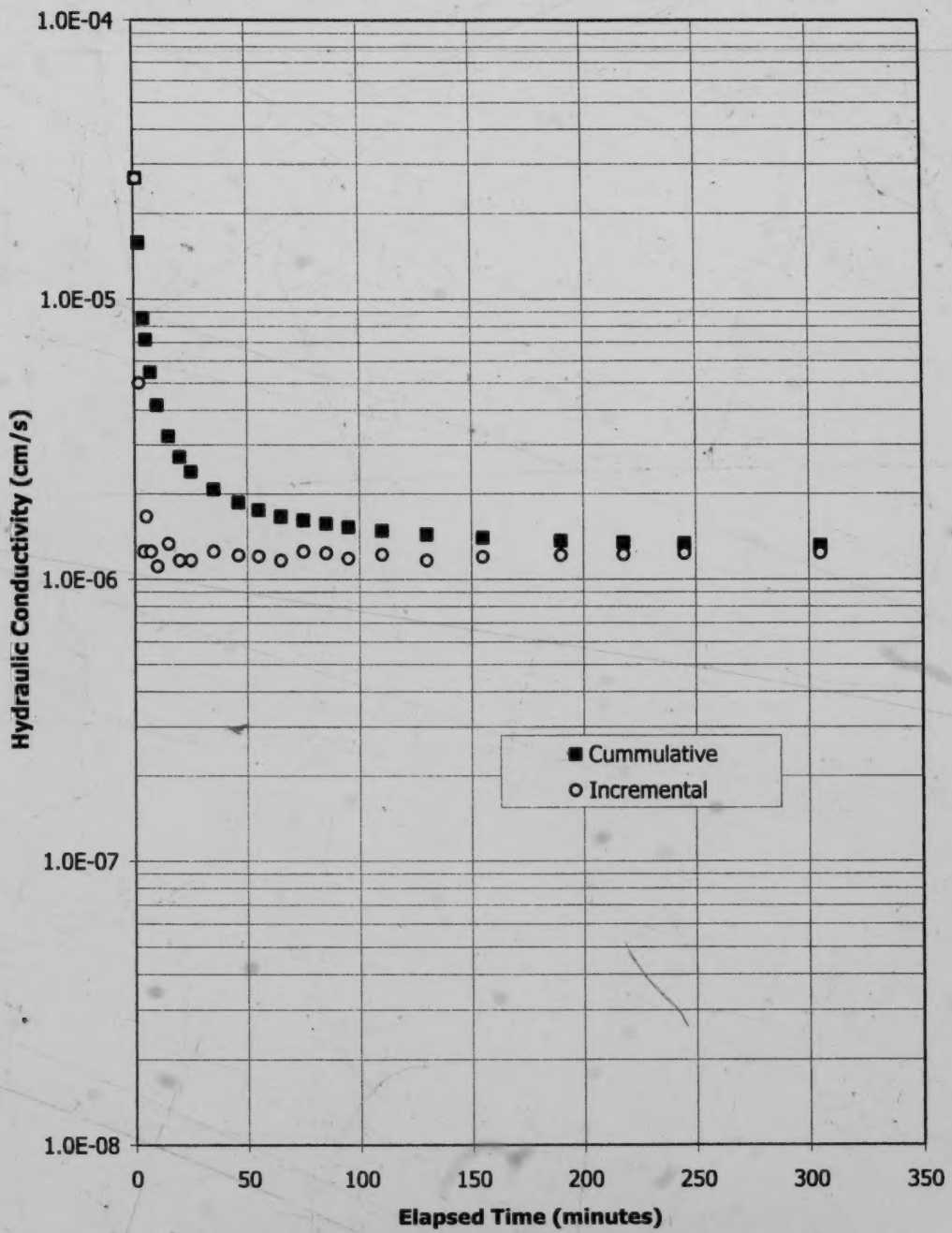

Figure D13: Hydraulic Conductivity vs. Time for C&P-4
Intially 62.5 % Solids, 20.6 % Fines, 3200 g/m^3 PG
After 1.2 kPa
Upward Flow

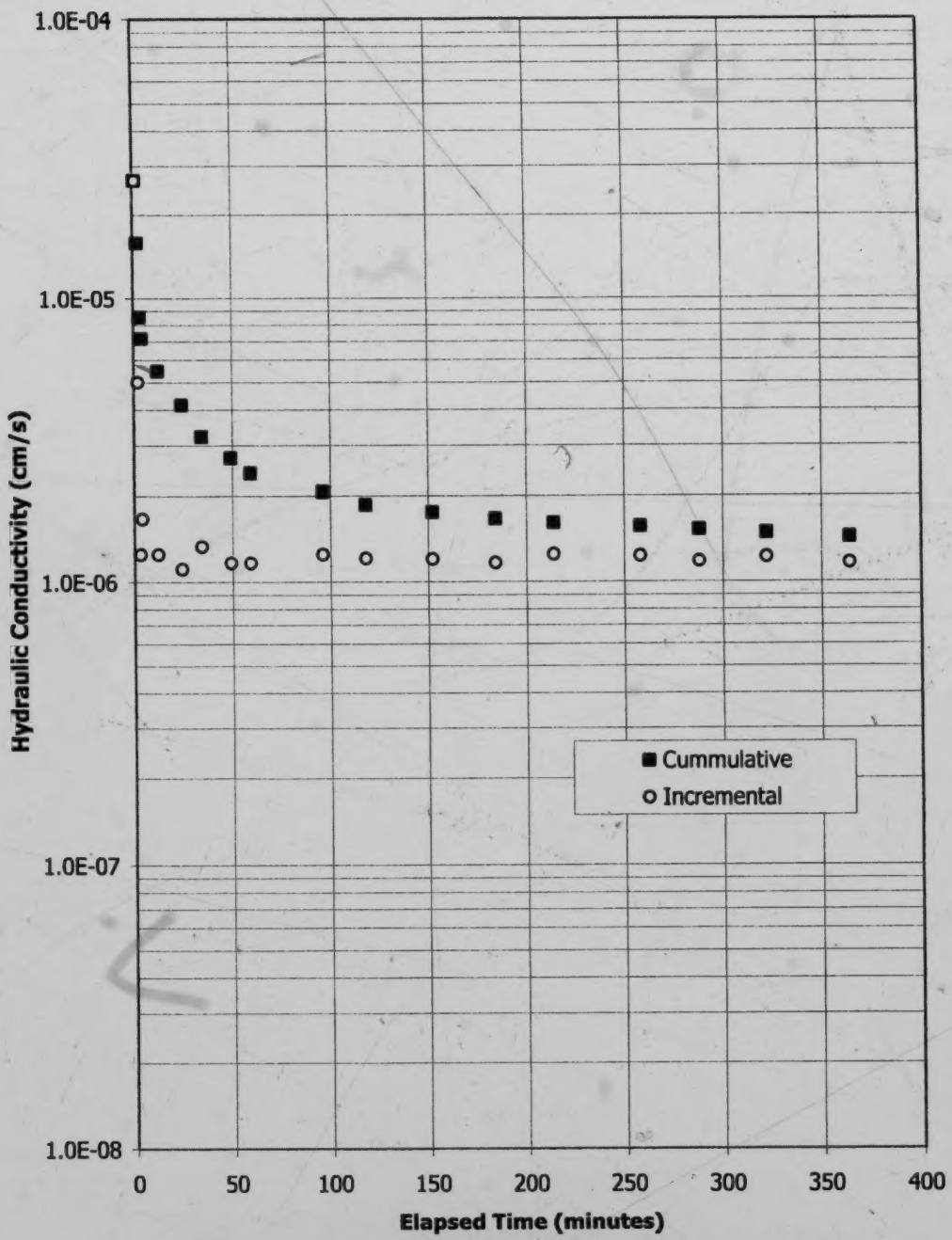

Figure D14: Hydraulic Conductivity vs. Time for C&P-4
Intially 62.5 % Solids, 20.6 % Fines, 3200 g/m^3 PG
After 2.6 kPa
Upward Flow

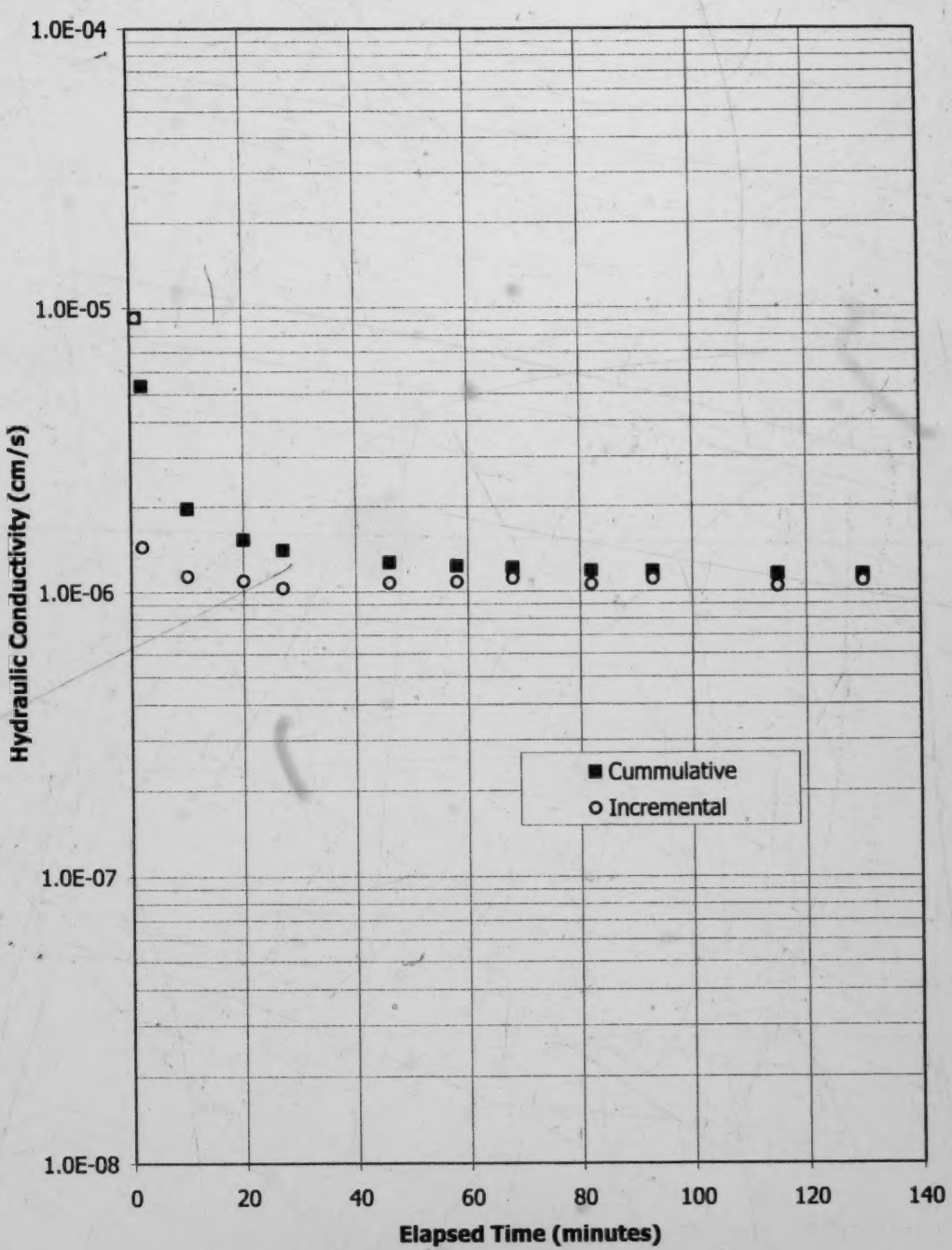

Figure D15: Hydraulic Conductivity vs. Time for C&P-4
Intially 62.5 % Solids, 20.6 % Fines, 3200 g/m^3 PG
After 5.0 kPa
Upward Flow

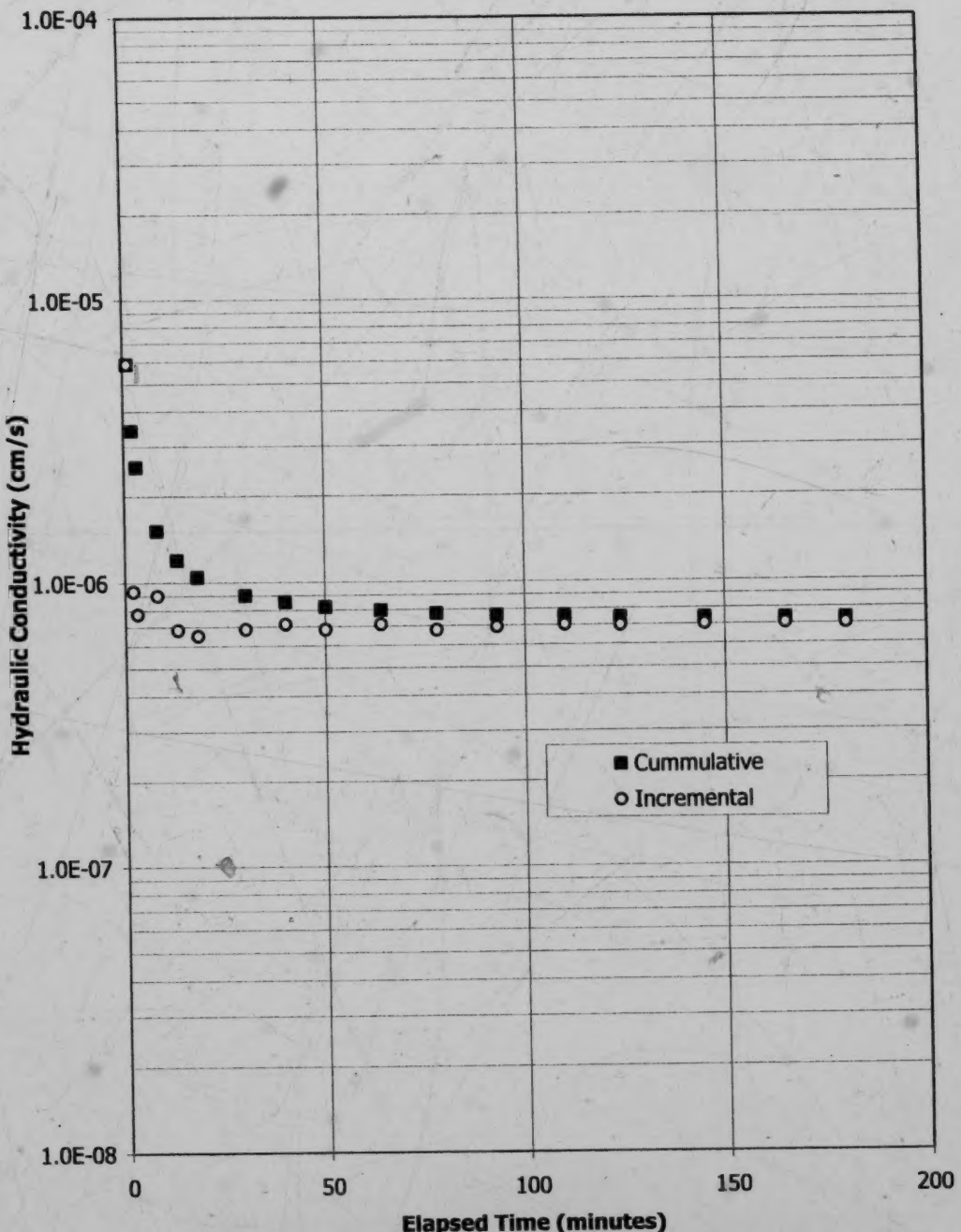

Figure D16: Hydraulic Conductivity vs. Time for C&P-4
Intially 62.5 % Solids, 20.6 % Fines, 3200 g/m^3 PG
After 10 kPa
Upward Flow

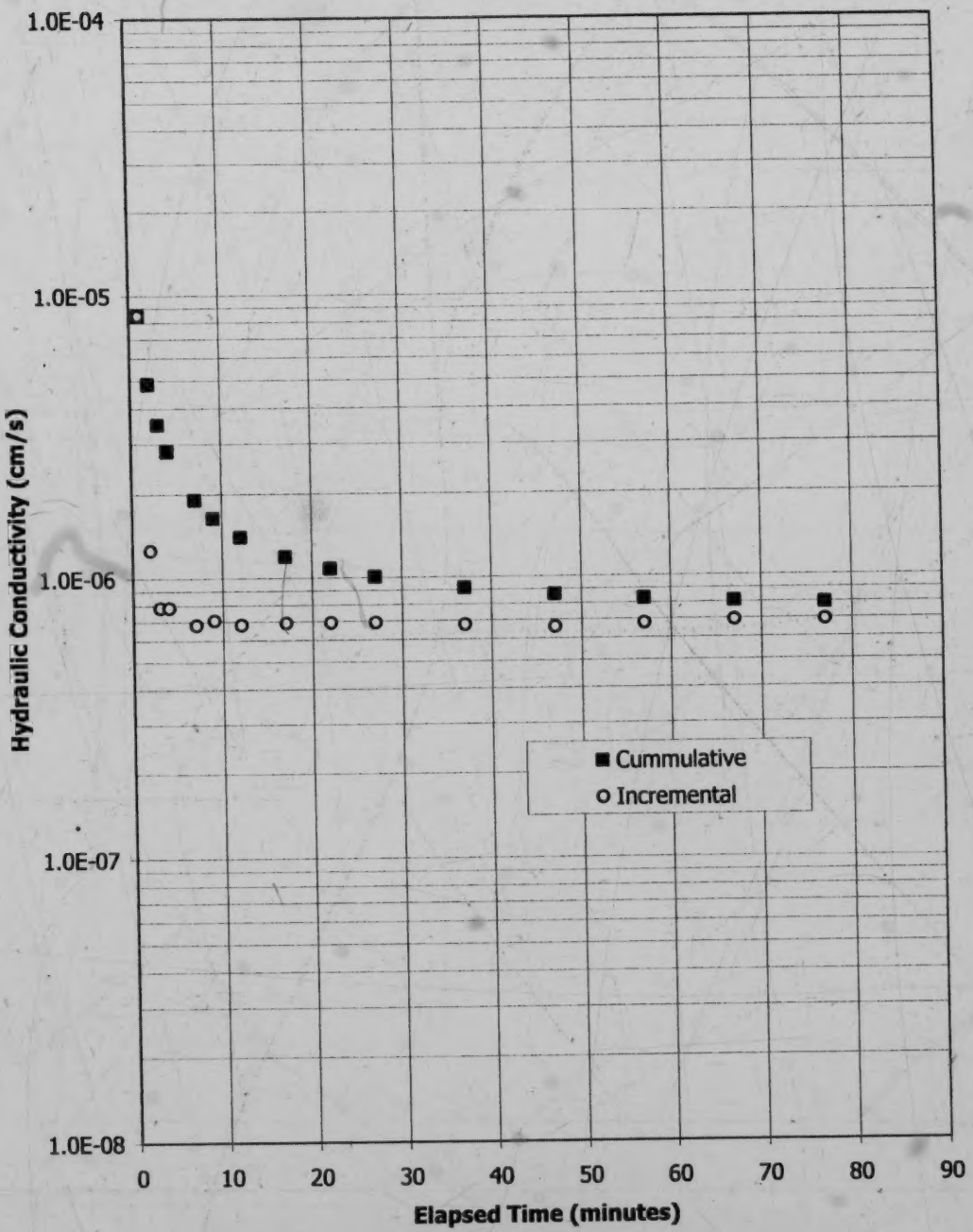

Figure D17: Hydraulic Conductivity vs. Time for C&P-4
Intially 62.5 % Solids, 20.6 % Fines, 3200 g/m^3 PG
After 20 kPa
Upward Flow

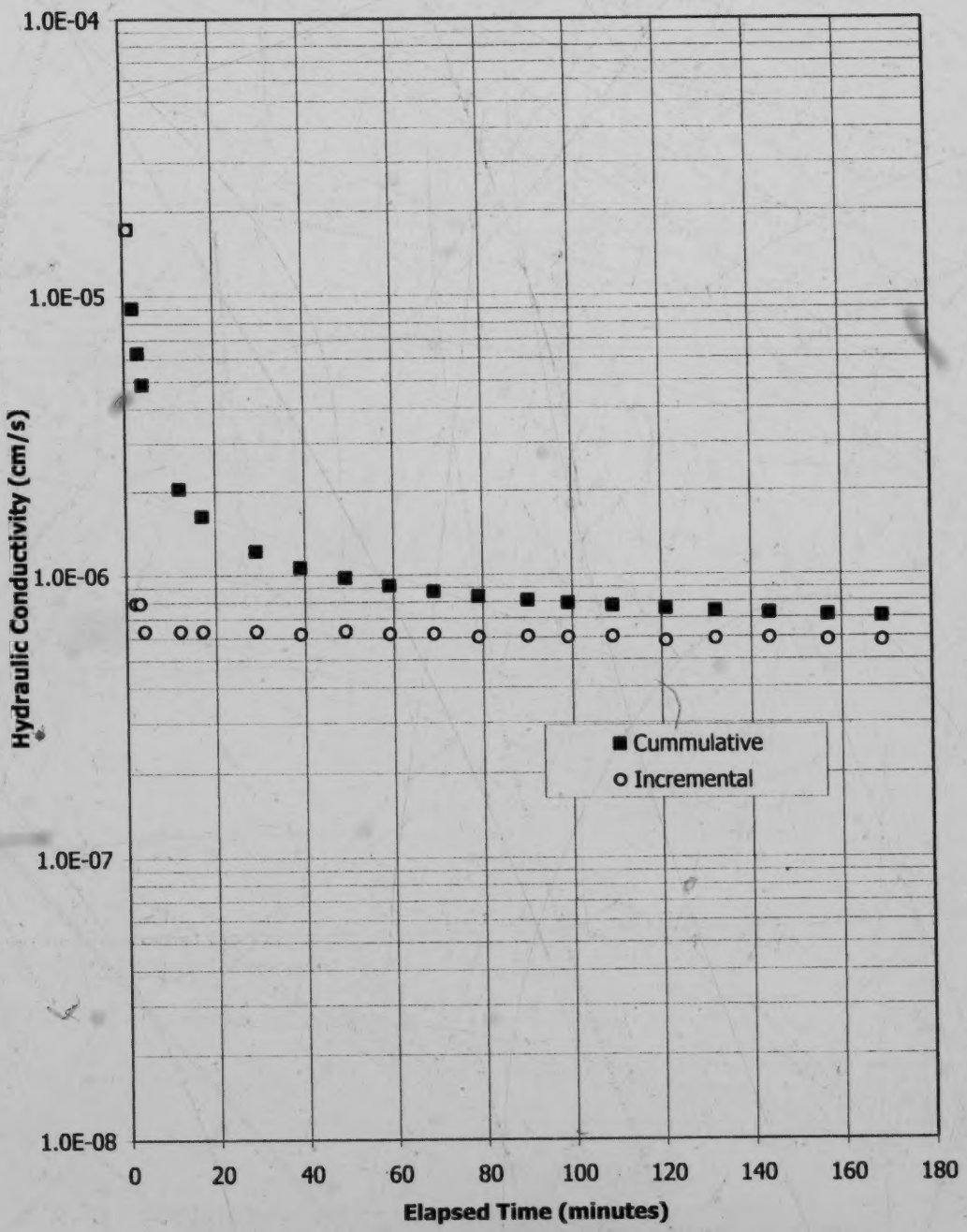

Figure D18: Hydraulic Conductivity vs. Time for C&P-4
Intially 62.5 % Solids, 20.6 % Fines, 3200 g/m^3 PG
After 40 kPa
Upward Flow

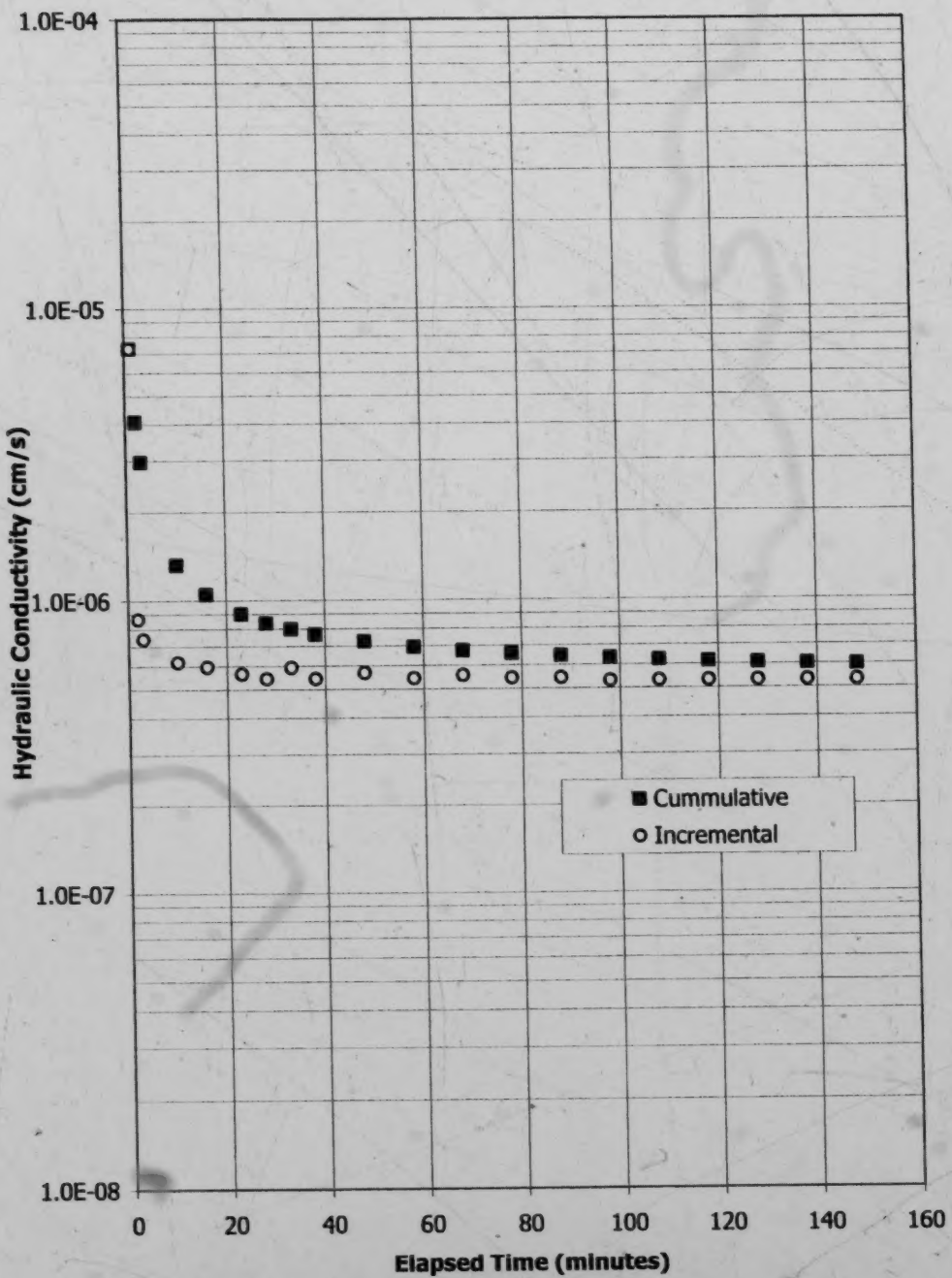

Figure D19: Hydraulic Conductivity vs. Time for C&P-4
Intially 62.5 % Solids, 20.6 % Fines, 3200 g/m^3 PG
After 80 kPa
Upward Flow

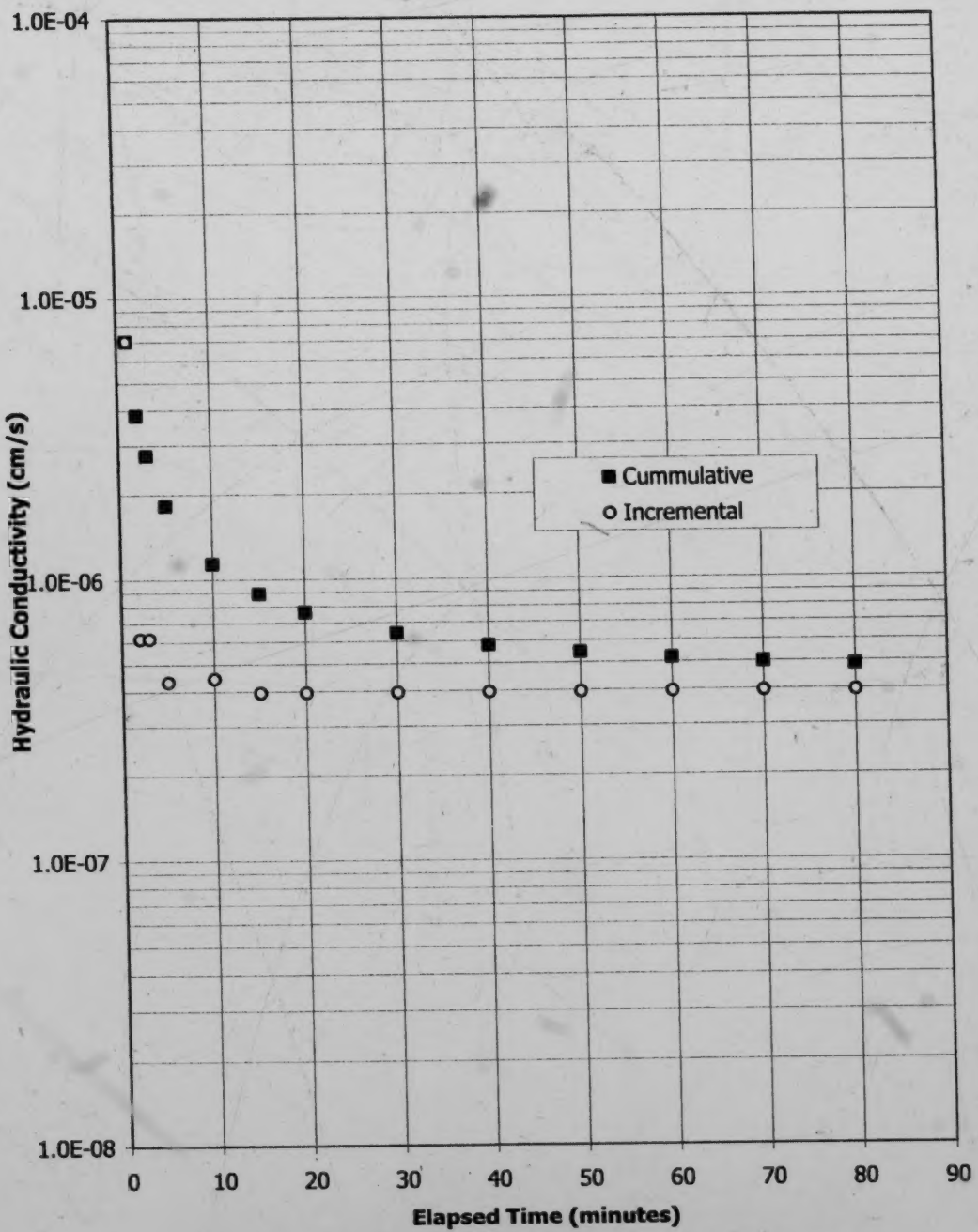

Figure D20: Hydraulic Conductivity vs. Time for C&P-4
Intially 62.5 % Solids, 20.6 % Fines, 3200 g/m^3 PG
After 160 kPa
Upward Flow

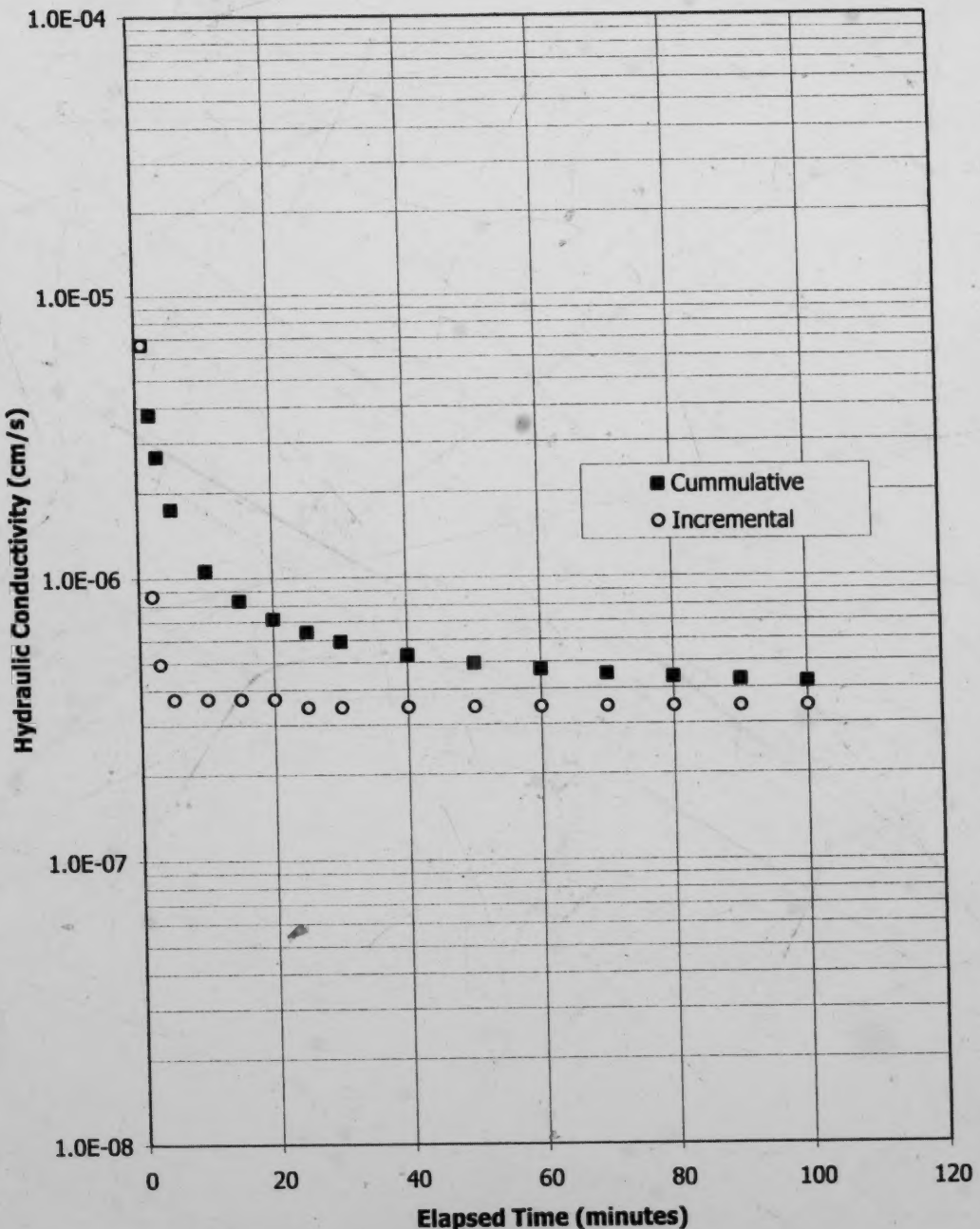

Figure D21: Hydraulic Conductivity vs. Time for C&P-4
Intially 62.5 % Solids, 20.6 % Fines, 3200 g/m^3 PG
After 293 kPa
Upward Flow

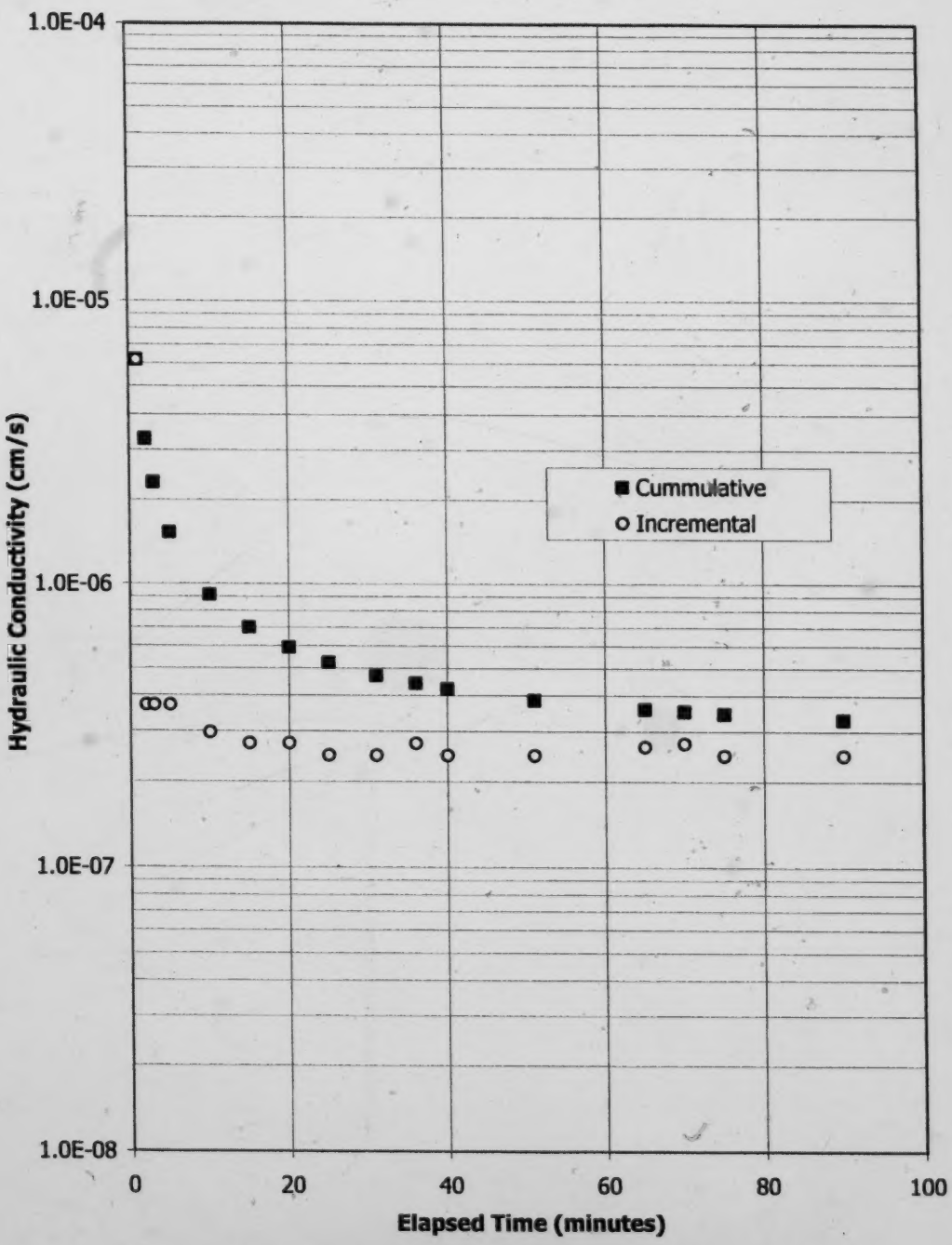

Figure D22: Hydraulic Conductivity vs. Time for C&P-4
Intially 62.5 % Solids, 20.6 % Fines, 3200 g/m^3 PG
After 700 kPa
Upward Flow